Use of tissue Doppler imaging and two-dimensional speckle tracking for quantification of left ventricular function in horses

Annelies Decloedt

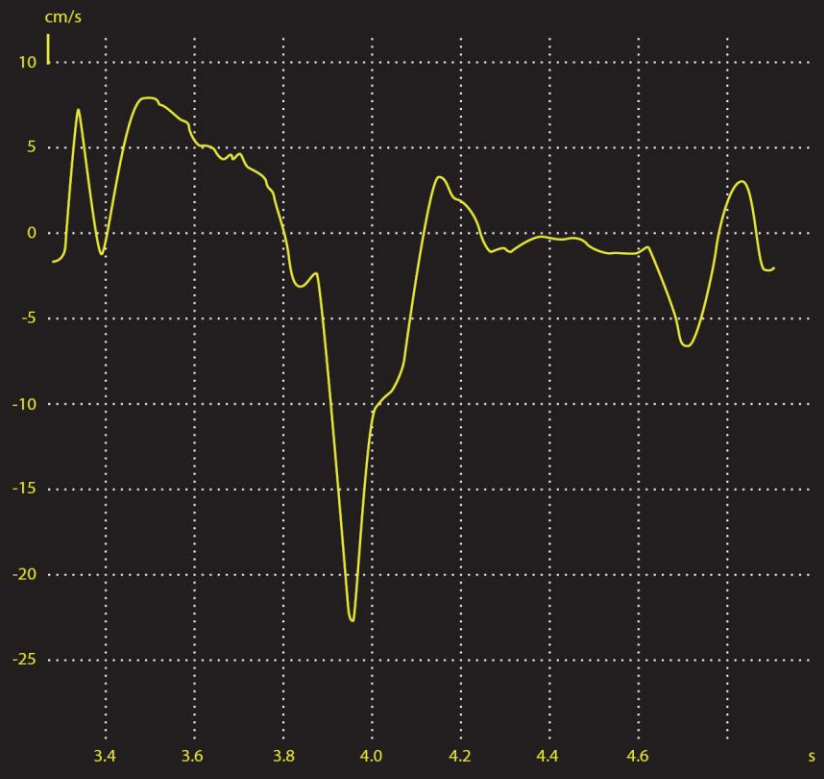

UNIVERSITEIT GENT

FACULTEIT DIERGENEESKUNDE
approved by EAEVE

Use of tissue Doppler imaging and two-dimensional speckle tracking for quantification of left ventricular function in horses

Annelies Decloedt

Dissertation submitted in fulfillment of the requirements for the degree of Doctor of Philosophy (PhD) in Veterinary Sciences, Faculty of Veterinary Medicine, Ghent University

May 2012

Promotor

Prof. Dr. G. van Loon

Co-promotor

Prof. Dr. P. Deprez

Department of Large Animal Internal Medicine
Salisburylaan 133, 9820 Merelbeke

ISBN 978-90-5864-293-6

Fonds Wetenschappelijk Onderzoek
Research Foundation – Flanders

This research was funded by the Research Foundation – Flanders / Dit onderzoek werd gesubsidieerd door het Fonds Wetenschappelijk Onderzoek (FWO) – Vlaanderen.
Aspirant 1172211N

A horse gallops with his lungs,
perseveres with his heart,
and wins with his character.

Federico Tesio

Table of contents

List of abbreviations

Chapter 1: General introduction **1**
1. Equine cardiology 1
2. Tissue Doppler imaging (TDI) 7
3. Two-dimensional speckle tracking (2DST) 16
4. Use of TDI and 2DST in veterinary and human medicine 20

Chapter 2: Scientific aims **39**

Chapter 3: Feasibility and reliability of tissue Doppler imaging and two-dimensional speckle tracking in healthy horses **41**

3.3 Quantification of left ventricular longitudinal strain, strain rate, velocity and displacement in healthy horses by two-dimensional speckle tracking 43

3.2 Two-dimensional speckle tracking for quantification of left ventricular circumferential and radial wall motion in horses 65

3.3 Tissue Doppler imaging for regional quantification of radial left ventricular wall motion in horses 91

Chapter 4: The influence of atrioventricular interaction on mitral valve closure and left ventricular isovolumic contraction **113**

Chapter 5: Tissue Doppler imaging and two-dimensional speckle tracking in horses with cardiomyopathy caused by ionophore intoxication **135**

5.1 Acute and long-term cardiomyopathy and delayed neurotoxicity after accidental lasalocid poisoning in horses 137

5.2 Tissue Doppler imaging and two-dimensional speckle tracking detect impaired left ventricular function in horses exposed to ionophores 155

Chapter 6: Cardiac changes in horses with atypical myopathy **177**

Chapter 7: General discussion **197**

Summary 217

Samenvatting 223

Curriculum vitae 229

Bibliography 231

Dankwoord 235

List of abbreviations

2D	two-dimensional
2DST	two-dimensional speckle tracking
A	late diastole
ADD	acyl-CoA dehydrogenase deficiency
AF	atrial fibrillation
AM	atypical myopathy
APD	atrial premature depolarization
AV	atrioventricular
AVC	aortic valve closure
AVC_a	time of aortic valve closure automatically calculated by 2DST software
AVC_{MM}	time of aortic valve closure measured by M-mode
AVO	aortic valve opening
bpm	beats per minute
CD	contraction duration
CF	color flow
cf	value corrected using Fridericia's correction method
CH	chordal level
CHF	congestive heart failure
CK	creatine kinase
CRT	cardiac resynchronization therapy
cTnI	cardiac troponin I
CV	coefficient of variation
CW	continuous wave
DCM	dilated cardiomyopathy
DHA	docosahexaenoic acid
DL_S	peak systolic longitudinal displacement
DR_S	peak systolic radial displacement
durA	duration of late diastolic peak
E	early diastole
EAD	early afterdepolarization
ECG	electrocardiography
EET	end ejection time
EF	ejection fraction
ET	ejection time
fps	frames per second
FS	fractional shortening
GRMD	Golden Retriever muscular dystrophy

HCM	hypertrophic cardiomyopathy
HR	heart rate
IVA	isovolumic acceleration
IVC	isovolumic contraction
IVCT	isovolumic contraction time
IVR	isovolumic relaxation
IVRT	isovolumic relaxation time
IVS	interventricular septum
LA	left atrium
LD_{50}	single oral median lethal dose
LLV	left region of left ventricular wall
LMM	linear mixed model
LQTS	long QT syndrome
LV	left ventricle
LVFW	left ventricular free wall
LVIDd	left ventricular end-diastolic internal diameter
LVIDs	left ventricular end-systolic internal diameter
MM	M-mode
MRI	magnetic resonance imaging
MVC	mitral valve closure
MVG	myocardial velocity gradient
MVO	mitral valve opening
nIVC	negative pre-ejectional velocity peak
NSR	normal sinus rhythm
PEP	pre-ejection period
PM	papillary muscle level
ppb	parts per billion
PRF	pulse repetition frequency
PW	pulsed wave
rA	recoil of the left ventricle following atrial contraction
RLV	right region of left ventricular wall
ROI	region of interest
Rot_S	peak systolic rotation
RVP	right ventricular pacing
SC	peak circumferential strain
SC_P	early-systolic positive circumferential strain
SD	standard deviation
SL	peak longitudinal strain
SL_G	peak maximal longitudinal strain

SL_P	peak positive longitudinal strain
SL_S	peak systolic longitudinal strain
SR	peak radial strain
SrC_A	late diastolic circumferential strain rate
SrC_E	early diastolic circumferential strain rate
SrC_S	systolic circumferential strain rate
SrL_A	late diastolic longitudinal strain rate
SrL_E	early diastolic longitudinal strain rate
SrL_S	systolic longitudinal strain rate
SrR_A	late diastolic radial strain rate
SrR_E	early diastolic radial strain rate
SrR_S	systolic radial strain rate
St	strain
STI	synchrony time index
Syst	systole
t	time
TDI	tissue Doppler imaging
V_A	peak radial wall motion velocity during late diastole
V_E	peak radial wall motion velocity during early diastolic filling
VF	ventricular fibrillation
VL_A	late diastolic longitudinal velocity
VL_E	early diastolic longitudinal velocity
VL_S	systolic longitudinal velocity
VO_2max	body mass specific maximal oxygen uptake
VPD	ventricular premature depolarization
V_{Syst}	peak radial wall motion velocity during systole
VT	ventricular tachycardia

Chapter 1: General introduction

1. Equine cardiology

1.1 The horse, a natural athlete

Centuries of selective breeding towards better athletic performance have made the horse one of the greatest mammalian athletes. The horse is a "natural blood doper", increasing both hematocrit and circulating blood volume by splenic contraction at the onset of exercise. Up to 12 liters of splenic blood can be released into the circulation, resulting in a great increase in circulating packed cell volume and blood viscosity (Persson, 1967). The cardiovascular system is also hugely compliant. The cardiac output can rise from 30-40 liters per minute at rest to 400 liters per minute during maximal exercise in trained racehorses (Poole and Erickson, 2008). This results in a spectacular body mass specific maximal oxygen uptake (VO_2max) of over 200 ml/kg/min in elite racehorses (Fig. 1) (Young et al., 2002). In human athletes, the highest VO_2max ever measured was 90 ml/kg/min in an elite cross-country skier. The high VO_2max in horses is required to fulfill the high oxygen demand of the skeletal muscle, which exceeds 50% of body weight (Hinchcliff et al., 2004).

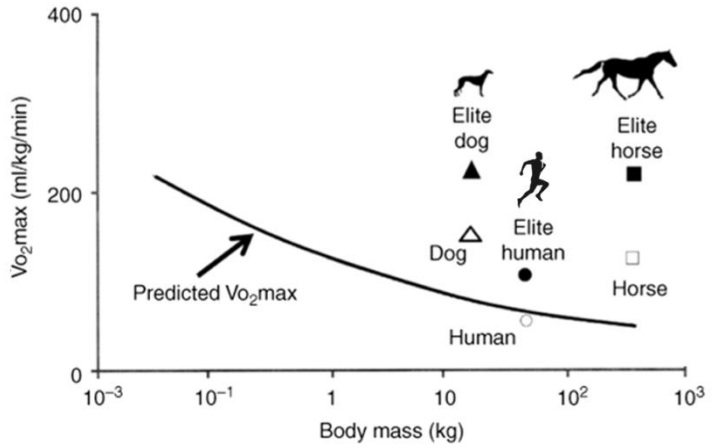

Figure 1: Body mass specific maximal oxygen uptake (VO_2max) plotted as a logarithmic function of body mass for a selection of mammals with body masses differing over 5 orders of magnitude. Horses and dogs show extraordinary values. (Adapted from: Poole and Erickson, 2011)

The cardiac output is determined by the wide heart rate range, from 20 to 240 beats per minute (bpm), and the large stroke volume, up to 1700 ml. The maximal heart rate cannot be influenced by training but decreases with age (Betros et al., 2002). Therefore the individual differences of cardiac output and thus aerobic capacity mainly depend on stroke volume, which is determined by heart size. The relative cardiac mass is very high in horses compared to other animals and man. While the human heart weighs on average about 0.5% of body mass, the equine heart weighs >1% of body mass (Gunn, 1989).

However, elite racehorses have been described to have even bigger hearts. The heart weight of the undefeated legendary racehorse *Eclipse* was alleged to be over 6 kg after death. The heart weight of another legend, *Secretariat*, was claimed to be over 10 kg, which means that his cardiac output would have exceeded 500 liters per minute (Young, 2003). The correlation between racing success and heart size was demonstrated in Thoroughbred racehorses. Left ventricular (LV) mass derived by echocardiography was positively associated with rating in horses racing over longer distances in jump races (Young et al., 2005).

1.2 Drawbacks of cardiovascular adaptations to exercise

Due to selective breeding for performance, horses rarely suffer from inherited or acquired degenerative cardiac diseases. However, the extreme cardiovascular adaptations not only result in improved aerobic capacity but also carry negative consequences. During maximal exercise, highly elevated pressures are reached in the right heart and the pulmonary artery. During exercise, the pulmonary artery pressure increases disproportionately compared to the systemic pressure, rising from 30 mmHg to over 100 mmHg (Manohar and Goetz, 1996). Combined with the negative alveolar pressure during inspiration, this results in extreme transmural pressures which may cause stress failure of the pulmonary capillaries. Exercise-induced pulmonary hemorrhage is reported in >80% of racehorses (Birks et al., 2002).

Another important problem is exercise-induced dysrhythmia as this can cause poor performance and even sudden death (Kiryu et al., 1999; Lyle et al., 2011). In 28% of racehorses, ventricular dysrhythmias were detected during recovery after maximal effort (Physick-Sheard and McGurrin, 2010). In normal performing dressage and jumping horses, atrial premature depolarizations were present in up to 89% of horses during exercise (Barbesgaard et al., 2010). Horses are also particularly susceptible to atrial fibrillation and its incidence is estimated around 2.5% (Else and Holmes, 1971).

Finally, equine athletes present a very high incidence of cardiac murmurs due to valvular regurgitation. Cardiac murmurs could be detected in 81% of Thoroughbred racehorses (Kriz et al., 2000). Although many of these murmurs are physiological ejection murmurs, mitral or aortic valvular regurgitation is present in up to 60% of horses (Young et al., 2008). Tricuspid regurgitation was found in up to 89% of horses, and this was suggested to be associated with training-induced eccentric hypertrophy. The prevalence and grade of mitral and tricuspid regurgitation increased significantly following physical training in Thoroughbreds and Standardbred trotters (Young and Wood, 2000; Buhl and Ersboll, 2012).

1.3 Examination of the horse with cardiovascular disease

1.3.1 Cardiac auscultation

Cardiac auscultation is a crucial diagnostic instrument for evaluating the equine heart. Abnormal findings are dysrhythmias and heart murmurs, which can both be physiological or pathological findings (Blissitt, 2010). The high vagal tone in horses often causes physiological dysrhythmia at rest, such as sinus arrhythmia and first and second degree atrioventricular (AV) block. Pathological dysrhythmias include premature depolarizations of ventricular or atrial origin and atrial fibrillation.

Cardiac murmurs can be classified as physiological or pathological based on the location, timing, quality, radiation and intensity of the murmur. Physiological or functional murmurs are caused by the high velocity blood flow into the great vessels during ejection. These murmurs are typically early to midsystolic, most often localized at the heart base and variable in intensity. Pathological murmurs are most often caused by valvular regurgitation, as valvular stenosis and congenital defects are rare in horses. Based on the point of maximal intensity and timing of the murmur, a differential diagnosis can be made. Systolic murmurs indicate atrioventricular valve regurgitation or a ventricular septal defect, while diastolic murmurs are a sign of aortic or pulmonary valve regurgitation. However, the main limitation of auscultation is that the intensity of the murmur is not always related to the severity of valvular regurgitation (Reef, 1995).

1.3.2 Electrocardiography

Electrocardiography (ECG) is an important tool for diagnosis and classification of dysrhythmias (Verheyen et al., 2010a). These can be classified based on their origin as sinoatrial nodal, atrial, AV nodal or ventricular (McGuirk and Muir, 1985; Verheyen et al., 2010b). Sinoatrial nodal dysrhythmias such as sinus bradycardia, sinus exit block and sinus arrest are often physiological and usually caused by a high vagal tone. They should disappear with increasing sympathetic tone during stress or exercise. Sinus arrhythmia is caused by alterations in vagal tone and is often present during recovery after exercise. Physiological AV nodal dysrhythmias include first and second degree AV blocks. Third degree AV block is a rare but pathological dysrhythmia, which is characterized by absence of conduction of the atrial impulses through the AV node and the presence of an idioventricular rhythm.

The clinically most important dysrhythmias are of atrial or ventricular origin. Atrial fibrillation (AF) is characterized by absence of P waves and an irregularly irregular rhythm.

Because of the high vagal tone, horses with AF often show a normal heart rate at rest. However, the heart rate can increase up to 400 bpm during exercise, causing rapid fatigue (Maier-Bock and Ehrlein, 1978). Atrial premature depolarizations are clinically less important but may preceed atrial fibrillation. Ventricular premature depolarizations, especially during exercise, are always regarded with caution. They might evolve into ventricular tachycardia or even ventricular fibrillation, causing collapse or sudden death of the horse with danger for the rider (Kiryu et al., 1999).

In contrast to small animal and human medicine, ECG analysis does not allow to determine the exact origin of the dysrhythmia, to detect myocardial disease nor to evaluate chamber size.

1.3.3 Cardiac catheterization

Before the introduction of echocardiography, right and left heart catheterization were used to diagnose valvular regurgitation or congenital defects in horses with cardiac murmurs. Right heart catheterization is performed through the jugular vein, left heart catheterization through the carotid artery. The catheter position can be determined from the pressure trace, which is typical for each chamber or vessel, or by fluoroscopy or echocardiography. The catheter length should be adapted to the size of the equine heart. A length of approximately 150 cm is needed to reach the pulmonary artery through the cervical jugular vein and the right ventricle (Patteson, 1996).

In horses with severe aortic regurgitation, the extreme arterial pressure difference between systole and diastole can be demonstrated in the carotid artery and the aorta. In horses with mitral regurgitation, the pulmonary wedge pressure is raised due to increased left atrial pressures (Gehlen et al., 2004). Increased right ventricular pressure can occur in horses with a large ventricular septal defect. However, right ventricular pressure increase can also be caused by pulmonary hypertension due to primary lung disease or pulmonary stenosis and thus catheterization findings are often non-specific. Oxygen tension measurements can provide additional information in the presence of shunts. A left to right shunt will cause an increased oxygen tension in the pulmonic circulation, while a right to left shunt will cause a decreased oxygen tension in the systemic circulation at the level of the shunt (Lombard et al., 1983).

Currently, cardiac catheterization is infrequently used in equine cardiology because of the non-specific findings and the risks involved with invasive catheterization, particularly of the carotid artery. Most diagnoses can now be made using echocardiography, a non-invasive and safe diagnostic method.

1.3.4 Echocardiography

The use of echocardiography was a major breakthrough in equine cardiology, allowing non-invasive quantification of cardiac chamber dimensions, evaluation of endo-, myo- or pericardial abnormalities, assessment of valvular function and measurements of LV function. For the quantification of cardiac dimensions, standardized two-dimensional (2D) and M-mode images are acquired from right and left parasternal short- and long-axis views (Long et al., 1992; Patteson et al., 1995). In adult horses, the acquisition of apical images is impossible due to anatomical constraints.

Valvular function can be evaluated by color flow (CF) Doppler imaging (Blissitt and Bonagura, 1995). The blood flow is color-coded and superimposed on the 2D image. The conventional color code displays flow away from the transducer in blue and flow towards the transducer in red. Valvular regurgitation results in a high-velocity turbulent jet, displayed in green (Fig. 2). The severity of valvular regurgitation is estimated subjectively, based on the duration, timing and area of the regurgitant jet. Therefore it is essential to evaluate this jet from different imaging planes. Furthermore, the pressure gradient between different cardiac chambers can be evaluated from the acceleration and deceleration of the jet measured by continuous wave (CW) Doppler.

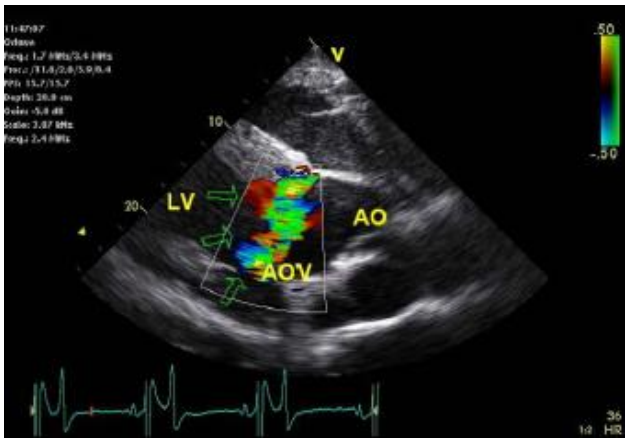

Figure 2: Right parasternal long-axis view of the left ventricular outflow tract in a horse, with color flow Doppler indicating aortic valve regurgitation. The regurgitant jet is color-coded green (indicated by the green arrows). LV = left ventricle, AOV = aortic valve, AO = aorta.

CW Doppler can accurately measure high blood velocities but does not allow depth discrimination. Therefore, peak blood flow velocity over the valve should be measured by pulsed wave (PW) Doppler. By PW Doppler, velocities are measured in a manually defined sample volume at a fixed distance from the transducer. Both CW and PW Doppler require good alignment of the ultrasound beam with the regurgitant jet or blood flow direction. As apical images cannot be obtained, this is rather difficult for mitral flow (Reef et al., 1989).

PW Doppler measurements of aortic flow can be used for quantification of LV systolic function. These measurements include peak flow velocity, the velocity time integral and flow acceleration. Cardiac output can be estimated based on the velocity time integral, vessel area and heart rate. In addition, systolic time intervals such as the pre-ejection period (PEP) and ejection time (ET) can be measured from the aortic flow profile and the ratio of PEP/ET can be calculated. Diastolic LV function can be assessed from the PW Doppler trace of inflow through the mitral valve based on the peak early (E) and late (A) diastolic flow velocities, the E/A ratio and the acceleration and deceleration of the E-wave (Blissitt et al., 1995).

The most common measurement of LV systolic function in horses is fractional shortening (FS), an M-mode measurement (Bonagura and Blissitt, 1995). FS is calculated from the LV internal diameter (LVID) measured at end-diastole (d) and end-systole (s) in a short-axis M-mode image at chordal level: $FS = \frac{(LVIDd - LVIDs)}{LVIDd} * 100$. This implies that FS is a focal and one-dimensional measurement, which can not detect regional abnormalities. Furthermore, FS is strongly load-dependent. This makes FS less reliable in horses with valvular disease, in which loading conditions can be altered significantly. Other indices such as ejection fraction (EF), LV mass and velocity of circumferential fibre shortening (VCF) have similar disadvantages since they are also calculated from M-mode measurements. Two-dimensional measurements such as LV myocardial area and fractional area change have been proposed but are infrequently used. In order to evaluate regional wall motion abnormalities, attempts were made to develop a visual wall motion scoring system (Gehlen et al., 2005). However, this is rather subjective.

Tissue Doppler imaging (TDI) and two-dimensional speckle tracking (2DST), two echocardiographic techniques that have been extensively studied in human medicine, might provide a better quantification of equine myocardial function.

2. Tissue Doppler imaging (TDI)

2.1 Principles

Ultrasound waves are generated by piezo-electric crystals which deform under the influence of an electric field. This generates longitudinal ultrasound waves, consisting of successive zones of compression and rarefaction oscillating back and forth in the direction of propagation. In a medium, sound waves propagate with a constant velocity. If the sound source is moving in the direction of propagation of the waves, the sound wave velocity is unaffected but the frequency increases. The frequency decreases if the sound source is moving in the opposite direction. This is called the Doppler effect (D'hooge et al., 2006).

The Doppler effect also applies if the sound source is stationary and the observer is moving. In echocardiography, an ultrasound wave is sent from a stationary transducer and reflected back to this transducer by moving tissue or blood. This results in a different frequency of the transmitted and reflected ultrasound wave. The Doppler shift or the difference between the observed and transmitted frequency can be calculated by the Doppler equation: $f_D = 2\, f_T \frac{v}{c} \cos(\alpha)$, where f_D is the Doppler shift, f_T the transmitted frequency, v the blood or tissue velocity relative to the transducer, c the velocity of sound and α the insonation angle between the velocity vector and the ultrasound beam (D'hooge et al., 2006). Tissue and blood velocities can be calculated from the Doppler shift of the reflected ultrasound wave: $v = -\frac{fD \,.\, c}{2\, fT \,.\, \cos\,(\alpha)}$. Blood or tissue moving away from the transducer will get a negative sign while velocities towards the transducer get a positive sign.

The calculation of velocity and direction from the Doppler shift was first applied to measure blood flow velocities using CF Doppler imaging. Tissue Doppler imaging (TDI) was described in 1989 as a modification of this technique (Isaaz et al., 1989). TDI measures the velocities of the myocardial walls, which show some major differences with blood flow velocities. The blood flow velocities are typically above 50 cm/s while myocardial wall velocities are usually below 35 cm/s. Furthermore, the blood pool is poorly reflective whereas the acoustic signal reflected from the myocardium has a high intensity. In conventional CF Doppler imaging, a high pass filter is used to reject the low myocardial velocities, and gain is adjusted to the low intensity blood flow signals. In contrast, a low pass filter is applied in TDI to reject high velocities and the ability to measure low velocities is improved. Gain is modified to eliminate the blood flow signals (McDicken et al., 1992; Miyatake et al., 1995).

As for conventional flow Doppler, two different modes may be used: PW and 2D color TDI (Van de Veire et al., 2008). By PW TDI, a sample volume is placed on the myocardium in the 2D grayscale image and the velocity curve within this sample volume is generated (Fig. 3A). Using color TDI, velocity signals are color-coded according to their direction and amplitude and superimposed on the 2D grayscale image (Fig. 3B). The color code is similar to CF Doppler imaging, with the myocardial walls colored red when moving towards the transducer and blue when moving away. The velocity curves are acquired by placing a sample area within the myocardium during off-line analysis. Data acquired by color TDI cannot be directly compared to PW TDI. Color TDI measures the mean peak velocities in the whole sample area calculated by the autocorrelation technique. By PW TDI, the maximal instantaneous velocities are measured in the sample volume by the Fast Fourier Transformation methodology (Pavlopoulos and Nihoyannopoulos, 2008). As a result, velocity measurements made by PW TDI are always slightly higher than those by color TDI (Kukulski et al., 2000).

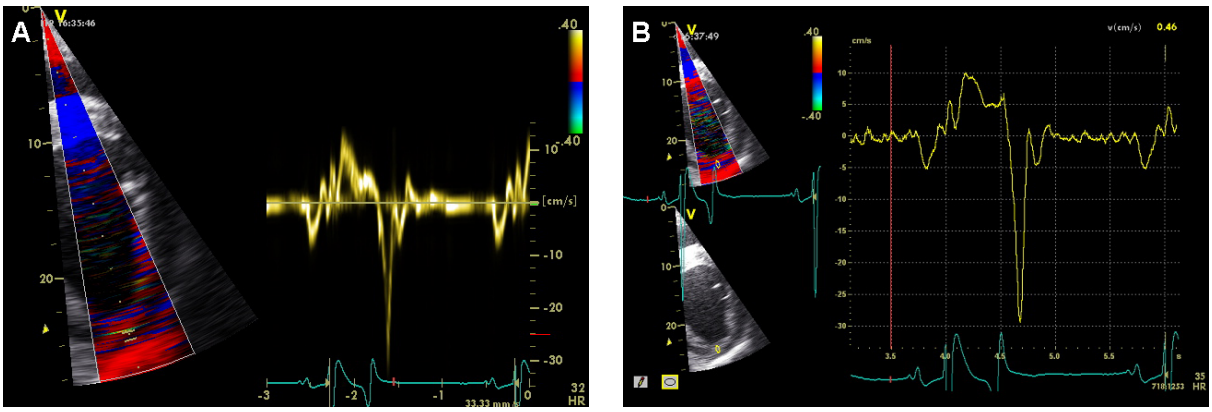

Figure 3: Tissue Doppler velocity curves of the left ventricular free wall from a right parasternal short-axis image at chordal level in a horse. (A) Pulsed wave tissue Doppler imaging. The sample volume is placed at a fixed distance from the transducer during image acquisition, as indicated in the 2D image on the left; (B) Color tissue Doppler imaging. The sample area is positioned on the myocardium during off-line analysis.

Although both modalities were used in the first TDI studies, the 2D color mode is preferred over PW TDI in recent studies in human medicine. Using PW TDI, the sample volume is positioned at a fixed distance from the transducer and the myocardial segment is moving through this sample area as the ventricle contracts. As a consequence, velocities of different parts of the myocardium are measured throughout the cardiac cycle. During color TDI postprocessing, the sample area or region of interest (ROI) can be manually moved through the different phases of the cardiac cycle, thus tracking myocardial motion. As a result, the

velocity of a specific myocardial segment can be measured throughout the entire cardiac cycle. A major limitation of the first color TDI applications in human medicine was the low temporal resolution of 30 to 60 frames per second (fps), compared to a frame rate of over 200 fps for PW TDI (Pellerin et al., 2003). However, by narrowing the sector width of the image, the new generations of commercially available systems can achieve frame rates of more than 180 fps. These frame rates are sufficient to resolve myocardial motion in all cardiac phases, even the fast isovolumic phases. Another limitation of color TDI is the off-line post-processing of the images, which is rather time consuming and requires operator expertise. On the other hand, this approach offers the possibility of evaluating several myocardial segments during the same cardiac cycle. This is especially advantageous for the assessment of ventricular asynchrony. It is also beneficial for the evaluation of several myocardial segments during stress echocardiography, which has a limited image acquisition time.

Due to the Doppler principle, velocities can only be measured correctly in the direction of the ultrasound beam. The amplitude of the velocity measurement depends on the angle between the ultrasound beam and the direction of wall motion. The relationship between the velocity measured by TDI and the actual myocardial wall velocity is described by the formula $v_{TDI} = v_{myocard} * \cos(\alpha)$. If the insonation angle α increases, the velocity measured by TDI will decrease, unless angle correction is applied. The velocity measurements are unacceptable if the insonation angle exceeds 15 to 20 degrees (Teske et al., 2007). Ideally, the insonation angle is 0 degrees. Optimal alignment of the ultrasound beam with myocardial wall motion direction should be obtained during image acquisition.

As the heart is a three-dimensional structure, wall motion occurs in three dimensions. During systole, three major directions of cardiac motion can be recognised (D'hooge et al., 2000): longitudinal shortening, radial thickening and circumferential shortening (Fig. 4). These three components are interrelated because of the incompressibility of the myocardium. In order to conserve myocardial volume, longitudinal and circumferential shortening are balanced by radial thickening (Teske et al., 2007). As TDI measurements are one-dimensional and angle-dependent, longitudinal shortening can only be assessed if the ultrasound beam is aligned parallel to the longitudinal direction of LV wall motion. This can be achieved in human and small animal medicine using apical views, although the curvature of the walls can still cause some angle deviation and the insonation angle can also vary during the cardiac cycle.

In equine cardiology, the acquisition of apical images is impossible as the apex is covered by the sternum. Only parasternal short- and long-axis images can be acquired, allowing the evaluation of radial wall motion by TDI.

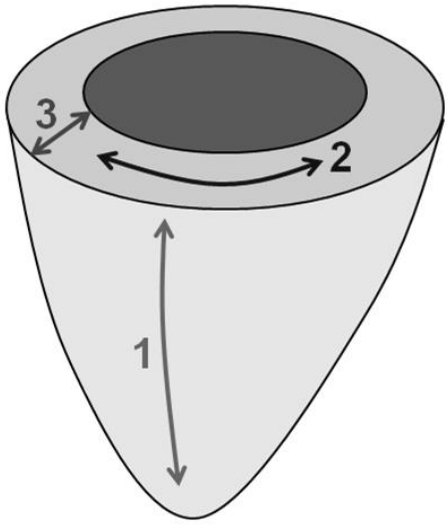

Figure 4: Schematic representation of the left ventricle, indicating the three major directions of wall motion:
(1) longitudinal; (2) circumferential; (3) radial.

2.2 Velocity, strain rate and strain

By TDI, tissue velocities are measured relative to the transducer. The major disadvantage of this technique is that intrinsic regional wall motion is measured together with total heart motion in the thorax (Edvardsen et al., 2002). In case of large total heart motion e.g. due to breathing, this results in an over- or underestimation of the regional wall motion velocities. This can be solved by acquiring TDI images in an end-expiratory state or by averaging at least three cardiac cycles. However, the myocardial velocities measured by TDI are also influenced by tethering between adjacent segments and cardiac translational motion (Smiseth and Ihlen, 2003).

The myocardial velocity gradient (MVG) has been proposed as a better measurement of intrinsic myocardial motion. In the radial direction, the endocardial border moves faster than the epicardial border, resulting in wall thickening during systole and wall thinning during diastole (Fig. 5). The MVG can be calculated as the difference between endocardial and epicardial velocities, divided by myocardial wall thickness (Uematsu et al., 1995). The main disadvantage of the MVG is that the calculation can not be performed in real time as it is based on the processed velocity data. Furthermore, the MVG is difficult to assess in longitudinal direction.

In order to overcome these limitations, two new modalities have been developed: strain and strain rate. These parameters are indices of myocardial deformation which are derived directly from the Doppler data (Heimdal et al., 1998).

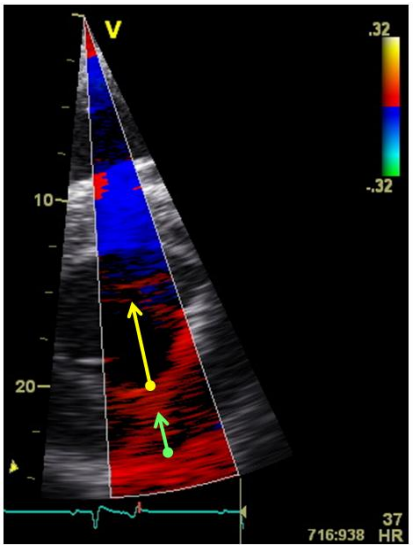

Figure 5:
Color tissue Doppler image of the left ventricle of a horse in a short-axis view at chordal level during systole. The left ventricular free wall is color-coded red as it is moving towards the transducer. The endocardial velocity (yellow arrow) is higher than the epicardial velocity (green arrow), resulting in a myocardial velocity gradient and radial wall thickening.

Strain is defined as the total amount of deformation of the myocardial wall at a certain point of time in the cardiac cycle, expressed as a percentage relative to the initial wall thickness or length. Strain values are positive if an object has thickened or lengthened, and negative if the object has thinned or shortened. Linear strain can be calculated by the Lagrangian formula: Lagrangian strain $\varepsilon_L = (L - L_0)/L_0$, where L_0 is the initial length and L is the length at a certain time point. Strain can also be expressed as deformation relative to the length at a previous instance instead of the initial length. This is the natural or Eulerian strain $\varepsilon_N = \int_{t0}^{t} d\varepsilon N(t)$, where $d\varepsilon N(t) = (L_{(t + dt)} - L_t)/L_t$ (D'hooge et al., 2000). Strain is usually expressed as Lagrangian strain. The change in strain per time unit or $\Delta\varepsilon/\Delta t$ is the strain rate. This is a measure of the rate of deformation and is expressed in s^{-1}. Strain rate can be calculated as the spatial derivative of the TDI velocities. Strain can then be calculated by temporal integration of the strain rate data (Fig. 6). From TDI velocities, natural or Eulerian strain rate is calculated, and temporal integration of these data results in natural strain. However, the TDI software converts this into Lagrangian strain (Geyer et al., 2010). Spatial integration of strain or temporal integration of velocity results in displacement. This measurement is infrequently used.

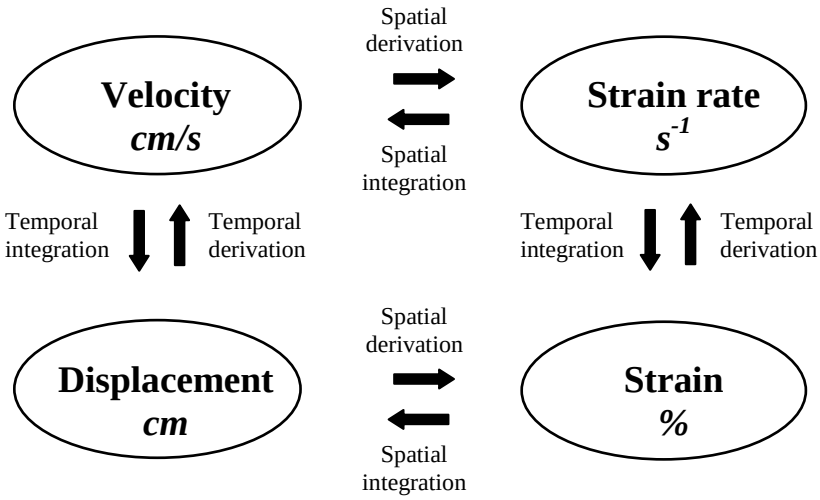

Figure 6: Mathematical relationship of velocity, strain rate, strain and displacement.

Strain and strain rate can also be displayed on the 2D grayscale image by color codes. Positive strain rate values (thickening or lengthening) are colored cyan to blue, while negative strain rate values are yellow to red. Positive strain values are colored blue, while negative strain values are red. These color codes facilitate a rapid visual assessment of myocardial wall motion (Brodin, 2004).

2.3 Pitfalls and artifacts

The main limitations associated with TDI are inherent to the Doppler technique. The importance of the insonation angle and total heart motion has already been mentioned. However, there are several other pitfalls that should be kept in mind. First, a correct sampling rate should be used to resolve myocardial motion during all phases of the cardiac cycle. Generally, the frame rate of CF Doppler images is quite low, about 10-20 fps. In comparison, the eye distinguishes 25 fps, which means a temporal resolution of 40 ms. In the first TDI studies in human medicine, the frame rate was enhanced to about 30-60 fps. This was sufficient to detect the changes from positive to negative myocardial velocity values for timing of systole and diastole. However, in order to measure peak values correctly, a frame rate of >100 fps is required for myocardial velocity data. Even higher frame rates are needed to resolve regional strain rate data (Brodin, 2004; Moladoust et al., 2008).

The frame rate is determined by several factors. A two-dimensional ultrasound image is built up by sending an ultrasound beam in one direction, waiting for the beam to return, and then sending out a second beam under a slightly different angle (Fig. 7A). To build up one frame, multiple beams are needed and the transducer has to sweep from one side to the other.

A higher number of beams per frame for a given sector width results in a better lateral resolution. By reducing image depth, the time from sending to receiving the pulses is reduced and the next pulse can be sent out earlier, thus increasing sweep speed and frame rate. By reducing sector width, less beams are needed for building up the entire image, which also increases frame rate (Fig. 7B). Furthermore, the number of beams for building up the sector can be reduced. This reduction of line density results in a decreased lateral resolution, particularly at larger image depths because of the diverging beams (Fig. 7C). As a result, myocardial velocities of adjacent regions cannot be differentiated from each other. In apical views, the strain rate calculations might erroneously be based on blood pool velocities if the beam width exceeds myocardial wall thickness (Hanekom et al., 2004). Enhancing frame rate should always be a compromise between decreasing sector size (depth and width) and decreasing line density (with decreased lateral resolution). For apical views, a decrease of the sector width implies that only single walls can be evaluated instead of acquiring a full four-chamber view. This prolongs data acquisition time and complicates the assessment of LV asynchrony.

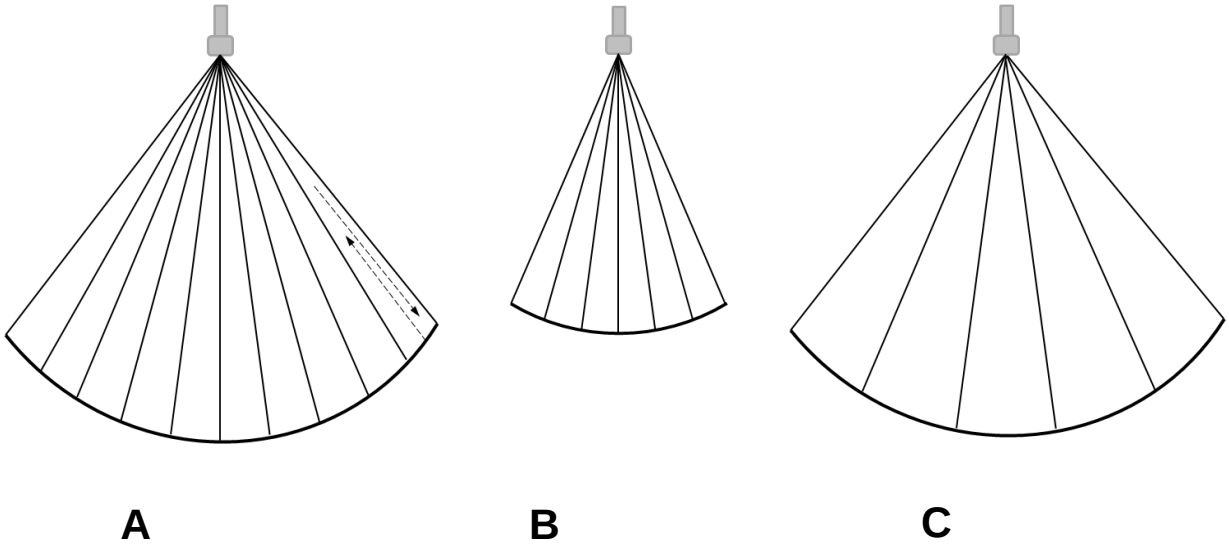

Figure 7: (A) Build-up of a two-dimensional ultrasound image; (B) Increasing frame rate by decreasing image width and depth; (C) Increasing frame rate by reducing line density.

In addition to frame rate optimization, the velocity scale also needs to be adjusted in order to perform correct TDI measurements. The Nyqvist limit determines the maximal frequency shift and thus the maximal velocity that can be measured. The Nyqvist limit is determined by the sampling rate or pulse repetition frequency (PRF). The PRF should be at least twice the maximal frequency shift of the Doppler signal. If the PRF is too low compared to the velocity

that should be measured, aliasing occurs. An everyday example of the aliasing phenomenon can be observed in movies when car wheels appear to go slowly backwards while the car is moving forward. This occurs when the rotational speed of the wheels exceeds half the frame rate or sampling frequency of the camera. In TDI velocity curves, aliasing is visible as a fast shift of high negative to high positive velocities or opposite (Fig. 8). If aliasing is present in the curve, the pulse repetition frequency should be increased by increasing the velocity scale during image acquisition (D'hooge et al., 2006).

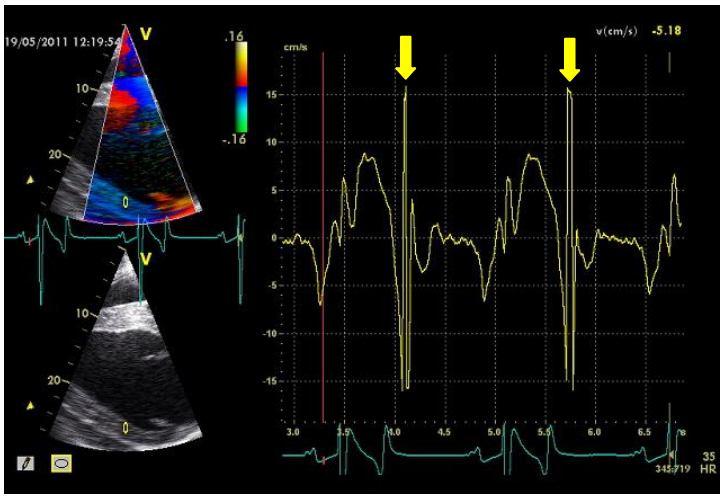

Figure 8: Tissue Doppler velocity curve generated in the left ventricular free wall from a right parasternal long-axis view in a horse. The velocity scale of +/- 16 cm/s is exceeded during early diastole, resulting in aliasing velocities (arrows). The velocity shifts from a high negative to high positive value.

TDI measurements are also very susceptible to the influence of artefacts. Attention should be paid to the presence of these artefacts during image acquisition and off-line analysis. Artefacts can be non-random or random. Non-random artefacts can be observed in the 2D grayscale image during image acquisition and include drop-out and reverberations. In these artefacts, the velocity measured is zero. This will lead to important changes in the calculated strain rate (Teske et al., 2007). The strain rate can even become opposite to the normal values, indicated as a band colored in the opposite color compared to the surrounding areas. This also happens at the endocardium, where the velocities of the blood pool are disturbing the strain rate calculations. If these color alterations are observed during off-line analysis, the region of interest (ROI) should be repositioned in order to avoid them.

A second category of artefacts is random noise caused by the limited precision of the velocity measurements (D'hooge et al., 2000). This noise is independent of the measured value. Therefore, low velocity values are relatively more noisy and thus have a lower signal-to-noise ratio. Canceling out random noise can be performed by smoothing the curves during post-processing using temporal or spatial averaging.

Temporal averaging is performed by averaging several consecutive points using Gaussian smoothing or by averaging consecutive cardiac cycles. Spatial averaging can be performed by using a larger ROI. Velocity measurements are the average of all pixel values within the ROI, therefore a larger ROI causes more noise reduction. Strain rate calculation is even more influenced by random noise as velocities are distracted from each other, resulting in a low velocity difference. The random variability of the velocity measurements is added up by this calculation, resulting in a very low signal-to-noise ratio (Urheim et al., 2000). This ratio can be increased by augmenting the distance over which strain rate is calculated, the strain length. This results in a larger velocity difference.

The integration to strain will also cancel out random noise. However, strain curves are very sensitive to integrational drift (D'hooge et al., 2000). Drifting of the curve occurs when the curve does not return to zero at the end of the cardiac cycle. This is caused by the accumulation of small non-random errors in the strain rate values. Drift can be compensated by the post-processing software in two ways. First, the strain value can be reset to zero at each cycle end, without changing the rest of the curve. The second method, linear drift compensation, is more often used and corrects the strain drift throughout the entire cardiac cycle, based on the assumption that drift is linearly distributed during the cardiac cycle.

3. Two-dimensional speckle tracking (2DST)

3.1 Principles

Two-dimensional speckle tracking (2DST) is based on tracking the movement of stable acoustic speckle patterns in the 2D grayscale image throughout the cardiac cycle. The speckles are created by the interference of ultrasound waves reflected by scatterers within the myocardium. In contrast to transitions between different tissues, scatterers within the myocardium produce reflections of small amplitudes. The interference of the reflections by different scatterers can be constructive, resulting in a high amplitude signal, or destructive, resulting in a low amplitude signal. When the radiofrequency signal is converted into the 2D image, high amplitude signals result in bright pixels and low amplitude signals result in dark pixels (D'hooge, 2007). The resulting speckle pattern is unique for each myocardial region (Fig. 9).

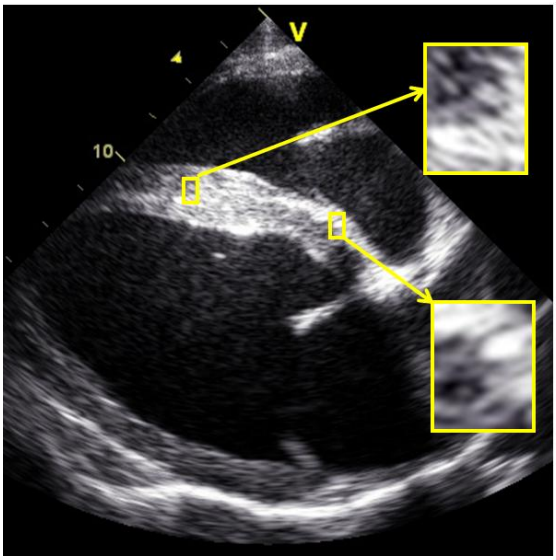

Figure 9:
Right parasternal four-chamber view of a horse, illustrating the unique speckle pattern in each myocardial region.

The speckle pattern is relatively stable throughout the cardiac cycle, which allows tracking of the speckle motion. This can be performed both on the radiofrequency data or on the 2D grayscale data. Tracking is based on recognizing the most similar speckle pattern from one frame to another (Leitman et al., 2004). The software selects speckles suited for tracking within the manually defined region of interest (ROI) in the grayscale image. The speckle size is about 20 to 40 pixels (Perk et al., 2007). These kernels are searched for in the next image frame in a region around their original position. The algorithm searches for an area with the smallest difference in the total sum of pixel values, which is the smallest sum of absolute difference. However, the ultrasound image is only two-dimensional while the myocardium

moves in three dimensions and is subjected to rotation and deformation. As a result, speckles can disappear. By searching on a frame-by-frame basis, this out-of-plane motion is sorted out since the speckle pattern usually disappears over a few frames, rather than within two consecutive frames. Therefore, the frame rate of the acquired images is crucial for correct tracking. The final result is a grayscale cineloop with the tracking of the speckles superimposed.

3.2 Two-dimensional velocity and deformation

The geometric shift of each speckle represents local tissue motion, which can be tracked in the two dimensions of the ultrasound image (Perk et al., 2007). This allows an angle-independent assessment of tissue velocity, strain and strain rate. Depending on the software manufacturer, myocardial velocity and deformation are calculated and represented in a different way (Nesser and Winter, 2009; Biaggi et al., 2011). By velocity vector imaging, vectors superimposed on the grayscale image display the dynamic vector field based on the individual speckle velocities in the ROI (Fig. 10A). Other applications, such as the 2D Strain tool from GE Healthcare used in our study, divide the ROI in several segments and calculate the mean velocity, displacement and deformation per segment (Fig. 10B).

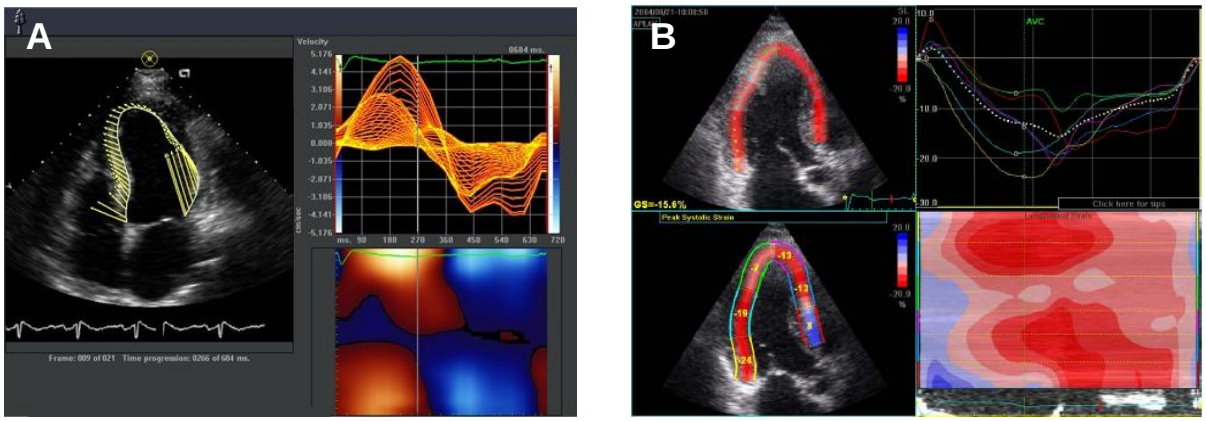

Figure 10: Different software applications based on speckle tracking technology. (A) syngo® Velocity Vector Imaging™ (VVI), Siemens Medical Solutions USA, Inc; (B) 2D Strain application, EchoPAC^{TM}, GE Healthcare, Horten, Norway.

In contrast to TDI, displacement and strain are measured directly by 2DST. Therefore the resulting strain value is Lagrangian strain. An important advantage compared to TDI is the angle-independency of 2DST. All measurements are performed in the two dimensions of the ultrasound image and not only in the direction of the ultrasound beam. Using short-axis images, both radial and circumferential motion can be quantified (Kawagishi, 2008).

In addition, rotation can be measured (Fig. 11A). When viewed from apex, the base rotates in a clockwise direction during systole while the apex rotates counterclockwise (Notomi et al., 2005). This results in LV torsion, which can be calculated from the rotation values measured in short-axis images at apical and basal level (Kim et al., 2007). In long-axis images, radial and longitudinal motion can be quantified. Radial motion is then designated as transverse motion (Fig. 11B).

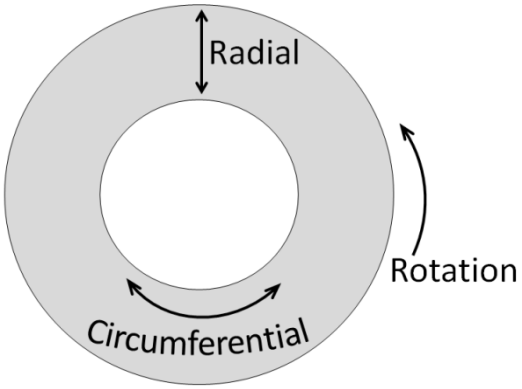

Figure 11A: Schematic drawing of a short-axis view of the left ventricle indicating radial and circumferential wall motion and rotation.

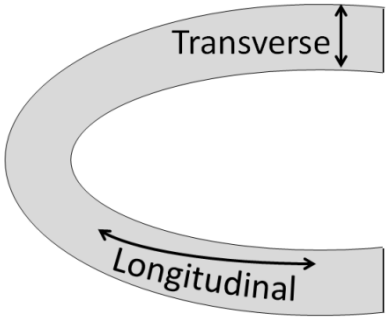

Figure 11B: Schematic drawing of a long-axis view of the left ventricle indicating transverse and longitudinal wall motion.

3.3 Pitfalls and artifacts

Like TDI, the 2DST method has some fundamental limitations. The insonation angle and the effect of total heart motion are less important because speckles are tracked in two dimensions and speckle motion is measured relative to other speckles instead of the transducer. However, an adequate frame rate is imperative. Too low frame rates cause large frame-to-frame changes of the speckle pattern which result in insufficient tracking quality. Furthermore, low frame rates may lead to undersampling, causing underestimation of peak values and even disappearance of short isovolumic peaks (Teske et al., 2007). The underestimation of peak values is especially important for diastolic velocity and strain rate, as these peaks are usually short and very high. The minimum required frame rate is 30 fps, but 40-70 fps and more is advised (Hurlburt et al., 2007). The frame rate can be enhanced by decreasing sector size (depth and width) or by decreasing line density at the cost of lateral resolution. For 2DST, a sufficiently high lateral resolution is crucial to ensure adequate tracking quality in the lateral direction (Amundsen et al., 2006). This is especially important at higher image depths where lateral resolution is always lower due to the diverging ultrasound beams (Fig. 12).

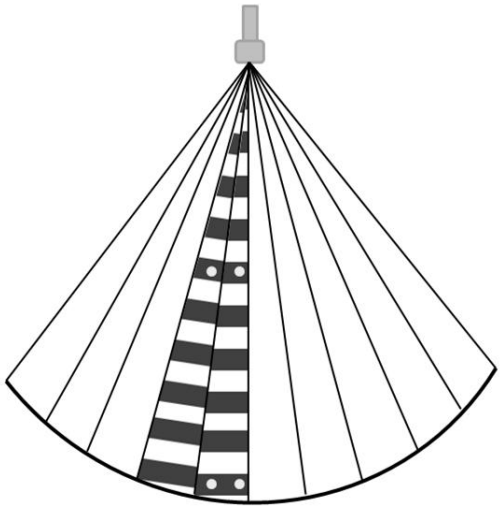

Figure 12:
Lateral resolution decreases with increasing image depth due to divergence of the ultrasound beams. Therefore adjacent speckles (white dots) can not be distinguished from each other in the far field while they can be distinguished from each other at a lower image depth.

Tracking quality can be improved by increasing the ROI width as this increases the number of speckles that can be tracked. Furthermore, the image quality is essential. Non-random artifacts such as drop-out or reverberations can be erroneously tracked by the software, resulting in abnormal velocity and deformation values. Random noise is less present in 2DST curves compared to TDI curves because of the extensive temporal and spatial smoothing applied by the software. Temporal averaging is performed similar to TDI, while spatial smoothing is performed along all segments of the ROI using model fitting. Because of this spatial smoothing, curves are even generated in segments of the ROI that are outside of the image, where no speckles are present to track. Excessive smoothing can also reduce the peak values, especially in the velocity and strain rate curves. Furthermore, small regional changes are difficult to detect by 2DST if they are surrounded by normal contractile myocardium.

Drift can be present in the 2DST strain and displacement curves because of "kernel slippage". Due to out-of-plane motion or tissue deformation, the speckle pattern may undergo too large frame-to-frame changes. As a result, a kernel is not correctly identified by the software in its new position in the next frame. Instead, the software selects another kernel based on the smallest sum of absolute difference and then continues tracking this kernel. This error is non-random as the software usually selects a wrong kernel closer to the original kernel position compared to the actual new position of the kernel. This results in a cumulated drift throughout the cardiac cycle, which is linearly compensated by the software (Perk et al., 2007; Teske et al., 2007).

Critical assessment of tracking quality should always be performed before measurements can be interpreted. The software itself automatically evaluates tracking quality and each segment receives a tracking score based on several criteria (Artis et al., 2008). First, the program tracks the speckles through several frames in a forward and backward direction. If this does not result in a return to baseline values, tracking is considered inadequate. Secondly, the software calculates strain drift. If excessive linear drift compensation is required, tracking quality is not approved. Finally, tissue velocities are compared within each wall segment. If significant velocity differences are found between adjacent speckles, tracking is not approved by the software (Perk et al., 2007). In addition to this automated evaluation of tracking quality, the subjective visual assessment of tracking remains crucial. If tracking is considered visually inadequate, the ROI should be repositioned and tracking should be repeated until acceptable tracking is achieved.

4. Use of TDI and 2DST in veterinary and human medicine

4.1 Quantification of myocardial function by TDI and 2DST

4.1.1. Normal curves

The most commonly used TDI and 2DST measurements for evaluation of myocardial function are velocity, strain rate and strain. Myocardial displacement is less frequently described. The velocity, strain rate and strain curves generated by TDI and 2DST are very similar (Fig. 14). In the velocity and strain rate curves, three major deflections are present: a systolic (Syst), early diastolic (E) and late diastolic (A) wave (Palka et al., 1995). The E-wave is usually the highest peak and can be followed by recoil of the myocardium in the opposite direction. In healthy young humans, the E/A-ratio is always higher than 1 (Rychik and Tian, 1996). Before and after ejection, two short isovolumic phases can be recognised. The isovolumic contraction (IVC) and relaxation (IVR) generally show a biphasic profile with a positive and negative peak.

The sign of the systolic velocity and strain rate peaks is opposite to that of the diastolic peaks. Velocities towards the transducer are indicated by a positive sign, velocities away from the transducer get a negative sign. For radial velocity assessed from a parasternal view, the sign of the peaks is opposite in the different myocardial segments (Fig. 13). For strain rate, the myocardial segments all show the same sign throughout the cardiac cycle. A positive sign indicates that myocardial wall thickening (in radial direction) or lengthening (in longitudinal or circumferential direction). A negative strain rate indicates wall thinning or shortening.

Strain curves show only one peak value. A positive strain value indicates that the walls have thickened or lengthened compared to end-diastole while a negative value indicates wall thinning or shortening compared to end-diastole (Fig. 14). Therefore, systolic longitudinal strain and strain rate values are negative because the myocardial walls are shortening during systole. Radial systolic strain and strain rate values are positive, reflecting wall thickening.

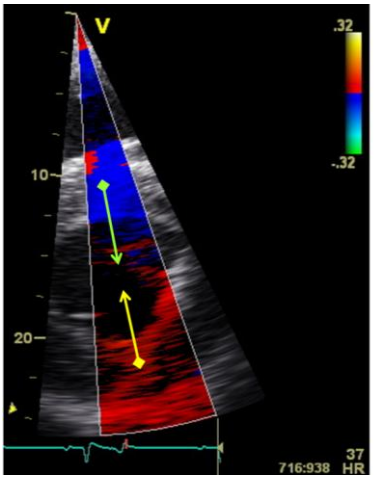

Figure 13:
Radial myocardial velocity measured by TDI in a right parasternal short-axis view of the left ventricle at chordal level. During systole, myocardial velocities in the left ventricular free wall are directed towards the transducer (yellow arrow) and thus positive, with a red color code. Velocities in the interventricular septum are directed away from the transducer (green arrow) and thus negative, with a blue color code.

Within the myocardial wall, the velocity profiles demonstrate a regional heterogeneity both in the radial and longitudinal direction. The radial endocardial velocities are significantly higher than the epicardial velocities (Donovan et al., 1995). Similarly, a gradient in longitudinal velocity is present with the highest myocardial velocities detected at the LV base while the apex is almost stationary. This velocity gradient reflects tethering of the myocardium due to deformation of adjacent segments. The strain rate and strain profile are more homogeneous in all myocardial segments.

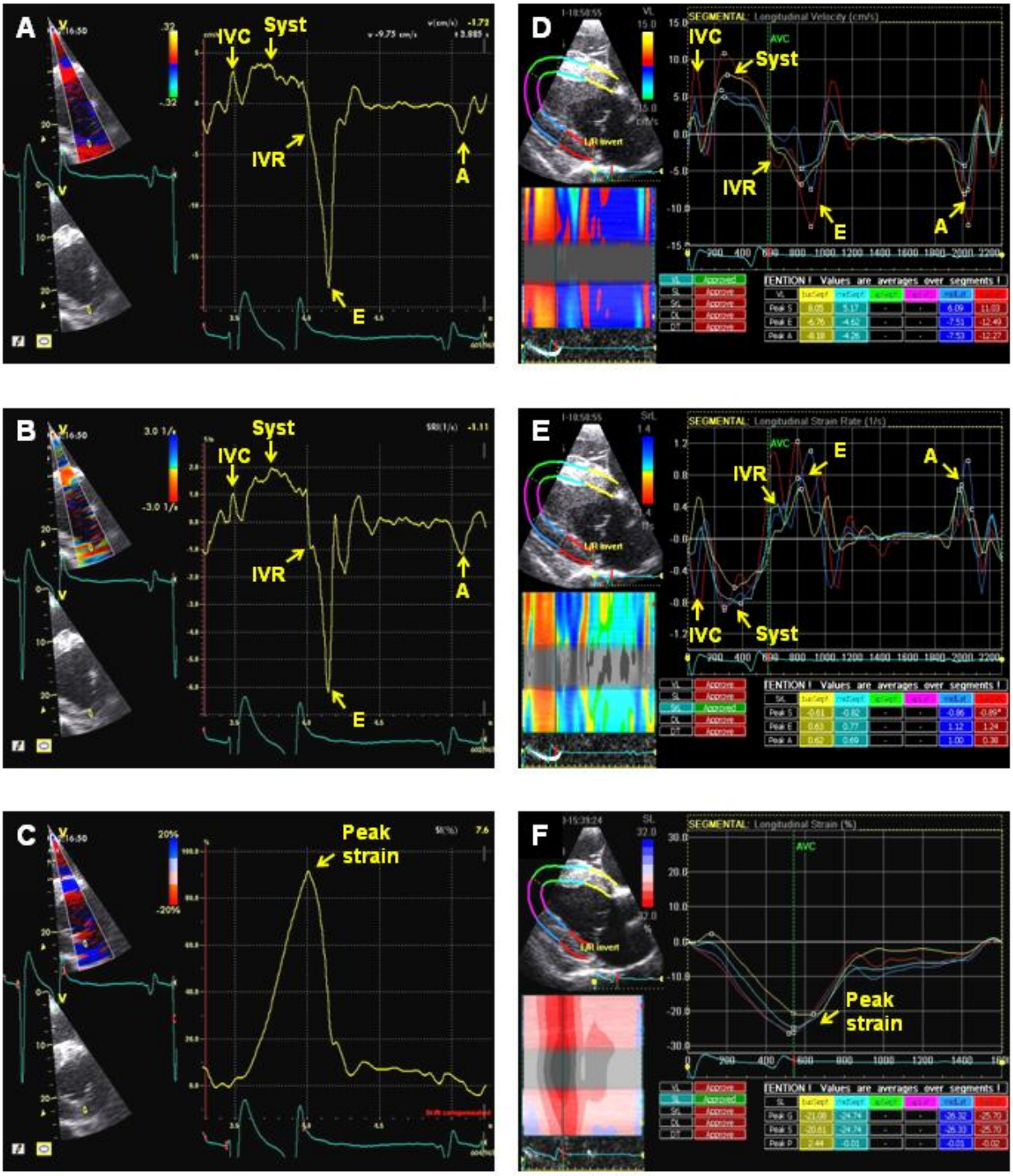

Figure 14: Examples of the velocity, strain rate and strain curves by tissue Doppler imaging and two-dimensional speckle tracking. (A) Radial velocity measured by TDI in the left ventricular free wall from a right parasternal short-axis view at chordal level; (B) Radial strain rate curve from the same segment; (C) Radial strain curve from the same segment; (D) Longitudinal velocity measured by 2DST in four left ventricular wall segments from a right parasternal long-axis modified four-chamber view; (E) Longitudinal strain rate curve in the same segments; (F) Longitudinal strain curve in the same segments.

IVC, isovolumic contraction; Syst, systolic; IVR, isovolumic relaxation; E, early diastole; A, late diastole

The velocity and strain rate curves can be used to measure systolic and diastolic time intervals of the cardiac cycle (Fig. 15). These are characterized by changes in wall motion seen as a change in sign or amplitude. Systolic time intervals include isovolumic contraction time (IVCT), pre-ejection period (PEP), ejection time (ET) and time to peak Syst. Diastolic time intervals include isovolumic relaxation time (IVRT), time to onset, peak and end of E and time to onset, peak and end of A. Time intervals can be measured within the curve or relative to onset QRS or P on the ECG. In human medicine, a good correlation was demonstrated between time intervals by color TDI and invasive hemodynamics (Zamorano et al., 1997).

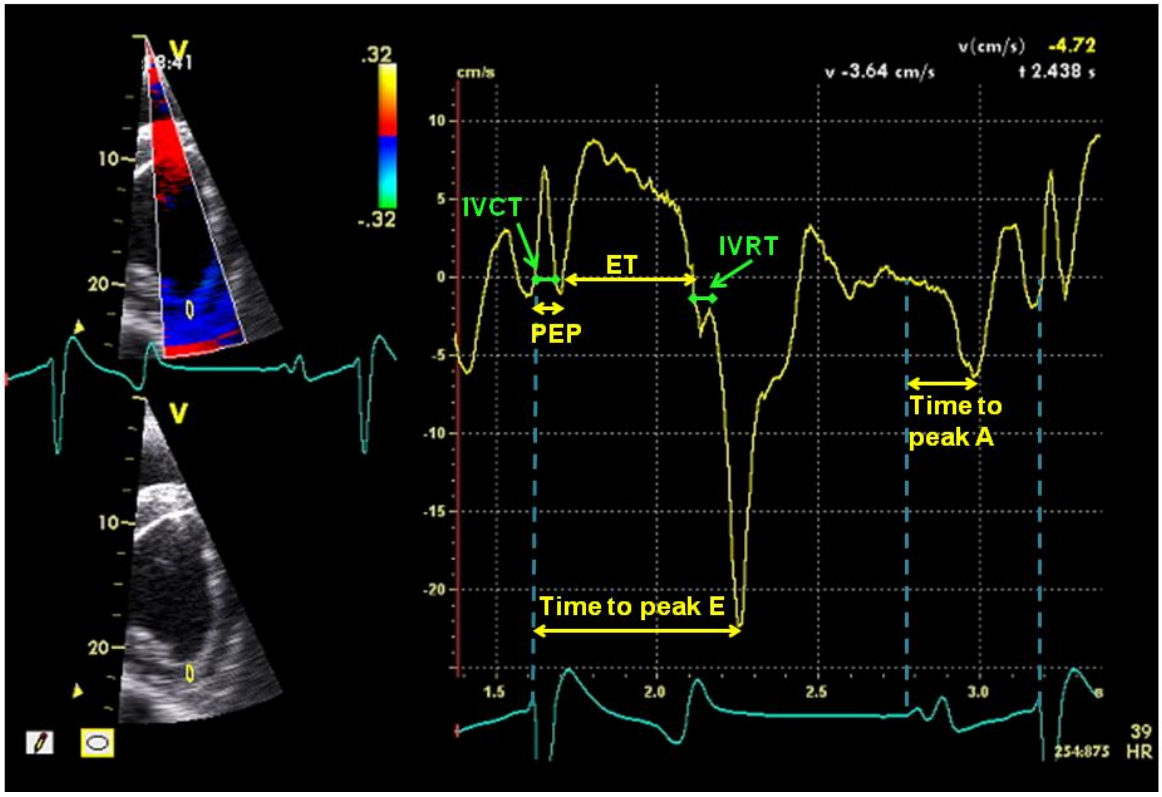

Figure 15: Examples of systolic and diastolic time interval measurements from a tissue Doppler velocity curve in the left ventricular free wall imaged from a right parasternal short-axis image at papillary muscle level. The blue dotted lines indicate the onset of QRS and onset of P on the ECG.

IVCT, isovolumic contraction time; PEP, pre-ejection period; ET, ejection time; IVRT, isovolumic relaxation time; E, peak early diastolic velocity; A, peak late diastolic velocity.

4.1.2. Validation of TDI and 2DST and use in healthy individuals

Validation of TDI and 2DST has been performed in vitro and in vivo using animal models and healthy individuals. The TDI technique was first validated on tissue-mimicking phantom models (Fleming et al., 1994; Miyatake et al., 1995). In the first validation studies of TDI in animal models, ultrasonic crystals were implanted in the myocardium of open-chest dogs to compare sonomicrometry to TDI measurements (Gorcsan et al., 1997; Urheim et al., 2000).

In healthy individuals, TDI measurements were well correlated with M-mode measurements and with tagged magnetic resonance imaging (MRI) (Donovan et al., 1995; Edvardsen et al., 2002). The validation of 2DST was performed in vitro using a tissue-mimicking gelatine block that was cyclically compressed (Korinek et al., 2005). In animal models, strain measurements were compared to sonomicrometry (Amundsen et al., 2006). In healthy individuals, 2DST measurements were correlated with tagged MRI (Korinek et al., 2005; Amundsen et al., 2006; Langeland et al., 2006). Most clinical studies using TDI and 2DST in human medicine only focus on longitudinal velocities and deformation. Normal values vary between publications and are strongly dependent on the software used (Kuznetsova et al., 2008; Dalen et al., 2010). Furthermore, ageing affects the velocity and deformation measurements, especially during diastole (Edner et al., 2000; Sun et al., 2004). Peak velocity and deformation are also influenced by training, with higher values reported in athletes (Baggish et al., 2008; Simsek et al., 2011).

In veterinary cardiology, numerous studies have demonstrated the feasibility and reliability of TDI in healthy cats and dogs. In 1999, PW TDI was used in healthy cats to measure diastolic longitudinal and radial LV motion (Gavaghan et al., 1999). Chetboul et al. demonstrated the feasibility of 2D color TDI measurements in healthy dogs and cats. Longitudinal LV velocity and deformation could be quantified from an apical four-chamber view, radial motion from a parasternal short-axis view (Chetboul et al., 2004a; Chetboul et al., 2006a). In larger studies, the normal range of TDI measurements was established. In dogs and cats, a significant association was found between TDI velocities and breed, which is probably a reflection of the large variation in body weight and heart size among different breeds (Chetboul et al., 2005; Chetboul et al., 2006b). In equine cardiology, the use of TDI was first described in 2005 for the evaluation of radial LV wall motion from left and right parasternal short-axis images (Sepulveda et al., 2005). Schwarzwald et al. demonstrated that several TDI measurements can be performed with a low to moderate variability in horses at rest, although color TDI was less reliable than PW TDI (Schwarzwald et al., 2009b). The acquisition of TDI measurements during post-exercise stress echocardiography was found to be technically difficult in one study, although it was feasible in another (Gehlen et al., 2009; Schefer et al., 2010).

The use of 2DST is a more recent development in veterinary cardiology. It was only in 2007 that the feasibility of 2DST in awake dogs was reported (Chetboul et al., 2007b). In this study, speckle tracking was performed in short-axis images at papillary muscle level, using a frame rate of 70-110 fps. Longitudinal LV function has also been described by 2DST and correlated

well with TDI measurements (Wess et al., 2011). In equine cardiology, few data on the use of 2DST are available. In right parasternal short-axis images of the left ventricle, 2DST analysis was feasible and radial and circumferential strain, strain rate, radial displacement and rotation could be measured at a frame rate between 59 and 73 fps (Schwarzwald et al., 2009a). Strain and strain rate measurements by 2DST were also feasible during post-exercise stress echocardiography (Schefer et al., 2010).

4.2 Clinical applications of TDI and 2DST

In human medicine, the use of TDI and 2DST has been studied extensively in coronary artery disease, cardiac resynchronization therapy, myocardial disease, heart failure and valvular insufficiency or stenosis (Sutherland et al., 2004). However, TDI and 2DST primarily remain research tools and the application in clinical practice is not widespread yet. A clinical application of TDI is the estimation of LV filling pressure by calculating the E/E' ratio of early diastolic PW Doppler mitral inflow velocity (E) and early diastolic TDI mitral annular velocity (E'). The mitral inflow velocity increases with greater filling pressure, while the mitral annular velocity remains the same. Therefore, the E/E' ratio increases with increased filling pressure, indicating diastolic dysfunction. The E/E' ratio correlated well with invasive measurements of pulmonary wedge pressure and mean LV diastolic pressure (Nagueh et al., 1997; Ommen et al., 2000). This correlation has also been found in cats and dogs (Schober et al., 2003; Oyama et al., 2004). In horses, this measurement is difficult to perform as the insonation angle is suboptimal from a parasternal view.

The main advantage of TDI and 2DST compared to conventional 2D and M-mode measurements is the increased sensitivity for detection of subtle myocardial dysfunction. In human medicine, strain and strain rate abnormalities are found in several conditions with subclinical cardiac involvement such as diabetes (Marwick, 2004), hypertension (Poulsen et al., 2003), amyloidosis (Piper et al., 2010) and cardiomyopathy after cancer treatment (Stoodley et al., 2011). The early detection of cardiomyopathy is also an important issue in small animal cardiology, as hereditary cardiomyopathy is present in many breeds. As most types of cardiomyopathy only become clinically important at a relatively late age, early detection could prevent breeding with affected animals. In dogs with overt dilated cardiomyopathy (DCM), systolic radial and longitudinal myocardial velocity gradients were significantly decreased and diastolic dysfunction could be detected (Chetboul et al., 2007a; O'Sullivan et al., 2007).

In Golden Retriever muscular dystrophy (GRMD), TDI could detect myocardial dysfunction before conventional echocardiographic measurements were altered. GRMD is a genetic neuromuscular disorder caused by a mutation in the dystrophin gene, which leads to DCM resulting in progressive heart failure. Young asymptomatic GRMD dogs showed a normal global ventricular function as assessed by conventional echocardiographic parameters, while the systolic and early diastolic radial and longitudinal myocardial velocity gradients were significantly decreased (Chetboul et al., 2004b). Similarly, TDI could detect myocardial dysfunction in cats with hypertrophic cardiomyopathy (HCM). While conventional echocardiography showed normal LV function, longitudinal peak velocity and strain were decreased in cats with echocardiographic evidence of HCM (Carlos Sampedrano et al., 2006; Wess et al., 2010). Diastolic dysfunction was also present in HCM cats, characterized by a prolonged isovolumic relaxation time, decreased early diastolic myocardial velocity and a reduction of the E/A ratio (Koffas et al., 2006). In Maine Coon cats, familial HCM is caused by a mutation of the cardiac myosin binding protein C gene. Cats with the heterozygous abnormal genotype but without evidence of hypertrophy showed decreased early diastolic longitudinal velocities compared to a control group, and velocities were even more reduced in a group with phenotypic evidence of HCM (MacDonald et al., 2007). However, no cut-off values could be determined yet for screening on an individual basis.

Another promising application of TDI and 2DST is the detection of subclinical myocardial dysfunction in valvular disease. In human medicine, TDI and 2DST are used to detect subclinical LV dysfunction in chronic aortic or mitral regurgitation and to determine the timing of surgery (Marciniak et al., 2009; Florescu et al., 2011; Smedsrud et al., 2011). In veterinary medicine, two studies with variable results were performed in dogs with chronic mitral valve disease and compensated or decompensated congestive heart failure (CHF). In one study, the E/E'-index was significantly increased in dogs with decompensated CHF and this was correlated with left atrial dilatation (Teshima et al., 2005). In contrast, another study described few changes in TDI measurements in dogs with myxomatous mitral valve disease with or without CHF compared to healthy control dogs (Tidholm et al., 2009). The TDI variables that were altered significantly were in most cases co-variate with changes in conventional echocardiographic parameters. In dogs with CHF, the systolic and diastolic myocardial velocities were increased, which is in agreement with the hyperkinesia seen by conventional echocardiography.

Furthermore, TDI and 2DST can be used for optimization of cardiac resynchronization therapy (CRT) in human patients. By biventricular pacing, CRT reduces the conduction delay between the two ventricles in heart failure patients with wide QRS and reduced LV function. This leads to an increased ejection fraction and improved NYHA class and exercise capacity (Philippon, 2004). Patient selection for CRT by echocardiography is based on the presence of mechanical dyssynchrony, which can be quantified by TDI or 2DST (Oyenuga et al., 2011). In a canine model of LV dyssynchrony, a large difference in time to peak radial strain was shown between 6 ventricular segments in a short-axis view at papillary muscle level. Biventricular pacing restored synchronous contraction (Tanabe et al., 2008). In dogs with pacing-induced heart failure with wide QRS, time to peak radial and circumferential strain by 2DST was superior to TDI indices for measuring dyssynchrony (Arita et al., 2007). In healthy horses, dyssynchrony has been evaluated based on the difference in time to peak radial strain by 2DST in 6 ventricular segments. However, the reliability of this parameter was very low and postsystolic radial motion, defined as thickening of the myocardium after aortic valve closure, was detected in many recordings (Schwarzwald et al., 2009a). The clinical relevance of postsystolic motion in supposedly healthy horses and the potential use of TDI and 2DST for detection of dyssynchrony in horses require further investigation.

Little is known about the use of TDI and 2DST for quantification of LV function in horses with cardiac disease. In 15 horses with atrial fibrillation, significant alterations of TDI parameters were described. As expected, the late diastolic wave was absent due to the absence of atrial contraction. The systolic and early diastolic peak values were significantly higher at rest and after stress echocardiography compared to healthy horses (Gehlen et al., 2009). In one mare with nutritional masseter degeneration, diastolic dysfunction could be detected by TDI. Systolic dysfunction was demonstrated by decreased radial and longitudinal peak strain, measured by 2DST (Schefer et al., 2011). The usefulness of TDI and 2DST for detection of subclinical myocardial dysfunction in horses with valvular disease, exercise-induced myocardial dysfunction or myocardial disease remains to be proven.

5. Summary

The equine heart is extremely adapted to athletic performance. However, the large cardiac size and enormous cardiovascular pressures during exercise also entail negative consequences such as the high prevalence of exercise-induced pulmonary hemorrhage, exercise-related dysrhythmia and valvular insufficiency. The routine cardiovascular examination of a horse consists of auscultation, electrocardiography and echocardiography.

Echocardiography has become an essential tool as it allows non-invasive quantification of cardiac chamber dimensions and assessment of valvular and myocardial function. Left ventricular systolic function is usually quantified by calculating fractional shortening, a one-dimensional, focal and load-dependent measurement. In contrast to human medicine, measurements of longitudinal left ventricular function and diastolic transmitral flow measurements are difficult because apical views are impossible to acquire in adult horses. Tissue Doppler imaging (TDI) and two-dimensional speckle tracking (2DST) are two echocardiographic techniques for quantification of myocardial function that might overcome these limitations.

By TDI, myocardial velocities are measured based on the Doppler principle. As a consequence, accurate measurements can only be performed in the direction of the ultrasound beam. Using parasternal images, radial wall motion can be assessed. From the velocity gradient between the endo- and epicardium, myocardial deformation can be calculated. The amount of wall thickening as a percentage of the end-diastolic state is expressed as strain, the speed of deformation is described as the strain rate (in s^{-1}). In contrast to TDI, 2DST allows two-dimensional quantification of myocardial velocity, strain rate and strain. The semi-automated software algorithm tracks the motion of acoustic speckle patterns which are unique for each myocardial region and stable throughout the cardiac cycle. Because tracking is performed in the two dimensions of the ultrasound image, longitudinal and circumferential left ventricular shortening as well as rotation can be measured in addition to radial wall thickening.

Both TDI and 2DST have been validated in vitro and in vivo. In human and small animal medicine, reference values for TDI and 2DST measurements have been established and both techniques have been extensively described in many cardiac diseases. TDI and 2DST measurements of myocardial velocity and deformation are often more sensitive for detection of subtle myocardial dysfunction than conventional two-dimensional and M-mode echocardiographic measurements. However, little information is available on the feasibility, reliability and diagnostic value of both techniques in horses.

References

Amundsen BH, Helle-Valle T, Edvardsen T, Torp H, Crosby J, Lyseggen E, Stoylen A, Ihlen H, Lima JA, Smiseth OA, Slordahl SA (2006). Noninvasive myocardial strain measurement by speckle tracking echocardiography: Validation against sonomicrometry and tagged magnetic resonance imaging. J Am Coll Cardiol 47, 789-793

Arita T, Sorescu GP, Schuler BT, Schmarkey LS, Merlino JD, Vinten-Johansen J, Leon AR, Martin RP, Sorescu D (2007). Speckle-tracking strain echocardiography for detecting cardiac dyssynchrony in a canine model of dyssynchrony and heart failure. Am J Physiol Heart Circ Physiol 293, H735-H742

Artis NJ, Oxborough DL, Williams G, Pepper CB, Tan LB (2008). Two-dimensional strain imaging: A new echocardiographic advance with research and clinical applications. Int J Cardiol 123, 240-248

Baggish AL, Yared K, Wang F, Weiner RB, Hutter AM, Picard MH, Wood MJ (2008). The impact of endurance exercise training on left ventricular systolic mechanics. Am J Physiol Heart Circ Physiol 295, H1109-H1116

Barbesgaard L, Buhl R, Meldgaard C (2010). Prevalence of exercise-associated arrhythmias in normal performing dressage horses. Equine Vet J 42 Suppl 38, 202-207

Betros CL, McKeever KH, Kearns CF, Malinowski K (2002). Effects of ageing and training on maximal heart rate and VO_2max. Equine Vet J 34 Suppl 34, 100-105

Biaggi P, Carasso S, Garceau P, Greutmann M, Gruner C, Tsang W, Rakowski H, Agmon Y, Woo A (2011). Comparison of two different speckle tracking software systems: Does the method matter? Echocardiography 28, 539-547

Birks EK, Shuler KM, Soma LR, Martin BB, Marconato L, Del Piero F, Teleis DC, Schar D, Hessinger AE, Uboh CE (2002). EIPH: Postrace endoscopic evaluation of Standardbreds and Thoroughbreds. Equine Vet J 34 Suppl 34, 375-378

Blissitt KJ (2010). Auscultation. In: Marr CM, editor. Cardiology of the horse (second edition), Elsevier, 91-104

Blissitt KJ, Bonagura JD (1995). Colour flow Doppler echocardiography in horses with cardiac murmurs. Equine Vet J 27 Suppl 19, 82-85

Blissitt KJ, Bonagura JD (1995). Pulsed wave Doppler echocardiography in normal horses. Equine Vet J 27 Suppl 19, 38-46

Bonagura JD, Blissitt KJ (1995). Echocardiography. Equine Vet J 27 Suppl 19, 5-17

Brodin LA (2004). Tissue Doppler, a fundamental tool for parametric imaging. Clin Physiol Funct Imaging 24, 147-155

Buhl R, Ersboll AK (2012). Echocardiographic evaluation of changes in left ventricular size and valvular regurgitation associated with physical training during and after maturity in Standardbred trotters. J Am Vet Med Assoc 240, 205-211

Carlos Sampedrano C, Chetboul V, Gouni V, Nicolle AP, Pouchelon JL, Tissier R (2006). Systolic and diastolic myocardial dysfunction in cats with hypertrophic cardiomyopathy or systemic hypertension. J Vet Intern Med 20, 1106-1115

Chetboul V, Athanassiadis N, Carlos C, Nicolle AP, Tissier R, Pouchelon JL, Concordet D, Lefebvre HP (2004a). Quantification, repeatability, and reproducibility of feline radial and longitudinal left ventricular velocities by tissue Doppler imaging. Am J Vet Res 65, 566-572

Chetboul V, Escriou C, Tessier D, Richard V, Pouchelon JL, Thibault H, Lallemand F, Thuillez C, Blot S, Derumeaux G (2004b). Tissue Doppler imaging detects early asymptomatic myocardial abnormalities in a dog model of Duchenne's cardiomyopathy. Eur Heart J 25, 1934-1939

Chetboul V, Gouni V, Sampedrano CC, Tissier R, Serres F, Pouchelon JL (2007a). Assessment of regional systolic and diastolic myocardial function using tissue Doppler and strain imaging in dogs with dilated cardiomyopathy. J Vet Intern Med 21, 719-730

Chetboul V, Sampedrano CC, Concordet D, Tissier R, Lamour T, Ginesta J, Gouni V, Nicolle AP, Pouchelon JL, Lefebvre HP (2005). Use of quantitative two-dimensional color tissue Doppler imaging for assessment of left ventricular radial and longitudinal myocardial velocities in dogs. Am J Vet Res 66, 953-961

Chetboul V, Sampedrano CC, Gouni V, Nicolle AP, Pouchelon JL, Tissier R (2006a). Ultrasonographic assessment of regional radial and longitudinal systolic function in healthy awake dogs. J Vet Intern Med 20, 885-893

Chetboul V, Sampedrano CC, Tissier R, Gouni V, Saponaro V, Nicolle AP, Pouchelon JL (2006b). Quantitative assessment of velocities of the annulus of the left atrioventricular valve and left ventricular free wall in healthy cats by use of two-dimensional color tissue Doppler imaging. Am J Vet Res 67, 250-258

Chetboul V, Serres F, Gouni V, Tissier R, Pouchelon JL (2007b). Radial strain and strain rate by two-dimensional speckle tracking echocardiography and the tissue velocity based technique in the dog. J Vet Cardiol 9, 69-81

D'hooge J, Heimdal A, Jamal F, Kukulski T, Bijnens B, Rademakers F, Hatle L, Suetens P, Sutherland GR (2000). Regional strain and strain rate measurements by cardiac ultrasound: Principles, implementation and limitations. Eur J Echocardiogr 1, 154-170

D'hooge J, Bijnens B (2006). The principles of ultrasound based motion and deformation estimation. In: Sutherland GR, Hatle L, Claus P, D'hooge J, Bijnens B, editors. Doppler myocardial imaging: A textbook, BSWK Scientific Consulting and Publishing, 23-48

D'hooge J (2007). Principles and different techniques for speckle tracking. In: Marwick TH, Yu C-M, Sun J, editors. Myocardial imaging: Tissue Doppler and speckle tracking, Wiley-Blackwell, 17-25

Dalen H, Thorstensen A, Aase SA, Ingul CB, Torp H, Vatten LJ, Stoylen A (2010). Segmental and global longitudinal strain and strain rate based on echocardiography of 1266 healthy individuals: The HUNT study in Norway. Eur J Echocardiogr 11, 176-183

Donovan CL, Armstrong WF, Bach DS (1995). Quantitative Doppler tissue imaging of the left ventricular myocardium: Validation in normal subjects. Am Heart J 130, 100-104

Edner M, Jarnert C, Muller-Brunotte R, Malmqvist K, Ring M, Kjerr AC, Lind L, Kahan T (2000). Influence of age and cardiovascular factors on regional pulsed wave Doppler myocardial imaging indices. Eur J Echocardiogr 1, 87-95

Edvardsen T, Gerber BL, Garot J, Bluemke DA, Lima JA, Smiseth OA (2002). Quantitative assessment of intrinsic regional myocardial deformation by Doppler strain rate echocardiography in humans: Validation against three-dimensional tagged magnetic resonance imaging. Circulation 106, 50-56

Else RW, Holmes JR (1971). Pathological changes in atrial fibrillation in the horse. Equine Vet J 3, 56-64

Fleming AD, McDicken WN, Sutherland GR, Hoskins PR (1994). Assessment of colour Doppler tissue imaging using test phantoms. Ultrasound in Medicine and Biology 20, 937-951

Florescu M, Benea DC, Sisu RR, Cerin G, Diena M, Lanzzillo G, Enescu OA, Cinteza M, Vinereanu D (2011). Myocardial systolic velocities and deformation assessed by speckle tracking for early detection of left ventricular dysfunction in asymptomatic patients with severe primary mitral regurgitation. Echocardiography Epub 8 Nov 2011, doi10.1111/j.1540-8175.2011.01563.x

Gavaghan BJ, Kittleson MD, Fisher KJ, Kass PH, Gavaghan MA (1999). Quantification of left ventricular diastolic wall motion by Doppler tissue imaging in healthy cats and cats with cardiomyopathy. Am J Vet Res 60, 1478-1486

Gehlen H, Bubeck K, Stadler P (2004). Pulmonary artery wedge pressure measurement in healthy warmblood horses and in warmblood horses with mitral valve insufficiencies of various degrees during standardised treadmill exercise. Res Vet Sci 77, 257-264

Gehlen H, Iversen C, Stadler P (2009). Tissue Doppler echocardiographic examinations at rest and after exercise in horses with atrial fibrillation. Pferdeheilkunde 25, 11-16

Gehlen H, Marnette S, Rohn K, Stadler P (2005). Echocardiographic analysis of segmental left ventricular wall motion at rest and after exercise in horses with and without heart disease. J Eq Vet Sci 25, 468-479

Geyer H, Caracciolo G, Abe H, Wilansky S, Carerj S, Gentile F, Nesser HJ, Khandheria B, Narula J, Sengupta PP (2010). Assessment of myocardial mechanics using speckle tracking echocardiography: Fundamentals and clinical applications. J Am Soc Echocardiogr 23, 351-369

Gorcsan J, 3rd, Strum DP, Mandarino WA, Gulati VK, Pinsky MR (1997). Quantitative assessment of alterations in regional left ventricular contractility with color-coded tissue Doppler echocardiography. Comparison with sonomicrometry and pressure-volume relations. Circulation 95, 2423-2433

Gunn HM (1989). Heart weight and running ability. J Anat 167, 225-233

Hanekom L, Lundberg V, Leano R, Marwick TH (2004). Optimisation of strain rate imaging for application to stress echocardiography. Ultrasound Med Biol 30, 1451-1460

Heimdal A, Stoylen A, Torp H, Skjaerpe T (1998). Real-time strain rate imaging of the left ventricle by ultrasound. J Am Soc Echocardiogr 11, 1013-1019

Hinchcliff KW, Kaneps AJ, Geor RJ, editors (2004). Equine sports medicine and surgery: Basic and clinical sciences of the equine athlete, Saunders, 1-704

Hurlburt HM, Aurigemma GP, Hill JC, Narayanan A, Gaasch WH, Vinch CS, Meyer TE, Tighe DA (2007). Direct ultrasound measurement of longitudinal, circumferential, and radial strain using 2-dimensional strain imaging in normal adults. Echocardiography 24, 723-731

Isaaz K, Thompson A, Ethevenot G, Cloez JL, Brembilla B, Pernot C (1989). Doppler echocardiographic measurement of low velocity motion of the left ventricular posterior wall. Am J Cardiol 64, 66-75

Kawagishi T (2008). Speckle tracking for assessment of cardiac motion and dyssynchrony. Echocardiography 25, 1167-1171

Kim HK, Sohn DW, Lee SE, Choi SY, Park JS, Kim YJ, Oh BH, Park YB, Choi YS (2007). Assessment of left ventricular rotation and torsion with two-dimensional speckle tracking echocardiography. J Am Soc Echocardiogr 20, 45-53

Kiryu K, Machida N, Kashida Y, Yoshihara T, Amada A, Yamamoto T (1999). Pathologic and electrocardiographic findings in sudden cardiac death in racehorses. J Vet Med Sci 61, 921-928

Koffas H, Dukes-McEwan J, Corcoran BM, Moran CM, French A, Sboros V, Simpson K, McDicken WN (2006). Pulsed tissue Doppler imaging in normal cats and cats with hypertrophic cardiomyopathy. J Vet Intern Med 20, 65-77

Korinek J, Wang J, Sengupta PP, Miyazaki C, Kjaergaard J, McMahon E, Abraham TP, Belohlavek M (2005). Two-dimensional strain - a Doppler-independent ultrasound method for quantitation of regional deformation: Validation in vitro and in vivo. J Am Soc Echocardiogr 18, 1247-1253

Kriz NG, Hodgson DR, Rose RJ (2000). Prevalence and clinical importance of heart murmurs in racehorses. J Am Vet Med Assoc 216, 1441-1445

Kukulski T, Voigt JU, Wilkenshoff UM, Strotmann JM, Wranne B, Hatle L, Sutherland GR (2000). A comparison of regional myocardial velocity information derived by pulsed and color Doppler techniques: An in vitro and in vivo study. Echocardiography 17, 639-651

Kuznetsova T, Herbots L, Richart T, D'hooge J, Thijs L, Fagard RH, Herregods MC, Staessen JA (2008). Left ventricular strain and strain rate in a general population. Eur Heart J 29, 2014-2023

Langeland S, Wouters PF, Claus P, Leather HA, Bijnens B, Sutherland GR, Rademakers FE, D'hooge J (2006). Experimental assessment of a new research tool for the estimation of two-dimensional myocardial strain. Ultrasound Med Biol 32, 1509-1513

Leitman M, Lysyansky P, Sidenko S, Shir V, Peleg E, Binenbaum M, Kaluski E, Krakover R, Vered Z (2004). Two-dimensional strain - a novel software for real-time quantitative

echocardiographic assessment of myocardial function. J Am Soc Echocardiogr 17, 1021-1029

Lombard CW, Scarratt WK, Buergelt CD (1983). Ventricular septal defects in the horse. J Am Vet Med Assoc 183, 562-565

Long KJ, Bonagura JD, Darke PG (1992). Standardised imaging technique for guided M-mode and Doppler echocardiography in the horse. Equine Vet J 24, 226-235

Lyle CH, Uzal FA, McGorum BC, Aida H, Blissitt KJ, Case JT, Charles JT, Gardner I, Horadagoda N, Kusano K, Lam K, Pack JD, Parkin TD, Slocombe RF, Stewart BD, Boden LA (2011). Sudden death in racing Thoroughbred horses: An international multicentre study of post mortem findings. Equine Vet J 43, 324-331

MacDonald KA, Kittleson MD, Kass PH, Meurs KM (2007). Tissue Doppler imaging in Maine Coon cats with a mutation of myosin binding protein C with or without hypertrophy. J Vet Int Med 21, 232-237

Maier-Bock H, Ehrlein HJ (1978). Heart rate during a defined exercise test in horses with heart and lung diseases. Equine Vet J 10, 235-242

Manohar M, Goetz TE (1996). Pulmonary vascular pressures of exercising Thoroughbred horses with and without endoscopic evidence of EIPH. J Appl Physiol 81, 1589-1593

Marciniak A, Sutherland GR, Marciniak M, Claus P, Bijnens B, Jahangiri M (2009). Myocardial deformation abnormalities in patients with aortic regurgitation: A strain rate imaging study. Eur J Echocardiogr 10, 112-119

Marwick TH (2004). Tissue Doppler imaging for evaluation of myocardial function in patients with diabetes mellitus. Curr Opin Cardiol 19, 442-446

McDicken WN, Sutherland GR, Moran CM, Gordon LN (1992). Colour Doppler velocity imaging of the myocardium. Ultrasound Med Biol 18, 651-654

McGuirk SM, Muir WW (1985). Diagnosis and treatment of cardiac arrhythmias. Vet Clin North Am Equine Pract 1, 353-370

Miyatake K, Yamagishi M, Tanaka N, Uematsu M, Yamazaki N, Mine Y, Sano A, Hirama M (1995). New method for evaluating left ventricular wall motion by color-coded tissue Doppler imaging: In vitro and in vivo studies. J Am Coll Cardiol 25, 717-724

Moladoust H, Mokhtari-Dizaji M, Ojaghi-Haghighi Z, Noohi F, Khajavi A (2008). Frame rate requirement for tissue Doppler imaging in different phases of cardiac cycle: Radial and longitudinal functions. Int J Cardiovasc Imaging 24, 377-387

Nagueh SF, Middleton KJ, Kopelen HA, Zoghbi WA, Quinones MA (1997). Doppler tissue imaging: A noninvasive technique for evaluation of left ventricular relaxation and estimation of filling pressures. J Am Coll Cardiol 30, 1527-1533

Nesser HJ, Winter S (2009). Speckle tracking in the evaluation of left ventricular dyssynchrony. Echocardiography 26, 324-336

Notomi Y, Lysyansky P, Setser RM, Shiota T, Popovic ZB, Martin-Miklovic MG, Weaver JA, Oryszak SJ, Greenberg NL, White RD, Thomas JD (2005). Measurement of

ventricular torsion by two-dimensional ultrasound speckle tracking imaging. J Am Coll Cardiol 45, 2034-2041

O'Sullivan ML, O'Grady MR, Minors SL (2007). Assessment of diastolic function by Doppler echocardiography in normal Doberman Pinschers and Doberman Pinschers with dilated cardiomyopathy. J Vet Intern Med 21, 81-91

Ommen SR, Nishimura RA, Appleton CP, Miller FA, Oh JK, Redfield MM, Tajik AJ (2000). Clinical utility of Doppler echocardiography and tissue Doppler imaging in the estimation of left ventricular filling pressures: A comparative simultaneous Doppler-catheterization study. Circulation 102, 1788-1794

Oyama MA, Sisson DD, Bulmer BJ, Constable PD (2004). Echocardiographic estimation of mean left atrial pressure in a canine model of acute mitral valve insufficiency. J Vet Intern Med 18, 667-672

Oyenuga OA, Onishi T, Gorcsan J, 3rd (2011). A practical approach to imaging dyssynchrony for cardiac resynchronization therapy. Heart Fail Rev 16, 397-410

Palka P, Lange A, Fleming AD, Sutherland GR, Fenn LN, McDicken WN (1995). Doppler tissue imaging: Myocardial wall motion velocities in normal subjects. J Am Soc Echocardiogr 8, 659-668

Patteson MW (1996). Diagnostic aids in equine cardiology. In: Patteson MW, editor. Equine cardiology, Blackwell Science, 70-115

Patteson MW, Gibbs C, Wotton PR, Cripps PJ (1995). Echocardiographic measurements of cardiac dimensions and indices of cardiac function in normal adult Thoroughbred horses. Equine Vet J 27 Suppl 19, 18-27

Pavlopoulos H, Nihoyannopoulos P (2008). Strain and strain rate deformation parameters: From tissue Doppler to 2D speckle tracking. Int J Cardiovasc Imaging 24, 479-491

Pellerin D, Sharma R, Elliott P, Veyrat C (2003). Tissue Doppler, strain, and strain rate echocardiography for the assessment of left and right systolic ventricular function. Heart 89 Suppl 3, iii9-17

Perk G, Tunick PA, Kronzon I (2007). Non-Doppler two-dimensional strain imaging by echocardiography-from technical considerations to clinical applications. J Am Soc Echocardiogr 20, 234-243

Persson S (1967). On blood volume and working capacity in horses. Studies of methodology and physiological and pathological variations. Acta Vet Scand Suppl 19,19-189

Philippon F (2004). Cardiac resynchronization therapy: Device-based medicine for heart failure. J Card Surg 19, 270-274

Physick-Sheard PW, McGurrin MK (2010). Ventricular arrhythmias during race recovery in Standardbred racehorses and associations with autonomic activity. J Vet Intern Med 24, 1158-1166

Piper C, Butz T, Farr M, Faber L, Oldenburg O, Horstkotte D (2010). How to diagnose cardiac amyloidosis early: Impact of ECG, tissue Doppler echocardiography, and myocardial biopsy. Amyloid 17, 1-9

Poole DC, Erickson HH (2008). Cardiovascular function and oxygen transport: response to exercise and training. In: Hinchcliff KW, Kaneps AJ, Geor RJ, editors. Equine exercise physiology: The science of exercise in the athletic horse, Saunders, 212-245

Poole DC, Erickson HH (2011). Highly athletic terrestrial mammals: Horses and dogs. Compr Physiol 1, 1-37

Poulsen SH, Andersen NH, Ivarsen PI, Mogensen CE, Egeblad H (2003). Doppler tissue imaging reveals systolic dysfunction in patients with hypertension and apparent "isolated" diastolic dysfunction. J Am Soc Echocardiogr 16, 724-731

Reef VB (1995). Heart murmurs in horses: Determining their significance with echocardiography. Equine Vet J 27 Suppl 19, 71-80

Reef VB, Lalezari K, De Boo J, van der Belt AJ, Spencer PA, Dik KJ (1989). Pulsed-wave Doppler evaluation of intracardiac blood flow in 30 clinically normal Standardbred horses. Am J Vet Res 50, 75-83

Rychik J, Tian ZY (1996). Quantitative assessment of myocardial tissue velocities in normal children with Doppler tissue imaging. Am J Cardiol 77, 1254-1257

Schefer KD, Bitschnau C, Weishaupt MA, Schwarzwald CC (2010). Quantitative analysis of stress echocardiograms in healthy horses with 2-dimensional (2D) echocardiography, anatomical M-mode, tissue Doppler imaging, and 2D speckle tracking. J Vet Intern Med 24, 918-931

Schefer KD, Hagen R, Ringer SK, Schwarzwald CC (2011). Laboratory, electrocardiographic, and echocardiographic detection of myocardial damage and dysfunction in an Arabian mare with nutritional masseter myodegeneration. J Vet Intern Med 25, 1171-1180

Schober KE, Fuentes VL, Bonagura JD (2003). Comparison between invasive hemodynamic measurements and noninvasive assessment of left ventricular diastolic function by use of Doppler echocardiography in healthy anesthetized cats. Am J Vet Res 64, 93-103

Schwarzwald CC, Schober KE, Berli AS, Bonagura JD (2009a). Left ventricular radial and circumferential wall motion analysis in horses using strain, strain rate, and displacement by 2D speckle tracking. J Vet Intern Med 23, 890-900

Schwarzwald CC, Schober KE, Bonagura JD (2009b). Methods and reliability of tissue Doppler imaging for assessment of left ventricular radial wall motion in horses. J Vet Intern Med 23, 643-652

Sepulveda MF, Perkins JD, Bowen IM, Marr CM (2005). Demonstration of regional differences in equine ventricular myocardial velocity in normal 2-year-old Thoroughbreds with Doppler tissue imaging. Equine Vet J 37, 222-226

Simsek Z, Gundogdu F, Alpaydin S, Gerek Z, Ercis S, Sen I, Akgun M, Karakelleoglu S (2011). Analysis of athletes' heart by tissue Doppler and strain/strain rate imaging. Int J Cardiovasc Imaging 27, 105-111

Smedsrud MK, Pettersen E, Gjesdal O, Svennevig JL, Andersen K, Ihlen H, Edvardsen T (2011). Detection of left ventricular dysfunction by global longitudinal systolic strain in patients with chronic aortic regurgitation. J Am Soc Echocardiogr 24, 1253-1259

Smiseth OA, Ihlen H (2003). Strain rate imaging: Why do we need it? J Am Coll Cardiol 42, 1584-1586

Stoodley PW, Richards DA, Meikle SR, Clarke J, Hui R, Thomas L (2011). The potential role of echocardiographic strain imaging for evaluating cardiotoxicity due to cancer therapy. Heart Lung Circ 20, 3-9

Sun JP, Popovic ZB, Greenberg NL, Xu XF, Asher CR, Stewart WJ, Thomas JD (2004). Noninvasive quantification of regional myocardial function using Doppler-derived velocity, displacement, strain rate, and strain in healthy volunteers: Effects of aging. J Am Soc Echocardiogr 17, 132-138

Sutherland GR, Di Salvo G, Claus P, D'hooge J, Bijnens B (2004). Strain and strain rate imaging: A new clinical approach to quantifying regional myocardial function. J Am Soc Echocardiogr 17, 788-802

Tanabe M, Lamia B, Tanaka H, Schwartzman D, Pinsky MR, Gorcsan J, 3rd (2008). Echocardiographic speckle tracking radial strain imaging to assess ventricular dyssynchrony in a pacing model of resynchronization therapy. J Am Soc Echocardiogr 21, 1382-1388

Teshima K, Asano K, Sasaki Y, Kato Y, Kutara K, Edamura K, Hasegawa A, Tanaka S (2005). Assessment of left ventricular function using pulsed tissue Doppler imaging in healthy dogs and dogs with spontaneous mitral regurgitation. J Vet Med Sci 67, 1207-1215

Teske AJ, De Boeck BW, Melman PG, Sieswerda GT, Doevendans PA, Cramer MJ (2007). Echocardiographic quantification of myocardial function using tissue deformation imaging, a guide to image acquisition and analysis using tissue Doppler and speckle tracking. Cardiovasc Ultrasound 5, 27-45

Tidholm A, Ljungvall I, Hoglund K, Westling AB, Häggström J (2009). Tissue Doppler and strain imaging in dogs with myxomatous mitral valve disease in different stages of congestive heart failure. J Vet Intern Med 23, 1197-1207

Uematsu M, Miyatake K, Tanaka N, Matsuda H, Sano A, Yamazaki N, Hirama M, Yamagishi M (1995). Myocardial velocity gradient as a new indicator of regional left ventricular contraction: Detection by a two-dimensional tissue Doppler imaging technique. J Am Coll Cardiol 26, 217-223

Urheim S, Edvardsen T, Torp H, Angelsen B, Smiseth OA (2000). Myocardial strain by Doppler echocardiography. Validation of a new method to quantify regional myocardial function. Circulation 102, 1158-1164

Van de Veire NR, De Sutter J, Bax JJ, Roelandt JR (2008). Technological advances in tissue Doppler imaging echocardiography. Heart 94, 1065-1074

Verheyen T, Decloedt A, De Clercq D, Deprez P, Sys SU, van Loon G (2010a). Electrocardiography in horses - part 1: How to make a good recording. Vlaams Dierg Tijdschrift 79, 331-336

Verheyen T, Decloedt A, De Clercq D, Deprez P, Sys SU, van Loon G (2010b). Electrocardiography in horses - part 2: How to read the equine ECG. Vlaams Dierg Tijdschrift 79, 337-344

Wess G, Keller LJ, Klausnitzer M, Killich M, Hartmann K (2011). Comparison of longitudinal myocardial tissue velocity, strain, and strain rate measured by two-dimensional speckle tracking and by color tissue Doppler imaging in healthy dogs. J Vet Cardiol 13, 31-43

Wess G, Sarkar R, Hartmann K (2010). Assessment of left ventricular systolic function by strain imaging echocardiography in various stages of feline hypertrophic cardiomyopathy. J Vet Intern Med 24, 1375-1382

Young LE (2003). Equine athletes, the equine athlete's heart and racing success. Exp Physiol 88, 659-663

Young LE, Marlin DJ, Deaton C, Brown-Feltner H, Roberts CA, Wood JL (2002). Heart size estimated by echocardiography correlates with maximal oxygen uptake. Equine Vet J 34 Suppl 34, 467-471

Young LE, Rogers K, Wood JL (2005). Left ventricular size and systolic function in Thoroughbred racehorses and their relationships to race performance. J Appl Physiol 99, 1278-1285

Young LE, Rogers K, Wood JL (2008). Heart murmurs and valvular regurgitation in Thoroughbred racehorses: Epidemiology and associations with athletic performance. J Vet Intern Med 22, 418-426

Young LE, Wood JL (2000). Effect of age and training on murmurs of atrioventricular valvular regurgitation in young Thoroughbreds. Equine Vet J 32, 195-199

Zamorano J, Wallbridge DR, Ge J, Drozd J, Nesser J, Erbel R (1997). Non-invasive assessment of cardiac physiology by tissue Doppler echocardiography. A comparison with invasive haemodynamics. Eur Heart J 18, 330-339

Chapter 2: Scientific aims

The echocardiographic evaluation of left ventricular (LV) function is important in horses, particularly in case of valvular regurgitation or poor performance. However, the most commonly used parameter of LV function, fractional shortening, is a focal, one-dimensional and load-dependent measurement, which does not take into account longitudinal LV function, regional myocardial dysfunction or diastolic dysfunction.

Tissue Doppler imaging (TDI) and two-dimensional speckle tracking (2DST) are two echocardiographic techniques used in human and small animal medicine. They allow a more extensive quantification of myocardial function and might overcome some of the above mentioned limitations. Numerous studies in human and small animal medicine have demonstrated that TDI and 2DST measurements are more sensitive than conventional echocardiographic measurements for the detection of subclinical LV dysfunction. However, little information is available on the use of TDI and 2DST in horses.

The general aim of this thesis was to evaluate the use of TDI and 2DST for quantification of LV function in horses.

The specific scientific aims were:

1. To determine the feasibility, reliability and reference values for TDI and 2DST measurements of systolic and diastolic LV myocardial velocity and deformation in healthy horses (Chapter 3).

2. To investigate experimentally the influence of the atrioventricular delay on mitral valve closure and LV peak velocity and acceleration measured by TDI during isovolumic contraction (Chapter 4).

3. To evaluate the use of TDI and 2DST in horses with myocardial dysfunction. For this purpose, two clinical studies were carried out. TDI and 2DST measurements were performed in horses with toxic cardiomyopathy caused by an ionophore intoxication (Chapter 5) and in horses with atypical myopathy (Chapter 6).

CHAPTER 3

Feasibility and reliability of tissue Doppler imaging and two-dimensional speckle tracking in healthy horses

Chapter 3.1

Quantification of left ventricular longitudinal strain, strain rate, velocity and displacement in healthy horses by two-dimensional speckle tracking

Adapted from:

Decloedt A, Verheyen T, Sys S, De Clercq D, van Loon G

Department of Large Animal Internal Medicine, Faculty of Veterinary Medicine, Ghent University, Belgium.

Quantification of left ventricular longitudinal strain, strain rate, velocity and displacement in healthy horses by two-dimensional speckle tracking.

Journal of Veterinary Internal Medicine (2011) 25, 330-338

Part of this work was presented at the 48th BEVA Congress, Birmingham, United Kingdom, September 9-12, 2009.

Summary

Background: The quantification of equine left ventricular (LV) function is generally limited to short-axis M-mode measurements. However, LV deformation is three-dimensional and consists of longitudinal shortening, circumferential shortening and radial thickening. In human medicine, longitudinal motion is the best marker of subtle myocardial dysfunction.

Objectives: To evaluate the feasibility and reliability of two-dimensional speckle tracking (2DST) for quantifying equine LV longitudinal function.

Animals: Ten healthy untrained trotter horses; 9.6 ± 4.4 years; 509 ± 58 kg.

Methods: Prospective study. Repeated echocardiographic examinations were performed by two observers from a modified four-chamber view. Global, segmental and averaged peak values and timing of longitudinal strain (SL), strain rate (SrL), velocity (VL) and displacement (DL) were measured in four LV wall segments. The inter- and intra-observer within- and between-day variability and measurement variability were assessed by calculating the coefficients of variation for repeated measurements.

Results: 2DST analysis was feasible in each exam. The variability of peak systolic values and peak timing was low to moderate, whereas peak diastolic values showed a higher variability. Significant segmental differences were demonstrated. DL and VL presented a prominent base-to-midwall gradient. SL and SrL values were similar in all segments except the basal septal segment, which showed a significantly lower peak SL occurring about 60 ms later compared to the other segments.

Conclusions and clinical importance: 2DST is a reliable technique for measuring systolic LV longitudinal motion in healthy horses. This study provides preliminary reference values which can be used when evaluating the technique in a clinical setting.

Introduction

The quantification of myocardial function is important in horses, particularly in cases of poor performance. The objective evaluation of left ventricular (LV) function is traditionally based on M-mode measurements such as fractional shortening and wall thickening (Long et al., 1992; Patteson et al., 1995). These measurements provide a rather rough estimate of global LV function, as they are focal and one-dimensional. Recently, new techniques have been introduced in equine cardiology that require further investigation. Tissue Doppler imaging (TDI) has been used to measure the systolic and diastolic velocities of the myocardial walls (Sepulveda et al., 2005; Gehlen et al., 2009; Schwarzwald et al., 2009b). However, these measurements are easily influenced by the insonation angle and total heart motion. This limitation has led to a growing interest in strain imaging in human medicine. Strain is a measure of the amount of deformation of the myocardial walls, expressed in %. Lengthening or thickening is indicated by a positive strain value, while shortening or thinning is negative. The rate of deformation is the strain rate, expressed in s^{-1}.

Two-dimensional speckle tracking (2DST) quantifies myocardial strain in the two dimensions of the ultrasound image based on tracking speckles in the myocardial walls (D'hooge et al., 2000; Teske et al., 2007). 2DST has been reliably applied in short-axis images for quantification of equine radial and circumferential LV motion (Schwarzwald et al., 2009a). However, LV contraction is a three-dimensional movement consisting of radial thickening, circumferential shortening and longitudinal shortening. In human medicine, longitudinal function is described as the best prognostic factor in several conditions such as valvular disease (Lancellotti et al., 2008; Mizuguchi et al., 2008; Marciniak et al., 2009). Although 2DST has recently been applied to measure equine LV longitudinal function during stress-echocardiography, no data are available on the reliability of these measurements (Schefer et al., 2010).

The purpose of this study was to assess global and regional LV longitudinal function in healthy horses at rest. We hypothesized that 2DST methods allow quantification of LV longitudinal strain, strain rate, velocity and displacement based on two-dimensional (2D) greyscale images. The 2DST technique and the feasibility and reliability of the evaluation of equine LV longitudinal function are described.

Material and methods

Study Population

The study population consisted of ten healthy untrained trotter horses (seven mares, three geldings) aged 9.6 ± 4.4 years (mean ± standard deviation SD) with a body weight of 509 ± 58 kg. Animal handling and care was performed following the guidelines of the local ethical committee. A comprehensive examination was performed prior to the study to exclude cardiovascular or respiratory disease. This consisted of a general physical examination, thorough cardiac auscultation, 30 minute electrocardiogram at rest and routine 2D, M-mode and color Doppler echocardiography.

Echocardiography

All horses were examined without sedation at heart rates below 45 beats per minute (bpm). Echocardiography was performed using an ultrasound unit (GE Vivid 7 Dimension, GE Healthcare, Horten, Norway) with phased array transducer (3S Phased Array Transducer, GE Healthcare, Horten, Norway) at a frequency of 1.6/3.2 MHz (octave harmonics). A base-apex ECG was recorded simultaneously. At least three non-consecutive cardiac cycles from each view were stored in cineloop format.

M-mode recordings of the aortic valve were made in the right parasternal LV outflow tract long-axis view. For the evaluation of LV longitudinal function, a standard right parasternal four-chamber view (Long et al., 1992) was obtained. The imaging depth ranged from 26 to 28 cm depending on LV size, with a single focus positioned at 20 cm. The sector width was reduced to 55° in order to achieve a frame rate of at least 40 frames per second (fps). The view was then slightly modified to include as much of the LV as possible while the mitral annulus remained visible throughout the entire cardiac cycle. As a result, the apex was not always visualized (Fig. 1).

Off-line analysis

Measurements were performed using a commercially available software package (EchoPAC Software Version 7.1.2, GE Healthcare, Horten, Norway). For each exam, three non-consecutive cardiac cycles per view were analysed one by one. The time of aortic valve closure (AVC_{MM}) was measured manually as the time interval between the R wave on the ECG and aortic valve closure in the M-mode image. The RR interval (in ms) was recorded and instantaneous heart rate was calculated as 60,000/RR interval.

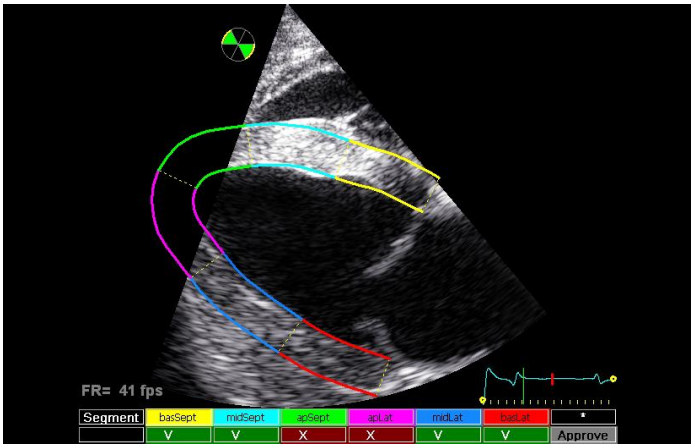

Figure 1: Modified four-chamber view for 2DST analysis of LV longitudinal function. The ROI is automatically divided into six segments: "basSept", "midSept" and "apSept" for the interventricular septum; "basLat", "midLat" and "apLat" for the LV free wall. Tracking quality is verified by the software and displayed at the bottom of the screen. Approved segments are marked with a green "V". The apical segments are rejected, as indicated by a red "X".

LV longitudinal function was assessed from the modified four-chamber view with the "2D Strain" application, using the "4CH" mode. A U-shaped region of interest (ROI) was placed on the myocardium in a frame at end-systole by tracing the endocardial border from the septal to the lateral wall insertion of the mitral valve, without following excessive bulging of the walls. This line was partially drawn outside the image where the apical endocardial border was expected. Afterwards, the ROI width was adjusted in order to cover the entire myocardium without including the epicardial borders. The software algorithm subdivided this ROI into six segments (Fig. 1). The apical segments were excluded from further analysis as these segments were not visualised. The midwall segments were manually corrected if they did not fit the image width. Next, the program automatically selected acoustic speckles that were tracked throughout the cardiac cycle in longitudinal and transverse (radial) direction. Based on the tracking quality, the software approved or rejected the segments for further analysis. In addition, tracking quality was evaluated by visual assessment during motion playback. If necessary, the ROI was adjusted and tracking was repeated until adequate tracking quality was achieved. Segments were excluded if they were rejected by the software or if tracking was visually insufficient. If tracking was visually accurate during systole but not during diastole, only systolic measurements were included for further analysis. Occasionally the last systolic frames were poorly tracked in some segments. As the effect of one or two poorly tracked frames was thought to be minimal, these segments were included for further analysis. However, this might have resulted in a small underestimation of strain values in these segments.

After tracking quality had been verified for all segments, the trace analysis screen was shown. The following curves were displayed: longitudinal velocity (VL), strain (SL), strain rate (SrL) and displacement (DL), and transverse displacement (DT). The default settings for spatial smoothing, temporal smoothing and drift compensation were used. The time of aortic valve closure (AVC_a) was calculated by the software based on the longitudinal strain curves of all LV segments. Segmental systolic ($_S$), early diastolic ($_E$) and late diastolic ($_A$) peak values were indicated on the curves and could be manually adjusted if necessary. Afterwards, the results were exported to a spreadsheet (Microsoft Office Excel 2003, Microsoft Corporation, Redmond, WA) for further analysis.

Timing of segmental peak values and AVC_a was automatically reported in the spreadsheet. Late diastolic timings were related to the onset of the preceding P wave, all others to the peak R wave. Global and averaged peak values were determined as measurements of global LV function. Global values were computed by the software from the whole ROI as a single segment. These values were not visible in the trace analysis screen but were included when all data were exported to a spreadsheet. Averaged values were calculated manually for all measurements as the average of the segmental values. Furthermore, a distinction was made between peak systolic (SL_S) and maximal (SL_G) strain. The highest longitudinal strain value before or at AVC_a was considered SL_S. SL_G was defined as the maximal strain value, which could occur before or after AVC_a. SL_P was measured as a small early-systolic positive longitudinal strain peak.

Reliability of echocardiographic variables

The reliability of 2DST measurements was evaluated by comparing repeated echocardiographic examinations and offline measurements by two experienced echocardiographers (AD and GvL). All horses were examined by observer 1 on two separate days with an interval of one day. On one of these occasions, this was repeated by observer 2 immediately before or after the first observer. Offline analysis was first performed by observer 1 for all echocardiographic exams (n=30). Next, on one exam of each horse (n=10), the same three non-consecutive cycles were measured by both observers on a separate occasion to determine measurement variability. At any time, observers were blinded to echocardiographer, horse, day and any previous results.

Statistical analysis

Statistical analyses were performed using dedicated computer software (SPSS Statistics 17.0, Rel. 17.0.1., SPSS Inc, Chicago, IL). Within- and between-day intra- and interobserver variability were determined based on the analysis of variance results of all measurements. The within-day interobserver variability was obtained by comparing the results of the exams performed on the same day by observer 1 and observer 2. The numerical values for the reported coefficients of variation (CV) were derived from the expressions of the expected mean square errors from a two-factor (observer and horse) analysis of variance of the natural logarithms of the measurements. In analogy, the between-day intra-observer variability was determined by comparing the exams recorded on two separate days by observer 1 using a two-factor (day and horse) analysis of variance. Similarly, the measurement variability was obtained by repeated measurements of thirty identical cycles (one exam per horse) on two different days (intra-observer measurement variability) or by two different observers (interobserver measurement variability). The degree of variability was defined based on the CV as follows: CV < 15%, low variability; CV 15-25%, moderate variability; CV > 25%, high variability (Schwarzwald et al., 2007).

Summary statistics for the different measurements (mean ± SD; n = 10 horses) were calculated using the average measurement of three non-consecutive cycles per horse. Peak values and timing in the different segments were compared by analysis of variance; post-hoc tests were performed using the Bonferroni correction method. These data were displayed as boxplots, with the box span indicating the middle half of the observations, the line in the box marking the median, and the whiskers indicating the range of observations. Extreme values were plotted individually at the end of the whiskers. Agreement between AVC_a and AVC_{MM} was assessed by Bland-Altman 95% limits of agreement. A paired t-test was used to compare both measurements of AVC and their corresponding heart rate, as well as to compare global and averaged values of SL and SrL. The level of significance was $\alpha = 0.05$.

Results

2DST analysis was feasible on three cycles of each exam using the modified four-chamber view at a frame rate of 41.1 fps. Fig. 2A-E shows an example of the curves displayed by the software after approval of tracking quality. The shape of these curves was similar in all horses and peak values could be easily distinguished. All apical segments were excluded as they were not visualized. Tracking quality was approved in 574 of the remaining 600 segments (95.7%). However, the tracking process was visually less accurate in diastole. In 6.1% of the approved segments, tracking was very poor and diastolic values were excluded from further analysis. Tracking quality of transverse motion was often visually inadequate and the variability of the measurements was very high (CV > 25%). Therefore these measurements are not further discussed.

Tables 1 and 2 show the peak values of global, averaged and segmental 2DST measurements in the study population. The global SL_G value was not significantly different from the averaged SL_G ($P = 0.06$). The global SrL values were slightly lower than the averaged SrL values ($P < 0.05$). Significant segmental differences were found. As illustrated in Fig. 3A-B, DL and VL presented a remarkable base-to-midwall gradient ($P < 0.01$). Conversely, SL and SrL values were similar in all segments except the basal septal segment (Fig. 3C-D). This segment showed a significantly less negative SL_S and SL_G ($P < 0.05$).

Table 1: Global[a] values of 2DST measurements of LV longitudinal function in 10 healthy adult trotter horses.

Variable	Mean	SD	Between-day intra-observer variability CV (%)	Within-day interobserver variability CV (%)	Intra-observer measurement variability CV (%)	Interobserver measurement variability CV (%)
HR (bpm)	33.4	3.88	7.7	7.0	3.2	3.2
AVC_a (ms)	528	26	6.1	5.7	3.6	3.6
SL_G (%)	-24.3	1.72	8.3	10.1	7.2	7.4
SrL_S (s^{-1})	-0.88	0.05	8.7	10.9	8.9	8.9
SrL_E (s^{-1})	0.98	0.09	10.8	11.3	10.7	9.3
SrL_A (s^{-1})	0.63	0.12	16.6	20.5	14.1	14.5

CV, coefficient of variation; SD, standard deviation
[a] Calculated by the software from the whole ROI as a single segment.

The mean AVC_a was 528 ms, which did not differ significantly from the AVC_{MM} of 537 ms (P = 0.07). A mean bias of -10 ms with a standard deviation of 14 ms was present, resulting in 95% limits of agreement between -36 and + 18 ms. The mean RR interval of 2DST and M-mode recordings did not differ significantly (P = 0.35).

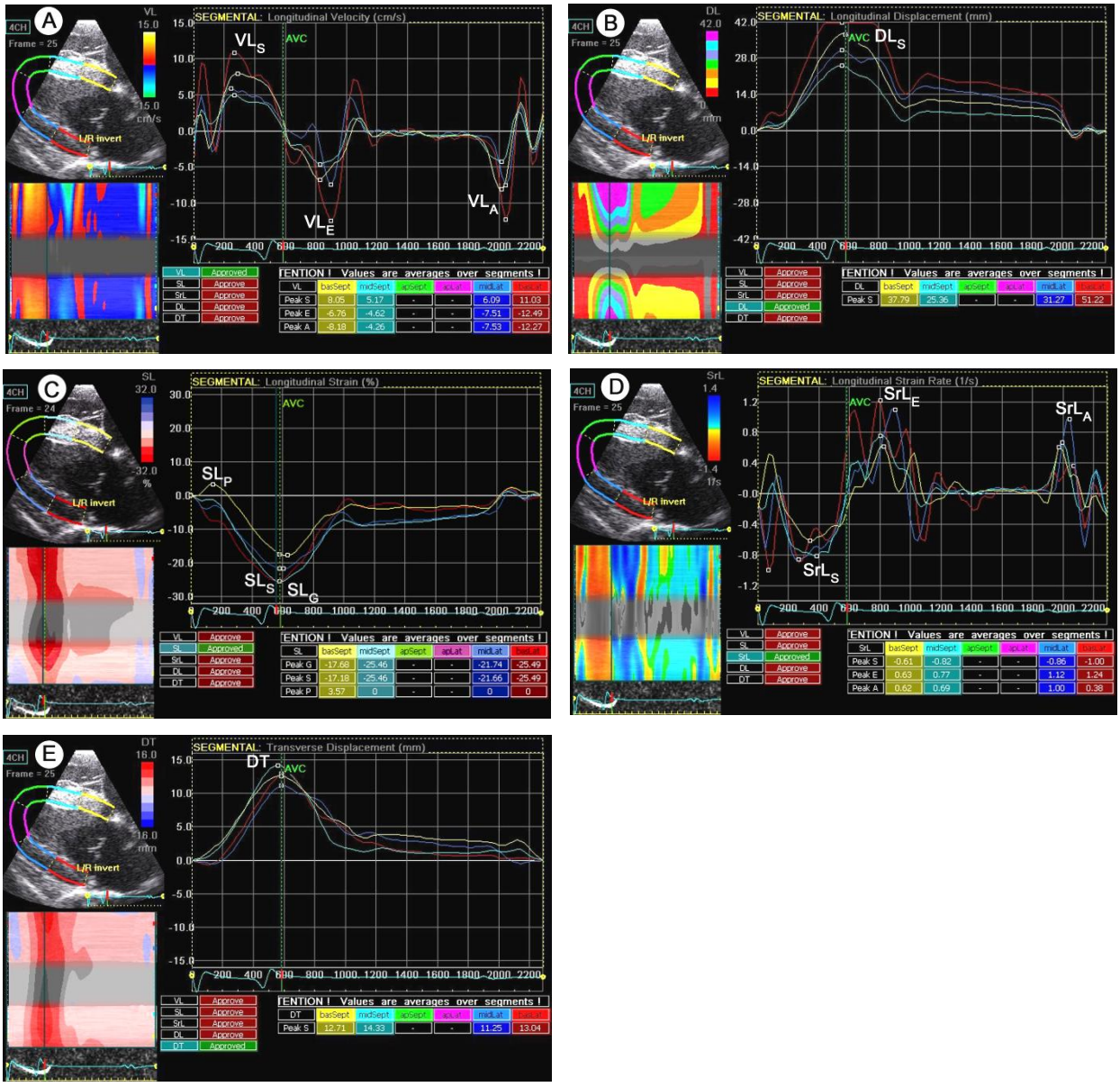

Figure 2A-E: Examples of the curves in the "Results" screen after approval of tracking quality. On the left, a 2D greyscale image is displayed showing the tracked ROI. A parametric color-coded M-mode is depicted below. On the right, the segmental traces are displayed. The vertical axis represents values of the selected variable; the horizontal axis shows time (ms) and the ECG. AVC_a is marked by a vertical green line. Peak values are automatically indicated on the curves and tabulated below. After verifying the correct position of these peaks, measurements can be approved in the column next to the table. (A) VL, longitudinal velocity; (B) DL, longitudinal displacement; (C) SL, longitudinal strain; (D) SrL, longitudinal strain rate; (E) DT, transverse displacement.

Table 2: Segmental and averaged peak values of 2DST measurements of LV longitudinal function in 10 healthy adult trotter horses.

Variable	Segment[a]	n	Mean	SD	Between-day intra-observer variability CV (%)	Within-day inter-observer variability CV (%)	Intra-observer meas. variability CV (%)	Inter-observer meas. variability CV (%)
SL_G (%)	Averaged		-24.80	2.36	8.0	11.1	7.1	6.5
	basLat	139	-25.19	3.83	13.7	15.4	11.7	13.4
	midLat	146	-26.27	2.65	12.0	14.1	10.2	10.4
	midSept	150	-25.36	2.83	8.7	9.9	6.3	6.2
	basSept	139	-22.47	2.15	12.7	15.3	9.8	8.0
SL_S (%)	Averaged		-24.49	2.52	8.0	11.2	7.2	6.5
	basLat	139	-25.08	3.84	13.7	15.1	11.7	13.6
	midLat	146	-26.24	2.63	12.0	14.2	10.2	10.4
	midSept	150	-25.23	2.94	8.8	9.9	6.3	6.2
	basSept	139	-21.48	2.28	14.3	16.2	11.3	9.5
SL_P (%)	Averaged		1.80	0.49	60.9	61.5	67.9	57.5
	basLat	51	0.98	0.51	102.0	154.1	61.9	63.9
	midLat	17	0.39	0.49	NA	NA	NA	NA
	midSept	86	0.86	0.46	124.7	109.8	85.2	82.3
	basSept	134	2.57	0.76	75.4	78.2	66.1	73.1
VL_S (m/s)	Averaged		8.37	0.44	10.1	10.1	7.6	7.7
	basLat	139	11.76	0.88	11.4	10.9	9.0	7.8
	midLat	146	6.96	1.09	26.1	26.3	16.4	15.7
	midSept	150	5.75	0.50	14.4	15.0	13.3	11.4
	basSept	139	9.41	0.61	5.9	7.4	5.0	6.9
VL_E (m/s)	Averaged		-7.71	0.50	11.9	11.9	10.3	10.5
	basLat	130	-11.14	0.80	13.6	10.0	9.3	8.8
	midLat	144	-6.17	0.98	21.7	20.7	20.1	19.7
	midSept	128	-5.32	0.45	17.5	14.4	14.4	11.1
	basSept	137	-8.33	1.15	11.5	12.3	7.9	8.2
VL_A (m/s)	Averaged		-7.46	0.76	11.5	11.7	9.0	9.2
	basLat	130	-9.68	0.99	16.0	15.4	15.1	17.1
	midLat	144	-6.19	0.95	21.2	21.0	17.3	18.3
	midSept	128	-5.25	0.48	13.8	19.1	13.1	13.2
	basSept	137	-8.52	1.54	13.8	15.0	7.6	8.3
SrL_S (s^{-1})	Averaged		-0.95	0.08	8.6	10.1	7.8	7.3
	basLat	139	-1.00	0.18	16.4	19.0	16.3	16.1
	midLat	146	-0.97	0.08	12.1	11.3	10.3	11.5
	midSept	150	-0.98	0.09	8.5	11.9	8.2	8.4
	basSept	139	-0.86	0.11	15.7	21.6	11.7	12.2

SrL_E (s^{-1})	Averaged		1.18	0.10	10.4	11.3	9.7	8.8
	basLat	130	1.51	0.20	21.5	24.6	19.9	17.0
	midLat	144	1.03	0.07	14.7	13.6	13.7	13.5
	midSept	128	1.03	0.11	11.0	13.6	10.6	10.1
	basSept	137	1.19	0.24	19.4	21.1	16.7	17.0
SrL_A (s^{-1})	Averaged		0.67	0.13	15.0	16.1	13.5	14.0
	basLat	130	0.55	0.15	45.9	45.1	44.6	41.4
	midLat	144	0.76	0.09	21.6	23.3	19.9	19.9
	midSept	128	0.69	0.15	16.5	18.8	11.8	13.1
	basSept	137	0.66	0.20	23.7	20.1	18.1	23.1
DL_S (mm)	Averaged		37.60	5.18	13.2	15.5	12.3	11.2
	basLat	139	53.60	6.91	11.1	12.9	9.6	9.2
	midLat	146	33.70	5.50	17.7	19.5	16.6	15.1
	midSept	150	25.60	4.24	17.0	18.7	18.9	14.3
	basSept	139	39.77	5.42	11.6	14.2	9.9	8.9

CV, coefficient of variation; n, number of segments in which the variable could be determined (on a total of 150); meas., measurement; NA, not available; SD, standard deviation
[a] Segments as illustrated in Fig. 1. Averaged = average of the approved segments.

The mean values of peak timing are provided in Supplementary Table 1. Some remarkable segmental differences were present. SL_G was reached significantly later in the basal septal segment compared to the other segments ($P < 0.01$) (Fig. 3E). The mean delay of this segment was 60 ms (95% confidence interval 37 to 84 ms). Consequently, SL_G occurred after AVC_a in 107 of the 139 (77%) basal septal segments and in only 74 of the 435 (17%) other segments. At the onset of systole, 96% of the analysed basal septal segments showed a small positive peak strain (SL_P), compared to only 35% of the other segments. Time to peak VL_A and SrL_A was significantly delayed in the lateral wall compared to the septum ($P < 0.001$) (Fig. 3F). The difference of means for VL_A and SrL_A was 31 ms (95% confidence interval 20 to 41 ms) and 25 ms (95% confidence interval 16 to 34 ms) respectively.

Reliability

As shown in Tables 1 and 2, the variability of segmental, global and averaged peak systolic values was low to moderate, whereas diastolic measurements showed a moderate to high variability. SL and SrL exhibited a lower variability than VL and DL. Conversely, the variability of SL_P was very high (CV 58–125%). The variability of peak timing was low, except for time to peak VL_S, SrL_S and SL_P, which showed a moderate to high variability (Supplementary Table 1).

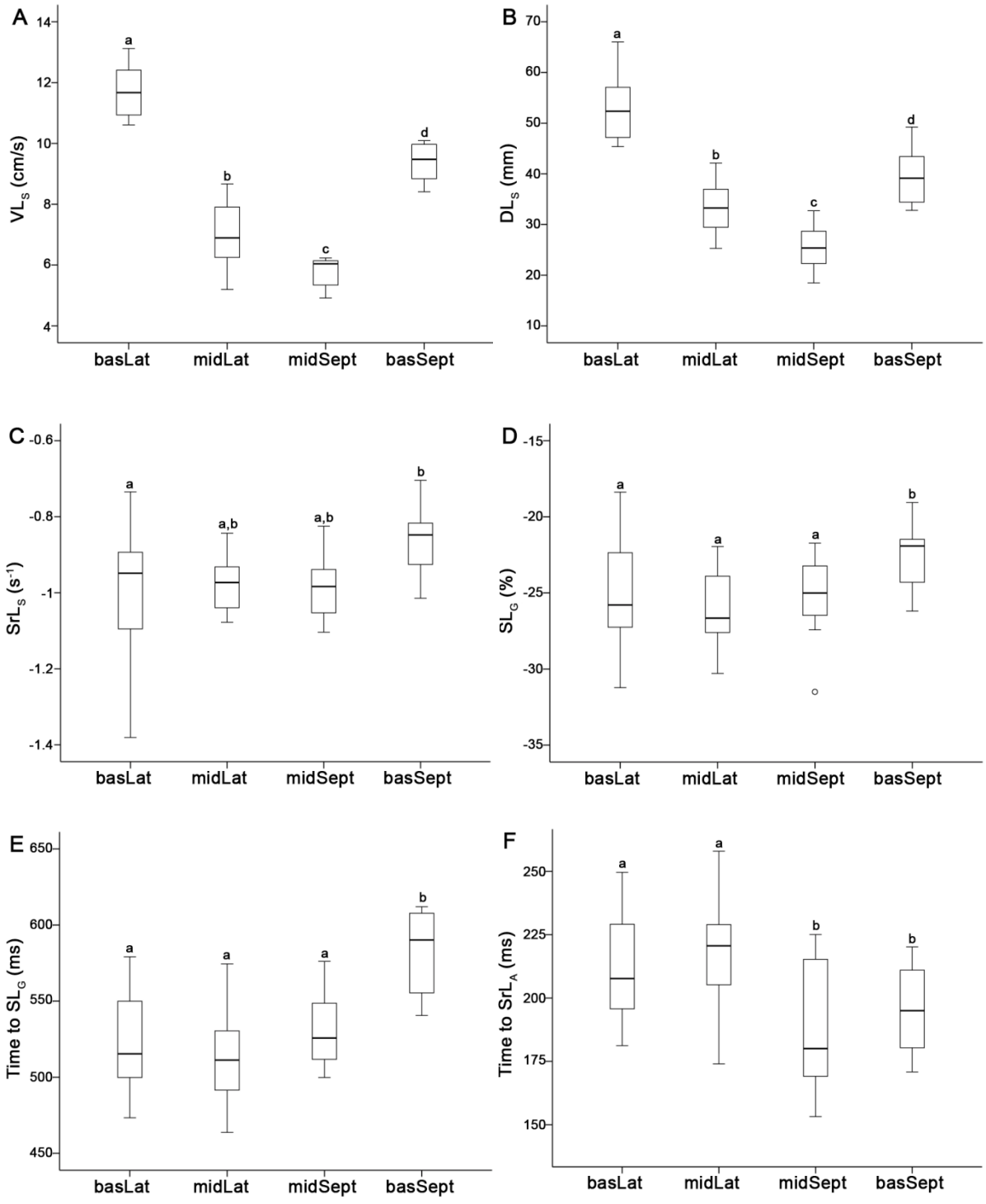

Figure 3A-F: Graphical illustration of segmental differences of 2DST measurements of LV longitudinal function. For each segment, the median and spread of the peak value or timing is indicated by a boxplot, based on the averaged measurement values for each horse (n = 10). Boxes marked with different letters are significantly different from each other. (A) VL_S: peak systolic longitudinal velocity (cm/s); (B) DL_S: peak systolic longitudinal displacement (mm); (C) SrL_S: peak systolic longitudinal strain rate (s^{-1}); (D) SL_G: peak maximal longitudinal strain (%); (E) time to SL_G (ms); (F) time to SrL_A: time to peak late diastolic longitudinal strain rate (ms).

Supplementary Table 1: Segmental and averaged peak timing of 2DST measurements of LV longitudinal function in 10 healthy adult trotter horses.

Variable	Segment[a]	Mean	SD	Between-day intra-observer variability CV (%)	Within-day interobserver variability CV (%)	Intra-observer measurement variability CV (%)	Interobserver measurement variability CV (%)
Time to SL_G (ms)	Averaged	537	23	6.1	5.3	3.6	3.5
	basLat	521	34	6.6	6.7	4.4	4.1
	midLat	516	32	4.9	4.7	3.2	3.1
	midSept	528	24	8.0	6.7	5.1	5.6
	basSept	582	27	7.3	6.8	6.1	5.3
Time to SL_S (ms)	Averaged	518	30	5.6	5.0	3.0	3.0
	basLat	515	32	6.0	6.1	3.8	3.6
	midLat	513	31	4.8	4.5	3.1	3.0
	midSept	517	30	6.1	4.9	3.0	3.1
	basSept	526	28	6.4	5.8	3.8	3.8
Time to SL_P (ms)	Averaged	82	16	37.0	36.1	38.0	32.8
	basLat	45	13	42.7	35.0	21.6	27.4
	midLat	42	39	NA	NA	NA	NA
	midSept	75	26	67.2	43.5	21.4	18.8
	basSept	100	16	36.2	38.5	27.8	27.6
Time to VL_S (ms)	Averaged	234	25	17.2	15.0	12.8	13.0
	basLat	238	37	29.1	25.5	20.4	20.3
	midLat	230	54	28.4	27.0	23.5	24.8
	midSept	227	32	17.0	17.9	13.8	13.8
	basSept	246	32	16.7	19.7	17.7	14.1
Time to VL_E (ms)	Averaged	756	44	4.1	4.2	3.6	3.6
	basLat	746	53	7.3	7.6	7.5	7.1
	midLat	766	53	6.2	6.7	7.2	7.4
	midSept	774	42	4.7	4.6	3.5	3.4
	basSept	742	45	5.1	6.3	4.2	3.9
Time to VL_A (ms)[c]	Averaged	212	23	8.9	9.9	7.2	7.2
	basLat	229	24	9.5	10.9	8.4	8.5
	midLat	227	25	9.2	10.9	7.4	7.1
	midSept	191	25	12.2	14.4	12.1	11.4
	basSept	202	27	9.1	11.4	8.0	8.1
Time to SrL_S (ms)	Averaged	293	48	15.2	16.3	12.2	12.3
	basLat	280	38	37.7	31.0	32.8	30.9
	midLat	270	52	33.0	26.6	23.0	24.2
	midSept	293	53	23.9	27.3	23.7	24.8
	basSept	336	65	25.8	31.8	21.7	25.5

Time to SrL_E (ms)	Averaged	705	45	4.5	5.1	3.9	3.6
	basLat	673	41	7.1	7.0	5.0	5.3
	midLat	701	63	9.6	9.2	8.6	9.1
	midSept	723	37	4.1	5.5	3.9	3.7
	basSept	722	54	6.4	8.3	6.1	5.5
Time to SrL_A (ms) [c]	Averaged	203	19	10.6	12.7	8.8	9.3
	basLat	214	22	23.3	23.1	18.1	21.7
	midLat	220	25	10.2	12.5	8.2	8.8
	midSept	185	25	10.3	15.3	10.1	9.8
	basSept	195	17	11.3	15.4	9.6	9.7
Time to DL_S (ms)	Averaged	501	31	5.3	4.0	2.7	2.8
	basLat	507	31	4.6	3.9	2.6	2.8
	midLat	503	32	5.5	3.9	3.1	3.0
	midSept	491	33	7.3	5.4	5.2	5.5
	basSept	506	31	5.3	4.5	2.8	2.8

CV, coefficient of variation; NA, not available; SD, standard deviation
[a] Time to peak measured from R-wave, unless indicated otherwise.
[b] Segments as illustrated in Fig. 1. Averaged = average of the approved segments.
[c] Time to peak measured from onset P-wave.

Discussion

This study describes the technique and demonstrates the feasibility of quantifying LV longitudinal function by 2DST in healthy horses at rest. Global and regional systolic myocardial strain, strain rate, velocity and displacement could be reliably measured using a modified right parasternal four-chamber view.

A frame rate of 41.1 fps was used, which is within the range of frame rates applied in human medicine (30 to 90 fps) (Suffoletto et al., 2006; Sutherland et al., 2006) and recommended by the software manufacturer (40 to 70 fps). Lower frame rates result in large frame-to-frame changes in speckle position and a decreased time resolution. This causes impaired tracking quality and underestimation of peak values, especially at increased heart rates (Teske et al., 2007). In this study, a sufficient frame rate was obtained by limiting the image width to 55°, which did not allow visualizing the entire LV throughout the cardiac cycle. The basal and midwall segments were chosen for analysis as these show the largest longitudinal movement. The frame rate was not increased by reducing the line density of the ultrasound beams, as this results in a decreased lateral resolution. Adequate lateral resolution is important for tracking quality, especially when measuring longitudinal strain from a right parasternal four-chamber view. The use of more advanced echocardiographic equipment and transducers may result in an improved lateral resolution, thus enabling the acquisition of higher frame rates at a wider imaging sector.

As 2DST is a new technique, a thorough evaluation of repeatability and reproducibility is crucial before clinical use. All systolic peak values showed a low to moderate variability and can thus be reliably investigated in future clinical studies. Our reliability data are similar to those reported for 2DST in human medicine, small animals and horses (Chetboul et al., 2007; Hurlburt et al., 2007; Schwarzwald et al., 2009a; Thorstensen et al., 2010). However, it should be noted that the comparison of different reliability studies is difficult due to different sample size and statistical methods for assessment of reliability. In our study, diastolic measurements were less reliable. Tracking was often visually inaccurate in early diastole because of the fast cardiac movement in this phase. Due to the relatively low frame rate, this early diastolic peak was underestimated by 2DST and early and late diastolic values were approximately equal. In reality, the early diastolic peak is probably much higher than the late diastolic peak in horses at rest, as has already been demonstrated for radial diastolic wall motion velocities by TDI (Schwarzwald et al., 2009b).

2DST analysis of LV longitudinal function was feasible in all exams, although 4.3% of segments were excluded because of inadequate tracking quality. Similarly, 5/90 segments (5.6%) were excluded at resting heart rate in a previous study on equine LV longitudinal function by 2DST (Schefer et al., 2010). The percentage of excluded segments in human medicine ranges from 2.2 to 20% in healthy and diseased study populations (Leitman et al., 2004; Amundsen et al., 2006; Suffoletto et al., 2006). In our study, the basal segments were most frequently excluded. It is important to note that some loops contained artefacts in the mitral annular region. Strict guidelines on the image quality in this region will lead to a lower number of excluded segments. Attention should be paid to an optimal gain and contrast for imaging the myocardium, thereby reducing artefacts. It is particularly important to avoid the presence of drop-out due to the ribs or the coronary region. Furthermore, the mitral annular ring has to remain visualised throughout the entire cardiac cycle, also during atrial contraction.

One of the main goals of this study was the quantification of global LV longitudinal function. For this purpose global and averaged SL_G were evaluated. These values were very similar and equally reliable. Global SrL values were 5-16% lower than the averaged SrL values. Because global values are computed automatically, they are more attractive to be used in a clinical setting. VL and DL are less applicable as measurements of global LV function due to large segmental differences. Because of the fixed position of the apex in the thorax, the mitral annular ring is pulled down towards the apex during systole. As a result, longitudinal velocity and displacement are largest in segments further away from the apex. The downward motion of the LV base not only results in ejection of blood from the ventricle, but also in passive filling of the atria. The longitudinal base-to-apex gradient is also present in man and small animals (Leitman et al., 2004; Chetboul et al., 2006a; Chetboul et al., 2006b). SL and SrL values did not show this gradient, indicating that all segments shorten almost equally. However, peak SL was significantly lower in the basal septal segment. The basal septal regions also exhibited the lowest contractile indices in the canine and human normal LV (Haendchen et al., 1983; Hurlburt et al., 2007).

Our results demonstrated significant segmental differences of peak timing. The automatically calculated AVC_a was in good agreement with AVC_{MM} and was thus considered the end of systole. Postsystolic motion, defined as SL_G occurring after AVC_a, was present in 31% of segments. This is comparable to human medicine, where postsystolic motion is recorded in about 30% of myocardial segments in healthy people (Voigt et al., 2003). The clinical

relevance of postsystolic motion in supposedly healthy horses requires further investigation. However, postsystolic shortening was predominantly observed in the basal septal segment. In the normal human LV, peak strain was also found to be 35 to 55 ms delayed in the basal septum, which is probably caused by a delayed activation of this segment (Kowalski et al., 2001; Sengupta et al., 2007). This hypothesis is supported by the frequent presence of early systolic SL_P in the basal septal segments in our study. This lengthening of the myocardium arises when a delayed activated segment is passively stretched while the other segments start to contract. In the basal septal segment, a small SL_P can probably be considered as normal. In healthy horses, the variability of SL_P measurements was very high due to the low peak values. However, the presence of a high SL_P in other segments than the basal septal might be useful in a clinical setting as a measure of dyssynchrony.

Surprisingly, a small but significant delay of VL_A and SrL_A in the LV free wall was found. This might be caused by a delayed activation of the left atrium. Due to the location of the sinoatrial node, the right atrium is depolarized before the left atrium. The septum and right ventricular free wall are stretched at the time of right atrial contraction, while stretching of the lateral wall is caused by the subsequent contraction of the left atrium.

The clinical value of LV longitudinal function is extensively documented in human medicine. Several studies have demonstrated that longitudinal function is a sensitive marker for impaired LV function (Lancellotti et al., 2008; Mizuguchi et al., 2008; Marciniak et al., 2009). In asymptomatic patients with mitral valve disease, myocardial dysfunction can be detected by a decrease in longitudinal shortening. This systolic dysfunction is present before changes in conventional echocardiographic measurements occur. The underlying mechanism is the high vulnerability of the subendocardial longitudinal fibres, whereas the circumferential fibres are less prone to myocardial damage and compensate for the loss of longitudinal function (Lee et al., 2004). Further studies are required to evaluate if equine LV longitudinal function is also altered by valvular regurgitation. As of yet, the only studies on the use of 2DST in equine cardiology were conducted on healthy adult horses at rest and after exercise (Schwarzwald et al., 2009a; Schefer et al., 2010). SL_G, SrL_S, DL_S and time to peak SL_G have been used to quantify LV longitudinal function. At resting heart rates, peak values and timing were similar to those reported in our study. Significant alterations were demonstrated during post-exercise stress echocardiography. However, it remains to be determined whether 2DST measurements can be used to detect stress-induced hypokinesia, akinesia or LV dyssynchrony.

The main limitations of our study were inherent to the 2DST technique. An adequate image quality is a prerequisite for accurate tracking. Artefacts such as reverberations and drop-out should be avoided during image acquisition, as they have a detrimental effect on the tracking quality. A thorough visual assessment of image quality is recommended before starting off-line analysis. A more hidden drawback of 2DST is the extensive smoothing of the curves. This might result in normally appearing curves even when visual tracking quality is poor. For this reason, visual evaluation of tracking quality is indispensable and should be performed before approving any results.

Measurements of longitudinal function were not compared to a gold standard, as there is no such technique available in horses. However, 2DST has been extensively validated in vitro, in animal models and in man, using sonomicrometry and MRI (Korinek et al., 2005; Amundsen et al., 2006; Sivesgaard et al., 2009). Therefore it can be assumed that the 2DST measurements are closely correlated to the actual deformation of the equine ventricular walls. It should be noted that our results may only be valid for 2DST analyses using the same ultrasound machine, transducer and off-line analysis software and settings.

Our study was performed on ten horses. A larger study population would have allowed to establish more accurate reference values and to identify influences of body weight, height, breed, sex and training. This was beyond the scope of this study. Nevertheless, based on our results, preliminary reference values for healthy horses could be formulated.

In conclusion, 2DST was found to be a reliable technique for measuring left ventricular systolic longitudinal strain, strain rate, velocity and displacement. These measurements offer new insights into equine ventricular motion and enable a more complete quantification of myocardial function. Further research should be performed in a larger population of healthy and diseased horses to evaluate the value of this technique in horses with cardiac disease.

References

Amundsen BH, Helle-Valle T, Edvardsen T, Torp H, Crosby J, Lyseggen E, Stoylen A, Ihlen H, Lima JA, Smiseth OA, Slordahl SA (2006). Noninvasive myocardial strain measurement by speckle tracking echocardiography: Validation against sonomicrometry and tagged magnetic resonance imaging. J Am Coll Cardiol 47, 789-793

Chetboul V, Sampedrano CC, Gouni V, Nicolle AP, Pouchelon JL, Tissier R (2006a). Ultrasonographic assessment of regional radial and longitudinal systolic function in healthy awake dogs. J Vet Intern Med 20, 885-893

Chetboul V, Sampedrano CC, Tissier R, Gouni V, Saponaro V, Nicolle AP, Pouchelon JL (2006b). Quantitative assessment of velocities of the annulus of the left atrioventricular valve and left ventricular free wall in healthy cats by use of two-dimensional color tissue Doppler imaging. Am J Vet Res 67, 250-258

Chetboul V, Serres F, Gouni V, Tissier R, Pouchelon JL (2007). Radial strain and strain rate by two-dimensional speckle tracking echocardiography and the tissue velocity based technique in the dog. J Vet Cardiol 9, 69-81

D'hooge J, Heimdal A, Jamal F, Kukulski T, Bijnens B, Rademakers F, Hatle L, Suetens P, Sutherland GR (2000). Regional strain and strain rate measurements by cardiac ultrasound: Principles, implementation and limitations. Eur J Echocardiogr 1, 154-170

Gehlen H, Iversen C, Stadler P (2009). Tissue Doppler echocardiographic examinations at rest and after exercise in horses with atrial fibrillation. Pferdeheilkunde 25, 11-16

Haendchen RV, Wyatt HL, Maurer G, Zwehl W, Bear M, Meerbaum S, Corday E (1983). Quantitation of regional cardiac function by two-dimensional echocardiography. I. Patterns of contraction in the normal left ventricle. Circulation 67, 1234-1245

Hurlburt HM, Aurigemma GP, Hill JC, Narayanan A, Gaasch WH, Vinch CS, Meyer TE, Tighe DA (2007). Direct ultrasound measurement of longitudinal, circumferential, and radial strain using 2-dimensional strain imaging in normal adults. Echocardiography 24, 723-731

Korinek J, Wang J, Sengupta PP, Miyazaki C, Kjaergaard J, McMahon E, Abraham TP, Belohlavek M (2005). Two-dimensional strain - a Doppler-independent ultrasound method for quantitation of regional deformation: Validation in vitro and in vivo. J Am Soc Echocardiogr 18, 1247-1253

Kowalski M, Kukulski T, Jamal F, D'hooge J, Weidemann F, Rademakers F, Bijnens B, Hatle L, Sutherland GR (2001). Can natural strain and strain rate quantify regional myocardial deformation? A study in healthy subjects. Ultrasound Med Biol 27, 1087-1097

Lancellotti P, Cosyns B, Zacharakis D, Attena E, Van Camp G, Gach O, Radermecker M, Pierard LA (2008). Importance of left ventricular longitudinal function and functional reserve in patients with degenerative mitral regurgitation: Assessment by two-dimensional speckle tracking. J Am Soc Echocardiogr 21, 1331-1336

Lee R, Hanekom L, Marwick TH, Leano R, Wahi S (2004). Prediction of subclinical left ventricular dysfunction with strain rate imaging in patients with asymptomatic severe mitral regurgitation. Am J Cardiol 94, 1333-1337

Leitman M, Lysyansky P, Sidenko S, Shir V, Peleg E, Binenbaum M, Kaluski E, Krakover R, Vered Z (2004). Two-dimensional strain - a novel software for real-time quantitative echocardiographic assessment of myocardial function. J Am Soc Echocardiogr 17, 1021-1029

Long KJ, Bonagura JD, Darke PG (1992). Standardised imaging technique for guided M-mode and Doppler echocardiography in the horse. Equine Vet J 24, 226-235

Marciniak A, Sutherland GR, Marciniak M, Claus P, Bijnens B, Jahangiri M (2009). Myocardial deformation abnormalities in patients with aortic regurgitation: A strain rate imaging study. Eur J Echocardiogr 10, 112-119

Mizuguchi Y, Oishi Y, Miyoshi H, Iuchi A, Nagase N, Oki T (2008). The functional role of longitudinal, circumferential, and radial myocardial deformation for regulating the early impairment of left ventricular contraction and relaxation in patients with cardiovascular risk factors: A study with two-dimensional strain imaging. J Am Soc Echocardiogr 21, 1138-1144

Patteson MW, Gibbs C, Wotton PR, Cripps PJ (1995). Echocardiographic measurements of cardiac dimensions and indices of cardiac function in normal adult Thoroughbred horses. Equine Vet J Suppl 19, 18-27

Schefer KD, Bitschnau C, Weishaupt MA, Schwarzwald CC (2010). Quantitative analysis of stress echocardiograms in healthy horses with 2-dimensional (2D) echocardiography, anatomical M-mode, tissue Doppler imaging, and 2D speckle tracking. J Vet Intern Med 24, 918-931

Schwarzwald CC, Schober KE, Berli AS, Bonagura JD (2009a). Left ventricular radial and circumferential wall motion analysis in horses using strain, strain rate, and displacement by 2D speckle tracking. J Vet Intern Med 23, 890-900

Schwarzwald CC, Schober KE, Bonagura JD (2007). Methods and reliability of echocardiographic assessment of left atrial size and mechanical function in horses. Am J Vet Res 68, 735-747

Schwarzwald CC, Schober KE, Bonagura JD (2009b). Methods and reliability of tissue Doppler imaging for assessment of left ventricular radial wall motion in horses. J Vet Intern Med 23, 643-652

Sengupta PP, Krishnamoorthy VK, Korinek J, Narula J, Vannan MA, Lester SJ, Tajik JA, Seward JB, Khandheria BK, Belohlavek M (2007). Left ventricular form and function revisited: Applied translational science to cardiovascular ultrasound imaging. J Am Soc Echocardiogr 20, 539-551

Sepulveda MF, Perkins JD, Bowen IM, Marr CM (2005). Demonstration of regional differences in equine ventricular myocardial velocity in normal 2-year-old Thoroughbreds with Doppler tissue imaging. Equine Vet J 37, 222-226

Sivesgaard K, Christensen SD, Nygaard H, Hasenkam JM, Sloth E (2009). Speckle tracking ultrasound is independent of insonation angle and gain: An in vitro investigation of agreement with sonomicrometry. J Am Soc Echocardiogr 22, 852-858

Suffoletto MS, Dohi K, Cannesson M, Saba S, Gorcsan J (2006). Novel speckle-tracking radial strain from routine black-and-white echocardiographic images to quantify dyssynchrony and predict response to cardiac resynchronization therapy. Circulation 113, 960-968

Sutherland GR, Hatle L, Claus P, Herbots L, Separovic J (2006). Normal data. In: Sutherland GR, Hatle L, Claus P, D'hooge J, Bijnens B, editors. Doppler myocardial imaging: A textbook, BSWK Scientific Consulting and Publishing, 49-102

Teske AJ, De Boeck BW, Melman PG, Sieswerda GT, Doevendans PA, Cramer MJ (2007). Echocardiographic quantification of myocardial function using tissue deformation imaging, a guide to image acquisition and analysis using tissue Doppler and speckle tracking. Cardiovasc Ultrasound 5, 27-45

Thorstensen A, Dalen H, Amundsen BH, Aase SA, Stoylen A (2010). Reproducibility in echocardiographic assessment of the left ventricular global and regional function, the HUNT study. Eur J Echocardiogr 11, 149-156

Voigt JU, Lindenmeier G, Exner B, Regenfus M, Werner D, Reulbach U, Nixdorff U, Flachskampf FA, Daniel WG (2003). Incidence and characteristics of segmental postsystolic longitudinal shortening in normal, acutely ischemic, and scarred myocardium. J Am Soc Echocardiogr 16, 415-423

Chapter 3.2

Two-dimensional speckle tracking for quantification of left ventricular circumferential and radial wall motion in horses

Adapted from:

Decloedt A, Verheyen T, Sys S, De Clercq D, van Loon G

Department of Large Animal Internal Medicine, Faculty of Veterinary Medicine, Ghent University, Belgium.

Two-dimensional speckle tracking for quantification of left ventricular circumferential and radial wall motion in horses.

Equine Veterinary Journal (2012) EPub Feb 22, doi: 10.1111/j.2042-3306.2012.00549.x

Part of this work was presented at the 8th International Conference on Equine Exercise Physiology, Cape Town, South Africa, November 7-12, 2010.

Summary

Background: The use of two-dimensional speckle tracking (2DST) for quantification of circumferential and radial left ventricular (LV) function has recently been described in horses using short-axis images at chordal but not at papillary muscle level.

Objectives: To compare the feasibility and reliability of 2DST for quantification of circumferential and radial LV function in short-axis images at papillary muscle and chordal level.

Animals: Ten healthy untrained trotter horses; 9.6 ± 4.4 years; 509 ± 58 kg.

Methods: Prospective study. Repeated echocardiographic examinations were performed by two observers from a right parasternal short-axis view at papillary muscle and chordal level. Segmental and averaged peak values and timing of circumferential and radial strain and strain rate, radial displacement and rotation were measured in six LV wall segments in each imaging plane. Global peak values were calculated for circumferential strain and strain rate. The inter- and intra-observer within- and between-day variability and measurement variability were assessed by calculating coefficients of variation for repeated measurements.

Results: 2DST analysis was feasible in each cardiac cycle although tracking was often inadequate during early diastole. Global and averaged systolic circumferential and radial strain and strain rate and radial displacement could be determined with low variability. Diastolic strain rate and systolic rotation showed a moderate variability. Radial segmental measurements were more reliable than circumferential measurements. The interventricular septum showed a higher circumferential and lower radial strain compared to the LV free wall.

Conclusions and clinical importance: 2DST measurements of global and regional circumferential and radial LV wall motion are feasible both at papillary muscle and chordal level. Several measurements showed a good reliability and can be used when evaluating the technique in a clinical setting.

Introduction

Echocardiography is the method of choice for non-invasive assessment of equine left ventricular (LV) function (Bonagura and Blissitt, 1995). Numerous studies have been devoted to the quantification of LV function at rest and post-exercise during stress echocardiography (Reef, 2001; Durando et al., 2006; Sandersen et al., 2006). This is especially important in horses with performance problems, valvular disease or ventricular dysrhythmias. Exercise-induced myocardial dysfunction has been suggested as a possible cause for poor performance (Reef, 2001). LV wall motion abnormalities were reported in horses with valvular disease (Gehlen et al., 2006). The early detection of subtle LV dysfunction in horses with subclinical valvular regurgitation might contribute to providing an accurate prognosis. The value of fractional shortening (FS) in these horses is limited as FS is highly load-dependent, and loading conditions can be altered significantly in horses with valvular disease. Furthermore, FS is a one-dimensional measurement, while LV wall motion occurs in three dimensions.

Two-dimensional speckle tracking (2DST) is a promising technique that allows a detailed quantification of LV wall motion, providing additional insights into global and regional cardiac function. 2DST enables a two-dimensional quantification of myocardial deformation based on tracking acoustic speckles in the greyscale image (Perk et al., 2007). Radial wall thickening during systole is described by a positive radial strain value. Systolic circumferential LV shortening is indicated by a negative circumferential strain value. The change in strain per time unit is the strain rate, expressed in s^{-1}.

2DST has recently been introduced in veterinary cardiology (Chetboul et al., 2007). Circumferential, radial and longitudinal deformation could be quantified in healthy horses at rest and after exercise, but measurements of circumferential strain were unreliable (Schwarzwald et al., 2009; Schefer et al., 2010; Decloedt et al., 2011). However, only short-axis images at chordal level were assessed for evaluation of circumferential and radial LV function. We hypothesized that the reliability of 2DST measurements might be better at papillary muscle level because of the thicker LV wall and less out-of-plane motion at this level. Furthermore, we hypothesized that regional differences exist between papillary muscle and chordal level and between the wall segments within each level.

The aim of this study was to compare the feasibility and reliability of 2DST for quantification of circumferential and radial LV function in short-axis images at papillary muscle and chordal level and to provide reference values for healthy horses.

Material and methods

Study population

The study population consisted of ten healthy untrained trotter horses (seven mares, three geldings) aged 9.6 ± 4.4 years (mean ± standard deviation SD) with a body weight of 509 ± 58 kg. Animal handling and care was performed following the guidelines of the local ethical committee. A comprehensive examination was performed to exclude cardiovascular or respiratory disease.

Echocardiography

All horses were examined at rest with heart rates (HR) below 45 beats per minute, using an ultrasound unit (GE Vivid 7 Dimension, GE Healthcare, Horten, Norway) with phased-array transducer (3S Phased Array Transducer, GE Healthcare, Horten, Norway). A base-apex ECG was recorded simultaneously. At least three non-consecutive cardiac cycles from each view were stored in cineloop format.

M-mode recordings of the aortic valve were made in the right parasternal LV outflow tract long-axis view. For 2DST, short-axis images were recorded at papillary muscle and chordal level. The imaging depth ranged from 26 to 28 cm depending on LV size, with a single focus positioned at 20 cm. A frequency of 1.6/3.2 MHz (octave harmonics) and sector width of 55° were used to achieve a frame rate of at least 40 frames per second (fps). Gain was adjusted for optimal imaging of the myocardium.

Off-line analysis

Off-line analysis was performed using dedicated software (EchoPAC Software Version 108.1.5, GE Healthcare, Horten, Norway). For each cycle, the RR interval and instantaneous HR were recorded. AVC_{MM} was measured as the interval between the peak R wave on the ECG and aortic valve closure in the M-mode image. 2DST measurements were performed semi-automated using the "2D Strain" application. A region of interest (ROI) was placed manually on the myocardium in a frame at end-systole. The inner margin of the ROI was drawn clockwise along the endocardial border, starting at the interventricular septum. The papillary muscles or chordae were not included, resulting in a smooth circular or oval shape. Afterwards, ROI width was adjusted to LV wall thickness. Speckle tracking started automatically, dividing the ROI into six segments (Fig. 1). Segments were defined automatically by the software and labelled based on human nomenclature. The orientation of

our short-axis images (right of the image is caudal) did not correspond to human guidelines. As a result, 'Sept' and 'AntSept' depict the interventricular septum, 'Ant' and 'Lat' depict the caudal free wall and 'Inf' and 'Post' the cranial free wall. Tracking quality for each segment was evaluated automatically by the software and checked visually by the operator. If no approval by the software and acceptable visual tracking were achieved after repeated adjustments of the ROI, the segment was excluded from further analysis. In numerous segments, tracking appeared too slow during early diastole. These segments were used for further analysis if tracking was visually correct during systole and tracking quality was approved by the software.

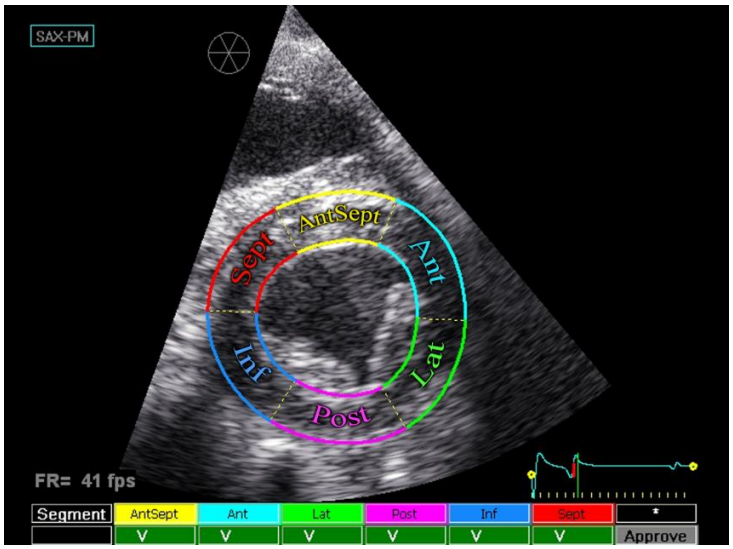

Figure 1: Right parasternal short-axis view at papillary muscle level for 2DST analysis. The right side of the image is caudal, which does not correspond to human guidelines. The ROI is automatically divided into six segments based on standard human nomenclature. Therefore, in our study "Sept" and "AntSept" indicate the interventricular septum; "Ant" and "Lat" the caudal LV free wall and "Post" and "Inf" the cranial LV free wall. Tracking quality is verified by the software and approved segments are marked with a green "V".

Measurements were made in the "Results" screen, providing a graphical and numerical display of the curves and peak values. Segmental traces were displayed for seven modalities: circumferential and radial strain and strain rate, radial displacement, rotation and rotation rate. Rotation rate was not measured as peak values were hard to identify. The default settings were used for spatial and temporal smoothing and for drift compensation. The time of aortic valve closure (AVC_a) was calculated automatically based on the weighted average of time to peak strain in each segment and indicated on the curves. Segmental peak values and timing were indicated automatically for circumferential and radial strain (SC and SR) and systolic (SrC_S and SrR_S), early (SrC_E and SrR_E) and late (SrC_A and SrR_A) diastolic strain rate, systolic radial displacement (DR_S) and rotation (Rot_S). SC_P was measured as a small early-systolic positive peak of circumferential strain (Fig. 2). The automatic detection of peak values was verified visually by the operator and manually adjusted if necessary. Afterwards, the results were exported to a spreadsheet (Microsoft Office Excel 2003, Microsoft Corporation, Redmond, WA) for further analysis.

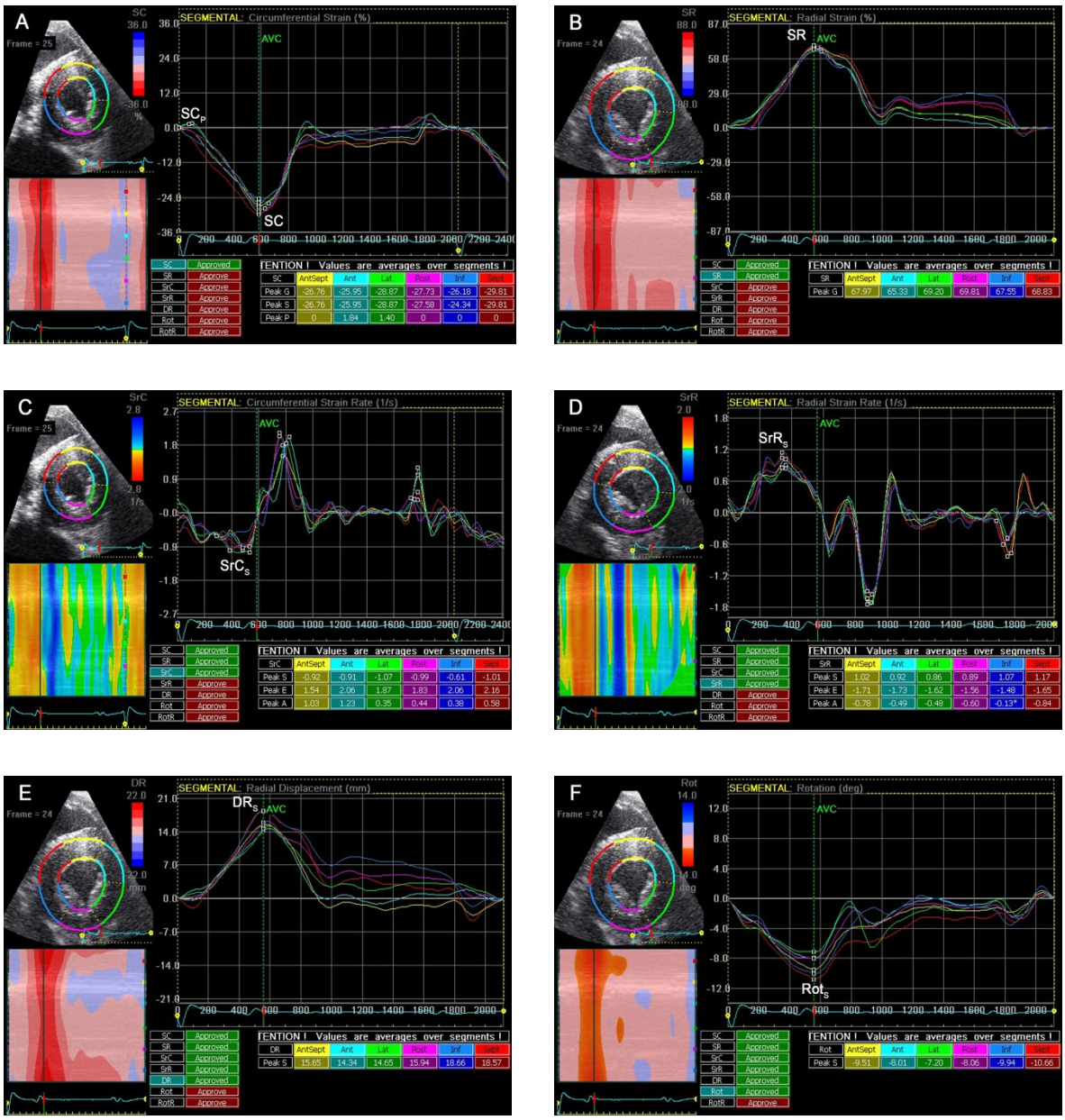

Figure 2: Examples of the segmental curves for a short-axis image at papillary muscle level. On the left, a grayscale image is displayed showing the tracked ROI. A parametric color-coded M-mode is depicted below. On the right, the segmental traces are displayed. The vertical axis represents values of the selected variable; the horizontal axis shows time (ms) and the ECG. AVC_a is marked by a vertical green line. Peak values are automatically indicated on the curves and tabulated below. After visual verification of peak detection and manual adjustment by the operator if necessary, measurements can be approved in the column next to this table. (A) Circumferential strain (%); (B) Radial strain (%); (C) Circumferential strain rate (s^{-1}); (D) Radial strain rate (s^{-1}); (E) Radial displacement (mm); (F) Rotation (°). See Table 1 for remainder of key.

Timing of segmental peak values and AVC_a was automatically reported in the spreadsheet. Late diastolic timings were related to the onset of the preceding P wave, all others to the peak R wave. Global and averaged values were determined as measurements of global LV function. Global values were computed by the software from the whole ROI as a single segment and automatically reported in the spreadsheet for SC and SrC_S. Averaged values were calculated manually as the average of the segmental values for all measurements. Segmental Rot was not tabulated as these measurements have little physiological importance since the heart muscle rotates as one entity. The average of three non-consecutive cycles was used for further analysis.

Reliability of echocardiographic variables

The reliability of 2DST measurements was evaluated by comparing repeated echocardiographic examinations and off-line measurements by two experienced echocardiographers (AD and GvL). All horses were examined by observer 1 on two separate days with an interval of one day. On one of these occasions, this was repeated by observer 2 immediately before or after the first observer. Off-line analysis was first performed by observer 1 for all echocardiographic exams (n=30). Next, on one exam of each horse (n=10), the same three non-consecutive cycles were measured by both observers on a separate occasion to determine measurement variability. At any time, observers were blinded to echocardiographer, horse, day and any previous results.

Data Analysis and Statistics

Statistical analyses were performed using dedicated computer software (SPSS Statistics 17.0, Rel.17.0.1., Chicago, IL). Reference values (mean ± SD; 10 horses) were calculated based on pooled measurements of all exams for each horse. Within-day interobserver variability was obtained by comparing the results of the echocardiographic exams performed on the same day by observer 1 and 2, both measured by observer 1, in a one-way repeated measures analysis of variance with the horse as the unit of repeated measure. The numerical values for the reported coefficients of variation (CV) were calculated by dividing the square root of the mean square error (MSE) by the grand mean, then multiplied by 100%. Similarly, between-day intra-observer variability was determined by comparing the exams recorded on two separate days by observer 1. Measurement variability was obtained by comparing the results of repeated off-line measurements of one exam per horse on two different days (intra-observer measurement variability) or by two different observers (interobserver measurement

variability). The degree of variability was defined based on the CV: CV<15%, low variability; CV 15-25%, moderate variability; CV>25%, high variability (Schwarzwald et al., 2007).

Peak values and timing in the different segments were compared by repeated measures analysis of variance. When significant ($P<0.05$), post-hoc comparisons were performed using the Bonferroni correction method. A paired t-test was used to compare AVC_a, AVC_{MM} and their corresponding HR, as well as global and averaged SC and SrC_S. Agreement between AVC_a and AVC_{MM} and between AVC_a at chordal and papillary muscle level was assessed by Bland-Altman analyses (Bland and Altman, 1986).

Results

2DST analysis was feasible in all cycles at a frame rate of 41 fps. Tracking quality was approved in 884/900 segments at papillary muscle and 872/900 segments at chordal level. Visual tracking quality was often inadequate in early diastole.

Fig. 2 shows examples of the circumferential and radial strain and strain rate, radial displacement and rotation curves. Tables 1, 2 and 3 show the peak values of global, averaged and segmental 2DST measurements in the study population. SC_P was present in only 325/872 segments at chordal and 287/884 segments at papillary muscle level, mainly in the LV free wall segments (Inf, Lat and Post). Global SrC_S was lower than averaged SrC_S at both levels ($P<0.001$; Table 1). Significant segmental differences were present. At papillary muscle level, SC was lower in Inf, Lat and Post ($P=0.001$; Table 2). At chordal level, SC and SrC_S were lower in Inf and Post ($P<0.001$) and SR was lower in the interventricular septum (Sept and AntSept; $P<0.001$; Table 3).

AVC_a was 507±32 ms at papillary muscle and 565±31 ms at chordal level, with a mean bias of 56 ms (95% limits of agreement 0-112 ms). Both differed significantly from AVC_{MM} (537±34 ms; $P<0.001$). The mean bias was -27 ms at papillary muscle level (95% limits of agreement -77 to 23 ms) and 28 ms at chordal level (95% limits of agreement -27 to 83 ms). The RR interval of 2DST and M-mode recordings did not differ significantly ($P=0.84$ for chordal level; $P=0.90$ for papillary level). Segmental peak timing is provided in Supplementary Tables 1 and 2. Time to peak SC and SR was significantly longer at chordal compared to papillary muscle level ($P<0.001$). Postsystolic radial motion, defined as a peak radial strain value after AVC_a, was present in 288/300 segments at papillary and 193/299 segments at chordal level, affecting all horses. Postsystolic circumferential motion was present in 132/300 segments at papillary and 122/299 segments at chordal level, affecting all horses.

Reliability

Variability of global and averaged peak values was low except for Rot_S and diastolic measurements (Table 1). The CV were generally slightly lower at papillary muscle compared to chordal level. Variability of segmental peak values ranged from low to high at both levels (Tables 2 and 3). Segmental SR could be reliably determined while SC showed a moderate to high variability in Inf, Lat and Post. SC_P showed a very high variability. The CV of peak timing were low, except for time to peak SC_P, SrC_S and SrR_S (Supplementary Tables 1 and 2).

Table 1: Global and averaged values of 2DST measurements of LV function at papillary muscle and chordal level in 10 horses.

Variable	View	Mean	SD	Between-day intra-observer variability CV (%)	Within-day interobserver variability CV (%)	Intra-observer measurement variability CV (%)	Interobserver measurement variability CV (%)
Global SC (%)	CH	-19.3	1.79	8.0	8.6	7.5	10.8
	PM	-19.7	1.88	7.3	10.1	3.5	7.3
Avg SC (%)	CH	-19.6	1.71	8.1	8.4	7.3	10.7
	PM	-19.7	1.86	6.9	10.3	3.4	7.9
Global SrC_S (s^{-1})	CH	-0.63	0.08	13.1	12.7	7.6	13.7
	PM	-0.69	0.09	8.9	8.3	4.6	9.8
Avg SrC_S (s^{-1})	CH	-0.89	0.11	9.2	8.9	5.5	9.9
	PM	-0.86	0.11	9.5	8.4	3.3	6.6
Global SrC_E (s^{-1})	CH	1.22	0.14	14.8	15.3	11.4	13.8
	PM	1.10	0.17	10.7	18.8	5.2	7.6
Avg SrC_E (s^{-1})	CH	1.51	0.16	10.6	13.9	15.7	10.8
	PM	1.40	0.11	8.9	12.8	5.7	6.4
Global SrC_A (s^{-1})	CH	0.38	0.08	20.5	22.4	11.6	14.5
	PM	0.40	0.09	23.1	12.0	7.1	6.2
Avg SrC_A (s^{-1})	CH	0.55	0.13	22.1	22.9	22.7	23.5
	PM	0.60	0.11	18.7	9.8	4.0	5.4
AVC_a (ms)	CH	565	31	3.2	4.0	0.0	0.0
	PM	507	32	3.2	4.5	0.0	0.0
Avg SR (%)	CH	63.0	4.13	8.2	4.4	5.7	4.7
	PM	63.7	3.22	7.3	9.1	2.7	2.4
Avg SrR_S (s^{-1})	CH	1.36	0.14	12.9	7.7	7.0	7.6
	PM	1.25	0.14	8.9	9.8	4.8	4.5
Avg SrR_E (s^{-1})	CH	-1.50	0.28	24.0	24.5	27.8	21.2
	PM	-1.60	0.14	14.5	21.8	6.5	6.7
Avg SrR_A (s^{-1})	CH	-0.70	0.23	43.8	41.4	45.4	47.1
	PM	-0.60	0.16	28.8	25.9	13.4	16.5
Avg DR_S (mm)	CH	16.1	1.17	5.7	3.6	3.7	6.9
	PM	15.4	1.20	6.2	9.2	2.4	5.0
Avg Rot_S (°)	CH	-7.00	1.61	20.9	22.6	19.1	12.1
	PM	-9.68	2.96	20.0	23.0	3.3	3.4

Avg, averaged; CH, chordal level; CV, coefficient of variation; PM, papillary muscle level; SD, standard deviation.

SC, circumferential strain; SrC_S, SrC_E, SrC_A, systolic, early diastolic, late diastolic circumferential strain rate; AVC_a, time of aortic valve closure; SR, radial strain; SrR_S, SrR_E, SrR_A, systolic, early diastolic, late diastolic radial strain rate; DR_S, systolic radial displacement; Rot_S, systolic rotation

Table 2: Segmental peak values of 2DST measurements at papillary muscle level in 10 horses.

Variable	Segment	n	Mean	SD	Between-day intra-observer variability CV (%)	Within-day interobserver variability CV (%)	Intra-observer measurement variability CV (%)	Interobserver measurement variability CV (%)
SC (%)	Ant	145	-22.0	2.02	13.7	14.1	6.1	6.5
	AntSept	148	-23.3	2.32	10.0	11.0	5.6	6.6
	Inf	150	-18.2	2.10	15.4	20.0	6.5	13.2
	Lat	150	-17.1	3.12	18.1	22.2	4.5	11.1
	Post	150	-15.1	3.39	15.5	24.1	9.4	22.9
	Sept	141	-22.5	2.84	12.8	13.7	3.5	8.7
SC_P (%)	Ant	20	0.5	0.37	31.3	8.2	NA	NA
	AntSept	17	0.3	0.43	126	NA	56.8	154
	Inf	73	0.9	0.38	156	67.9	35.3	51.9
	Lat	55	1.1	0.81	168	114	34.4	72.0
	Post	92	1.9	1.03	121	105	28.4	27.0
	Sept	30	0.6	1.18	227	366	17.1	179.4
SrC_S (s^{-1})	Ant	145	-0.9	0.11	9.0	10.9	8.7	7.3
	AntSept	148	-0.9	0.13	17.1	17.1	4.6	9.8
	Inf	150	-0.8	0.13	16.0	15.2	7.5	10.1
	Lat	150	-0.8	0.13	9.7	11.7	7.8	13.2
	Post	150	-0.8	0.13	18.0	16.3	10.4	15.2
	Sept	141	-0.9	0.13	11.1	13.0	6.5	7.8
SrC_E (s^{-1})	Ant	145	1.6	0.22	14.3	15.7	8.7	13.3
	AntSept	148	1.5	0.18	14.7	20.8	8.5	12.9
	Inf	150	1.5	0.29	17.9	19.2	9.1	15.5
	Lat	150	1.2	0.15	15.6	19.7	7.8	7.6
	Post	150	1.2	0.20	11.6	13.7	7.5	10.2
	Sept	141	1.5	0.20	14.6	19.8	8.2	12.6
SrC_A (s^{-1})	Ant	145	0.9	0.21	21.5	12.4	5.2	5.4
	AntSept	148	0.7	0.15	24.5	25.6	6.4	10.8
	Inf	147	0.4	0.08	35.9	26.6	10.3	7.9
	Lat	150	0.6	0.19	28.3	36.9	8.1	9.9
	Post	148	0.4	0.11	38.7	32.4	8.5	18.0
	Sept	141	0.5	0.17	32.8	27.1	14.4	14.0
SR (%)	Ant	145	63.2	5.43	5.2	9.2	4.1	3.0
	AntSept	148	63.9	6.06	5.9	10.4	3.1	2.9
	Inf	150	64.1	4.06	14.1	12.8	3.5	5.6
	Lat	150	62.8	2.91	8.2	9.3	6.6	4.7
	Post	150	63.9	3.16	11.3	9.8	4.1	3.7
	Sept	141	64.3	4.93	9.0	11.7	3.0	5.5
SrR_S (s^{-1})	Ant	145	1.2	0.16	13.6	14.4	5.3	6.6
	AntSept	148	1.2	0.15	15.4	13.0	3.6	6.5
	Inf	150	1.3	0.19	10.1	12.1	8.5	7.2
	Lat	150	1.2	0.15	15.7	14.9	7.6	7.3
	Post	150	1.2	0.15	11.9	12.6	9.6	8.1
	Sept	141	1.3	0.16	13.7	11.5	3.7	7.1

SrR_E (s^{-1})	Ant	145	-1.8	0.22	12.1	25.6	8.3	11.0
	AntSept	148	-1.6	0.24	17.3	22.7	6.4	7.3
	Inf	150	-1.5	0.19	27.3	21.5	12.8	13.4
	Lat	150	-1.6	0.16	11.2	24.7	8.7	10.8
	Post	150	-1.5	0.18	19.3	23.9	6.2	13.1
	Sept	141	-1.6	0.24	22.4	24.5	21.5	9.7
SrR_A (s^{-1})	Ant	139	-0.6	0.17	36.4	33.7	11.6	15.7
	AntSept	144	-0.6	0.18	36.0	36.7	8.8	17.2
	Inf	135	-0.6	0.20	27.1	33.5	32.7	36.2
	Lat	141	-0.6	0.16	32.0	25.9	16.0	22.6
	Post	138	-0.6	0.17	24.8	23.6	25.1	33.4
	Sept	129	-0.6	0.21	36.3	37.9	30.8	23.8
DR_S (mm)	Ant	145	11.9	1.72	17.7	13.6	4.5	7.6
	AntSept	148	15.0	2.69	9.8	9.5	3.1	4.3
	Inf	150	19.4	1.85	10.8	10.2	2.7	5.4
	Lat	150	11.8	2.63	21.7	23.7	4.6	9.4
	Post	150	15.7	2.43	9.1	13.2	3.6	8.3
	Sept	141	18.8	2.66	11.3	11.3	2.7	4.7

CV, coefficient of variation; n, number of segments in which the variable could be determined (on a total of 150); NA, not available; SD, standard deviation.
SC, circumferential strain; SC_P, early-systolic positive circumferential strain; SrC_S, SrC_E, SrC_A, systolic, early diastolic, late diastolic circumferential strain rate; AVC_a, time of aortic valve closure; SR, radial strain; SrR_S, SrR_E, SrR_A, systolic, early diastolic, late diastolic radial strain rate; DR_S, systolic radial displacement.

Table 3: Segmental peak values of 2DST measurements at chordal level in 10 horses.

Variable	Segment	n	Mean	SD	Between-day intra-observer variability CV (%)	Within-day interobserver variability CV (%)	Intra-observer measurement variability CV (%)	Interobserver measurement variability CV (%)
SC (%)	Ant	148	-23.8	2.97	11.2	9.5	3.0	7.0
	AntSept	149	-23.6	2.96	12.8	14.2	5.2	10.1
	Inf	142	-14.5	2.14	13.7	15.7	17.2	21.1
	Lat	147	-20.2	4.25	11.4	13.8	9.4	13.2
	Post	139	-13.7	4.63	32.4	21.7	16.5	20.7
	Sept	147	-21.6	2.07	14.3	15.5	11.6	15.5
SC_P (%)	Ant	5	0.3	0.22	NA	NA	NA	NA
	AntSept	16	0.2	0.14	227	198	178	83.0
	Inf	108	1.4	0.78	98.0	64.6	38.0	51.8
	Lat	45	0.5	0.36	124	144	88.3	65.1
	Post	96	2.5	1.25	77.0	82.6	35.5	37.9
	Sept	55	0.5	0.49	67.9	170	83.2	67.0
SrC_S (s^{-1})	Ant	148	-1.0	0.15	6.5	14.8	5.1	9.4
	AntSept	149	-0.9	0.15	11.7	15.2	8.6	8.0
	Inf	142	-0.8	0.10	21.8	16.7	11.2	16.0
	Lat	147	-0.9	0.14	16.3	10.0	5.6	15.0
	Post	139	-0.8	0.17	32.7	20.2	15.3	23.6
	Sept	147	-0.9	0.12	18.2	10.6	9.6	12.6
SrC_E (s^{-1})	Ant	148	1.7	0.16	22.8	19.7	8.1	10.0
	AntSept	149	1.5	0.24	30.2	21.5	16.0	15.1
	Inf	142	1.4	0.27	18.6	19.2	8.7	15.4
	Lat	147	1.4	0.33	10.7	13.4	12.3	11.0
	Post	139	1.5	0.35	23.2	12.8	13.7	13.9
	Sept	147	1.6	0.24	11.6	18.0	18.2	21.8
SrC_A (s^{-1})	Ant	147	0.8	0.21	21.6	25.9	12.9	11.7
	AntSept	149	0.6	0.17	24.6	39.0	8.1	22.5
	Inf	138	0.4	0.16	40.4	48.6	23.2	34.5
	Lat	147	0.6	0.16	24.8	23.9	19.0	11.8
	Post	139	0.6	0.18	30.3	22.3	11.3	15.3
	Sept	142	0.4	0.15	34.9	28.3	22.3	27.4
SR (%)	Ant	148	65.4	5.02	8.9	7.6	3.6	2.2
	AntSept	149	59.9	6.71	14.4	8.3	6.4	5.8
	Inf	142	63.1	4.23	12.0	10.4	10.1	9.9
	Lat	147	66.3	4.86	6.1	7.2	6.6	5.8
	Post	139	66.1	4.57	8.6	5.5	5.5	8.1
	Sept	147	57.3	6.23	12.1	13.8	15.4	10.4
SrR_S (s^{-1})	Ant	148	1.3	0.14	11.2	8.4	9.7	9.8
	AntSept	149	1.1	0.12	13.7	9.1	6.2	7.2
	Inf	142	1.5	0.21	16.4	15.5	13.2	13.7
	Lat	147	1.5	0.17	15.2	10.4	8.7	8.6
	Post	139	1.5	0.20	22.9	15.1	10.2	11.1
	Sept	147	1.3	0.18	16.6	17.5	9.5	10.2

SrR_E (s^{-1})	Ant	148	-1.7	0.51	21.8	18.4	11.9	13.1
	AntSept	149	-1.5	0.32	16.6	14.9	10.3	10.6
	Inf	142	-1.3	0.28	27.1	10.7	25.4	28.5
	Lat	147	-1.6	0.47	25.2	20.0	15.6	17.4
	Post	139	-1.4	0.34	26.7	19.7	18.4	20.0
	Sept	147	-1.4	0.25	21.2	18.6	22.5	29.1
SrR_A (s^{-1})	Ant	121	-0.6	0.24	33.9	25.2	24.9	32.7
	AntSept	133	-0.5	0.20	25.9	23.4	14.4	16.2
	Inf	134	-0.9	0.23	41.0	39.1	48.7	40.9
	Lat	126	-0.7	0.31	19.0	36.5	25.3	38.5
	Post	129	-0.8	0.31	24.8	35.1	41.1	49.6
	Sept	136	-0.7	0.24	34.3	35.8	29.8	26.8
DR_S (mm)	Ant	148	14.9	2.16	14.2	13.5	3.8	5.3
	AntSept	149	14.3	2.16	12.7	12.5	4.7	6.7
	Inf	142	18.4	2.02	11.7	13.4	7.6	10.9
	Lat	147	15.8	2.14	19.3	19.3	4.4	8.2
	Post	139	17.5	1.65	6.1	8.0	5.1	10.5
	Sept	147	15.8	2.63	19.3	21.5	4.6	8.5

CV, coefficient of variation; n, number of segments in which the variable could be determined (on a total of 150); NA, not available; SD, standard deviation.
SC, circumferential strain; SC_P, early-systolic positive circumferential strain; SrC_S, SrC_E, SrC_A, systolic, early diastolic, late diastolic circumferential strain rate; AVC_a, time of aortic valve closure; SR, radial strain; SrR_S, SrR_E, SrR_A, systolic, early diastolic, late diastolic radial strain rate; DR_S, systolic radial displacement

Discussion

This study demonstrates the feasibility and reliability of 2DST for quantification of circumferential and radial LV function in short-axis images at papillary muscle and chordal level. Global, averaged and regional measurements of peak systolic strain, strain rate and displacement could be determined with low to moderate variability.

2DST measurements were feasible in all cycles at both levels and only 2-3% of segments were excluded due to poor tracking. In long-axis images, 4.3% of segments were excluded in a study using the same horses and conducted by the same observers (Decloedt et al., 2011). In contrast, the feasibility of 2DST in healthy children and adults was better in long-axis than short-axis views (Bussadori et al., 2009). In horses, image quality is generally better and the LV wall is thicker, which might explain the more accurate tracking of short-axis views. However, inadequate tracking was present in early diastole. The frame rate in our study was 41.1 fps, which is within the guidelines of 40 to 90 fps, especially if the low heart rate is taken into consideration. However, higher frame rates might be needed to resolve the fast early diastolic motion by decreasing the frame-to-frame shift of the speckles. Furthermore, the poor early diastolic tracking might also be caused by restrictions in the software algorithm, which is not adapted to the large equine heart.

Peak values were easily identified in all curves except rotation rate, as previously described (Schwarzwald et al., 2009). SC_P was often absent. This peak is caused by stretching of delayed-activated or dysfunctional segments following contraction of adjacent segments (Bijnens et al., 2009). Therefore SC_P should be absent or very small in healthy horses with normal LV activation. SC_P was mainly present in the LV free wall segments (Inf, Lat and Post). This might indicate delayed onset of contraction in these segments. However, the higher imaging depth of the free wall causes less accurate circumferential measurements due to decreased lateral resolution as the ultrasound beams of a curvilinear or phased-array image diverge at higher depth (Shapiro et al., 1998). This reduces lateral tracking quality, which might contribute to the presence of SC_P and the lower SC and SrC_S values in Inf, Lat and Post. The lower SC and SrC_S peak values in the LV free wall have been previously described in horses (Schwarzwald et al., 2009). SR was lower in the interventricular septum at chordal level. This corresponds to the lower strain found in the basal septal segment using longitudinal 2DST (Decloedt et al., 2011). In man and dogs, this region also showed the lowest contractile indexes (Haendchen et al., 1983). The lower wall thickening is

physiologically beneficial to avoid obstruction of the LV outflow tract. In the study of Schwarzwald et al. (2009), SR was lowest in 'Ant' and 'Lat', which represented part of the interventricular septum and LV cranial free wall.

Time to peak SR and SC was longer at chordal level. This is reflected in the automatically calculated AVC_a, which was 56 ms later at chordal compared to papillary muscle level. The different AVC_a should be considered when evaluating postsystolic motion, defined as peak strain occurring after AVC. A high degree of postsystolic motion is associated with myocardial ischemia or hypertrophy in human medicine (Voigt et al., 2003). In our study, postsystolic circumferential and radial strain was present in all horses. This is consistent with previous data on 2DST demonstrating postsystolic radial wall thickening in 80/180 segments, affecting 5/6 apparently healthy horses (Schwarzwald et al., 2009). Therefore postsystolic motion might be physiological in horses.

In contrast to a previous study on 2DST in short-axis images at chordal level (Schwarzwald et al., 2009), global and averaged circumferential strain could be reliably determined. This might be caused by differences in lateral resolution, image quality or the number of animals used. Segmental SC showed a moderate to high variability in the LV free wall segments. Conversely, SR could be reliably quantified in all segments. For global and averaged measurements, variability was slightly higher at chordal compared to papillary muscle level. This may be caused by inferior image quality at chordal level where acoustic shadowing due to coronary fat or the annular ring was present in some loops. The ventricular walls are also thicker at papillary muscle level, resulting in a larger ROI which may explain more accurate tracking. Furthermore, due to systolic longitudinal shortening of the left ventricle towards the apex, the out-of-plane motion is higher at chordal level. Consequently, papillary muscle level seems better suited for 2DST analysis of LV global function. Both global and averaged measurements can be used. However, global SrC_S was significantly lower than averaged SrC_S. This is due to the smoothened global strain rate curve shape, whereas the segmental traces showed short high peaks based on which the averaged value was calculated.

In small animals and man, 2DST has been applied to evaluate LV function in different cardiac diseases. LV radial and circumferential strain rate are useful markers of LV systolic function in patients with chronic MR (Kim et al., 2009). In addition, 2DST allows the evaluation of LV synchrony based on segmental peak timing. Time to peak radial strain was accurate in detecting LV dyssynchrony in a canine model and in human patients for prediction of the

response to cardiac resynchronization therapy (Arita et al., 2007; Delgado et al., 2008). In horses, the accurate quantification of LV dysfunction might contribute to the assessment of subclinical valvular disease. 2DST-derived measurements allow a more complete evaluation of LV function than fractional shortening, which is only one-dimensional and highly load-dependent. The evaluation of LV synchrony by 2DST has already been attempted in healthy horses at rest and after exercise but the reliability of an LV synchrony index was low (Schwarzwald et al., 2009; Schefer et al., 2010).

The use of short-axis images at different LV levels offers the opportunity to calculate LV twist. LV twist or torsion is defined as counter-directional apical rotation relative to the basal rotation around the long axis. Systolic LV twist facilitates the ejection of blood and stores potential energy. The release of this energy by untwisting causes the LV pressure drop and provides suction force for filling (Sengupta et al., 2008). Therefore, twist mechanics play an important role in LV systolic and diastolic function. In dogs, measurements of systolic LV torsion by 2DST were reliable (Chetboul et al., 2008). Unfortunately, Rot_S showed a high variability in our study. Therefore LV torsion was not calculated. Furthermore, the direction of rotation was negative both at papillary muscle and chordal level. This is consistent with the positive peak rotation found by Schwarzwald et al. (2009) as the orientation of short-axis images in our study was opposite. These results indicate a clockwise rotation as viewed from the apex both at papillary and chordal level. In man and dogs, the base also rotates clockwise but the apex rotates counterclockwise. A limitation of this study is that no images were acquired at apical or mitral level. These might provide additional insights into LV twist in horses.

Another limitation is that our results may only be valid for 2DST analyses using the same ultrasound machine, transducer and off-line analysis software and settings. Different settings might result in different variability of certain measurements. 2DST measurements were not compared to a gold standard, as there is no such technique available in horses. However, 2DST has been validated in vitro, in animal models and man, using sonomicrometry and MRI (Korinek et al., 2005; Amundsen et al., 2006). Therefore it can be assumed that the 2DST measurements are closely correlated to the actual deformation of the LV walls. A larger study population would have allowed to establish more accurate reference values and to identify influences of body weight, height, breed, sex and training. This was beyond the scope of this study. Nevertheless, preliminary reference values for healthy horses were formulated.

In conclusion, global, averaged and regional 2DST measurements of circumferential and radial LV wall motion are feasible using short-axis images both at papillary muscle and chordal level. For evaluation of global LV function, global and averaged systolic radial and circumferential strain and strain rate and radial displacement showed a good reliability and can be used in further clinical studies. For evaluation of regional LV function, segmental peak timing and radial strain can be used.

Supplementary Table 1: Peak timing of 2DST measurements at papillary muscle level in 10 horses.

Variable	Segment	Mean	SD	Between-day intra-observer variability CV (%)	Within-day interobserver variability CV (%)	Intra-observer measurement variability CV (%)	Interobserver measurement variability CV (%)
Time to SC (ms)	Ant	512	31	5.8	6.7	1.2	2.3
	AntSept	506	34	4.1	4.5	1.1	1.9
	Inf	522	33	4.8	4.9	2.8	1.1
	Lat	501	39	7.7	7.7	2.8	2.3
	Post	510	28	2.6	4.9	0.8	9.2
	Sept	512	31	4.7	3.9	2.4	3.6
Time to SC_P (ms)	Ant	52	31	79.7	89.5	NA	NA
	AntSept	31	17	128.3	NA	73.7	125.2
	Inf	52	21	95.0	34.0	26.9	50.4
	Lat	72	40	126.0	121.7	45.8	32.3
	Post	84	43	83.7	71.5	42.0	50.6
	Sept	32	23	60.7	93.0	19.7	67.9
Time to SrC_S (ms)	Ant	272	57	16.9	21.1	14.6	23.3
	AntSept	256	71	21.5	13.9	18.9	22.1
	Inf	341	42	15.7	14.9	10.1	9.0
	Lat	308	61	19.1	25.4	16.5	17.6
	Post	332	39	17.3	19.0	11.2	11.5
	Sept	279	49	25.9	25.2	20.0	34.8
Time to SrC_E (ms)	Ant	740	45	4.2	4.1	0.6	2.9
	AntSept	735	43	4.0	3.4	5.3	3.0
	Inf	683	26	5.2	3.0	2.4	3.4
	Lat	707	63	5.4	4.7	5.2	2.3
	Post	670	38	6.3	7.4	2.8	4.3
	Sept	704	45	6.4	3.6	2.6	3.4
Time to SrC_A (ms)	Ant	227	25	7.3	7.4	2.7	2.3
	AntSept	218	27	5.2	9.4	2.8	4.7
	Inf	224	32	17.8	14.9	3.8	3.9
	Lat	201	27	7.5	10.2	2.4	1.3
	Post	201	27	15.5	15.4	2.0	7.9
	Sept	217	28	12.0	10.3	6.0	8.3
Time to SR (ms)	Ant	550	27	7.7	5.5	2.5	2.8
	AntSept	557	29	6.0	5.4	3.0	2.9
	Inf	552	29	4.0	3.9	3.3	2.7
	Lat	543	29	5.3	4.5	2.6	1.0
	Post	541	27	4.4	3.4	2.9	1.4
	Sept	562	27	5.3	5.4	3.5	5.8
Time to SrR_S (ms)	Ant	258	35	22.1	20.6	7.8	9.7
	AntSept	248	36	13.9	18.5	9.8	13.2
	Inf	267	32	17.7	13.3	5.8	19.4
	Lat	261	34	18.6	20.0	5.7	14.6
	Post	258	30	22.1	14.2	5.7	14.4
	Sept	256	34	16.3	18.1	11.4	10.7

Time to SrR_E (ms)	Ant	765	38	3.8	3.2	2.0	0.7
	AntSept	773	41	3.1	3.1	0.6	0.7
	Inf	751	49	4.3	4.9	1.9	1.4
	Lat	760	39	4.6	3.1	2.0	2.2
	Post	750	45	5.3	3.4	3.3	2.4
	Sept	766	43	2.4	2.9	1.0	1.9
Time to SrR_A (ms)	Ant	231	21	12.8	13.7	4.6	3.4
	AntSept	229	22	11.4	11.6	3.7	5.5
	Inf	212	29	10.8	9.0	7.8	6.9
	Lat	230	22	13.0	12.3	4.3	3.1
	Post	224	22	13.7	9.1	6.1	5.8
	Sept	219	24	10.5	10.9	7.9	9.1
Time to DR_S (ms)	Ant	502	30	3.2	5.1	0.0	0.3
	AntSept	501	33	3.5	4.2	0.6	0.5
	Inf	503	30	2.9	4.3	0.7	0.5
	Lat	502	30	3.2	5.1	0.0	0.0
	Post	506	32	3.0	4.3	0.0	0.0
	Sept	497	29	3.6	3.8	0.8	0.8

CV, coefficient of variation; NA, not available; SD, standard deviation.
SC, circumferential strain; SC_P, early-systolic positive circumferential strain; SrC_S, SrC_E, SrC_A, systolic, early diastolic, late diastolic circumferential strain rate; AVC_a, time of aortic valve closure; SR, radial strain; SrR_S, SrR_E, SrR_A, systolic, early diastolic, late diastolic radial strain rate; DR_S, systolic radial displacement.

Supplementary Table 2: Peak timing of 2DST measurements at chordal level in 10 horses.

Variable	Segment	Mean	SD	Between-day intra-observer variability CV (%)	Within-day interobserver variability CV (%)	Intra-observer measurement variability CV (%)	Interobserver measurement variability CV (%)
Time to SC (ms)	Ant	540	22	3.8	5.3	2.3	4.0
	AntSept	566	48	6.4	6.0	2.5	4.5
	Inf	585	45	3.8	6.0	3.8	3.5
	Lat	531	31	6.2	5.3	2.3	3.5
	Post	563	38	7.8	5.7	6.1	4.3
	Sept	571	32	4.5	5.6	3.3	2.6
Time to SC_P (ms)	Ant	21	11	NA	NA	NA	NA
	AntSept	17	9	199.2	187.7	140.5	173.6
	Inf	86	30	93.2	83.1	51.1	72.9
	Lat	46	35	121.8	168.0	23.2	54.7
	Post	130	55	71.5	65.2	30.4	32.1
	Sept	29	17	71.9	116.1	76.8	26.0
Time to SrC_S (ms)	Ant	279	48	18.8	24.2	24.0	19.5
	AntSept	259	44	27.1	28.4	15.1	20.2
	Inf	368	46	21.0	15.0	13.3	21.1
	Lat	338	75	19.6	15.7	13.3	19.6
	Post	357	63	27.9	22.4	19.9	19.3
	Sept	274	58	21.2	23.2	22.9	20.5
Time to SrC_E (ms)	Ant	723	36	4.1	3.3	0.6	1.3
	AntSept	715	37	3.3	2.1	2.0	2.5
	Inf	680	30	3.7	2.7	2.6	3.9
	Lat	681	31	2.2	3.2	2.3	2.0
	Post	678	28	5.8	2.9	3.7	8.0
	Sept	684	35	2.2	2.3	1.0	1.8
Time to SrC_A (ms)	Ant	216	17	6.5	6.8	5.6	2.6
	AntSept	210	21	14.1	12.8	3.5	5.5
	Inf	200	26	16.5	17.6	7.9	13.8
	Lat	201	23	6.3	7.2	3.3	5.2
	Post	185	30	13.4	11.6	3.6	9.9
	Sept	209	30	9.5	17.5	12.2	13.2
Time to SR (ms)	Ant	573	25	6.3	4.8	3.9	5.3
	AntSept	597	34	4.1	5.2	4.0	3.8
	Inf	584	25	4.6	6.3	4.0	3.3
	Lat	563	24	4.9	3.4	3.1	6.7
	Post	568	26	5.4	4.0	2.5	5.6
	Sept	609	37	4.0	5.8	3.8	2.8
Time to SrR_S (ms)	Ant	233	33	19.0	26.6	22.4	22.1
	AntSept	221	36	18.2	24.0	16.1	31.9
	Inf	247	25	23.9	16.4	21.7	21.8
	Lat	247	31	17.8	20.3	16.1	13.5
	Post	253	29	18.2	16.8	15.5	21.4
	Sept	228	21	25.0	16.3	14.8	22.5

Time to SrR_E (ms)	Ant	728	30	2.7	2.6	2.6	3.4
	AntSept	729	38	2.3	3.1	1.6	2.1
	Inf	731	21	4.4	3.0	3.0	4.6
	Lat	732	22	3.0	4.9	1.9	5.0
	Post	733	24	4.7	5.1	3.5	5.2
	Sept	733	34	2.9	4.1	4.4	2.9
Time to SrR_A (ms)	Ant	223	21	5.9	9.8	6.4	12.3
	AntSept	212	23	10.7	14.7	9.5	6.8
	Inf	218	17	7.9	8.5	6.6	6.7
	Lat	222	22	4.4	7.3	5.0	6.4
	Post	215	19	7.6	6.2	13.5	11.5
	Sept	215	20	6.6	9.0	7.3	6.3
Time to DR_S (ms)	Ant	557	29	3.8	3.8	0.8	0.4
	AntSept	550	31	2.9	3.0	1.9	2.2
	Inf	549	37	3.1	3.9	1.5	2.4
	Lat	557	29	2.7	4.1	0.6	0.5
	Post	553	29	5.3	3.2	0.9	1.1
	Sept	547	42	4.7	4.2	1.4	1.7

CV, coefficient of variation; NA, not available; SD, standard deviation.
SC, circumferential strain; SC_P, early-systolic positive circumferential strain; SrC_S, SrC_E, SrC_A, systolic, early diastolic, late diastolic circumferential strain rate; AVC_a, time of aortic valve closure; SR, radial strain; SrR_S, SrR_E, SrR_A, systolic, early diastolic, late diastolic radial strain rate; DR_S, systolic radial displacement.

References

Amundsen BH, Helle-Valle T, Edvardsen T, Torp H, Crosby J, Lyseggen E, Stoylen A, Ihlen H, Lima JA, Smiseth OA, Slordahl SA (2006). Noninvasive myocardial strain measurement by speckle tracking echocardiography: Validation against sonomicrometry and tagged magnetic resonance imaging. J Am Coll Cardiol 47, 789-793

Arita T, Sorescu GP, Schuler BT, Schmarkey LS, Merlino JD, Vinten-Johansen J, Leon AR, Martin RP, Sorescu D (2007). Speckle-tracking strain echocardiography for detecting cardiac dyssynchrony in a canine model of dyssynchrony and heart failure. Am J Physiol Heart Circ Physiol 293, H735-H742

Bijnens BH, Cikes M, Claus P, Sutherland GR (2009). Velocity and deformation imaging for the assessment of myocardial dysfunction. Eur J Echocardiogr 10, 216-226

Bland JM, Altman DG (1986). Statistical-methods for assessing agreement between 2 methods of clinical measurement. Lancet 1, 307-310

Bonagura JD, Blissitt KJ (1995). Echocardiography. Equine Vet J 27 Suppl 19, 5-17

Bussadori C, Moreo A, Di Donato M, De Chiara B, Negura D, Dall'Aglio E, Lobiati E, Chessa M, Arcidiacono C, Dua JS, Mauri F, Carminati M (2009). A new 2D-based method for myocardial velocity strain and strain rate quantification in a normal adult and paediatric population: Assessment of reference values. Cardiovasc Ultrasound 7, 8

Chetboul V, Serres F, Gouni V, Tissier R, Pouchelon JL (2007). Radial strain and strain rate by two-dimensional speckle tracking echocardiography and the tissue velocity based technique in the dog. J Vet Cardiol 9, 69-81

Chetboul V, Serres F, Gouni V, Tissier R, Pouchelon JL (2008). Noninvasive assessment of systolic left ventricular torsion by 2-dimensional speckle tracking imaging in the awake dog: Repeatability, reproducibility, and comparison with tissue Doppler imaging variables. J Vet Intern Med 22, 342-350

Decloedt A, Verheyen T, Sys S, De Clercq D, van Loon G (2011). Quantification of left ventricular longitudinal strain, strain rate, velocity, and displacement in healthy horses by 2-dimensional speckle tracking. J Vet Intern Med 25, 330-338

Delgado V, Ypenburg C, van Bommel RJ, Tops LF, Mollema SA, Marsan NA, Bleeker GB, Schalij MJ, Bax JJ (2008). Assessment of left ventricular dyssynchrony by speckle tracking strain imaging - comparison between longitudinal, circumferential, and radial strain in cardiac resynchronization therapy. J Am Coll Cardiol 51, 1944-1952

Durando MM, Slack J, Reef VB, Birks EK (2006). Right ventricular pressure dynamics and stress echocardiography in pharmacological and exercise stress testing. Equine Vet J 38 Suppl 36, 183-192

Gehlen H, Sundermann T, Rohn K, Stadler P (2006). Feasability of stress-echocardiography for detecting exercise induced myocardial dysfunction in horses with heart valve insufficiencies. Pferdeheilkunde 22, 757-766

Haendchen RV, Wyatt HL, Maurer G, Zwehl W, Bear M, Meerbaum S, Corday E (1983). Quantitation of regional cardiac function by two-dimensional echocardiography. I. Patterns of contraction in the normal left ventricle. Circulation 67, 1234-1245

Kim MS, Kim YJ, Kim HK, Han JY, Chun HG, Kim HC, Sohn DW, Oh BH, Park YB (2009). Evaluation of left ventricular short- and long-axis function in severe mitral regurgitation using 2-dimensional strain echocardiography. Am Heart J 157, 345-351

Korinek J, Wang J, Sengupta PP, Miyazaki C, Kjaergaard J, McMahon E, Abraham TP, Belohlavek M (2005). Two-dimensional strain - a Doppler-independent ultrasound method for quantitation of regional deformation: Validation in vitro and in vivo. J Am Soc Echocardiogr 18, 1247-1253

Perk G, Tunick PA, Kronzon I (2007). Non-Doppler two-dimensional strain imaging by echocardiography - from technical considerations to clinical applications. J Am Soc Echocardiogr 20, 234-243

Reef VB (2001). Stress echocardiography and its role in performance assessment. Vet Clin North Am Equine Pract 17, 179-189, viii

Sandersen C, Detilleux J, Art T, Amory H (2006). Exercise and pharmacological stress echocardiography in healthy horses. Equine Vet J Suppl 36, 159-162

Schefer KD, Bitschnau C, Weishaupt MA, Schwarzwald CC (2010). Quantitative analysis of stress echocardiograms in healthy horses with 2-dimensional (2D) echocardiography, anatomical M-mode, tissue Doppler imaging, and 2D speckle tracking. J Vet Intern Med 24, 918-931

Schwarzwald CC, Schober KE, Berli AS, Bonagura JD (2009). Left ventricular radial and circumferential wall motion analysis in horses using strain, strain rate, and displacement by 2D speckle tracking. J Vet Intern Med 23, 890-900

Schwarzwald CC, Schober KE, Bonagura JD (2007). Methods and reliability of echocardiographic assessment of left atrial size and mechanical function in horses. Am J Vet Res 68, 735-747

Sengupta PP, Tajik AJ, Chandrasekaran K, Khandheria BK (2008). Twist mechanics of the left ventricle: Principles and application. JACC. Cardiovasc imag 1, 366-376

Shapiro RS, Wagreich J, Parsons RB, Stancato-Pasik A, Yeh HC, Lao R (1998). Tissue harmonic imaging sonography: Evaluation of image quality compared with conventional sonography. AJR. Am J Roentgenol 171, 1203-1206

Voigt JU, Lindenmeier G, Exner B, Regenfus M, Werner D, Reulbach U, Nixdorff U, Flachskampf FA, Daniel WG (2003). Incidence and characteristics of segmental postsystolic longitudinal shortening in normal, acutely ischemic, and scarred myocardium. J Am Soc Echocardiogr 16, 415-423

Chapter 3.3

Tissue Doppler imaging for regional quantification of radial left ventricular wall motion in horses

Adapted from:

Decloedt A, Verheyen T, Sys S, De Clercq D, van Loon G

Department of Large Animal Internal Medicine, Faculty of Veterinary Medicine, Ghent University, Belgium.

Tissue Doppler imaging for regional quantification of radial left ventricular wall motion in horses.

American Journal of Veterinary Research (2012). Revised manuscript submitted.

Part of this work was presented at the 42nd European Veterinary Conference (Voorjaarsdagen), Amsterdam, The Netherlands, April 23-24, 2009

Summary

Background: Tissue Doppler imaging (TDI) is increasingly used in veterinary cardiology for quantification of left ventricular (LV) function.

Objectives: To compare the feasibility and reliability of TDI for quantifying radial myocardial velocity and deformation from different imaging planes in horses and to correlate TDI-derived cardiac event time intervals to M-mode- and pulsed wave (PW) Doppler-derived cardiac event time intervals.

Animals: Ten healthy untrained trotter horses; 9.6 ± 4.4 years; 509 ± 58 kg.

Procedures: Repeated echocardiographic examinations were performed by two observers from right and left parasternal short-axis views at papillary muscle and chordal level. TDI measurements of systolic and diastolic peak velocity, strain rate and strain and time intervals were performed in two LV wall segments per view. The inter- and intra-observer within- and between-day variability and measurement variability were assessed by calculating coefficients of variation for repeated measurements. The correlation between TDI-derived, M-mode- and PW Doppler-derived time measurements was calculated.

Results: TDI measurements of velocity, strain rate and strain were feasible in each loop, although strain rate and strain could often not be measured in the LV free wall from right parasternal views. Systolic and diastolic time intervals could be determined with low to moderate variability while peak amplitude variability ranged from low to high. TDI-based time measurements were significantly correlated to M-mode and PW Doppler measurements.

Conclusions and Clinical Relevance: TDI measurements of radial LV velocity and deformation were feasible in two LV segments from four views (right and left short-axis views at papillary muscle and chordal level). This study appoints measurements with reasonable reliability that need to be further assessed in a clinical setting.

Introduction

Tissue Doppler imaging (TDI) is increasingly used in veterinary cardiology to evaluate left ventricular (LV) function. TDI allows quantification of systolic and diastolic myocardial velocities based on the Doppler principle. Conventional color flow Doppler measures the high frequency, low amplitude signals from the blood pool using high pass filtering. In contrast, TDI captures the high intensity, low velocity myocardial signals using a low pass filter (Brodin, 2004). A limitation of the Doppler principle is that measurements are restricted to the direction of the ultrasound beam. As the acquisition of apical images is impossible in adult horses, only radial myocardial velocity and deformation can be assessed by TDI using parasternal images. Deformation indices are calculated from the myocardial velocity gradient between the endo- and epicardium (Pellerin et al., 2003). Strain is defined as the total amount of myocardial deformation, expressed as a percentage relative to the end-diastolic wall thickness. The change in strain per time unit is the strain rate, expressed in s^{-1}.

In small animals, the reliability of TDI and its use for early detection of impaired LV function in cardiomyopathy have been extensively described (Chetboul et al., 2005; O'Sullivan et al., 2007; Wess et al., 2010). In equine cardiology, the feasibility and reliability of TDI have been studied in healthy horses at rest and post-exercise (Sepulveda et al., 2005; Schwarzwald et al., 2009; Schefer et al., 2010). In a horse with nutritional masseter myodegeneration, systolic and diastolic myocardial dysfunction could be quantified by pulsed wave (PW) TDI (Schefer et al., 2011). However, the reliability of TDI measurements in horses has been assessed in only one LV free wall segment from a right parasternal short-axis view (Schwarzwald et al., 2009). In this study, deformation indices were unreliable. It is unknown whether the use of other segments and left parasternal views might allow strain and strain rate measurements in horses. Furthermore, TDI allows accurate timing of cardiac events because of the high frame rate. However, the relationship between TDI-based and M-mode or PW Doppler-based cardiac event timings has not been studied in horses yet.

The aim of this study was to compare the feasibility and reliability of TDI for quantification of myocardial velocity and deformation in eight LV wall segments from right and left parasternal short-axis views at papillary muscle and chordal level. TDI-derived cardiac event timing by TDI was compared to measurements obtained by M-mode and PW Doppler.

Material and methods

Study population

The study population consisted of ten healthy untrained trotter horses (seven mares, three geldings) aged 9.6 ± 4.4 years (mean ± standard deviation SD) with a body weight of 509 ± 58 kg. Animal handling and care was performed following the guidelines of the local ethical committee. A comprehensive examination was performed prior to the study to exclude cardiovascular or respiratory disease.

Echocardiography

All horses were examined at heart rates below 45 beats per minute, using an ultrasound unit (GE Vivid 7 Dimension, GE Healthcare, Horten, Norway) with phased array transducer (3S Phased Array Transducer, GE Healthcare, Horten, Norway) at a frequency of 1.7/3.4 MHz. A base-apex ECG was recorded simultaneously. Right parasternal LV outflow tract M-mode recordings were made for timing of aortic valve opening and closure. Aortic flow was measured by PW Doppler from a left parasternal imaging plane. Mitral valve motion was assessed from a right parasternal short-axis M-mode image. At least three non-consecutive cardiac cycles from each view were stored in cineloop format.

For color-coded tissue Doppler images, the greyscale width was reduced to 30° and the TDI sector was narrowed maximally. The imaging depth ranged from 26 to 28 cm depending on LV size, with a single focus positioned at 20 cm. The velocity scale was set from +32 to –32 cm/s, resulting in a frame rate of 183 frames per second (fps). Right and left parasternal short-axis views were acquired both at papillary and chordal level. The probe was turned 90° counterclockwise to obtain short-axis images of the LV. As a result, the right side of LV cross-section was caudal for the right parasternal short-axis views and cranial for the left parasternal views. The image was tilted for optimal alignment of radial wall motion to the ultrasound beam. At least three consecutive cardiac cycles from each view were stored in cineloop format.

Determination of M-mode and PW Doppler indices

All off-line measurements were performed using dedicated software (EchoPAC Software Version 108.1.5, GE Healthcare, Horten, Norway). Time to aortic valve opening (AVO_{MM}) and closure (AVC_{MM}) and mitral valve opening (MVO_{MM}) were measured as the time interval between the peak R wave on the ECG and valve opening or closure in the M-mode image.

Timing of aortic valve opening and closure by PW Doppler (AVO_{PW} and AVC_{PW}) were measured as the time interval between the R wave and onset or end of aortic flow. The average of three non-consecutive cycles was used for further analysis.

Determination of TDI indices

Loops of three consecutive cycles were analysed using the "Q-analysis"-mode of the software. The interventricular septum (IVS) and LV free wall (LVFW) were evaluated from right parasternal views (Fig. 1). From the left parasternal imaging planes, the left and right region of the LV wall (LLV and RLV) were assessed (Sepulveda et al., 2005). Fig. 2 and 3 show the position of sample areas in each segment. Sample area length (12-17 mm) and width (5-6 mm) were adapted to wall thickness. The sample area was anchored inside the myocardium using the proprietary software available in the workstation. This facilitated tracking of the motion of the myocardial segments during the cardiac cycle. The sample area was set to the inside of the myocardium at the time of peak R on the ECG and at the end of systole, early diastole, diastasis and atrial contraction.

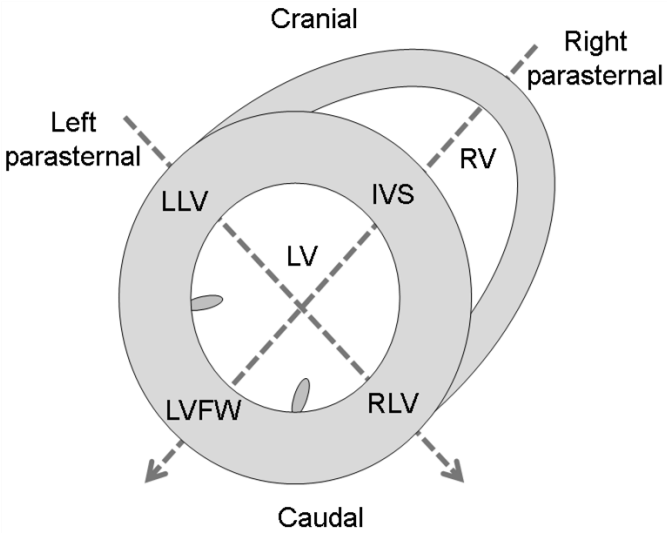

Fig. 1: Schematic short-axis cross-section of the equine left (LV) and right (RV) ventricle at chordal level. The dashed arrows indicate the direction of the ultrasound beam from a left and right parasternal view. The four left ventricular segments that can be assessed are indicated by their abbreviations. IVS, interventricular septum; LLV, left region of the left ventricular wall; LVFW, left ventricular free wall; RLV, right region of the left ventricular wall.

The software displayed segmental velocity, strain rate and strain curves. A 30 ms temporal smoothing filter was applied. Strain was calculated over a strain length or offset distance of 12 mm and linear drift compensation was used. The cine compound function was used to convert the last cycle into the average of the three consecutive cycles. Measurements were made in this cycle. In the velocity and strain rate curves, peak values and timing were measured during isovolumic contraction (IVC), systole (Syst), isovolumic relaxation (IVR), early (E) and late (A) diastole (Fig. 2A-B and Fig. 3A-B). All late diastolic timings were

related to the onset of the preceding P wave, all others to the peak R wave. The time to onset and end of systole were defined as the pre-ejection period (PEP) and end-ejection time (EET). The time to onset of E and A were measured and duration of the late diastolic peak (dur A) was calculated as end A–onset A. In the strain curve, peak strain (St) and its timing were measured (Fig. 2C and 3C).

Reliability of echocardiographic variables

The reliability of TDI measurements was evaluated by comparing repeated echocardiographic examinations and offline measurements performed by two experienced echocardiographers (AD and GvL). All horses were examined by observer 1 on two separate days with a one day interval. On one of these occasions, the examination was repeated by observer 2 immediately before or after observer 1. Offline analysis was first performed by observer 1 for all exams (n=30). Next, on one exam of each horse (n=10), the same three consecutive cycles were measured by both observers on a separate occasion. At any time, observers were blinded to echocardiographer, horse, day and any previous results.

Statistical analysis

Statistical analyses were performed using dedicated software (SPSS Statistics 17.0, Rel.17.0.1., SPSS Inc, Chicago, IL). Reference values (mean ± SD; 10 horses) were calculated based on pooled measurements of all exams for each horse. Within-day interobserver variability was obtained by comparing the results of the echocardiographic exams performed on the same day by observer 1 and 2, both measured by observer 1, in a one-way repeated measures analysis of variance with the horse as the unit of repeated measure. The numerical values for the reported coefficients of variation (CV) were calculated by dividing the square root of the mean square error (MSE) by the grand mean, then multiplied by 100%. Similarly, between-day intra-observer variability was determined by comparing the exams recorded on two separate days by observer 1. Measurement variability was obtained by comparing the results of repeated off-line measurements of one exam per horse on two different days (intra-observer measurement variability) or by two different observers (interobserver measurement variability). The degree of variability was defined based on the CV: CV<15%, low variability; CV 15-25%, moderate variability; CV>25%, high variability (Schwarzwald et al., 2007b).

Measurements from different segments and views were compared by a linear mixed model (level of significance $P<0.05$). Agreement between conventional and TDI-based timings was assessed by simple linear regression.

Results

TDI curves could be obtained in each segment from all views at a frame rate of 183 fps. Peak values and timing could be easily identified in most curves, although the IVC and IVR peaks were often absent. At both papillary muscle and chordal level, IVC was most often absent in the velocity curves of IVS and the velocity and strain rate curves of RLV. IVR was more often absent at chordal compared to papillary muscle level in all segments. Furthermore, some peaks could not be identified due to inadequate curve quality. This mainly affected strain rate and strain in LVFW, which could frequently not be measured. As a result, the coefficients of variation of these measurements could not be calculated.

Mean peak values and timing in the eight LV segments are shown in Tables 1-4. In all velocity and strain rate curves, peak E was higher than Syst. The velocity E/A-ratio in LVFW, RLV and LLV was highly variable but was always higher than 1 in all horses. In the IVS and RLV velocity curves, the A-wave was biphasic, consisting of both a negative and a positive peak velocity. In the IVS at chordal level, the positive peak which was measured as A was often absent. Segmental timing differences were present. In the velocity curves, PEP and EET were significantly shorter in IVS ($P<0.001$). In contrast, the strain rate PEP and EET measurements showed no segmental differences except for shorter PEP in IVS and RLV at chordal level ($P=0.005$). Time to peak E velocity and strain rate was longer in IVS ($P=0.016$) and at papillary compared to chordal level ($P<0.001$). Onset A occurred earlier in IVS and RLV at both levels in the velocity curves ($P<0.001$). Peak strain occurred later in IVS and RLV at chordal level ($P<0.001$).

When compared to M-mode and PW Doppler measurements, EET measured in the velocity and strain rate curves of the different segments was significantly correlated to AVC_{MM} (range of correlation coefficient r 0.54–0.80; all $P<0.05$) and AVC_{PW} (r 0.54–0.89; all $P<0.05$), except for strain rate in LVFW. Similarly, onset E correlated significantly with MVO_{MM} (r 0.45–0.83; all $P<0.01$). PEP was only moderately correlated to AVO_{MM} and AVO_{PW}. In the segments with significant correlations ($P<0.05$), r ranged from 0.39 to 0.59 and 0.38 to 0.58, respectively.

The variability of TDI measurements is indicated in Tables 1-4. Variability was low for most systolic and diastolic timing measurements but ranged from low to high for peak values. However, for several peak values, between-day intra-observer and within-day interobserver variability were moderate to high while measurement variability was low.

Figure 2: Tissue Doppler (TDI) curves from a right parasternal short-axis view at papillary muscle level. On the left, the TDI color cineloop and a grayscale cineloop are displayed showing the sample area positions. Right on the image is caudal. Segmental traces are displayed for LVFW (yellow) and IVS (green). The horizontal axis shows time (ms) and the ECG. Peak values and timing are indicated on the LVFW curve. (A) Velocity; (B) Strain rate; (C) Strain. See Table legend for key.

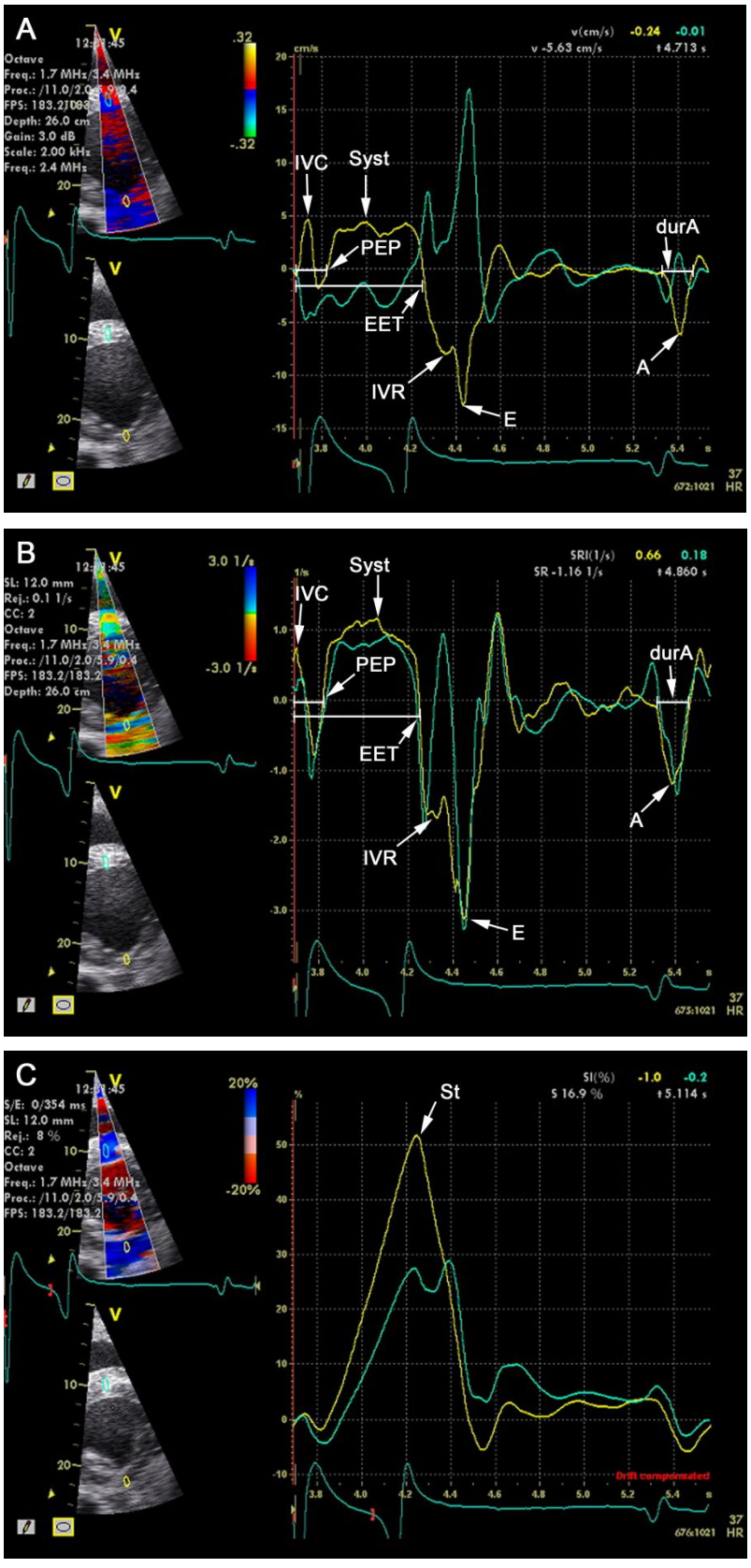

Figure 3: Tissue Doppler (TDI) curves from a left parasternal short-axis view at chordal level. On the left, the TDI color cineloop and a grayscale cineloop are displayed showing the sample area positions. Right on the image is cranial. Segmental traces are displayed for LLV (yellow) and RLV (green). The horizontal axis shows time (ms) and the ECG. Peak values and timing are indicated on the LLV curve. (A) Velocity; (B) Strain rate; (C) Strain. See Table legend for key.

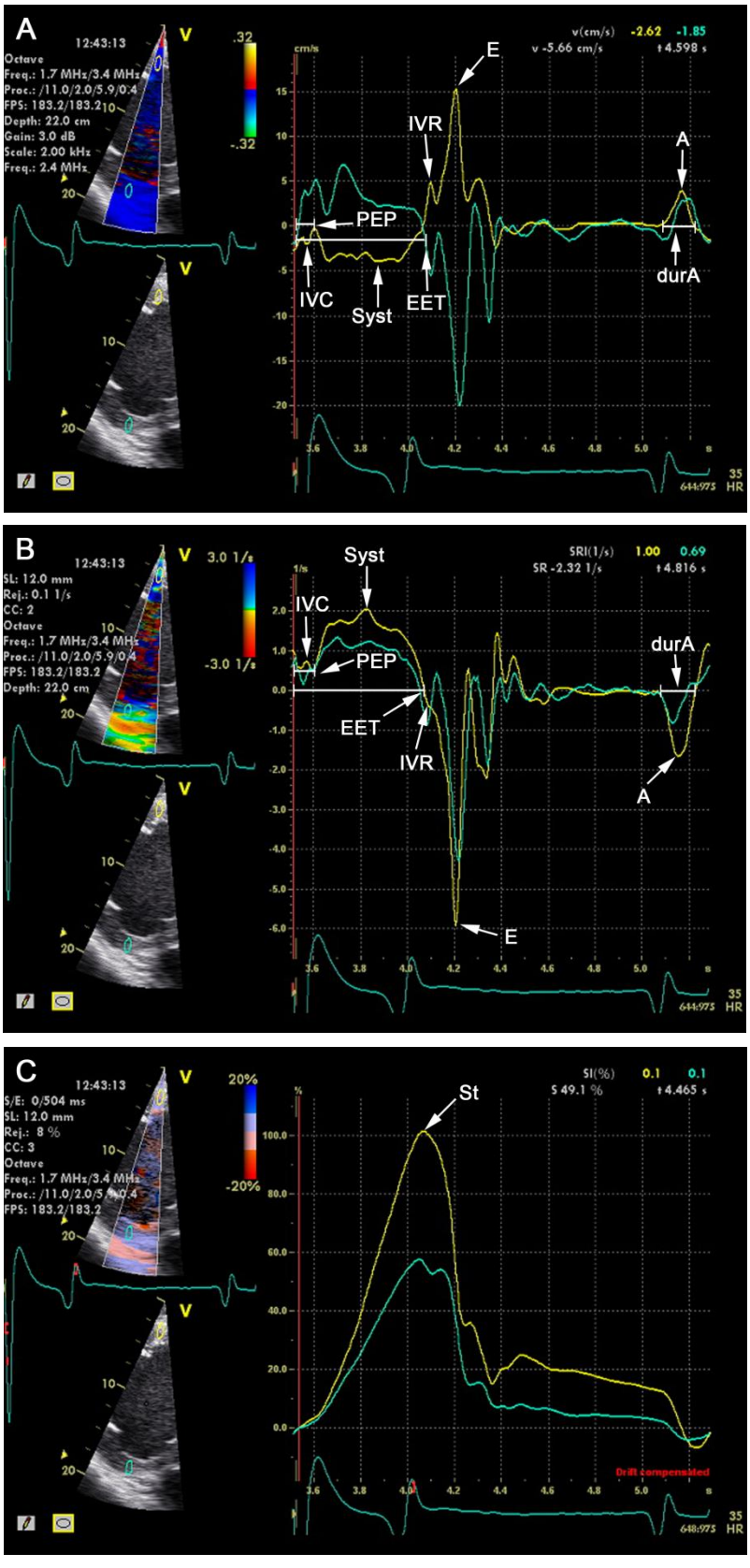

Table legend:

LVFW	Left ventricular free wall
IVS	Interventricular septum
LLV	Left region of left ventricular free wall
RLV	Right region of left ventricular free wall
SD	Standard deviation
n	Number of measurements (on a total of 50)
CV	Coefficient of variation
CV_{bd}	CV of between-day intra-observer variability
CV_{wd}	CV of within-day interobserver variability
CV_{dm}	CV of intra-observer measurement variability
CV_{om}	CV of interobserver measurement variability
*	All CV<15%
†	Measurement CV<15%
NA	Not available due to numerous missing values
IVC	Peak isovolumic contraction
tIVC	Time to peak isovolumic contraction (from peak R wave)
PEP	Pre-ejection period (from peak R wave)
Syst	Systolic peak
tSyst	Time to peak systole (from peak R wave)
EET	End ejection time (from peak R wave)
IVR	Peak isovolumic relaxation
tIVR	Time to peak isovolumic relaxation (from peak R wave)
onset E	Time to onset of early diastole (from peak R wave)
E	Early diastolic peak
tE	Time to peak early diastole (from peak R wave)
onset A	Time to onset of late diastole (from onset P wave)
A	Late diastolic peak
tA	Time to peak late diastole (from onset P wave)
dur A	Duration of late diastolic peak (end – onset)
St	Peak strain
tSt	Time to peak strain (from onset R wave)

Table 1: Mean, standard deviation and coefficients of variation of TDI measurements of left ventricular function from a right parasternal short-axis view at chordal level

	LVFW						IVS					
Velocity	**Mean**	**SD**	**n**	**CV_{bd}**	**CV_{wd}**	**CV_{dm}**	**CV_{om}**	**Mean**	**SD**	**n**	**CV_{bd}**	**CV_{wd}**	**CV_{dm}**	**CV_{om}**
IVC(cm/s)	5.35†	1.8	47	33.9	28.8	9.5	9.2	-3.66†	1.5	40	15.6	26.4	13.3	12.1
tIVC(ms)	38†	7	47	20.5	26.0	7.8	5.6	31†	15	40	40.1	45.2	12.2	10.8
PEP(ms)	101*	19	49	11.9	7.9	4.3	5.8	64†	15	41	20.1	30.6	6.4	5.5
Syst(cm/s)	7.39*	1.2	50	7.9	14.8	10.2	5.5	-4.26†	1.3	50	21.5	28.9	5.6	5.3
tSyst(ms)	215	42	50	30.7	18.1	23.0	11.8	118	23	50	14.0	26.1	21.5	4.6
EET(ms)	531*	27	49	4.5	4.7	1.4	1.2	475*	34	48	3.2	4.1	2.6	3.2
IVR(cm/s)	-5.13†	1.6	41	17.9	29.4	13.4	5.0	3.11†	1.8	45	38.9	33.1	11.7	12.7
tIVR(ms)	570*	31	41	4.2	4.3	1.4	2.0	536*	24	45	3.1	3.0	2.4	0.7
onset E(ms)	602*	33	41	3.9	4.5	1.3	1.5	628*	25	50	3.4	3.2	1.4	1.3
E(cm/s)	-19.19†	3.4	50	7.5	23.7	11.2	8.1	12.69†	2.7	50	12.6	18.7	9.1	8.7
tE(ms)	689*	34	50	2.9	3.7	0.6	0.7	727*	27	50	2.8	2.5	1.6	0.8
onset A(ms)	137†	19	50	21.4	23.2	4.8	3.8	77†	15	50	32.7	42.2	12.7	11.6
A(cm/s)	-7.20†	2.7	50	25.8	27.8	8.1	6.8	3.34	3.5	35		NA		
tA(ms)	217*	17	50	13.6	13.9	2.8	2.5	212	34	35		NA		
dur A(ms)	144†	13	50	13.9	16.4	6.8	5.5	169†	40	50	15.6	16.4	10.2	5.9
Strain rate														
IVC(s^{-1})	1.11	0.6	30		NA			0.88†	0.3	47	21.6	27.8	15.0	12.5
tIVC(ms)	43	17	30		NA			23†	9	47	34.7	45.6	15.0	14.4
PEP(ms)	99	17	29		NA			81*	13	50	13.6	14.1	6.7	5.5
Syst(s^{-1})	1.94	0.4	30		NA			1.23†	0.2	50	11.5	15.3	7.0	9.0
tSyst(ms)	231	48	30		NA			182	30	50	11.3	33.1	15.4	24.5
EET(ms)	514	36	29		NA			511*	25	48	3.2	4.3	1.2	0.5
IVR(s^{-1})	-1.51	0.8	25		NA			-0.71	0.4	42	88.9	78.5	31.9	10.9
tIVR(ms)	542	33	25		NA			537*	26	42	4.4	4.8	1.4	0.9
onset E(ms)	598	31	26		NA			620*	28	50	2.5	2.9	1.6	0.6
E(s^{-1})	-4.74	0.5	29		NA			-3.00†	0.7	50	14.0	17.7	13.3	8.7
tE(ms)	683	38	29		NA			709*	30	50	3.4	2.6	1.2	0.9
onset A(ms)	126	26	29		NA			118†	25	50	31.4	27.6	6.2	7.1
A(s^{-1})	-1.90	0.6	29		NA			-1.24†	0.5	50	36.4	33.5	10.5	12.4
tA(ms)	204	36	29		NA			197*	26	50	9.7	12.9	4.6	5.9
dur A(ms)	158	18	29		NA			150†	17	50	21.8	26.0	7.9	6.7
Strain														
St(%)	74.63	16.1	30		NA			49.58†	6.3	50	15.5	18.8	7.2	8.6
tSt(ms)	531	34	30		NA			589*	36	50	8.6	7.5	4.3	1.1

Table 2: Mean, standard deviation and coefficients of variation of TDI measurements of left ventricular function from a right parasternal short-axis view at papillary muscle level

	LVFW						IVS					
Velocity	**Mean**	**SD**	**n**	**CV_{bd}**	**CV_{wd}**	**CV_{dm}**	**CV_{om}**	**Mean**	**SD**	**n**	**CV_{bd}**	**CV_{wd}**	**CV_{dm}**	**CV_{om}**
IVC(cm/s)	4.48	1.8	49	35.4	30.7	15.0	16.2	-4.29†	2.1	41	18.1	33.0	4.6	7.8
tIVC(ms)	41†	11	49	24.6	16.7	9.6	12.9	43†	15	41	64.3	48.1	7.4	4.7
PEP(ms)	112*	26	50	12.8	7.4	6.6	7.8	85†	31	47	34.0	25.9	8.9	8.6
Syst(cm/s)	5.88†	0.8	50	18.6	13.3	10.8	11.2	-4.49†	1.2	50	13.8	17.4	6.7	5.9
tSyst(ms)	238	54	50	17.1	24.6	26.0	24.1	129†	19	50	31.9	14.6	9.3	3.7
EET(ms)	536*	26	50	2.2	3.2	1.1	1.2	478*	32	50	3.7	5.5	1.4	1.7
IVR(cm/s)	-5.40	2.0	50	29.9	31.1	17.5	20.8	5.26	2.2	50	38.4	35.4	29.5	22.9
tIVR(ms)	587*	33	50	4.1	3.6	1.2	1.4	553*	24	50	1.8	2.8	3.3	1.9
onset E(ms)	647*	30	50	5.8	4.3	1.1	0.9	644*	30	49	3.8	5.4	1.7	0.7
E(cm/s)	-13.74†	1.7	50	21.4	19.2	6.7	7.0	13.02	2.7	50	23.7	21.2	16.8	14.9
tE(ms)	731*	27	50	4.0	3.1	1.5	1.1	756*	25	50	3.3	3.1	0.8	0.8
onset A(ms)	141*	26	50	7.6	7.5	5.0	4.4	79†	14	50	25.5	26.2	14.0	7.4
A(cm/s)	-7.18	2.5	50	26.3	25.3	15.4	11.5	3.56	3.2	39	53.4	38.7	19.9	19.0
tA(ms)	224*	29	50	7.1	9.6	2.9	2.6	237*	44	39	6.1	5.5	5.8	4.2
dur A(ms)	142†	15	50	16.9	15.8	8.5	6.5	189†	43	50	24.0	24.5	7.1	10.5
Strain rate														
IVC(s^{-1})	0.96	0.3	29		NA			0.83†	0.2	46	30.5	28.7	9.7	12.7
tIVC(ms)	41	10	29		NA			25	14	46	45.8	42.5	23.9	25.3
PEP(ms)	106	19	33		NA			101*	22	50	12.6	12.8	2.4	5.1
Syst(s^{-1})	1.62	0.6	36		NA			1.26*	0.2	50	10.8	14.1	5.7	5.8
tSyst(ms)	218	65	36		NA			213†	43	50	36.9	40.7	14.1	6.3
EET(ms)	528	25	34		NA			515*	21	50	3.2	3.7	1.2	1.8
IVR(s^{-1})	-1.46	0.6	29		NA			-1.40	0.5	50	51.9	50.0	9.8	46.6
tIVR(ms)	579	30	29		NA			555*	22	50	3.7	3.9	0.9	0.9
onset E(ms)	638	27	28		NA			657*	23	50	4.8	5.5	1.9	0.8
E(s^{-1})	-3.84	1.0	30		NA			-3.20	0.7	50	13.3	16.4	13.9	16.8
tE(ms)	716	31	30		NA			752*	23	50	4.6	4.1	1.7	1.7
onset A(ms)	122	19	33		NA			136†	34	50	37.6	22.1	6.6	5.5
A(s^{-1})	-1.54	0.5	33		NA			-1.51†	0.9	50	34.2	50.1	4.4	6.8
tA(ms)	207	20	33		NA			220*	28	50	9.8	10.4	4.1	3.9
dur A(ms)	155	23	33		NA			138†	28	50	30.0	27.9	12.9	12.8
Strain														
St(%)	54.79	13.2	35		NA			44.38†	6.0	50	16.4	19.1	6.0	7.2
tSt(ms)	542	23	35		NA			559*	55	50	11.2	12.2	1.5	1.1

Table 3: Mean, standard deviation and coefficients of variation of TDI measurements of left ventricular function from a left parasternal short-axis view at chordal level

	LLV							RLV						
Velocity	**Mean**	**SD**	**n**	**CV_{bd}**	**CV_{wd}**	**CV_{dm}**	**CV_{om}**	**Mean**	**SD**	**n**	**CV_{bd}**	**CV_{wd}**	**CV_{dm}**	**CV_{om}**
IVC(cm/s)	-3.60	2.9	50	44.3	44.1	18.2	13.0	8.05†	2.8	47	14.6	18.1	8.8	10.3
tIVC(ms)	46*	10	50	14.8	11.3	8.4	9.4	58†	10	47	9.7	18.1	6.1	5.8
PEP(ms)	106*	16	50	10.5	13.7	3.9	2.1	133†	32	48	21.1	15.7	6.3	6.1
Syst(cm/s)	-4.63	1.5	50	15.0	16.9	9.0	16.9	5.58*	0.6	50	9.4	8.9	4.8	4.9
tSyst(ms)	319	72	50	22.0	15.6	18.7	10.6	208†	28	50	16.7	8.0	6.4	3.3
EET(ms)	525*	31	50	2.5	4.2	1.1	1.5	527*	33	50	5.0	6.1	1.4	2.3
IVR(cm/s)	2.53	1.0	47	57.9	50.0	19.9	19.1	-3.15	1.3	45	36.0	36.2	18.3	13.5
tIVR(ms)	559*	39	47	3.2	4.9	1.2	1.1	558*	38	45	2.9	4.1	2.2	3.2
onset E(ms)	610*	47	50	3.4	4.3	1.7	1.5	595*	32	50	3.2	4.5	1.9	2.6
E(cm/s)	13.52	1.6	50	14.9	23.7	24.6	18.9	-18.44†	1.8	50	16.2	18.8	12.8	14.4
tE(ms)	696*	44	50	3.8	3.5	0.9	2.2	692*	37	50	3.8	4.0	1.5	1.5
onset A(ms)	130	21	50	16.6	16.7	17.9	16.2	79†	27	49	52.2	30.8	14.1	13.2
A(cm/s)	2.48	1.2	50	51.5	43.0	16.5	13.1	-1.88	0.6	48	28.7	28.6	14.5	14.3
tA(ms)	214*	17	50	9.6	10.6	11.2	10.4	150	21	48	18.0	19.3	4.6	5.3
dur A(ms)	148*	17	50	11.2	12.6	10.2	5.6	218†	23	49	15.6	12.8	4.9	6.5
Strain rate														
IVC(s^{-1})	1.63	1.2	49	39.1	38.2	18.1	20.3	0.57	0.3	26		NA		
tIVC(ms)	43†	8	49	17.1	31.5	10.6	6.3	33	12	26		NA		
PEP(ms)	100†	15	49	10.4	21.4	6.4	5.6	88†	16	48	13.0	15.3	11.3	13.7
Syst(s^{-1})	2.34*	0.4	50	12.2	10.1	7.4	12.1	1.49†	0.2	50	15.5	9.7	5.6	4.9
tSyst(ms)	291†	51	50	20.2	27.8	10.5	11.0	294	36	50	31.8	31.2	27.4	25.7
EET(ms)	530*	30	50	4.2	6.9	2.4	2.7	525*	42	50	4.1	5.1	2.9	3.3
IVR(s^{-1})	-0.89	0.6	32		NA			-0.53	0.4	34		NA		
tIVR(ms)	553	39	32		NA			549	43	34		NA		
onset E(ms)	601*	39	46	4.8	6.2	1.2	1.8	619*	38	48	3.5	6.4	2.7	1.5
E(s^{-1})	-5.94†	1.4	50	17.1	18.7	12.0	14.3	-5.29	0.8	49	29.4	20.8	23.5	16.6
tE(ms)	694*	45	50	3.8	4.8	1.5	2.5	709*	41	49	2.6	4.7	1.4	2.2
onset A(ms)	114†	18	50	18.5	14.4	4.1	6.2	107†	30	49	43.5	24.6	9.5	14.4
A(s^{-1})	-1.70	0.4	50	40.5	26.7	29.4	16.0	-1.36	0.5	49	40.3	18.7	29.7	14.1
tA(ms)	202*	27	50	12.2	12.1	12.2	12.1	179†	28	49	21.3	18.2	7.6	6.2
dur A(ms)	169*	12	50	9.8	7.1	6.9	6.4	143†	19	49	20.0	14.1	7.2	13.8
Strain														
St(%)	109.95†	18.0	50	18.5	12.6	12.5	12.1	69.18†	9.5	50	17.8	15.3	12.7	9.1
tSt(ms)	556*	39	50	4.6	6.3	2.9	3.3	605*	33	50	7.5	7.8	2.9	2.2

Table 4: Mean, standard deviation and coefficients of variation of TDI measurements of left ventricular function from a left parasternal short-axis view at papillary muscle level

	LLV						RLV					
Velocity	**Mean**	**SD**	**n**	**CV_{bd}**	**CV_{wd}**	**CV_{dm}**	**CV_{om}**	**Mean**	**SD**	**n**	**CV_{bd}**	**CV_{wd}**	**CV_{dm}**	**CV_{om}**
IVC(cm/s)	-5.42†	3.0	50	25.8	27.1	12.4	12.1	5.52†	3.5	42	47.9	21.7	8.7	7.1
tIVC(ms)	40†	8	50	25.6	32.1	11.2	10.8	47†	21	42	38.7	19.6	7.0	14.1
PEP(ms)	102*	16	50	11.4	11.6	3.9	3.2	126†	41	45	20.5	19.6	3.4	5.6
Syst(cm/s)	-4.43	1.4	50	19.7	15.3	18.6	11.5	4.69†	0.7	50	20.4	19.4	6.9	8.4
tSyst(ms)	211	42	50	38.8	32.1	23.7	38.7	215†	45	50	28.9	29.8	8.0	2.8
EET(ms)	521*	32	50	4.3	4.8	2.7	1.1	537*	34	50	4.0	4.3	1.9	1.6
IVR(cm/s)	3.51	1.0	50	33.2	49.5	28.0	16.3	-3.64	1.7	45	16.4	29.5	41.3	14.9
tIVR(ms)	566*	35	50	5.4	5.0	4.2	1.0	571*	38	45	3.3	3.9	2.1	2.9
onset E(ms)	651*	53	50	4.7	5.0	1.6	2.3	610*	32	45	4.0	4.9	2.0	2.7
E(cm/s)	9.00†	3.5	50	29.1	22.0	14.3	12.0	-13.60†	2.6	50	25.6	14.6	12.9	14.5
tE(ms)	740*	50	50	5.0	4.2	1.7	1.3	714*	38	50	3.8	4.0	2.3	2.4
onset A(ms)	126†	23	50	17.3	13.1	12.1	14.4	81	19	50	36.6	39.7	24.6	39.4
A(cm/s)	4.20	1.1	50	30.1	20.4	14.8	23.3	-1.33	0.5	45	35.4	46.2	5.8	21.2
tA(ms)	220*	25	50	12.9	7.6	2.5	4.3	144	24	45	20.8	22.9	7.6	7.2
dur A(ms)	160*	13	50	12.0	9.6	8.7	8.3	222†	24	50	15.1	11.8	10.6	11.4
Strain rate														
IVC(s^{-1})	2.00	1.0	50	37.4	49.8	12.2	16.0	1.40	0.6	40	23.6	18.4	13.5	22.0
tIVC(ms)	39†	9	50	30.0	32.5	11.8	8.4	38	14	40	17.2	36.8	5.0	17.7
PEP(ms)	94†	19	50	16.7	18.5	9.4	9.8	99†	19	44	23.7	12.8	7.9	8.7
Syst(s^{-1})	2.28†	0.3	50	12.4	20.8	8.8	11.6	1.29†	0.3	45	13.2	17.0	7.6	11.1
tSyst(ms)	220	46	50	17.3	46.9	25.6	31.2	272	64	45	26.6	42.1	30.5	37.0
EET(ms)	514*	31	50	3.8	4.5	2.1	1.5	516*	31	45	4.6	3.5	2.8	2.3
IVR(s^{-1})	-1.91	0.9	47	46.6	30.5	33.1	31.1	-1.42	0.6	44	58.9	18.3	26.2	17.4
tIVR(ms)	566*	40	47	5.1	4.5	5.0	2.9	558*	39	44	4.7	3.3	3.2	2.7
onset E(ms)	631*	49	47	4.8	5.9	2.9	2.6	643*	47	45	6.2	4.9	1.9	1.8
E(s^{-1})	-3.77	0.7	50	20.9	21.7	21.0	18.3	-4.34	1.0	45	36.3	18.2	31.6	34.6
tE(ms)	720*	56	50	6.3	6.1	3.4	2.7	724*	48	45	6.0	4.5	1.9	2.6
onset A(ms)	112	21	50	19.7	18.0	17.8	18.5	123†	27	44	35.9	23.4	11.6	13.0
A(s^{-1})	-2.14	0.6	50	21.4	26.0	10.6	21.8	-0.97	0.3	44	50.5	30.0	17.4	21.3
tA(ms)	208*	23	50	6.1	9.2	14.4	6.2	198*	25	44	13.0	14.4	3.9	5.6
dur A(ms)	169*	13	50	11.3	10.5	8.8	10.3	130	33	44	13.1	10.3	7.7	19.5
Strain														
St(%)	93.65†	14.2	50	21.1	22.5	7.4	11.5	53.28†	12.0	45	13.9	15.7	6.3	8.5
tSt(ms)	514*	27	50	5.4	4.4	2.0	1.2	534*	45	45	6.2	2.9	5.4	4.7

Discussion

This study demonstrates the feasibility and reliability of color-coded TDI with off-line quantitative analysis for quantification of radial wall motion in eight LV segments from right and left parasternal short-axis images at papillary muscle and chordal level. Myocardial velocity and deformation could be measured in all segments, although some peaks could often not be identified due to inadequate curve quality. This mainly affected the strain rate and strain curves in the LVFW from right parasternal views. Peak values showed a higher variability compared to timing measurements. Timings by TDI correlated with conventional measurements.

The velocity and strain rate curves showed three major deflections: one during systole (Syst) and two during diastole (E and A). IVC and IVR were smaller and often biphasic. These peaks were frequently absent, which might be caused by smoothing of the curves using the cine compound function. The numerical values of peak amplitudes and timing measured in the LVFW at chordal level were very similar to those found by Schwarzwald et al. (2009). The peak amplitudes measured in IVS, LLV and RLV at chordal level were generally equal to or lower than those described by Sepulveda et al. (2005). The velocity E/A-ratio was higher than 1 in all horses, as previously described in healthy dogs (Chetboul et al., 2005). Impaired LV relaxation in the early stages of diastolic dysfunction causes prolonged isovolumic relaxation time, reduced early filling and increased dependence on atrial contraction, resulting in E/A<1. In human medicine, this can be easily assessed by PW transmitral flow measurements (Nishimura and Tajik, 1997). In horses, these measurements are highly variable due to poor alignment and TDI might be an easier alternative to assess diastolic function. In a horse with nutritional masseter myopathy, diastolic dysfunction could be demonstrated both by TDI and transmitral flow Doppler (Schefer et al., 2011).

Strain rate and strain could be measured in each horse in all segments except LVFW, which was probably caused by the image depth of this segment. Strain rate and strain offer several advantages over velocity measurements. A non-contractile myocardial segment will show no intrinsic active deformation while wall motion because of tethering by the adjacent segments can be present. As a result, myocardial velocities can be close to normal, while strain rate and strain curves are altered (Heimdal et al., 1998). Furthermore, deformation indices are not affected by total heart motion (D'hooge et al., 2000). However, the possible advantages of TDI-based deformation indices in horses with cardiac disease require further investigation.

Because of the high frame rate (> 180 fps), TDI also allows accurate time measurements. The main advantage of TDI is that systolic and diastolic time intervals can be acquired from one single image. A good correlation of systolic and diastolic time intervals measured by TDI and by invasive hemodynamics has been demonstrated in human medicine (Zamorano et al., 1997). In our study, TDI-based measurements of PEP, EET and onset E correlated with M-mode and PW-Doppler measurements. Correlation was better for EET and onset E than for PEP. Because PEP is very short, the measurement error of all methods is relatively large. Furthermore, TDI-based and conventional measurements were made in different cycles, thereby adding physiological variability of heart rate and inotropy. In the horse with nutritional masseter myopathy and myocardial damage, an increased ratio of PEP/ejection time and a longer isovolumic relaxation time could be measured by TDI, indicating both systolic and diastolic dysfunction (Schefer et al., 2011).

Significant segmental differences of peak timing were demonstrated that should be taken into account when evaluating LV dyssynchrony. Differences were mainly found in the velocity curves which is probably due to total heart motion and interaction with right ventricular motion. Strain rate timing measurements showed less segmental differences, indicating a synchronous contraction pattern in these healthy horses at resting heart rate. The longer time to peak strain found in IVS and RLV at chordal level is similar to the delayed peak longitudinal strain in the basal septal segment measured by 2D speckle tracking (Decloedt et al., 2011) since RLV is located at the transition of the septum and LV free wall. The earlier onset of velocity peak A in IVS and RLV is caused by the delay in left compared to right atrial activation. This also explains the biphasic shape of the A-wave.

Most peak values showed a moderate to high variability while time measurements showed a low variability. This might be attributed to measurement error during off-line analysis. Sample area positioning has little impact on timings but significantly influences peak values because of the myocardial velocity gradient from endocardium to epicardium. However, this is refuted by the fact that the intra- and interobserver measurement variability of peak values was often low while between-day intra-observer and within-day interobserver variability was moderate to high. This possibly reflects biological variability due to temporary changes of inotropic state or variation during image acquisition such as a different insonation angle. Similar results were found in previous studies in healthy dogs and cats (Chetboul et al., 2004; Chetboul et al., 2005), however, variability was lower in our study compared to previous

studies in horses (Sepulveda et al., 2005; Schwarzwald et al., 2009). This might be caused by the higher frame rate (>180 fps).

The use of TDI in veterinary cardiology is a relatively recent development. TDI was shown to be more sensitive than conventional echocardiography for detection of systolic and diastolic myocardial dysfunction in cats with hypertrophic cardiomyopathy (Koffas et al., 2006; Wess et al., 2010). Dogs with occult dilated cardiomyopathy showed impaired LV relaxation as measured by TDI but not by conventional measurements (O'Sullivan et al., 2007). TDI could also detect diastolic dysfunction in dogs with chronic mitral valve regurgitation and decompensated congestive heart failure (Teshima et al., 2005). This was correlated with left atrial dilatation and might be clinically applied to detect left atrial volume overload. In contrast, another study described few changes of TDI measurements in dogs with mitral valve regurgitation (Tidholm et al., 2009). The significantly different TDI measurements were co-variate with changes of conventional parameters. Few studies are available on the use of TDI in larger groups of horses with cardiac disease. In 15 horses with atrial fibrillation, systolic and early diastolic velocities were significantly higher whereas the late diastolic wave was absent (Gehlen et al., 2009). TDI has also been applied for follow up of recovery of left atrial function after cardioversion of atrial fibrillation (Schwarzwald et al., 2007a). A future application of TDI might be the early detection of myocardial dysfunction in horses with valvular disease.

The main limitations of this study were inherent to the Doppler technique. Velocities are measured relative to the transducer, in the direction of the ultrasound beam. Velocity measurements are therefore affected by total heart motion and by the insonation angle between the ultrasound beam and wall motion. An adequate velocity scale is also a prerequisite. The Nyqvist limit of velocity measurements is based on the pulse repetition frequency in relation to the observed velocity. Exceeding this limit results in aliasing velocities, visible as a fast shift of high negative to high positive velocities or opposite. Homogeneous myocardial coloring during acquisition indicates the absence of aliasing or artefacts. Our results were not compared to a gold standard technique as this is not available in horses. However, TDI has been extensively validated in vitro, in animal models and in man by comparison with tagged MRI and sonomicrometry (Fleming et al., 1994; Gorcsan et al., 1997; Edvardsen et al., 2002). Our study included a relatively small study population. A larger group would have allowed to establish more accurate reference values and identify influences of body weight, breed, heart rate and training.

In conclusion, TDI measurements of radial velocity, strain rate and strain are feasible in eight LV segments from right and left parasternal short-axis images at papillary muscle and chordal level. TDI allowed accurate timing of cardiac events which was correlated to M-mode and PW Doppler measurements. All timing measurements and several peak amplitudes showed good reliability and can be used in further clinical studies.

References

Brodin LA (2004). Tissue Doppler, a fundamental tool for parametric imaging. Clin Physiol Funct Imaging 24, 147-155

Chetboul V, Athanassiadis N, Carlos C, Nicolle AP, Tissier R, Pouchelon JL, Concordet D, Lefebvre HP (2004). Quantification, repeatability, and reproducibility of feline radial and longitudinal left ventricular velocities by tissue Doppler imaging. Am J Vet Res 65, 566-572

Chetboul V, Sampedrano CC, Concordet D, Tissier R, Lamour T, Ginesta J, Gouni V, Nicolle AP, Pouchelon JL, Lefebvre HP (2005). Use of quantitative two-dimensional color tissue Doppler imaging for assessment of left ventricular radial and longitudinal myocardial velocities in dogs. Am J Vet Res 66, 953-961

D'hooge J, Heimdal A, Jamal F, Kukulski T, Bijnens B, Rademakers F, Hatle L, Suetens P, Sutherland GR (2000). Regional strain and strain rate measurements by cardiac ultrasound: Principles, implementation and limitations. Eur J Echocardiogr 1, 154-170

Decloedt A, Verheyen T, Sys S, De Clercq D, van Loon G (2011). Quantification of left ventricular longitudinal strain, strain rate, velocity, and displacement in healthy horses by 2-dimensional speckle tracking. J Vet Intern Med 25, 330-338

Edvardsen T, Gerber BL, Garot J, Bluemke DA, Lima JA, Smiseth OA (2002). Quantitative assessment of intrinsic regional myocardial deformation by Doppler strain rate echocardiography in humans: Validation against three-dimensional tagged magnetic resonance imaging. Circulation 106, 50-56

Fleming AD, McDicken WN, Sutherland GR, Hoskins PR (1994). Assessment of colour Doppler tissue imaging using test-phantoms. Ultrasound Med Biol 20, 937-951

Gehlen H, Iversen C, Stadler P (2009). Tissue Doppler echocardiographic examinations at rest and after exercise in horses with atrial fibrillation. Pferdeheilkunde 25, 11-16

Gorcsan J, 3rd, Strum DP, Mandarino WA, Gulati VK, Pinsky MR (1997). Quantitative assessment of alterations in regional left ventricular contractility with color-coded tissue Doppler echocardiography. Comparison with sonomicrometry and pressure-volume relations. Circulation 95, 2423-2433

Heimdal A, Stoylen A, Torp H, Skjaerpe T (1998). Real-time strain rate imaging of the left ventricle by ultrasound. J Am Soc Echocardiogr 11, 1013-1019

Koffas H, Dukes-McEwan J, Corcoran BM, Moran CM, French A, Sboros V, Simpson K, McDicken WN (2006). Pulsed tissue Doppler imaging in normal cats and cats with hypertrophic cardiomyopathy. J Vet Intern Med 20, 65-77

Nishimura RA, Tajik AJ (1997). Evaluation of diastolic filling of left ventricle in health and disease: Doppler echocardiography is the clinician's Rosetta stone. J Am Coll Cardiol 30, 8-18

O'Sullivan ML, O'Grady MR, Minors SL (2007). Assessment of diastolic function by Doppler echocardiography in normal doberman pinschers and doberman pinschers with dilated cardiomyopathy. J Vet Intern Med 21, 81-91

Pellerin D, Sharma R, Elliott P, Veyrat C (2003). Tissue Doppler, strain, and strain rate echocardiography for the assessment of left and right systolic ventricular function. Heart 89 Suppl 3, iii9-17

Schefer KD, Bitschnau C, Weishaupt MA, Schwarzwald CC (2010). Quantitative analysis of stress echocardiograms in healthy horses with 2-dimensional (2D) echocardiography, anatomical M-mode, tissue Doppler imaging, and 2D speckle tracking. J Vet Intern Med 24, 918-931

Schefer KD, Hagen R, Ringer SK, Schwarzwald CC (2011). Laboratory, electrocardiographic, and echocardiographic detection of myocardial damage and dysfunction in an Arabian mare with nutritional masseter myodegeneration. J Vet Intern Med 25, 1171-1180

Schwarzwald CC, Schober KE, Bonagura JD (2007a). Echocardiographic evidence of left atrial mechanical dysfunction after conversion of atrial fibrillation to sinus rhythm in 5 horses. J Vet Intern Med 21, 820-827

Schwarzwald CC, Schober KE, Bonagura JD (2007b). Methods and reliability of echocardiographic assessment of left atrial size and mechanical function in horses. Am J Vet Res 68, 735-747

Schwarzwald CC, Schober KE, Bonagura JD (2009). Methods and reliability of tissue Doppler imaging for assessment of left ventricular radial wall motion in horses. J Vet Intern Med 23, 643-652

Sepulveda MF, Perkins JD, Bowen IM, Marr CM (2005). Demonstration of regional differences in equine ventricular myocardial velocity in normal 2-year-old Thoroughbreds with Doppler tissue imaging. Equine Vet J 37, 222-226

Teshima K, Asano K, Sasaki Y, Kato Y, Kutara K, Edamura K, Hasegawa A, Tanaka S (2005). Assessment of left ventricular function using pulsed tissue Doppler imaging in healthy dogs and dogs with spontaneous mitral regurgitation. J Vet Med Sci 67, 1207-1215

Tidholm A, Ljungvall I, Hoglund K, Westling AB, Häggström J (2009). Tissue Doppler and strain imaging in dogs with myxomatous mitral valve disease in different stages of congestive heart failure. J Vet Intern Med 23, 1197-1207

Wess G, Sarkar R, Hartmann K (2010). Assessment of left ventricular systolic function by strain imaging echocardiography in various stages of feline hypertrophic cardiomyopathy. J Vet Intern Med 24, 1375-1382

Zamorano J, Wallbridge DR, Ge J, Drozd J, Nesser J, Erbel R (1997). Non-invasive assessment of cardiac physiology by tissue Doppler echocardiography. A comparison with invasive haemodynamics. Eur Heart J 18, 330-339

Chapter 4

The influence of atrioventricular interaction on mitral valve closure and left ventricular isovolumic contraction

Adapted from:

Decloedt A[1], Verheyen T[1], Sys S[1], De Clercq D[1], Bijnens B[2], van Loon G[1]

[1] Department of Large Animal Internal Medicine, Faculty of Veterinary Medicine, Ghent University, Belgium.
[2] ICREA-Universitat Pompeu Fabra, Barcelona, Spain

The influence of atrioventricular interaction on mitral valve closure and left ventricular isovolumic contraction

Ready for submission.

Part of this work was presented at the EUROECHO & other Imaging Modalities Congress 2011, Budapest, Hungary, December 7-10, 2011

Summary

Purpose: To evaluate the relationship between atrioventricular (AV) delay, mitral valve closure (MVC) and left ventricular (LV) isovolumic contraction (IVC), using the horse as an animal model because of the low heart rate (25–45 bpm) and physiologically long AV delay.

Methods: Six unsedated horses were evaluated during normal sinus rhythm (NSR), ventricular pacing without preceding atrial contraction (RVP) and dual-chamber pacing at AV delays of 150 to 350 ms, programmed at a constant rate. Modified right parasternal four-chamber views were recorded for simultaneous measurements of MVC by anatomical M-mode and TDI-based LV pre-ejectional peak velocity and isovolumic acceleration (IVA).

Results: During NSR and long AV delays (≥300 ms), two positive pre-ejectional velocity peaks were present. The first peak was identified as LV recoil during atrial relaxation and consistently preceded MVC. The second peak was called LV isovolumic contraction, occurring after MVC. This suggests MVC caused by atrial relaxation, followed by a true isovolumic contraction. However, during short AV delays (<300 ms) and RVP, MVC occurred significantly later. Only one pre-ejectional peak was present, of which the end coincided with MVC. These findings suggest MVC caused by LV contraction. Peak velocity and IVA were significantly higher, as the mitral valve was still open at the onset of LV contraction.

Conclusions: Depending on the AV delay, MVC can be atrio- or ventriculogenic, resulting in significant alterations of the pre-ejectional peak LV velocity and IVA.

Introduction

Left ventricular (LV) peak velocity and acceleration measured by tissue Doppler imaging (TDI) during isovolumic contraction (IVC) have been proposed as load-independent measurements of myocardial contractility (Pellerin et al., 1998; Vogel et al., 2003). However, the myocardial mechanics during IVC have not yet been completely elucidated. Both longitudinal and transverse motion have been described, which resulted in a more spherical external LV shape (Goetz et al., 2005). By TDI, a biphasic wall motion can be detected. This has been attributed to asynchronous deformation of the subendocardial and subepicardial myocardial layers, with subendocardial shortening in the right-handed helical direction accompanied by transient lengthening in the cross-fiber left-handed helical direction (Sengupta et al., 2005). The biphasic myocardial velocity spike might also be explained by interaction with mitral valve closure (MVC). Good agreement has been demonstrated between the timing of MVC and the interruption of pre-ejection shortening (Remme et al., 2008). In patients with severe mitral valve regurgitation, the peak pre-ejection velocity spike was significantly higher before valve surgery.

The exact mechanism of MVC is still debated. Convention holds that MVC is caused by the reversed flow following atrioventricular pressure cross-over due to the LV pressure rise at the initiation of LV contraction (Silbiger and Bazaz, 2009). However, the left atrium (LA) might also play an important role. Reduced atrial contraction during occlusion of the proximal left circumflex coronary artery in sheep resulted in delayed MVC (Timek et al., 2002). This might be caused by the absence of inward flow during atrial contraction. The cessation of this forward flow has been described to cause negative pressures at the mitral valve leaflets (Little, 1979). Furthermore, the presence of late diastolic vortices along the ventricular surfaces of the leaflets might facilitate leaflet appositioning (Kim et al., 1995). Recently, electromechanical coupling of the LA, mitral annulus and mitral valve leaflets has been described. At the onset of IVC, annular area reduction and valve stiffening through contraction of myocytes in the basal portion of the anterior leaflet occur after atrial activation, by an electrical connection through the AV-node (Timek et al., 2001; Swanson et al., 2011).

The aim of this study was to investigate the influence of the atrioventricular (AV) delay on MVC and its relationship with IVC as measured by TDI. The horse was used as an animal model because of its low heart rate at rest (25 – 45 bpm) and physiologically long AV delay, so that a wide range of AV delays could be studied using pacing.

Measurements were performed during spontaneous sinus rhythm (SR), AV pacing with different AV delays and ventricular pacing without preceding atrial contraction (RVP). Pre-ejection LV wall motion could be measured simultaneously with mitral valve motion using a color TDI four-chamber view. We hypothesized that the AV delay would influence the time of MVC and that this would affect the LV myocardial velocity and acceleration during IVC.

Material and methods

Experimental preparation

This study included six horses (four mares, two geldings) with a mean bodyweight of 568 ± 63 kg, aged 12.5 ± 4 years. The experiment was approved by the Ethical Committee of the Faculty of Veterinary Medicine of Ghent University (2011/015). Animal handling and care were performed following their guidelines.

The study was carried out on the standing horses at rest without sedatives. Two horses had a permanent implanted dual-chamber pacemaker (Thera DR 7960i and Kappa KDR 901, Medtronic, Minneapolis, MN). Four horses were instrumented with temporary pacing leads. Two introducer sheaths (Baxter Intro-Flex 8.5Fr, I350BF85, Edwards Life Sciences, Irvine, CA) were placed in the proximal third of the right jugular vein after local anesthesia with procaine (Procaine hydrochloride 4%, VMD, Arendonk, Belgium). Two bipolar pacing catheters (Bipolar Intracardiac Electrode, USCI Division, C.R. Bard Inc., Billerica, MA) were inserted and positioned in the right ventricular apex and the right atrium. Catheter placement was guided by analysis of the intracardiac ECG and echocardiography and stable positioning of the catheters was checked repeatedly throughout the study. Both catheters were connected to an external pacing device (Programmer 9790, Medtronic, Minneapolis, MN). Pacing was performed at twice the diastolic threshold amplitude.

Pacing protocol

Pacing was performed at a constant rate in excess of sinus rate. A stabilization period of one minute was allowed for each pacing modality before measurements were started. Measurements were performed during spontaneous sinus rhythm (SR), dual-chamber pacing at different AV delays and right ventricular pacing without preceding atrial contraction (RVP), programmed in a random sequence. The AV delay during dual-chamber pacing ranged from 150 to 350 ms (150-200-250-300-320-350 ms). For RVP, care was taken to obtain ventricular contractions that were not preceded by spontaneous atrial depolarization.

Echocardiography

Images were acquired using a Vivid 7 Dimension ultrasound machine equipped with a 3S Phased Array transducer (GE Healthcare, Horten, Norway). A base-apex surface ECG was recorded simultaneously. Color TDI loops of four consecutive cardiac cycles were acquired at a frequency of 1.7/3.4 MHz from a right-parasternal four-chamber view.

The image depth was 28 cm, with a single focus positioned at 22 cm. The greyscale sector width was decreased to 45° and the velocity scale was set from -16 to +16 cm/s in order to obtain frame rates exceeding 100 frames per second (fps). As a result, the LV apex and LA dorsal wall were not imaged, however, the mitral valve was visualised throughout the entire cardiac cycle. Care was taken to ensure optimal alignment of the ultrasound beam with radial motion of the LV free wall at chordal level. For each pacing modality, additional M-mode recordings of aortic valve opening and closure were obtained from the right parasternal LV outflow tract long-axis view.

Off-line analysis

All measurements were performed off-line using commercially available software (EchoPAC Software Version 108.1.5, GE Healthcare, Horten, Norway). For TDI measurements, a sample area of 12x4 mm was placed in the LV free wall at chordal level. The cine compound function was used to obtain an average of three consecutive cycles and a 30 ms temporal smoothing filter was applied. Peak myocardial velocities were measured during late diastole (A) and the pre-ejection period. Isovolumic acceleration (IVA) was calculated as the mean slope of the pre-ejection wave ($v_{max} – v_0$/acceleration time; unit m/s^2), where v_{max} represents the maximal LV velocity during IVC and v_0 the velocity at the onset of the pre-ejection wave. If two pre-ejection velocity spikes were present, IVA was measured from the second peak. If biphasic pre-ejection motion was present, the negative velocity peak occurring before ejection was called nIVC. All timings were measured relative to onset QRS. Onset and end of the velocity peaks were measured where the curve crossed the zero line or where a clear deviation occurred. The time between onset QRS and end of IVC was measured. Duration of the late diastolic peak (durA) was calculated as end A – onset A.

The time of mitral valve closure (MVC) was measured as the time of leaflet coaptatation in an anatomical color-coded TDI M-mode image through the mitral valve on the same loop as the TDI measurements. Similarly, an anatomical M-mode at chordal level (Grenacher et al., 2010) was used for measuring fractional shortening (FS), which was calculated from the LV internal diameter (LVID) measured at end-diastole (d) and end-systole (s): FS = ((LVIDd – LVIDs) / LVIDd) * 100. The time of aortic valve opening (AVO) and closure (AVC) was measured from a long-axis LV outflow tract M-mode image. The pre-ejection period was defined as the time between the onset of QRS and AVO, the ejection time was defined as the time between AVO and AVC.

From these measurements, the ratio of LV pre-ejection period and ejection time (LVPEP/ET) was calculated. The isovolumic contraction time (IVCT) was calculated as the time between MVC and AVO. To minimize measurement variability, all recordings were performed and analysed by one experienced echocardiographer (AD).

Statistical analysis

Data are reported as mean ± standard deviation (SD). Pre-ejection peak velocity and IVA, TDI time measurements and timing of valve events during SR, RVP and pacing at different AV delays were compared by a linear mixed model (LMM) with type of stimulation as a fixed categorical effect and the horses as subjects. A global significance level of 0.05 was used; for multiple comparisons the Bonferroni adjustment was applied. To compare SR and long AV delays (≥ 300 ms) versus RVP and short AV delays (< 300 ms), a custom hypothesis was tested within the LMM. In order to compare the difference between timing of pre-ejection velocity peaks and mitral valve closure, similar LMM's were used.

Results

The resting heart rate in sinus rhythm was 36 ± 4 bpm with a mean PQ interval of 392 ± 62 ms. Pacing was performed at 40 bpm in four horses and at 45 bpm in two horses. Good quality TDI images could be acquired at a frame rate of 105 fps in all horses. Late diastolic and pre-ejection LV velocity peaks could be easily identified. For each pacing mode, the PQ interval, TDI measurements and M-mode measurements are tabulated in Table 1.

Peak myocardial velocity during atrial contraction (A) did not differ significantly between pacing modes (P=0.60). However, duration of A was significantly shorter at AV delay 150 and 200 ms (P=0.02), as atrial contraction was interrupted by MVC. During SR and long AV delays, two positive pre-ejection velocity peaks were present (Fig. 1B). The first peak was identified as recoil of the LV during atrial relaxation (rA). The second peak was coinciding with LV isovolumic contraction (IVC). During RVP and short AV delays, only one pre-ejection peak was present, which was called IVC as this peak occurred after the onset of QRS (Fig. 1A).

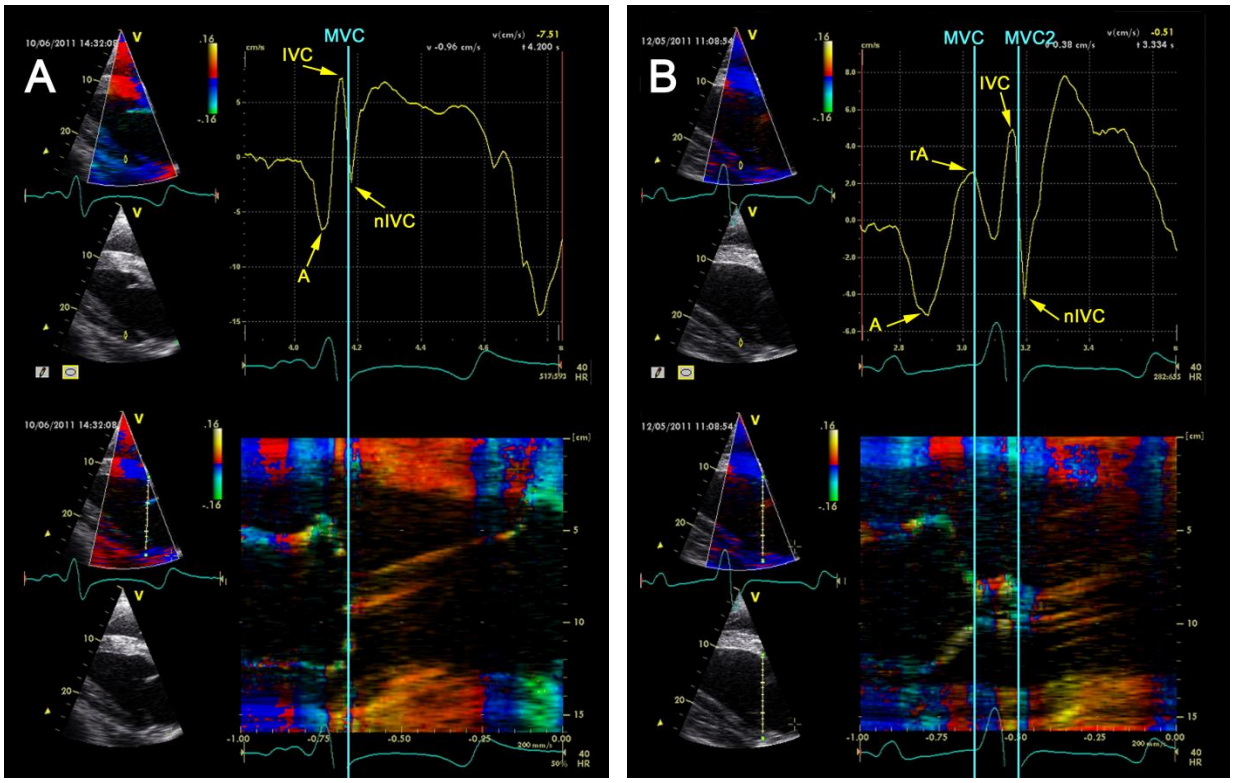

Figure 1: Example of a TDI velocity curve in the left ventricular free wall and an anatomical M-mode through the mitral valve, derived from the same right parasternal modified four-chamber view. (A) During dual-chamber pacing at an atrioventricular delay of 150 ms; (B) During dual-chamber pacing at an atrioventricular delay of 350 ms.
A, atrial contraction; IVC, peak left ventricular isovolumic contraction velocity; MVC, mitral valve closure; MVC2, second mitral valve closure after minor valve reopening; nIVC, negative velocity peak following IVC; rA, recoil of the left ventricle during atrial relaxation

Peak IVC velocity was remarkably higher when only one peak was present during RVP and short AV delays (P<0.001, Fig. 2A). IVA was significantly higher as well (P<0.001, Fig. 2B). The time of end IVC did not differ significantly between short and long AV delays (P=0.51). Biphasic pre-ejection motion was present in most horses during short AV delays and RVP, with IVC followed by a negative velocity peak (nIVC). During long AV delays and SR, this peak was often absent and significantly less negative if present (P=0.001, Fig. 2C).

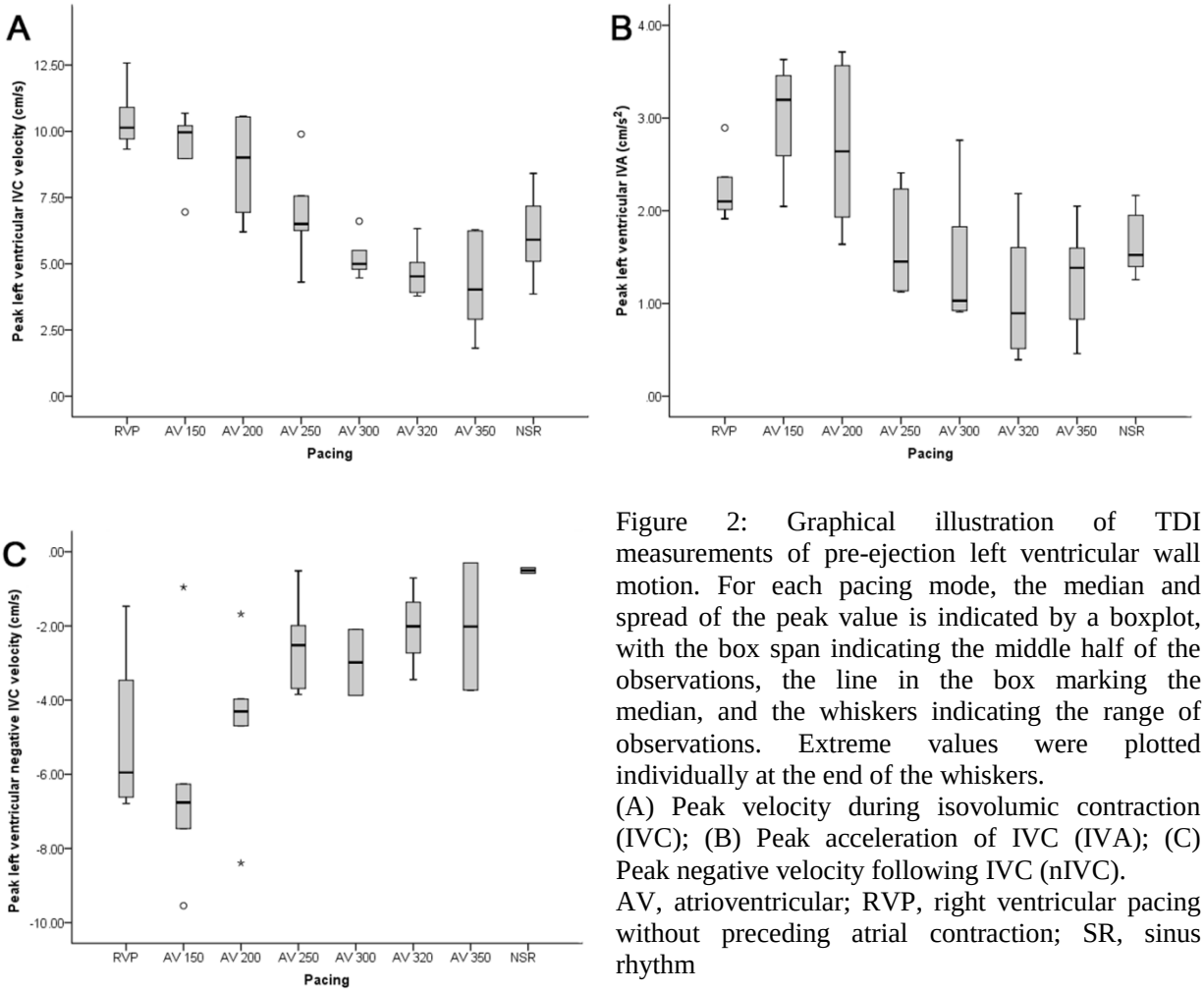

Figure 2: Graphical illustration of TDI measurements of pre-ejection left ventricular wall motion. For each pacing mode, the median and spread of the peak value is indicated by a boxplot, with the box span indicating the middle half of the observations, the line in the box marking the median, and the whiskers indicating the range of observations. Extreme values were plotted individually at the end of the whiskers.
(A) Peak velocity during isovolumic contraction (IVC); (B) Peak acceleration of IVC (IVA); (C) Peak negative velocity following IVC (nIVC).
AV, atrioventricular; RVP, right ventricular pacing without preceding atrial contraction; SR, sinus rhythm

During short AV delays and RVP, MVC occurred after onset QRS (Fig. 1A) and coincided with end IVC (Fig. 3) with a mean difference of -1.5 ± 10 ms which was independent of the pacing mode (P=0.251). MVC occurred significantly earlier during long AV delays and SR (P<0.001) and was consistently preceded by rA by 33 ± 17 ms, independent of the pacing mode (P=0.63, Fig. 3). Minor valve reopening during pre-ejection often occurred at long AV delays, mostly at 350 ms and during SR (Fig. 1B). This resulted in double valve closure. The second closure was called MVC2 and coincided with end IVC with a mean difference of -0.3 ± 12 ms, independent of the pacing mode (P=0.32).

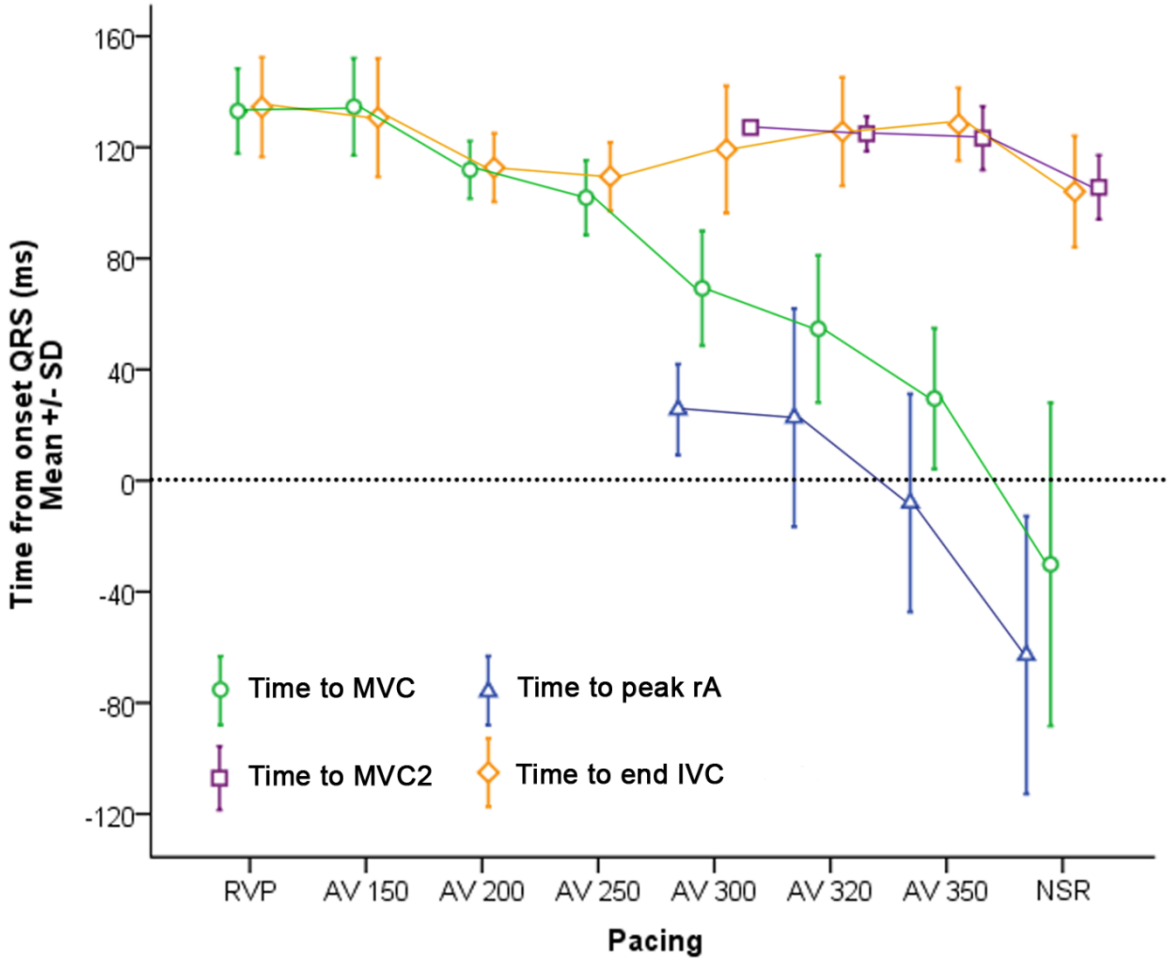

Figure 3: Timing of mitral valve closure (MVC), second mitral valve closure after minor valve reopening (MVC2), end of isovolumic contraction (end IVC) and recoil of the left ventricle during atrial relaxation (rA) relative to the time of onset QRS measured on the ECG (represented by the dotted line).

AV, atrioventricular; RVP, right ventricular pacing without preceding atrial contraction; SD, standard deviation; NSR, normal sinus rhythm

AVO occurred latest during RVP and earliest during SR, with a trend of earlier AVO at longer AV delays. However, due to the significantly earlier timing of MVC at long AV delays and SR, the true isovolumic period (AVO-MVC) was significantly longer compared to short AV delays and RVP ($P<0.001$, Fig. 4A). However, if MVC2 was considered for calculation of the true isovolumic period, no significant difference was present (Fig. 4B). LVPEP/ET as measured by M-mode was not altered by the AV delay during AV pacing but was significantly higher during RVP and lower during SR ($P<0.001$). FS was lower during long AV delays and SR compared to short AV delays and RVP ($P=0.001$).

Table 1: ECG, tissue Doppler (TDI) and M-mode measurements (mean±standard deviation) in six horses during different pacing modalities

Measurement		RVP	AV 150	AV 200	AV 250	AV 300	AV 320	AV 350	SR
ECG	PQ interval	NA	159 ± 12	212 ± 35	246 ± 20	299 ± 13	316 ± 12	350 ± 10	392 ± 62
TDI	A (cm/s)	NA	-5.91 ± 2.33	-6.94 ± 1.60	-6.76 ± 1.58	-7.40 ± 1.82	-6.94 ± 1.04	-7.07 ± 2.04	-6.66 ± 0.72
	durA (ms)	NA	90 ± 31^{ab}	136 ± 17^{ac}	173 ± 17^{c}	161 ± 20^{c}	173 ± 21^{c}	170 ± 18^{c}	176 ± 13^{c}
	rA (cm/s)	NA	NA	NA	NA	2.47 ± 1.21	3.33 ± 1.11	3.34 ± 0.86	2.87 ± 0.84
	# rA	0	0	0	0	3	5	6	6
	IVC (cm/s)	10.46 ± 1.16^{ab}	9.46 ± 1.35^{ab}	8.71 ± 1.83^{b}	6.84 ± 1.84^{d}	5.22 ± 0.76^{cd}	4.69 ± 0.94^{cd}	4.22 ± 1.83^{cd}	6.06 ± 1.61^{cd}
	IVA (m/s^2)	2.23 ± 0.36	3.02 ± 0.61^{ab}	2.69 ± 0.85^{b}	1.63 ± 0.56^{c}	1.41 ± 0.75^{c}	1.08 ± 0.69^{c}	1.28 ± 0.58^{c}	1.64 ± 0.35^{c}
	end IVC (ms)	135 ± 18^{a}	131 ± 21^{a}	113 ± 12	110 ± 12	119 ± 23	126 ± 20	128 ± 13	104 ± 20^{cd}
	nIVC (cm/s)	-5.04 ± 2.45	-6.29 ± 2.86^{a}	-4.61 ± 2.42	-2.51 ± 1.23	-2.98 ± 1.26	-2.05 ± 1.37	-2.02 ± 2.42	-0.5 ± 0.11^{c}
	# nIVC	4	6	5	6	2	3	2	2
M-mode	MVC (ms)	133 ± 15^{ab}	135 ± 18^{ab}	112 ± 10^{ab}	102 ± 13^{ab}	69 ± 21^{acd}	55 ± 27^{acd}	30 ± 25^{acd}	-30 ± 58^{bcd}
	MVC2 (ms)	NA	NA	NA	NA	127	125 ± 6	123 ± 11	106 ± 12
	# MVC2	0	0	0	0	1	2	5	6
	AVO (ms)	199 ± 28^{abc}	170 ± 26^{ad}	168 ± 22^{ad}	174 ± 18^{ad}	165 ± 21^{ad}	166 ± 12^{ad}	158 ± 15^{ad}	125 ± 17^{bcd}
	LVPEP/ET	0.57 ± 0.11^{ab}	0.43 ± 0.10^{ad}	0.43 ± 0.06^{ad}	0.43 ± 0.07^{ad}	0.41 ± 0.07^{ad}	0.42 ± 0.05^{ad}	0.39 ± 0.05^{ad}	0.30 ± 0.05^{d}
	FS (%)	38.1 ± 1.4^{a}	37.6 ± 3.9^{a}	37.7 ± 2.2^{a}	37.1 ± 1.9	37.5 ± 3.0^{a}	36.2 ± 3.3	35.8 ± 2.0	34.0 ± 3.3^{cd}

#, number of horses in which the peak was present (on a total of 6); A, atrial contraction; AV, atrioventricular pacing; AVO, aortic valve opening; durA, duration of atrial contraction; end IVC, time between onset QRS and end IVC; IVA, isovolumic acceleration; IVC, isovolumic contraction; IVCT, isovolumic contraction time; FS, fractional shortening; LVPEP/ET, pre-ejection period/ejection time; MVC, mitral valve closure; MVC2, mitral valve closure after valve reopening; NA, not available; nIVC, negative velocity peak following IVC; rA, recoil of left ventricle during atrial relaxation; SR, normal sinus rhythm; TDI, tissue Doppler; RVP, ventricular pacing.

Superscript indicates significant difference ($P<0.05$) from ^{a}, SR; ^{b}, AV 350 ms; ^{c}, AV 150 ms; ^{d}, RVP.

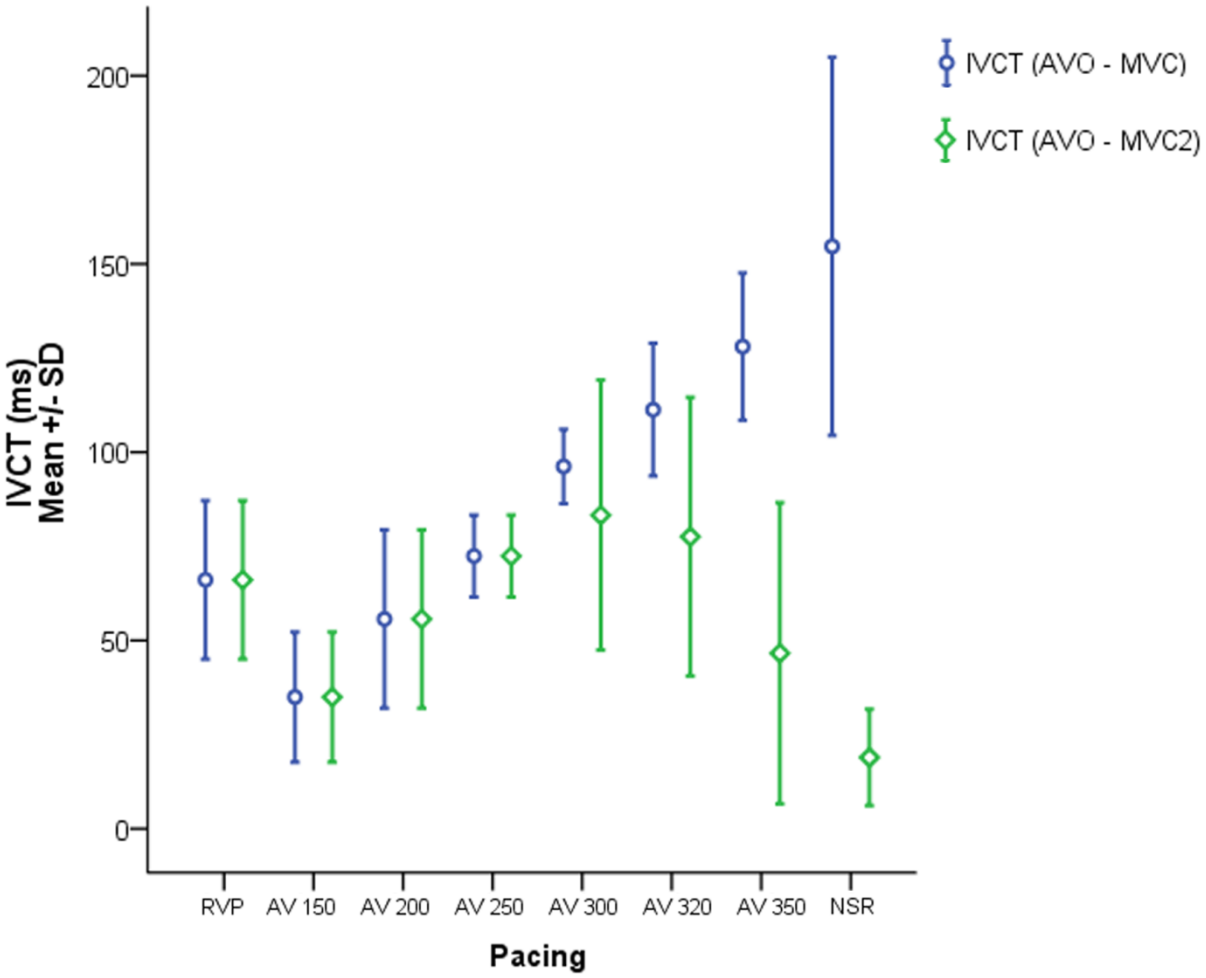

Figure 4: Isovolumic contraction time (IVCT) calculated based on aortic valve opening (AVO) and mitral valve closure (MVC) measured by M-mode. Blue error bars represent IVCT calculated as AVO – MVC, green error bars represent IVCT calculated as AVO – MVC2 if a second closure of the mitral valve (MVC2) was present after minor valve reopening during long atrioventricular delays. The error bars display mean ± 1 standard deviation (SD).

Discussion

This study demonstrates the influence of AV interaction on:

1. The morphology of the pre-ejection velocity spikes
2. The peak pre-ejection LV velocity and acceleration measured by TDI
3. The time of MVC

During SR and long AV delays, the TDI curves showed two pre-ejection peaks in the LV free wall. MVC was induced by atrial relaxation, later followed by a true isovolumic velocity peak. During RVP and short AV delays, MVC occurred significantly later and coincided with the end of IVC, suggesting the role of LV pressure development for MVC. The TDI curves showed one pre-ejection peak with a significantly higher velocity and acceleration.

Morphology of the pre-ejection velocity spikes

Radial myocardial velocity curves in normal adult humans usually show one positive pre-ejection peak (Lind et al., 2004). Similarly, one peak was present during pacing at short AV delays in this study. However, two peaks were observed during long AV delays. This is in agreement with a study of pacing at a long AV delay (300 ms) in patients with third degree AV block which resulted in two pre-ejection velocity waves, while pacing at a short (50 ms) and nominal (130 ms) delay revealed only one pre-ejection peak (Remme et al., 2008). The first peak can be explained by atrial relaxation or by passive recoil of the LV following expansion after atrial contraction. The second peak was identified as true isovolumic contraction.

Peak IVC velocity and IVA measured by TDI

Peak IVC velocity and acceleration were significantly influenced by AV interaction. Both measurements are often used as measurerements of LV function. Peak IVC velocity is a strong marker of myocardial dysfunction in severely ischemic and dyskinetic myocardium (Edvardsen et al., 2002). IVA has been proposed as a load-independent index of LV contractility (Vogel et al., 2003; Margulescu et al., 2010). Changes in IVA during dobutamine and esmolol infusion were correlated to invasively measured systolic elastance, the "gold standard" of contractility. IVA was unaffected by preload reduction within a physiological range, whereas dP/dt_{max} and systolic myocardial velocities changed significantly. In patients, IVA remained unchanged during inferior vena cava occlusion or after closure of an atrial septal defect while myocardial velocities were significantly altered (Pauliks et al., 2005; Duan

et al., 2006). In contrast, other investigators revealed that IVA is not load-independent and can be altered by experimental volume loading and caval constriction (Lyseggen et al., 2005). Similarly, in our study, we demonstrated that IVC velocities and acceleration differed during dual-chamber pacing dependent on the timing of atrial and ventricular contraction, with higher peak IVC velocity and IVA during short AV delays and RVP. We hypothesize that this can be explained by the delayed MVC. As a consequence, the mitral valve is still open at the onset of contraction of the LV, which sees an initially lower afterload resulting in higher LV velocities.

The concept of a true isovolumic contraction phase has been debated before. Goetz et al. (2005) demonstrated that MVC does not occur until after three-quarters of the pre-ejection period. Remme et al. (2008) hypothesized that the myocardial pre-ejection velocity spikes might be caused by a simple mechanism: at the onset of systole, LV wall shortening closes the valve leaflets and moves them toward the left atrium. When leaflet motion is stopped by the chordae tendinae, wall shortening is interrupted which results in a biphasic spike on the TDI velocity curve. Our findings support this hypothesis. During short AV delays and RVP, MVC coincided with the end of IVC and was followed by a highly negative velocity peak (nIVC). During long AV delays and SR, MVC occurred before IVC and nIVC was often absent. However, other mechanisms such as layer-dependent wall deformation have been proposed to explain the radial biphasic wall motion during IVC. Subendocardial fiber shortening accompanied by subepicardial fiber stretch results in wall thickening within the isovolumic constraint (Ashikaga et al., 2009). The subepicardial pre-ejection stretch might be important to adjust the cardiac myosin power to variations in load (Sengupta et al., 2005).

Mitral valve closure

Although the influence of the AV delay on MVC has been previously demonstrated, the exact mechanism of MVC is not yet fully clarified. MVC is initiated by the LA/LV pressure cross-over, but this might be caused both by increased LV pressure following LV contraction or by decreased LA pressure following LA relaxation. In patients paced at AV delays of 50 to 250 ms, MVC was correlated to onset of ventricular systole at short AV delays but this correlation was lost at long AV delays (Von Bibra et al., 1986). Similarly, during long AV delays in our study, MVC was associated with atrial relaxation and could even occur before onset QRS. This indicates that MVC can be caused by atrial relaxation alone during long AV delays.

Atrial relaxation results in a decreased LA pressure which falls below LV pressure, resulting in a deceleration of mitral flow until flow is reversed and simultaneous movement of the valve leaflets toward closure occurs (Meisner et al., 1985). Other mechanisms can also explain the role of the LA in the mechanism of MVC. Presystolic mitral annular contraction facilitates valve closure by approximating the mitral leaflets. This annular reduction is functionally coupled to left atrial depolarization and 89% of this reduction occurs before ventricular systole (Glasson et al., 1997; Bothe et al., 2009). In addition, myocytes occupying the basal portion of the leaflets are activated after atrial depolarization, causing anterior mitral valve leaflet stiffening which aids valve closure (Swanson et al., 2011). However, leaflet stiffening and annular reduction seem to be induced by activation through the AV-node, suggesting that it plays a role in the MVC associated with IVC rather than with atrial relaxation itself.

During long AV delays and SR in our study, minor mitral valve re-opening occurred after atriogenic MVC, followed by a second ventriculogenic MVC. Similarly, both atrial relaxation and ventricular contraction could close the valve at long AV delays in a patient with a prosthetic mitral valve and complete heart block, resulting in double closure (Hamby et al., 1973). However, sustained MVC after atrial systole or diastolic mitral valve "locking" has also been described during pacing. A critical LV volume is required to prevent passive reopening of the valve (David et al., 1986).

Clinical implications

Late diastolic mitral regurgitation (MR) before MVC or during re-opening of the mitral valve has been described at prolonged AV delays in patients with implanted DDD pacemakers (Ishikawa et al., 1999). In patients with AV block, mitral and tricuspid diastolic regurgitation occurred about 240 to 330 ms after onset P, after the mitral valve reached near closure following atrial relaxation (Schnittger et al., 1988). However, our results suggest that mitral regurgitation can also occur during RVP and pacing at short AV delays, when ventricular contraction interrupts leaflet motion toward the ventricle (Tsakiris et al., 1976). This is reflected by the increased FS values during RVP and pacing at short AV delays. Similarly, it was shown that ventricular pacing in sheep resulted in a greater end-diastolic leaflet opening angle, delayed MVC and a higher regurgitant fraction compared to atrial pacing (Langer et al., 2005).

This might be particularly important in patients with atrial fibrillation (AF). During AF, both normal LA contraction and electrical activation are absent. The absence of electrical activation causes a loss of the presystolic mitral annular reduction (Pai et al., 2003). The altered mechanism of MVC during AF might be important in the pathogenesis of "atrial function MR", a secondary, normal leaflet motion MR which is often present in patients with AF and an enlarged mitral annulus (Gertz et al., 2011). In addition, LV peak IVC velocity and IVA might be different in AF compared to sinus rhythm.

Finally, AV delay optimization is increasingly important in cardiac resynchronization therapy (CRT). Both patients with a short AV delay and blunting of the A wave and patients with a prolonged AV delay and diastolic MR have a high likelihood of being a clinical CRT responder (Parsai et al., 2009). AV delay optimization results in changes in stroke volume and diastolic filling, which can be assessed by pulsed or continuous wave Doppler of the aortic or mitral valve (Waggoner et al., 2008). Peak IVC velocity or IVA might be additional parameters to consider as surrogates for assessing mitral valve dynamics (rather than contractility).

Limitations

Ventricular pacing possibly influenced the activation pattern and pre-ejection motion of the LV. Although this may complicate the comparison with sinus rhythm, the pacing catheter position was stable throughout the study and pacing could thus not interfere with the influence of the AV delay during dual-chamber pacing. Furthermore, no indications for severe dyssynchrony, such as a wide QRS complex or a septal flash (Parsai et al., 2009) were present. The sequence of pacing modes might also affect results. Therefore, pacing was performed in a random sequence and each recording period was preceded by a stabilization period of 1 minute. Invasive studies have demonstrated a stabilization period of 5–20 seconds sufficient to achieve hemodynamic equilibrium (Porciani et al., 2005).

Apical images are impossible to obtain in adult horses due to anatomical restrictions. As a consequence, radial velocity measurements were performed from parasternal images, and accurate transmitral inwards and regurgitant flow measurements could not be achieved. Invasive measurements of LA and LV pressure would have provided additional information but are difficult to obtain in horses without sedation or anesthesia, which might in turn influence LV contractility.

Conclusions

The AV interaction significantly influences the timing of MVC and pre-ejection LV wall motion. Depending on the AV delay, MVC can be atrio- or ventriculogenic, resulting in a significantly higher pre-ejection LV peak velocity and IVA if the mitral valve is still open at the onset of LV contraction.

References

Ashikaga H, van der Spoel TI, Coppola BA, Omens JH (2009). Transmural myocardial mechanics during isovolumic contraction. JACC. Cardiovasc Imaging 2, 202-211

Bothe W, Nguyen TC, Roberts ME, Timek TA, Itoh A, Ingels NB, Jr., Miller DC (2009). Presystolic mitral annular septal-lateral shortening is independent from left atrial and left ventricular contraction during acute volume depletion. Eur J Cardiothorac Surg 36, 236-242

David D, Michelson EL, Naito M, Chen CC, Schaffenburg M, Dreifus LS (1986). Diastolic 'locking' of the mitral valve: Possible importance of diastolic myocardial properties. Circulation 73, 997-1005

Duan YY, Harada K, Toyono M, Ishii H, Tamura M, Takada G (2006). Effects of acute preload reduction on myocardial velocity during isovolumic contraction and myocardial acceleration in pediatric patients. Pediatr Cardiol 27, 32-36

Edvardsen T, Urheim S, Skulstad H, Steine K, Ihlen H, Smiseth OA (2002). Quantification of left ventricular systolic function by tissue Doppler echocardiography: Added value of measuring pre- and postejection velocities in ischemic myocardium. Circulation 105, 2071-2077

Garcia MJ, Rodriguez L, Ares M, Griffin BP, Klein AL, Stewart WJ, Thomas JD (1996). Myocardial wall velocity assessment by pulsed Doppler tissue imaging: Characteristic findings in normal subjects. Am Heart J 132, 648-656

Gertz ZM, Raina A, Saghy L, Zado ES, Callans DJ, Marchlinski FE, Keane MG, Silvestry FE (2011). Evidence of atrial functional mitral regurgitation due to atrial fibrillation: Reversal with arrhythmia control. J Am Coll Cardiol 58, 1474-1481

Glasson JR, Komeda M, Daughters GT, Foppiano LE, Bolger AF, Tye TL, Ingels NB, Jr., Miller DC (1997). Most ovine mitral annular three-dimensional size reduction occurs before ventricular systole and is abolished with ventricular pacing. Circulation 96, 115-123

Goetz WA, Lansac E, Lim HS, Weber PA, Duran CM (2005). Left ventricular endocardial longitudinal and transverse changes during isovolumic contraction and relaxation: A challenge. Am J Physiol Heart Circ Physiol 289, H196-201

Grenacher PA, Schwarzwald CC (2010). Assessment of left ventricular size and function in horses using anatomical M-mode echocardiography. J Vet Cardiol 12, 111-121

Hamby RI, Aintablian A, Wisoff BG (1973). The role of atrial systole in valve closure. Report of patient with complete heart block and a mitral prosthetic valve. Chest 64, 197-202

Ishikawa T, Sumita S, Kimura K, Kikuchi M, Kosuge M, Kuji N, Endo T, Sugano T, Sigemasa T, Kobayashi I, Tochikubo O, Usui T (1999). Prediction of optimal atrioventricular delay in patients with implanted DDD pacemakers. Pacing Clin Electrophysiol 22, 1365-1371

Kim WY, Walker PG, Pedersen EM, Poulsen JK, Oyre S, Houlind K, Yoganathan AP (1995). Left ventricular blood flow patterns in normal subjects: A quantitative analysis by

three-dimensional magnetic resonance velocity mapping. J Am Coll Cardiol 26, 224-238

Langer F, Tibayan FA, Rodriguez F, Timek T, Zasio MK, Liang D, Daughters GT, Ingels NB, Miller DC (2005). Altered mitral valve kinematics with atrioventricular and ventricular pacing. J Heart Valve Dis 14, 286-294

Lind B, Nowak J, Cain P, Quintana M, Brodin LA (2004). Left ventricular isovolumic velocity and duration variables calculated from colour-coded myocardial velocity images in normal individuals. Eur J Echocardiogr 5, 284-293

Little RC (1979). The mechanism of closure of the mitral valve: A continuing controversy. Circulation 59, 615-618

Lyseggen E, Rabben SI, Skulstad H, Urheim S, Risoe C, Smiseth OA (2005). Myocardial acceleration during isovolumic contraction: Relationship to contractility. Circulation 111, 1362-1369

Margulescu AD, Thomas DE, Ingram TE, Vintila VD, Egan MA, Vinereanu D, Fraser AG (2010). Can isovolumic acceleration be used in clinical practice to estimate ventricular contractile function? Reproducibility and regional variation of a new noninvasive index. J Am Soc Echocardiogr 23, 423-431

Meisner JS, McQueen DM, Ishida Y, Vetter HO, Bortolotti U, Strom JA, Frater RW, Peskin CS, Yellin EL (1985). Effects of timing of atrial systole on LV filling and mitral valve closure: Computer and dog studies. Am J Physiol 249, H604-619

Pai RG, Varadarajan P, Tanimoto M (2003). Effect of atrial fibrillation on the dynamics of mitral annular area. J Heart Valve Dis 12, 31-37

Parsai C, Bijnens B, Sutherland GR, Baltabaeva A, Claus P, Marciniak M, Paul V, Scheffer M, Donal E, Derumeaux G, Anderson L (2009). Toward understanding response to cardiac resynchronization therapy: Left ventricular dyssynchrony is only one of multiple mechanisms. Eur Heart J 30, 940-949

Pauliks LB, Chan KC, Chang D, Kirby SK, Logan L, DeGroff CG, Boucek MM, Valdes-Cruz LM (2005). Regional myocardial velocities and isovolumic contraction acceleration before and after device closure of atrial septal defects: A color tissue Doppler study. Am Heart J 150, 294-301

Pellerin D, Berdeaux A, Cohen L, Giudicelli JF, Witchitz S, Veyrat C (1998). Pre-ejectional left ventricular wall motions studied on conscious dogs using Doppler myocardial imaging: Relationships with indices of left ventricular function. Ultrasound Med Biol 24, 1271-1283

Porciani MC, Dondina C, Macioce R, Demarchi G, Pieragnoli P, Musilli N, Colella A, Ricciardi G, Michelucci A, Padeletti L (2005). Echocardiographic examination of atrioventricular and interventricular delay optimization in cardiac resynchronization therapy. Am J Cardiol 95, 1108-1110

Remme EW, Lyseggen E, Helle-Valle T, Opdahl A, Pettersen E, Vartdal T, Ragnarsson A, Ljosland M, Ihlen H, Edvardsen T, Smiseth OA (2008). Mechanisms of preejection and postejection velocity spikes in left ventricular myocardium: Interaction between wall deformation and valve events. Circulation 118, 373-380

Schnittger I, Appleton CP, Hatle LK, Popp RL (1988). Diastolic mitral and tricuspid regurgitation by Doppler echocardiography in patients with atrioventricular block: New insight into the mechanism of atrioventricular valve closure. J Am Coll Cardiol 11, 83-88

Sengupta PP, Khandheria BK, Korinek J, Wang J, Belohlavek M (2005). Biphasic tissue Doppler waveforms during isovolumic phases are associated with asynchronous deformation of subendocardial and subepicardial layers. J Appl Physiol 99, 1104-1111

Silbiger JJ, Bazaz R (2009). Contemporary insights into the functional anatomy of the mitral valve. Am Heart J 158, 887-895

Swanson JC, Krishnamurthy G, Kvitting JP, Miller DC, Ingels NB, Jr. (2011). Electromechanical coupling between the atria and mitral valve. Am J Physiol Heart Circ Physiol 300, H1267-1273

Timek T, Dagum P, Lai DT, Green GR, Glasson JR, Daughters GT, Ingels NB, Jr., Miller DC (2001). The role of atrial contraction in mitral valve closure. J Heart Valve Dis 10, 312-319

Timek TA, Lai DT, Tibayan F, Daughters GT, Liang D, Dagum P, Lo S, Miller DC, Ingels NB, Jr. (2002). Atrial contraction and mitral annular dynamics during acute left atrial and ventricular ischemia in sheep. Am J Physiol Heart Circ Physiol 283, H1929-1935

Tsakiris AG, Gordon DA, Mathieu Y, Padiyar R, Labrosse C (1976). Sudden interruption of leaflet opening by ventricular contractions: A mechanism of mitral regurgitation. J Appl Physiol 40, 132-137

Vogel M, Cheung MMH, Li J, Kristiansen SB, Schmidt MR, White PA, Sorensen K, Redington AN (2003). Noninvasive assessment of left ventricular force-frequency relationships using tissue Doppler-derived isovolumic acceleration validation in an animal model. Circulation 107, 1647-1652

von Bibra H, Wirtzfeld A, Hall R, Ulm K, Blomer H (1986). Mitral valve closure and left ventricular filling time in patients with VDD pacemakers. Assessment of the onset of left ventricular systole and the end of diastole. Br Heart J 55, 355-363

Waggoner AD, de las Fuentes L, Davila-Roman VG (2008). Doppler echocardiographic methods for optimization of the atrioventricular delay during cardiac resynchronization therapy. Echocardiography 25, 1047-1055

CHAPTER 5

Tissue Doppler imaging and two-dimensional speckle tracking in horses with cardiomyopathy caused by ionophore intoxication

Chapter 5.1

Acute and long-term cardiomyopathy and delayed neurotoxicity after accidental lasalocid poisoning in horses

Adapted from:

Decloedt A[1], Verheyen T[1], De Clercq D[1], Sys S[1], Vercauteren G[2], Ducatelle R[2], Delahaut P[3], van Loon G[1]

[1]Department of Large Animal Internal Medicine, Faculty of Veterinary Medicine, Ghent University, Belgium
[2]Department of Pathology, Bacteriology and Avian Diseases, Faculty of Veterinary Medicine, Ghent University, Merelbeke, Belgium
[3]Département Santés animale et humaine, Centre d'Economie Rurale, Marloie, Belgium

Acute and long-term cardiomyopathy and delayed neurotoxicity after accidental lasalocid poisoning in horses.

Journal of Veterinary Internal Medicine (2012) EPub Apr 21, doi 10.1111/j.1939-1676.2012.00933.x

Part of this work was presented at the 50th BEVA Congress, Liverpool, United Kingdom, September 7-10, 2011.

Summary

Background: Horses are extremely susceptible to ionophore intoxication. Although numerous reports are available regarding monensin, little is known about lasalocid toxicity.

Objectives: To describe accidental lasalocid poisoning on a farm in Belgium.

Animals: Eighty-one horses, of which fourteen demonstrated clinical signs from day 0–21 after being fed a new concentrate batch. One horse died on day 20 and another on day 27.

Methods: The most severe cases (n=7), admitted to the Department of Large Animal Internal Medicine on day 29–46, underwent cardiac examination and blood biochemical analysis including determination of plasma cardiac troponin I (cTnI) at admission and during follow-up. On day 57–70, cardiac examination, cTnI determination or both were undertaken on 72 remaining horses.

Results: Short-term effects of lasalocid intoxication included inappetance, lethargy, sweating and muscular weakness. All seven horses admitted to the clinic demonstrated signs of myocardial degeneration such as increased cTnI, dysrhythmia and impaired myocardial function. Four horses developed ataxia on day 40–50. Five horses died or were euthanized on day 30–370, two horses recovered fully and returned to previous athletic use. None of the 72 remaining horses exhibited clinical signs between day 57–70, but 34 had dysrhythmia and 13 had increased cTnI concentrations. After a period of rest, all horses returned to their previous work. Lasalocid was detected in hepatic tissue of two necropsied horses.

Conclusions and clinical importance: Lasalocid intoxication induced myocardial and neurological damage. Although uncommon, this should be included as differential diagnosis for unexplained inappetance, signs of depression, cardiomyopathy and ataxia in horses.

Introduction

Ionophores are a group of polyether antibiotics used as feed additives in poultry and ruminants. Their biological activity is exerted by the formation of lipid-soluble complexes with cations, thereby facilitating transmembrane ion transport. They can be classified based on their affinity for different cation types. Monovalent ionophores such as monensin primarily bind Na^+ and K^+, while divalent ionophores such as lasalocid have a high affinity for Ca^{2+} and Mg^{2+} (Gad et al., 1985).

Ionophore intoxication may occur due to overdosage in target species. In non-target species, intoxication can be caused by accidental mixing in feed or malicious intent. Toxicity is caused by the disruption of transmembrane ion concentration gradients and electrical potentials, which results in an overload of the active cation efflux channels, leading to ATP depletion. Furthermore, the increased Ca^{2+} influx results in excess mitochondrial uptake, causing mitochondrial damage and lack of cellular energy production (Mollenhauer et al., 1981). Ca^{2+} also interferes with the cellular enzyme systems. These mechanisms eventually result in cell death (Novilla, 1992). The influx of Ca^{2+} is especially detrimental in excitable cells such as those in myocardium, skeletal muscles and nervous tissue (Doebler, 2000).

The single oral median lethal dose (LD_{50}) of ionophores varies largely between species. Horses are more sensitive to the toxic effects of ionophores than cattle or poultry. Monensin toxicosis in horses is well documented in the literature as this is the most widely used ionophore antibiotic (Kamphues et al., 1990; Bezerra et al., 1999; Bila et al., 2001; Peek et al., 2004). The main toxic effects of monensin result from myocardial and muscular damage. Acute intoxication causes anorexia, sweating, ataxia, tachydysrhythmia and possibly death. Long-term effects have also been described and include cardiac failure, poor performance or muscular weakness and stiffness (Muylle et al., 1981; Hughes et al., 2009). Horses are also susceptible to intoxication by other ionophores such as salinomycin or lasalocid (Novilla, 1992; Aleman et al., 2007). Although lasalocid toxicosis has been described in several animal species, the short- and long-term consequences of accidental lasalocid intoxication in horses have not previously been reported (Hanson et al., 1981; Galitzer et al., 1986; Segev et al., 2004; Kart and Bilgili, 2009).

The aims of this study were to describe accidental lasalocid poisoning on a Belgian farm with eighty-one horses and to describe the presence of acute and chronic myocardial and neurological damage due to lasalocid intoxication.

Material and methods

Study population

The study population consisted of eighty-one horses on a Belgian farm. Breeds included warmblood horses (n=50), riding ponies (n=25), Shetland ponies (n=4) and Norwegian Fjord horses (n=2). Mean height was 151±20 cm and mean age was 12±5 years. Sex distribution was 44 mares, 33 geldings and 4 stallions. All horses were vaccinated against influenza and tetanus (Duvaxyn IE-PLUS-T, Fort Dodge, Naarden, The Netherlands). The next day, a new batch of concentrate was delivered. This day will be referred to as day 0.

Biochemical examination

Biochemical examination of horses admitted to the Department of Large Animal Internal Medicine (Ghent University) between day 29 and 46 was performed at admission and during follow-up examination and included electrolyte concentrations, serum activities of creatine kinase and plasma cardiac troponin I (cTnI) concentration.

In the remaining horses at the farm, only cTnI was measured on day 37 and during follow-up. After blood was collected in lithium heparin tubes, the samples were centrifuged as quickly as possible. Maximum time between sample collection and centrifugation was 6 hours. The samples were then immediately stored at -18°C and cTnI concentration was determined within one week by a validated immuno-assay (Acces Accu-TnI, Beckman Coulter Inc, Fullerton, CA).

Cardiac examination

The cardiologic examination (performed between day 30 and 490) included an echocardiogram, resting and exercising ECG. Echocardiography was performed using an ultrasound unit (GE Vivid 7 Dimension, GE Healthcare, Horten, Norway) with phased array transducer (3S Phased Array Transducer, GE Healthcare, Horten, Norway). Left ventricular (LV) function was assessed by M-mode, tissue Doppler imaging and two-dimensional speckle tracking. Fractional shortening was calculated as the conventional measurement of LV systolic function.

ECGs were recorded at rest and during a lunging exercise test with a telemetric recording system (Televet 100® Version 4.1.3., Kruuse, Marslev, Denmark). The test consisted of five minutes walk, ten minutes trot, four minutes canter and one minute gallop.

The test was discontinued if horses demonstrated signs of fatigue or if pathological ECG abnormalities were detected such as polymorphic ventricular premature depolarizations (VPDs) or ventricular tachycardia (VT).

Necropsy findings

Gross pathological and histopathological lesions were identified and recorded. Toxicological analysis of the liver was performed in two horses that died on day 30 and 37. Samples were analysed by liquid chromatography coupled to tandem mass spectrometry. The extraction of target coccidiostats was based on liquid extraction with an organic solvent (acetonitrile). This method allows quantification and confirmation of ten coccidiostatics (maduramycin, narasin, lasalocid, monensin, salinomycin, halofuginone, robenidin, nicarbazin, diclazuril and decoquinate), with a detection limit of 0.5 parts per billion (ppb) for most compounds. Quantification was performed with a Quality Control (QC) sample, analysed with each samples batch. This sample is a matrix sample spiked with target coccidiostatics, at a level corresponding to the detection limit. Retention time of the chromatography as well as ion ratios (i.e. relative intensities of the two product ions) are used as identification criterion, as stated by Decision 2002/657/EC.

Feed analysis

Samples of the concentrate present at the farm on day 30 were analysed for the presence of ionophores. As a new batch was delivered every two weeks, the concentrate supply fed at day 0 was no longer available. Samples taken during the production process of the batches delivered on day 0 and 15 were provided by the manufacturer. In addition, analyses were performed on dust accumulated in the dust pipe of the silo used to store feed at the farm. The presence and concentration of ionophores in concentrate and dust were assessed by the same method as the liver samples.

Data Analysis and Statistics

Data are reported as median and range.

Results

Clinical course

Between day 0 and 21, 14 horses demonstrated inappetance (n=11), lethargy (n=9), swelling of the neck at the vaccination site (n=7), diffuse sweating (n=2), increased body temperature (n=3) or hind limb weakness (n=3). These clinical signs were assumed to be due to vaccination and horses were treated with antibiotics and non-steroidal anti-inflammatory drugs for several days to weeks. One horse was treated with trimethoprim and sulfadiazine administered orally during ten days. Two ponies were referred to a private referral practice on day 17. Despite intensive treatment, both ponies suddenly became recumbent and died on day 20 and 27.

Between day 29 and 46, 7 horses with persistent anorexia and lethargy were admitted to the Department of Large Animal Internal Medicine, Ghent University (Table 1). These horses were treated according to their clinical status by intravenous administration of crystalloid fluids, flunixin (IV), supplementation of magnesium and potassium (PO or IV), and supplementation of vitamin E (PO). Two horses showed sustained polymorphic VT and were treated by a lidocaine bolus (IV) followed by a constant rate infusion. In horse 1, VT progressed to development of ventricular fibrillation (VF) and death of the horse within twenty-four hours despite anti-dysrhythmic treatment. In horse 4, treatment initially effectively suppressed ectopy but after one week, this animal was euthanized because of severe weakness, increased respiratory effort and collapse. The five other horses also had signs of mild to severe myocardial damage such as dysrhythmia, increased plasma cTnI concentrations, impaired LV function or all three. In addition, four of them developed weakness, ataxia or paresis between day 40 and 50. These horses were additionally supplemented orally with thiamine. In horse 6, mild ataxia was present which resolved fully after three months. However, horse 3 and 5 were euthanized on day 55 and 56 due to severe ataxia, decubitus and excitation. Horse 2 showed severe ataxia of the hind limbs and paresis of the front limbs but recovered at the nine month re-evaluation period.

Feeding of the concentrate batch present at the farm was immediately discontinued from day 30 onward. The 72 remaining horses were rested and their plasma cTnI concentration was determined on day 37. Between day 57 and 70, 60 of the 72 horses underwent a full cardiac examination. Five of these horses had shown clinical signs between day 0 and 21, but clinical examination between day 57 and 70 revealed no abnormalities.

Table 1: Clinical course, echocardiographic and ECG findings of seven horses admitted to the clinic with persistent lethargy or anorexia on day 29–46 after accidental lasalocid poisoning

Horse	$cTnI_{max}$ (ng/mL)	Day of $cTnI_{max}$	Day of admission	ECG findings	Echocardiographic findings	Clinical course	Outcome
1	123	29	29	sustained polymorphic VT	severely impaired LV function	ventricular fibrillation	death (day 30)
2	88.8	34	29	paroxysmal polymorphic VT	severely impaired LV function	improved LV function, severe ataxia	fully recovered (after 9 months)
3	145	29	29	paroxysmal polymorphic VT	severely impaired LV function	improved LV function, severe ataxia	euthanized (day 55)
4	816	34	30	sustained polymorphic VT	severely impaired LV function	weakness, dyspnea, mesenterial hemorrhage	euthanized (day 37)
5	8.43	43	43	frequent APD, occasional VPD	normal function	severe ataxia	euthanized (day 56)
6	1.39	37	46	occasional APD and VPD	normal function	mild ataxia	fully recovered (after 3 months)
7	3.32	46	46	paroxysmal polymorphic VT	myocardial fibrosis, severely impaired LV function	continuing paroxysmal VT, impaired LV function	euthanized (day 370)

$cTnI_{max}$, maximal plasma concentration of cardiac troponin I; LV, left ventricular; VT, ventricular tachycardia; APD, VPD, atrial, ventricular premature depolarization; VF, ventricular fibrillation.

Biochemical examination

The seven horses initially admitted to the clinic were hypokalemic, hypocalcemic and hypomagnesemic. Despite electrolyte supplementation, these plasma electrolyte disturbances remained in some horses up to three weeks after admission. Serum activities of creatine kinase were increased in six horses (median 341.5 mU/mL, range 214–1564 mU/mL; reference range 10–146 mU/mL). Plasma cTnI concentrations were increased above reference values in all seven horses with a median peak value of 88.78 ng/mL (1.39–816 ng/mL, reference range 0–0.10 ng/mL). Thirteen of the 72 remaining horses had increased cTnI concentrations on day 37 or during follow-up. The median peak cTnI concentration was 0.19 ng/mL (0.11–2.01 ng/mL). Plasma cTnI concentrations generally decreased throughout the period of follow-up but remained increased for months in several horses (Fig. 1A-B). In 8/13 horses at the premises the cTnI concentration was slightly increased at one or more sampling dates during follow-up.

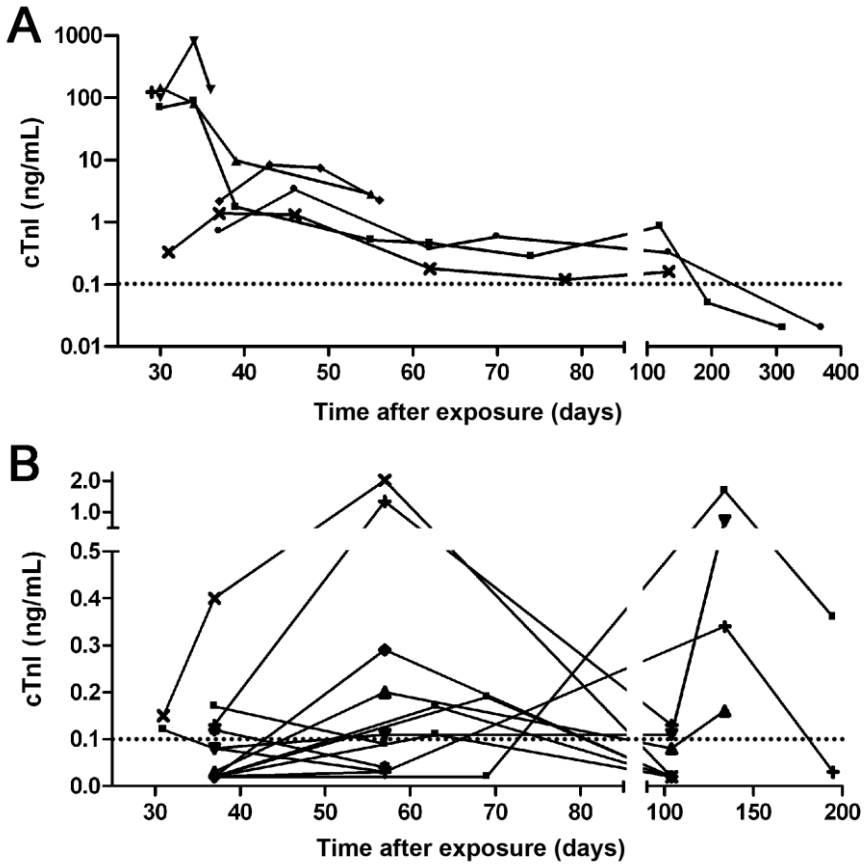

Figure 1A-B: Plasma concentrations of cardiac troponin I (cTnI) over time in horses exposed to lasalocid. The X-axis displays time expressed as days after the new batch of concentrate was delivered to the farm (presumed time of exposure). The dotted line indicated the upper reference limit of 0.10 ng/mL). (A) cTnI concentrations of seven horses admitted to the clinic between day 29 and 46 with persistent lethargy or anorexia; (B) cTnI concentrations of thirteen horses at the premises which showed increased cTnI concentrations.

Cardiac examination

Ventricular dysrhythmia was detected in all seven horses initially admitted to the clinic (Table 1). By echocardiography, anechogenic fluid could be demonstrated in the pericardial space of three horses. Five horses showed severely depressed LV systolic function (FS<25%). The median FS was 19% (range 5–24%; reference range 29.4–44.7%). Long-term follow-up could be performed in three horses. Horse 3 had improved LV systolic function one week before it had to be euthanized due to neurological abnormalities. In horse 2, FS returned to normal values after four months. Horse 7 showed impaired LV systolic function (FS=24%), severe myocardial fibrosis demonstrated by hyperechoic regions in the LV walls and frequent ventricular premature depolarizations (VPDs) at admission. At repeated follow-up until day 370, myocardial fibrosis, multiple VPDs and paroxysmal VT persisted and the horse was euthanized at the owner's request.

Cardiac auscultation of 60 horses at the farm revealed no dysrhythmias. In two horses, a pathological murmur was detected due to valvular regurgitation as confirmed by color flow Doppler. Conventional echocardiography showed normal LV diameters and systolic function in all horses. However, 34 horses presented a dysrhythmia (Table 2). Two horses with more than ten VPDs during exercise were re-examined on day 134 and day 195. In both horses, VPDs were still present on both occasions. However, after one year all surviving horses had returned to their previous level of exercise.

Table 2: Classification of dysrhythmias present in 60 horses at the premises between day 57 and 70 on an ECG at rest (30 minutes) and during a standardized exercise test (25 minutes)

Dysrhythmia	Horses with increased cTnI (n=13)		Horses with normal cTnI (n=47)	
	Number per horse (median and range)	Number of horses (%)	Number per horse (median and range)	Number of horses (%)
sinus/AV-block at >70 bpm	1	2 (15.4)	2 (1–3)	6 (12.8)
APDs at rest	47 (1–92)	2 (15.4)	3 (1–31)	8 (17.0)
APDs during exercise	0	0 (0.0)	1 (1–19)	10 (21.3)
APDs rest and exercise	47 (1–92)	2 (15.4)	2 (1–50)	13 (27.7)
VPDs at rest	7 (1–9)	3 (23.1)	2 (1–4)	6 (12.8)
VPDs during exercise	23 (16–30)	2 (15.4)	1 (1–4)	15 (32.0)
VPDs rest and exercise	23 (1–30)	3 (23.1)	2 (1–6)	18 (38.3)
All dysrhythmias		6 (46.2)		28 (59.6)

AV, atrioventricular; APD, VPD, atrial, ventricular premature depolarization; bpm, beats per minute; HR, heart rate

Necropsy

Six horses were necropsied: one pony that died at the referral practice on day 27 and five horses that died at the clinic on day 30, 37, 55, 56 and 370. Gross pathological lesions revealed signs of myocardial degeneration in all horses. These included multifocal pale areas in the myocardium, left and right cardiac dilation and hydropericardium. Small subendocardial pale, irregular lesions were present in the interventricular septum. Horse 7 had evidence of severe myocardial fibrosis, especially in the septum. The pony that died at the referral practice, horse 1 and horse 4 showed secondary signs of heart failure including pulmonary edema, hepatic venous congestion and ascites. Horse 4 had a severe mesenteric haemorrhage.

Histopathological examination demonstrated acute to chronic myocardial degeneration, with multifocal to coalescent hyalinisation, fragmentation and loss of striation of cardiomyocytes combined with interstitial edema, fibroblast proliferation or fibrosis and infiltration of macrophages, neutrophils and lymphocytes. The most severe lesions were located subendocardially and subepicardially, with subendocardial deposition of mineraloid matrix in the septum. Horse 3 and 5, euthanized eight weeks after the onset of clinical signs, also presented myocardial regeneration with mild anisokaryosis. Hepatic lesions were due to chronic hepatic congestion, characterized by dilation of centrolobular veins and atrophy of paracentral hepatocytes with diffuse vacuolar degeneration. Renal histopathological lesions included signs of congestion, haemorrhage, calcification and degeneration of the tubuli. Hind limb skeletal muscles showed mild degeneration and regeneration in horse 3 and 5. The sciatic and tibial nerve of both horses demonstrated myelin sheath swelling and focal axonal degeneration, with formation of digestion chambers. In both horses, multifocal axonal swelling was detected along the spinal cord from the cervical segments to the cauda equina.

Toxicological analysis of liver tissue of horse 1 and 4 (collected on day 30 and 37) demonstrated lasalocid concentrations of 0.5 ppb lasalocid in the liver samples. No other ionophores were detected.

Feed analysis

Samples of the feed concentrate present at the farm on day 30 contained low concentrations of lasalocid (6 ppb) and robenidin (170 ppb). Samples taken from the batches delivered on day 0 and 15 contained 1 ppb lasalocid and 80 ppb robenidin. Several ionophores were detected in the dust accumulated in the dust pipe of the silo: 1 ppb nicarbazin, 0.7 ppb monensin, 1 ppb salinomycin, 1 ppb narasin, 15 ppb lasalocid and 100 ppb robenidin.

Discussion

This study describes accidental lasalocid poisoning on a premises with 81 horses. Fourteen horses had clinical signs between day 0 and 21, including anorexia, lethargy, profuse sweating and muscular weakness. Two horses died at a referral practice. Seven horses admitted to the Department of Large Animal Internal Medicine demonstrated signs of myocardial damage such as increased cTnI, dysrhythmias and impaired LV systolic function. Four horses developed a delayed neuropathy between day 40 and 50 characterized by ataxia and paresis. Five of the seven horses died or were euthanized and two horses recovered fully. None of the 72 remaining horses exhibited clinical signs between day 57 and 70, but 34 had dysrhythmias and 13 had increased cTnI concentrations. Diagnosis was confirmed by lasalocid detection in liver tissue but not in feed.

Horses are very susceptible to ionophore intoxication and accidental poisoning is well described. The LD_{50} of monensin in horses is estimated to be between 2 and 3 mg/kg body weight (Matsuoka, 1976). This is very low compared to the LD_{50} in cattle (26 mg/kg body weight) and chickens (200 mg/kg body weight) (Todd et al., 1984; Oehme and Pickrell, 1999). Lasalocid is less toxic and the LD_{50} in horses has been estimated to be 21.5 mg/kg body weight (Hanson et al., 1981). However, this estimate has been questioned as it is based on the data from four horses that died after being fed concentrate providing 15 to 26 mg/kg body weight (Kronfeld, 2002). In the current study, the total ingested dose of lasalocid could not be determined. The feed was not withdrawn until four weeks after the onset of clinical signs, and at that time two new batches of concentrate had already been delivered. The horses could have ingested low daily doses of lasalocid over a two-week period, resulting in a more chronic intoxication instead of a single oral dose. The short-term effects of lasalocid intoxication are similar to other ionophores. Inappetance is one of the first clinical signs and often the ingestion of concentrate is refused. Profuse sweating had not previously been reported for lasalocid, but is an acute clinical sign of monensin intoxication (Matsuoka, 1976; Novilla, 1992). Increased serum activities of muscle enzymes indicated muscle cell damage. The post-injection neck swelling probably resulted from mild muscular damage due the vaccination which may have been exacerbated by the ionophore. Furthermore, plasma electrolyte disturbances were present. These are caused by the ability of the ionophores to bind cations, as described in several cases of monensin intoxication (Boemo et al., 1991).

In total, 14/81 horses (17%) showed clinical signs between day 0 and 21. Full cardiac examination between day 30 and 70 revealed abnormal findings such as increased cTnI concentration, dysrhythmia or impaired LV systolic function in 48/67 horses (72%). Seven horses died or had to be euthanized whilst all other horses recovered fully. This is consistent with the large individual variations of ionophore susceptibility described in the literature. Even after experimental administration of monensin, clinical signs differ, ranging from absence of clinical abnormalities to sudden death (Matsuoka, 1976; Divers et al., 2009; Kraus et al., 2010). In the case of accidental poisoning, variation may be larger due to different amounts of concentrates ingested, inhomogeneous partitioning of the ionophore in the feed and other components in the diet. Anti-oxidants, such as vitamin E, act as a protective factor against intoxication and were used in the treatment of affected animals (Van Vleet and Rebar, 1985). Vitamin E status in these horses was unknown but might have contributed to individual variation in clinical signs. Horse 1 in this study showed severely depressed LV function and ectopy, and died due to VF despite intensive anti-dysrhythmic treatment. This horse had been treated at the farm with sulfonamides, which are known to enhance lasalocid toxicity (Espino et al., 2003; Aleman et al., 2007).

For monensin intoxication, it has been suggested that permanent cardiac damage can occur. Several studies have demonstrated reduced LV systolic function and ventricular dysrhythmias two to four months after ingestion of feed containing monensin (Peek et al., 2004; Hughes et al., 2009). Similarly, two months after the onset of clinical signs in this study, 13/72 (18%) of the remaining horses at the premises demonstrated increased cTnI concentrations and 21/60 (35%) demonstrated ventricular dysrhythmias at rest or during exercise. APDs, sinus exit block or first and second degree AV block at high heart rates were present in 22/60 (37%) horses. The higher prevalence of first and second degree AV block has been previously described in a case of salinomycin intoxication (Van Amstel and Guthrie, 1985). Histopathologically, the long-term effects of intoxication include marked cardiac fibrosis, as previously reported in six cases within five months after exposure to monensin (Muylle et al., 1981). In this study, all horses necropsied showed gross and histopathological signs of mild to severe myocardial degeneration and fibrosis.

Cardiac troponin I is a sensitive marker of myocardial injury and can be measured using human assays (Wells and Sleeper, 2008). This molecule is primarily bound to the contractile apparatus, although a small percentage remains free in the cytosol. Myocardial cell necrosis or membrane damage result in cTnI leakage into the circulation. The upper limit of the reference

range for the assay used in this study has been estimated at 0.10 ng/mL (Jesty et al., 2009). After experimental administration of monensin to healthy horses, the highest cTnI concentrations (>50 ng/mL) were reached in the horses that died or were euthanized due to severe cardiac disease (Divers et al., 2009; Kraus et al., 2010). Similarly, the highest cTnI concentrations in this study were generally found in horses with the most severe echocardiographic and electrocardiographic signs. The maximal cTnI concentration was as high as 816 ng/mL in a fatal case with severely depressed LV systolic function and VT. In some surviving horses, the cTnI concentration remained increased for several months, which is likely due to ongoing release from damaged myocytes (Wells and Sleeper, 2008). Similarly, experimentally-induced monensin intoxication resulted in increased plasma cTnI up to seven months after monensin administration (Kraus et al., 2010). Remarkably, cTnI concentrations increased during follow-up in some of our cases. This might be explained by the fact that some owners did not put their horses at rest although this was recommended. Conversely, in the horse with severe LV fibrosis, the cTnI concentration remained high for five months but had returned to normal values at the time of euthanasia after one year of rest.

Delayed neurotoxicity occurred in four horses at six weeks after the onset of clinical signs. Ataxia has been described as an acute clinical sign of monensin toxicosis. Furthermore, ataxia, hind limb weakness and muscle atrophy over a period of a week to several months have been reported in cases of accidental monensin and salinomycin poisoning (Boemo et al., 1991; Aleman et al., 2007). Delayed neuropathy due to lasalocid intoxication has not yet been described in horses. However, lasalocid induces axonal degeneration in other species. In dogs, accidental lasalocid ingestion results in tetraparesis, hyporeflexia and hypotonia. Mental status and pain perception are not affected, indicating a generalized lower motor neuron deficit. Most dogs recover fully over two to fifty days (Safran et al., 1993; Espino et al., 2003; Segev et al., 2004). The mechanism of neurotoxicity has been investigated in broiler chickens and rats. The mitochondrial energy deficit and impaired osmoregulation due to influx of Ca^{2+} ions lead to myelin edema and demyelination with secondary axonal degeneration. Histopathological lesions of neural tissue included axonal swelling with the presence of digestion chambers and vacuolation (Gregory et al., 1995; Kart et al., 2005; Kart and Bilgili, 2009). These lesions are very similar to those found in horse 3 and 5 in this study. In the two other affected horses, clinical signs were completely reversible.

The diagnosis of lasalocid intoxication is difficult since ionophores are not deposited in high concentrations in target tissues (Aleman et al., 2007). Horses that survived an LD_{50} dose of monensin longer than twenty-four hours had no detectable monensin in the liver (<0.05 ppm) even though they eventually died (Donoho, 1984). In this study, lasalocid could be demonstrated in the liver of two horses at low concentrations which confirmed exposure of these horses to lasalocid. Unfortunately, no sample was available at the premises from the concentrate batch delivered at the onset of clinical signs. A sample of this batch taken during the production process did not contain high lasalocid concentrations. However, contamination might have occurred during feed transportation. In addition, the ionophore concentration in concentrate is often nonuniform in cases of feed mixing errors (Hall, 2001). Therefore the final diagnosis of lasalocid intoxication was primarily based on the clinical signs, histopathological lesions and the presence of lasalocid in hepatic tissue of two horses. The dust collected from the silo at the farm contained several other ionophores. These might have accumulated in the dust pipe over a long period due to electrostatic adherence. However, the potential role of these ionophores could not be ruled out entirely because of the delay between ingestion and necropsy and the possible difference in pharmacokinetics between individual ionophores.

In conclusion, lasalocid intoxication induced myocardial and neurological damage, resulting in various short-term and long-term clinical signs. Although uncommon, lasalocid intoxication should be included as a differential diagnosis for unexplained inappetance, signs of depression, cardiac disease and ataxia.

References

Aleman M, Magdesian KG, Peterson TS, Galey FD (2007). Salinomycin toxicosis in horses. J Am Vet Med Assoc 230, 1822-1826

Bezerra PS, Driemeier D, Loretti AP, Riet-Correa F, Kamphues J, de Barros CS (1999). Monensin poisoning in Brazilian horses. Vet Human Toxicol 41, 383-385

Bila CG, Perreira CL, Gruys E (2001). Accidental monensin toxicosis in horses in Mozambique. J S Afr Vet Assoc 72, 163-164

Boemo CM, Tucker JC, Huntington PJ, Rawlin GT, Drennen PW (1991). Monensin toxicity in horses. An outbreak resulting in the deaths of ten horses. Aust Eq Vet 9, 4

Divers TJ, Kraus MS, Jesty SA, Miller AD, Mohammed HO, Gelzer AR, Mitchell LM, Soderholm LV, Ducharme NG (2009). Clinical findings and serum cardiac troponin I concentrations in horses after intragastric administration of sodium monensin. J Vet Diagn Invest 21, 338-343

Doebler JA (2000). Effects of neutral ionophores on membrane electrical characteristics of NG108-15 cells. Toxicol Lett 114, 27-38

Donoho AL (1984). Biochemical-studies on the fate of monensin in animals and in the environment. J Anim Sci 58, 1528-1539

Espino L, Suarez ML, Mino N, Goicoa A, Fidalgo LE, Santamarina G (2003). Suspected lasalocid poisoning in three dogs. Vet Human Toxicol 45, 241-242

Gad SC, Reilly C, Siino K, Gavigan FA, Witz G (1985). Thirteen cationic ionophores: Their acute toxicity, neurobehavioral and membrane effects. Drug Chem Toxicol 8, 451-468

Galitzer SJ, Oehme FW, Bartley EE, Dayton AD (1986). Lasalocid toxicity in cattle: Acute clinicopathological changes. J Anim Sci 62, 1308-1316

Gregory DG, Vanhooser SL, Stair EL (1995). Light and electron microscopic lesions in peripheral nerves of broiler chickens due to roxarsone and lasalocid toxicoses. Avian Dis 39, 408-416

Hall JO (2001). Toxic feed constituents in the horse. Vet Clin North Am Equine Pract 17, 479-489, vii

Hanson LJ, Eisenbeis HG, Givens SV (1981). Toxic effects of lasalocid in horses. Am J Vet Res 42, 456-461

Hughes KJ, Hoffmann KL, Hodgson DR (2009). Long-term assessment of horses and ponies post exposure to monensin sodium in commercial feed. Equine Vet J 41, 47-52

Jesty SA, Kraus M, Gelzer A, Rishniw M, Moise NS (2009). Effect of transvenous electrical cardioversion on plasma cardiac troponin I concentrations in horses with atrial fibrillation. J Vet Intern Med 23, 1103-1107

Kamphues J, Meyer H, Liebler EM, Johannsen A (1990). Animal nutrition for veterinarians - Recent cases of clinical disorders in horses after intake of ionophore-containing feed. Deut Tierarztl Woch 97, 537-539

Kart A, Bilgili A (2009). Effects of organophosphate phenyl saligenin phosphate and polyether carboxylic ionophore lasalocid on motor nerve conduction velocity, neuropathy target esterase enzyme activity, and clinical ataxia in chickens. Toxicol Mech Methods 19, 351-355

Kart A, Vanhooser SL, Sangiah S (2005). Oral administration of lasalocid causes peripheral neuropathy in Sprague Dawley rats: Effect of water salinity on lasalocid-induced peripheral neuropathy. J Anim Vet Adv 4, 719-722

Kraus MS, Jesty SA, Gelzer AR, Ducharme NG, Mohammed HO, Mitchell LM, Soderholm LV, Divers TJ (2010). Measurement of plasma cardiac troponin I concentration by use of a point-of-care analyzer in clinically normal horses and horses with experimentally induced cardiac disease. Am J Vet Res 71, 55-59

Kronfeld DS (2002). Lasalocid toxicosis is inadequately quantified for horses. Vet Human Toxicol 44, 245-247

Matsuoka T (1976). Evaluation of monensin toxicity in the horse. J Am Vet Med Assoc 169, 1098-1100

Mollenhauer HH, Rowe LD, Cysewski SJ, Witzel DA (1981). Ultrastructural observations in ponies after treatment with monensin. Am J Vet Res 42, 35-40

Muylle E, Vandenhende C, Oyaert W, Thoonen H, Vlaeminck K (1981). Delayed monensin sodium toxicity in horses. Equine Vet J 13, 107-108

Novilla MN (1992). The veterinary importance of the toxic syndrome induced by ionophores. Vet Human Toxicol 34, 66-70

Oehme FW, Pickrell JA (1999). An analysis of the chronic oral toxicity of polyether ionophore antibiotics in animals. Vet Human Toxicol 41, 251-257

Peek SF, Marques FD, Morgan J, Steinberg H, Zoromski DW, McGuirk S (2004). Atypical acute monensin toxicosis and delayed cardiomyopathy in Belgian draft horses. J Vet Intern Med 18, 761-764

Safran N, Aizenberg I, Bark H (1993). Paralytic syndrome attributed to lasalocid residues in a commercial ration fed to dogs. J Am Vet Med Assoc 202, 1273-1275

Segev G, Baneth G, Levitin B, Shlosberg A, Aroch I (2004). Accidental poisoning of 17 dogs with lasalocid. Vet Rec 155, 174-176

Todd GC, Novilla MN, Howard LC (1984). Comparative toxicology of monensin sodium in laboratory animals. J Anim Sci 58, 1512-1517

van Amstel SR, Guthrie AJ (1985). Salinomycin poisoning in horses: Case report. Proc 31st Ann AAEP Conv, Beltsville, Maryland 10

Van Vleet JA, HE, Rebar H (1985). Effects of pretreatment with selenium-vitamin E on monensin toxicosis in cattle. Am J Vet Res 46, 2221-2228

Wells SM, Sleeper M (2008). Cardiac troponins. J Vet Emerg Crit Car 18, 235-245

Chapter 5.2

Tissue Doppler imaging and two-dimensional speckle tracking detect impaired left ventricular function in horses exposed to ionophores

Adapted from:

Decloedt A, Verheyen T, Sys S, De Clercq D, van Loon G

Department of Large Animal Internal Medicine, Faculty of Veterinary Medicine, Ghent University, Belgium.

Tissue Doppler imaging and two-dimensional speckle tracking detect impaired left ventricular function in horses exposed to ionophores

Journal of Veterinary Internal Medicine (2012). Revised manuscript submitted.

Part of this work was presented at the 44th European Veterinary Conference (Voorjaarsdagen), Amsterdam, The Netherlands, April 27-29, 2011.

Summary

Background: Tissue Doppler imaging (TDI) and two-dimensional speckle tracking (2DST) have not yet been described for quantifying left ventricular (LV) function in horses with myocardial dysfunction due to ionophore intoxication.

Objectives: To evaluate LV function by TDI and 2DST following accidental ionophore intoxication.

Animals: Sixty-seven horses underwent a detailed cardiac examination after lasalocid exposure.

Methods: Repeated cardiac troponin I (cTnI) and echocardiographic measurements were performed. By TDI, radial systolic velocity and strain were measured. By 2DST, circumferential (SC) and radial (SR) strain at papillary muscle and chordal level and longitudinal (SL) strain were measured. LV fractional shortening (FS) was calculated for comparison.

Results: Twenty horses with signs of myocardial damage were included. Five horses showed severe myocardial damage (increased cTnI and ventricular tachycardia) and fifteen mild myocardial damage (increased cTnI without ventricular tachycardia). Forty-nine exams were performed between day 30 and 490 after suspected onset of exposure. Horses with mild myocardial damage showed few significant differences compared to a control group. Horses with severe myocardial damage showed severely decreased TDI, 2DST and FS measurements, indicating impaired LV function. Long-term follow-up of two surviving horses demonstrated full recovery in one horse and permanent myocardial fibrosis in the other. The lowest measurements per horse (n=20) for all TDI measurements, SL, SR at chordal level and FS correlated significantly with maximal cTnI ($P<0.05$). Over all examinations (n=49), TDI and 2DST measurements correlated well with FS ($P<0.05$).

Conclusions and clinical importance: TDI and 2DST measurements allowed accurate detection and quantification of LV systolic dysfunction.

Introduction

Horses are extremely susceptible to myocardial damage caused by the toxic effects of ionophore antibiotics, which result in increased concentrations of plasma cardiac troponin I (cTnI), cardiac dysrhythmia and depressed LV systolic function. This has been extensively described for the most commonly used ionophore, monensin, but other ionophores such as lasalocid can cause similar clinical signs (Matsuoka, 1976; Hanson et al., 1981; Peek et al., 2004; Divers et al., 2009; Decloedt et al., 2012). In the acute stages, horses typically show inappetence, signs of depression, ataxia, sweating and tachycardia. In peracute cases, horses may die within hours after ingestion without obvious clinical signs. Chronic cases occur with continuous or intermittent ingestion of sublethal doses which results in delayed cardiomyopathy with reduced LV systolic function due to fibrosis (Blomme et al., 1999). In some horses, LV systolic function recovers after several weeks to months (Hughes et al., 2009).

Left ventricular (LV) systolic function in horses is traditionally evaluated by M-mode measurements such as fractional shortening (FS). However, FS is a one-dimensional and focal measurement and may be unaffected in case of regional myocardial dysfunction. Furthermore, FS is highly load-dependent (Mahler et al., 1975; Colan et al., 1984). Recently, the reliability of tissue Doppler imaging (TDI) and two-dimensional speckle tracking (2DST) has been described in horses (Sepulveda et al., 2005; Schwarzwald et al., 2009a; Schwarzwald et al., 2009b; Schefer et al., 2010; Decloedt et al., 2011). These techniques allow a more extensive quantification of global and regional myocardial function. By TDI, myocardial velocities are measured based on the Doppler principle and myocardial deformation can be calculated. The amount of wall deformation relative to the end-diastolic state is expressed as strain (%) and the rate of deformation as strain rate (s^{-1}). Due to the Doppler principle, the quantification of strain and strain rate is limited to the direction of the ultrasound beam. Using left and right parasternal images, radial wall thickening can be evaluated (Sepulveda et al., 2005; Schwarzwald et al., 2009b). In contrast, 2DST allows the quantification of strain and strain rate by tracking myocardial acoustic speckles in the two dimensions of the ultrasound image. Using short-axis images, both radial wall thickening and circumferential shortening can be evaluated (Schwarzwald et al., 2009a; Schefer et al., 2010). Using long-axis images, longitudinal shortening can be measured (Decloedt et al., 2011). So far, TDI and 2DST have been primarily reported in healthy horses at rest or after exercise. The use of these techniques in horses with cardiac disease requires further investigation.

The goal of this study was to evaluate the use of TDI and 2DST for the quantification of LV function in horses with different stages of myocardial dysfunction due to accidental lasalocid intoxication. TDI and 2DST measurements were compared to FS and the correlation of echocardiographic findings and plasma cTnI concentrations was investigated.

Material and methods

Study population

The study population consisted of 67 horses from a farm in Belgium which underwent a detailed cardiac examination after accidental exposure to lasalocid (Decloedt et al., 2012). At the farm, fourteen horses had shown inappetence or lethargy within three weeks after a new batch of concentrate had been delivered. Seven horses with complaints of persistent inappetence and lethargy were admitted to the Department of Large Animal Internal Medicine (Ghent University) between day 29 and 46 after this suspected onset of exposure to lasalocid. As the concentrate supply fed at the onset of clinical signs was no longer available at the farm, diagnosis of lasalocid intoxication was based on the presence of lasalocid in hepatic tissue of two necropsied horses.

Plasma concentration of cardiac troponin I (cTnI) was determined in all 67 horses between day 30 and 37. Detailed echocardiography and an ECG recording with a duration of at least one hour were performed on the seven horses admitted to the clinic between day 30 and 46. Between day 34 and 490, full follow-up examinations with cTnI determination, echocardiography and ECG were performed on these horses until full recovery, death or euthanasia of the horse. In sixty horses from the same premises without clinical signs, plasma cTnI determination was repeated and detailed echocardiography and an ECG recording with a duration of at least one hour were performed between day 57 and 70. Full follow-up examinations with cTnI determination, echocardiography and ECG were performed on two of these horses on day 134 and 195.

Horses were included in the study if they showed myocardial damage, which was defined as having a plasma cTnI concentration above reference values (>0.10 ng/mL) (Jesty et al., 2009) on at least one occasion. Based on the presence of polymorphic ventricular tachycardia (VT) on the one hour ECG, they were further categorized as having severe myocardial damage (increased cTnI with VT) or mild myocardial damage (increased cTnI without VT). For comparison of echocardiographic measurements, a control group was examined consisting of ten healthy horses not related to the farm (seven mares and three geldings, 509±58 kg, 9.6±4.4 years), in which plasma cTnI concentrations were within the reference range (<0.10 ng/mL).

Biochemical examination

After collection of jugular venous blood in tubes containing lithium heparin, the samples were centrifuged as quickly as possible and stored at -18°C. The maximum time between sample collection and centrifugation was 6 hours. The cTnI concentration was determined within one week by use of a validated immuno-assay (Acces Accu-TnI, Beckman Coulter Inc, Fullerton, CA).

Image acquisition

Echocardiography was performed by one observer throughout the entire study period, using an ultrasound unit (GE Vivid 7 Dimension, GE Healthcare, Horten, Norway) with phased array transducer (3S Phased Array Transducer, GE Healthcare, Horten, Norway) at a frequency of 1.7/3.4 MHz (octave harmonics). A base-apex ECG was recorded simultaneously. Standardized right and left parasternal B-mode, M-mode and color flow Doppler images were recorded for assessment of left atrial and LV dimensions and valvular function (Long et al., 1992).

M-mode, color-coded TDI and 2DST measurements were recorded for the evaluation of LV function. A right parasternal short-axis M-mode image of the left ventricle was acquired at chordal level for calculation of FS. Aortic valve motion was assessed from a right parasternal long-axis LV outflow tract M-mode recording.

For TDI, the greyscale sector width was reduced to 30°. The velocity scale ranged from –32 to +32 cm/s. Consequently, a frame rate of 183 frames per second (fps) was achieved. The LV walls were imaged from a right and left parasternal short-axis view at chordal level. The tilt function was used to obtain optimal alignment of radial wall motion to the ultrasound beam.

For 2DST, the frequency was set to 1.6/3.2 MHz (octave harmonics). Greyscale images were acquired using a sector width of 55° in order to achieve a frame rate of at least 40 fps. For evaluation of longitudinal strain, a four-chamber view was acquired which did not visualize the apex due to the decreased image width (Decloedt et al., 2011). Short-axis images of the entire LV were recorded at chordal and papillary muscle level for evaluation of circumferential and radial strain.

Off-line data analysis

Off-line analysis was performed using dedicated software (EchoPAC Software Version 108.1.5, GE Healthcare, Horten, Norway). Image acquisition and off-line analysis were performed by one experienced observer, who performed caliper positioning blinded to the results of the measurements as well as to previous results. From the short-axis M-mode image at chordal level, LV end-diastolic internal diameter (LVIDd) and FS were measured. LV pre-ejection period (LVPEP) was measured as the time interval between the R wave on the ECG and aortic valve opening in the LV outflow tract M-mode. LV ejection time (LVET) was measured as the time interval between aortic valve opening and closure and the ratio LVPEP/ET was calculated (Long et al., 1992). The average of three cardiac cycles per view was used for further analysis.

Color-coded TDI images were analysed in the Q-analysis mode. From the right parasternal view, the interventricular septum (IVS) and LV free wall (LVFW) were evaluated. From left parasternal, the left and right region of the LV wall (LLV and RLV) were assessed. In each segment, a sample area was placed with a length (range 11-17 mm) and width (range 5-6 mm) adapted to wall thickness. The sample area was anchored inside the myocardium throughout the cardiac cycle. The cine compound function was used to convert the last cycle into the average of the three consecutive cycles per loop. Segmental peak systolic velocity (Vsyst) and strain (St) were measured.

For 2DST, the calculation of strain and strain rate was performed semi-automated using the "2D Strain" application of the ultrasound software. First, the correct view type was selected: "4CH" for the four-chamber view, "SAX-MV" for the short-axis view at chordal level and "SAX-PM" for papillary muscle level. A region of interest (ROI) was drawn along the LV endocardial border in a frame at end-systole and ROI width was adjusted to wall thickness. Speckle tracking started automatically, dividing the ROI into 6 segments. Segmental and global peak values were measured for longitudinal strain (SL), and for circumferential (SC) and radial (SR) strain at chordal ($_{CH}$) and papillary muscle ($_{PM}$) level. Three cardiac cycles were analysed per view and the average was used for further analysis.

Data Analysis and Statistics

Statistical analyses were performed using dedicated computer software (SPSS Statistics 19.0, Chicago, IL). Data are reported as median and range.

The values reported are the lowest values for each measurement per horse (if repeated examinations were performed). M-mode, TDI and 2DST measurements of horses with mild and severe myocardial damage were compared to the control group using a Kruskal-Wallis one-way analysis of variance with post hoc Dunn test. To facilitate graphical comparison of the different measurements of LV function, the results were transformed to z-scores based on the data of the control group. The z-score was calculated by subtracting the population mean from the measured value, and dividing this by the population standard deviation. The correlation of measurements of LV function with each other and with plasma cTnI concentrations was performed using Spearman's rank correlation coefficient. Segmental comparisons for 2DST within one horse were made by a repeated measures ANOVA with Bonferroni correction. The level of significance was $\alpha = 0.05$.

Results

The clinical course of the lasalocid intoxication, detailed blood biochemistry and ECG findings have been described previously (Decloedt et al., 2012). Twenty of the sixty-seven horses presented a plasma cTnI concentration >0.10 ng/mL at one or more occasions and were included in this study: the seven horses admitted to the clinic and thirteen of the sixty horses at the premises. Five horses were categorized as having severe myocardial damage (defined as increased cTnI and VT): four mares and one gelding, 434±110 kg, 11±4 years old. All five horses had been admitted to the clinic. In total, twenty-six examinations were performed on these horses between day 30 and 490 (Fig. 1). Fifteen horses were categorized as having mild myocardial damage (defined as increased cTnI without VT): five mares and ten geldings, 496±125 kg, 14±5 years old. In total, twenty-three examinations were performed on these horses. Six examinations were performed between day 43 and 134 on two horses that were admitted to the clinic. Seventeen examinations were performed on the thirteen horses without clinical signs between day 57 and 195.

Left atrial and LV dimensions were within reference values in all horses. None of the horses with myocardial damage showed significant valvular regurgitation. Table 1 shows the results of the measurements of LV function in the horses with myocardial damage. Compared to the control group, the group with mild myocardial damage showed no significant differences except for a higher SR_{PM} and shorter LVET. The five horses with severe myocardial damage showed significantly lower values for all measurements except $Vsyst_{IVS}$ and SR_{PM}. In these horses, LV systolic function improved during follow-up. Fig. 1A shows the progression over time of St values in the IVS calculated by TDI. A similar progression of LV function could be demonstrated using other TDI measurements, 2DST measurements such as SL (Fig. 1B), and FS (Fig. 1C). Three horses were lost for long-term follow-up because of death or euthanasia (on day 30–56). One horse showed normal cTnI concentrations and normal LV systolic function after nine months and returned to previous athletic use. In the second horse, the cTnI concentrations returned to normal but little improvement of LV systolic function was observed over a period of almost one year. In this horse, regional myocardial fibrosis was demonstrated by echocardiography and confirmed by necropsy on day 370.

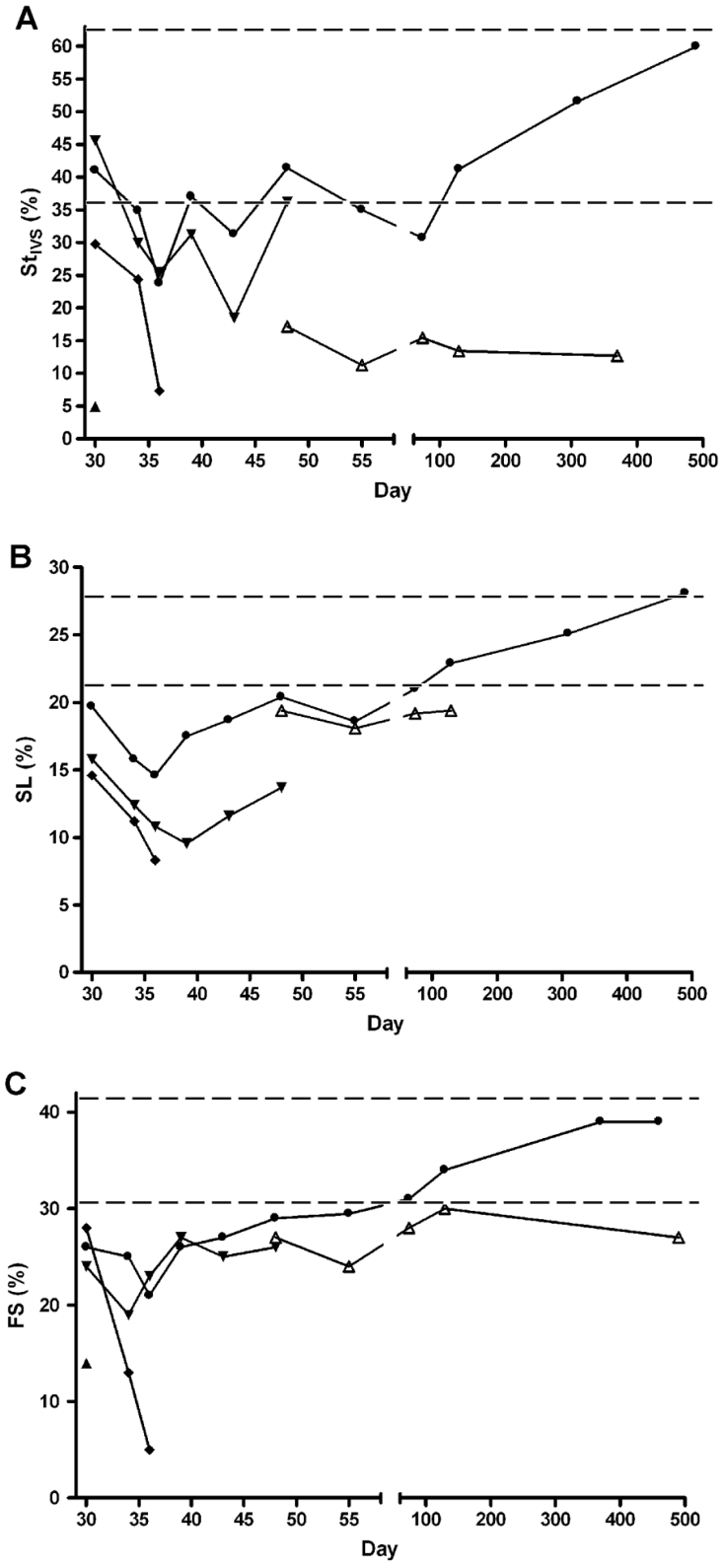

Figure 1: Progression of left ventricular function in five horses with severe myocardial damage (increased cTnI and ventricular tachycardia). The vertical axis represents peak values of the selected parameter. The horizontal axis represents time in days after suspected onset of exposure to lasalocid. The normal range is indicated by the dashed horizonal lines. (A) St_{IVS}, radial strain in interventricular septum by TDI; (B) SL, global longitudinal strain by 2DST. This measurement could not be performed in one horse due to poor image quality; (C) FS, fractional shortening.

Table 1: Measurements of LV function in horses with severe myocardial damage and mild myocardial damage, compared to a control group of healthy horses.

	Measurement	Severe myocardial damage		Mild myocardial damage		Healthy horses
		Median (range)	P	Median (range)	P	Median (range)
	number of horses	5		15		10
	heart rate (bpm)	51 (42–76)	<0.001	40 (29–48)	0.50	36 (29–42)
	cTnI (ng/mL)	124 (3.3–816)	<0.001	0.2 (0.03–8.4)	<0.001	<0.10
TDI	$Vsyst_{LVFW}$ (cm/s)	2.8 (2.0–3.7)	0.003	8.0 (4.8–10.5)	0.71	7.9 (6.0–8.7)
	$Vsyst_{IVS}$ (cm/s)	-1.7 (-0.2–-5.8)		-4.8 (-1.7–-11.3)		-4.3 (-1.9–-6.0)
	St_{LVFW} (%)	7.8 (5.8–16.9)	0.003	63.6 (38.4–92.2)	0.62	64.5 (51.4–97.6)
	St_{IVS} (%)	11.3 (4.9–23.8)	0.02	64.3 (38.4–79.3)	0.07	51.3 (39.4–58.4)
	$Vsyst_{LLV}$ (cm/s)	-1.6 (-0.7–-2.8)	0.003	-4.6 (-2.1–-9.6)	0.99	-4.6 (-2.9–-7.4)
	$Vsyst_{RLV}$ (cm/s)	3.0 (2.1–4.5)	0.01	6.7 (2.8–13.1)	0.45	5.5 (4.5–7.1)
	St_{LLV} (%)	23.1 (13.4–55.6)	<0.001	91.6 (54.4–125.3)	0.08	114.0 (83.2–139.4)
	St_{RLV} (%)	18.3 (12.3–33.9)	<0.001	59.6 (51.5–82.2)	0.13	68.1 (47.0–83.1)
2DST	SL (%)	-12.1 (-8.3–-18.1)	0.002	-24.1 (-17.1–-27.6)	0.49	-24.5 (-22.2–-27.0)
	SC_{CH} (%)	-10.4 (-7.3–-11.2)	0.01	-21.1 (-17.0–-23.8)	0.99	-19.7 (-18.6–-23.0)
	SR_{CH} (%)	24.3 (11.7–34.9)	0.003	61.3 (52.7–75.5)	0.32	64.2 (56.0–67.1)
	SC_{PM} (%)	-7.2 (-5.3–-9.5)	0.02	-21.5 (-15.2–-24.3)	0.37	-20.5 (-16.6–-22.6)
	SR_{PM} (%)	16.1 (11.0–33.1)	0.09	68.0 (57.1–70.1)	0.02	63.1 (55.0–67.1)
M-mode	FS (%)	19 (5–24)	0.008	37 (30–45)	0.28	36 (32–41)
	LVIDd (cm)	10.9 (10.2–11.7)		11.1 (8.1–12.8)		11.2 (10.5–13.3)
	LVPEP (ms)	133 (123–151)	0.01	92 (66–115)	0.42	93 (79–114)
	LVET (ms)	286 (266–301)	<0.001	401 (301–469)	<0.001	441 (416–483)
	LVPEP/ET	0.43 (0.36–0.48)	0.002	0.22 (0.14–0.28)	0.57	0.21 (0.19–0.25)

P = P-value for comparison with the control group using a post hoc Dunn test, performed if a Kruskal-Wallis one-way analysis of variance between the three groups reached significance (P<0.05). This field is blank if the Kruskal-Wallis analysis did not reach significance.

bpm, beats per minute; CH, chordal level; cTnI, cardiac troponin I; FS, fractional shortening; LVFW, left ventricular free wall; LVIDd, end-diastolic left ventricular internal diameter; LLV, left region of left ventricular free wall; IVS, interventricular septum; n, number; NA, not available; PM, papillary muscle level; RLV, right region of left ventricular free wall; SC, circumferential strain; SL, longitudinal strain; SR, radial strain; St, peak strain; Vsyst, peak systolic velocity.

Figure 2 shows the z-scores for TDI, 2DST and FS measurements. In the control group and the group with mild myocardial damage, the values of the measurements were normally distributed. A z-value lower than -1.96 or higher than 1.96 indicates a value outside the 95th percentile of the control group. Eight horses with mild myocardial damage showed z-values lower than -1.96 for one or more TDI, 2DST or FS measurements.

While only one horse showed low FS, four horses demonstrated low SL. In the group with severe myocardial damage, the z-values cannot be used for quantitative analysis as the values of the measurements were non-normally distributed. Graphically, all five horses with severe myocardial damage showed high negative z-values for each measurement except $Vsyst_{IVS}$.

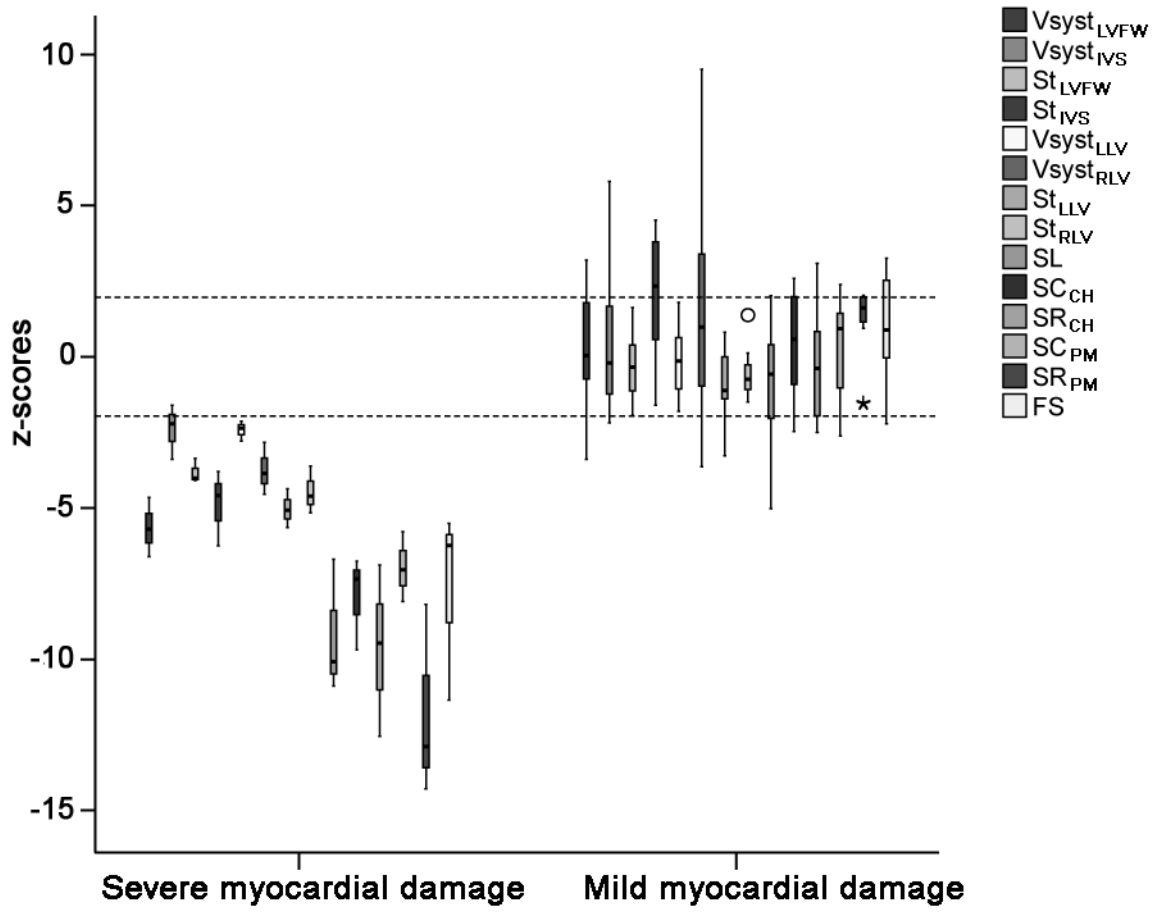

Figure 2: Graphical representation of the TDI, 2DST and FS measurements in 5 horses with severe myocardial damage (increased cTnI and ventricular tachycardia) and 15 horses with mild myocardial damage (increased cTnI without ventricular tachycardia) using z-scores calculated based on the mean and standard deviation of the control group. The dotted lines represent the 2.5th percentile (z-value -1.96) and the 97.5th percentile (z-value +1.96) of the control group. Z-scores of the group with severe myocardial damage cannot be numerically compared to the control group as the measurements were non-normally distributed. For each measurement, the median and spread of the z-scores is indicated by a boxplot, based on the lowest measurement values for each horse (n=20).

FS, fractional shortening; Vsyst, peak systolic velocity; LVFW, left ventricular free wall; IVS, interventricular septum; St, peak strain; LLV, left region of left ventricular free wall; RLV, right region of left ventricular free wall; SL, longitudinal strain; SC, circumferential strain; SR, radial strain; CH, chordal level; PM, papillary muscle level.

The highest cTnI concentration was compared to the lowest value for each measurement per horse (n = 20). All TDI measurements, SL and SR_{CH} correlated significantly with cTnI (Table 2). FS was also significantly correlated with cTnI (correlation coefficient -0.622, P=0.003). Over all 49 examinations, all TDI and 2DST measurements were significantly correlated to FS (Table 2, Fig. 3).

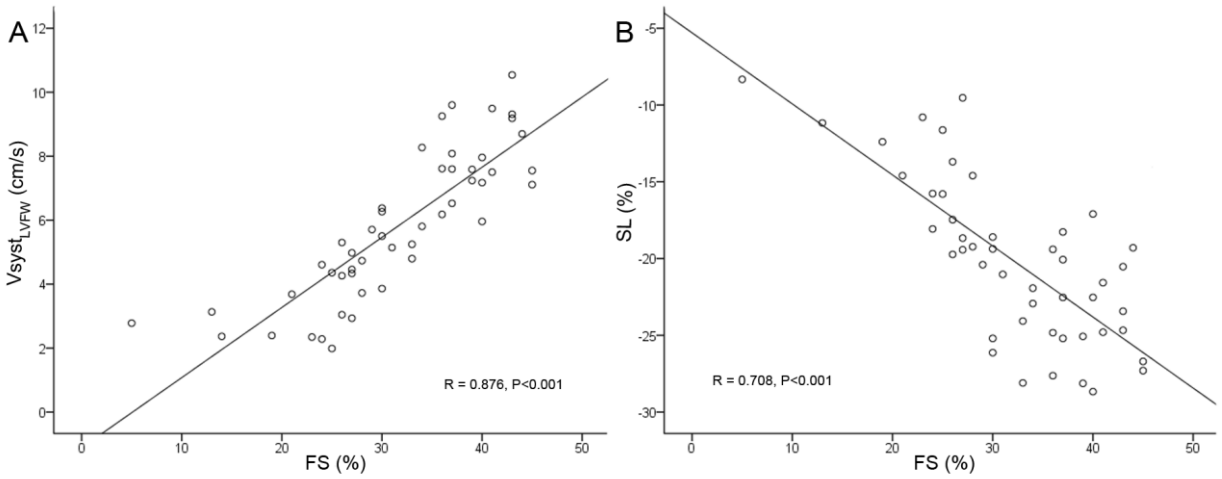

Figure 3: Scatterplot illustrating the correlation of TDI and 2DST measurements with fractional shortening (FS) over all examinations (n=49). (A) Correlation between FS and radial peak systolic velocity in the left ventricular free wall ($Vsyst_{LFW}$) measured by TDI; (B) Correlation between FS and peak longitudinal strain (SL) measured by 2DST.

Table 2: Correlation of TDI and 2DST measurements of LV function with plasma cardiac troponin I concentration and fractional shortening in 20 horses with myocardial damage.

	Correlation with plasma cTnI		Correlation with FS	
Measurement	Correlation coefficient	P	Correlation coefficient	P
$Vsyst_{LVFW}$ (cm/s)	-0.628	0.003	0.876	<0.001
$Vsyst_{IVS}$ (cm/s)	0.516	0.02	0.332	0.02
St_{LVFW} (%)	-0.638	0.003	0.825	<0.001
St_{IVS} (%)	-0.749	<0.001	0.794	<0.001
$Vsyst_{LLV}$ (cm/s)	0.557	0.01	0.700	<0.001
$Vsyst_{RLV}$ (cm/s)	-0.598	0.005	0.734	<0.001
St_{LLV} (%)	-0.704	0.001	0.791	<0.001
St_{RLV} (%)	-0.755	<0.001	0.847	<0.001
SL (%)	0.549	0.02	0.708	<0.001
SC_{CH} (%)	0.296	0.23	0.773	<0.001
SR_{CH} (%)	-0.601	0.008	0.739	<0.001
SC_{PM} (%)	0.375	0.13	0.774	<0.001
SR_{PM} (%)	-0.253	0.31	0.712	<0.001

cTnI, cardiac troponin I; FS, fractional shortening; Vsyst, peak systolic velocity; LVFW, left ventricular free wall; IVS, interventricular septum; St, peak strain; LLV, left region of left ventricular free wall; RLV, right region of left ventricular free wall; SL, longitudinal strain; SC, circumferential strain; SR, radial strain; CH, chordal level; PM, papillary muscle level.

The ability of TDI and 2DST to detect regional myocardial dysfunction was evaluated in the horse with echocardiographic evidence of myocardial fibrosis. At necropsy, fibrosis was confirmed to be predominantly located in the septum. Over all examinations of this horse, SL was significantly lower in the midseptal and basoseptal segment compared to the midlateral and basolateral segment (Fig. 4, $P<0.01$). By TDI, St_{IVS} was extremely low (Fig. 1A, horse indicated by open triangles) but could not be compared to St_{LVFW} because of inferior image quality due to the fibrosis. Inferior image quality was also present in the short-axis 2DST images. Therefore segmental SR and SC could not be measured.

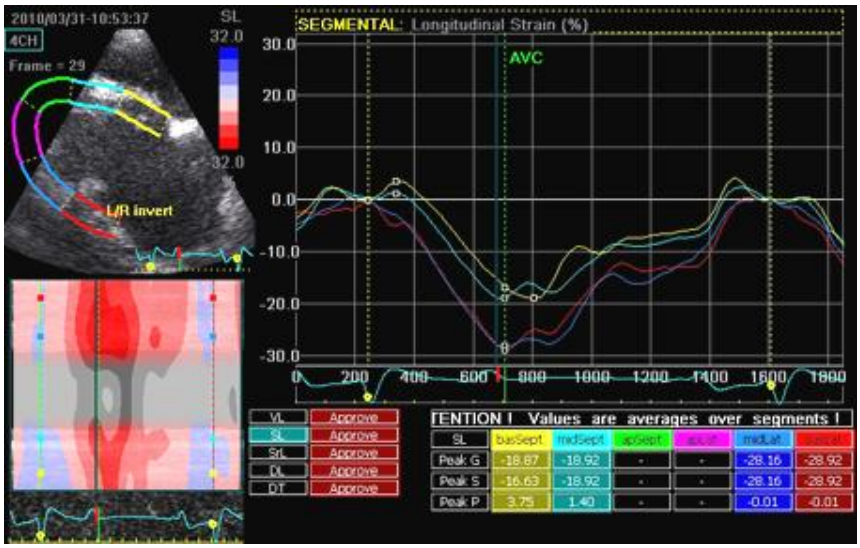

Figure 4: Segmental longitudinal strain measured by 2DST. Longitudinal strain is lower in the septal segments (yellow and light blue) compared to the free wall segments (red and dark blue). The septal segments also showed echodense regions. Necropsy confirmed that fibrosis was predominantly present in the interventricular septum.

Discussion

This study describes the long-term effects of an accidental lasalocid intoxication on LV systolic myocardial function. Impaired LV function could be detected and followed up by TDI, 2DST and FS. All TDI measurements, SL, SR_{CH} and FS correlated well with plasma cTnI concentration. All TDI and 2DST measurements were significantly correlated to FS. TDI and 2DST could detect regional myocardial dysfunction due to fibrosis in one horse.

To our knowledge, this study is the first to report on TDI and 2DST measurements in horses with myocardial dysfunction due to ionophore intoxication. In five horses with severe myocardial damage, which was defined as increased plasma cTnI concentration and presence of VT, TDI and 2DST measurements were significantly decreased. The use of TDI and 2DST in horses is a recent development in equine cardiology and few reports are available on the use of both techniques in horses with cardiac disease. In horses with atrial fibrillation, the late diastolic velocity wave was absent in the interventricular septum and the LV free wall. Myocardial velocities were significantly higher during systole and early diastole (Gehlen et al., 2009). Furthermore, TDI was used to quantify atrial remodeling after conversion of atrial fibrillation to sinus rhythm. Left atrial dysfunction at 24 hours after conversion was characterized by a significantly prolonged ratio of time to onset versus duration of atrial contraction (Schwarzwald et al., 2007). In one mare with nutritional masseter myodegeneration, systolic dysfunction was demonstrated by decreased radial and longitudinal peak strain as measured by 2DST (Schefer et al., 2011).

In small animal and human medicine, several reports describe higher sensitivity of TDI and 2DST for quantification of subclinical regional or global myocardial dysfunction. Toxic cardiomyopathy often occurs in human cancer patients as a complication of chemotherapy. In patients treated with the chemotherapeutic agents doxorubicin or trastuzumab, decreased strain and strain rate could be detected while LV ejection fraction (EF) remained unchanged (Ganame et al., 2007; Hare et al., 2009). In mice exposed to doxorubicin, decreased TDI-derived peak endocardial systolic velocity and strain rate preceded a reduction of EF. The reduction of systolic velocity and strain rate correlated with future LV dysfunction and could predict mortality (Neilan et al., 2006).

In this study, it could not be demonstrated whether one or more TDI or 2DST measurements were more sensitive than FS for detection of myocardial dysfunction. The alterations of the TDI and 2DST measurements in the horses with severe myocardial damage were

accompanied by changes in FS. As a result, all TDI and 2DST measurements correlated well with FS and with each other. However, in the group of horses with mild myocardial damage, only one horse showed a FS value slightly below the reference range of the control group while one or more TDI or 2DST measurements were below reference values in eight horses. This might indicate subtle myocardial dysfunction in these horses which was not detected by FS measurements. Four horses demonstrated SL values below the reference range. In human medicine, SL has been shown to be more sensitive for detection of myocardial dysfunction than other echocardiographic measurements of LV function in several diseases (Blessberger and Binder, 2010; Geyer et al., 2010). On the other hand, several horses in the group with mild myocardial damage also showed values above the reference range. This larger spread of the measurements might be explained by the larger variation of body weight and age in this group compared to the control group. Some of the affected horses also had higher heart rates and exhibited signs of stress whereas the control group consisted of horses acquainted to the echocardiographic examinations.

We were able to demonstrate a correlation between the plasma cTnI concentration and echocardiographic measurements of LV systolic function by comparing the maximal cTnI concentration and the lowest measurements of LV systolic function per horse. This has not yet been described in horses. In human cancer patients receiving high-dose chemotherapy, increased concentrations of cTnI were correlated to decreased LV ejection fraction during follow-up (Sawaya et al., 2011). Similarly, a linear correlation between cardiac troponin T and dP/dtmax, an invasive measurement of myocardial contractility, has been demonstrated in rabbits with anthracycline-induced cardiomyopathy (Simunek et al., 2003). In cattle with monensin-induced heart failure, cTnI was significantly associated with FS and myocardial histopathological lesion score (Varga et al., 2009). Cardiac troponin I is released from the myocardial cells in case of necrosis or damage to the cardiomyocyte membrane and is therefore a marker of acute myocardial damage. Consequently, it is possible that the plasma cTnI concentration returns to normal while chronic myocardial damage is present. The cTnI concentration in the horse with myocardial fibrosis had returned to reference values after one year although LV systolic function was still impaired. This has previously been described in a Belgian draft horse which demonstrated a FS of 25% while cTnI was within reference range at two months after accidental ingestion of monensin (Peek et al., 2004).

Two horses with severe myocardial damage were followed up for more than 10 months after admission. In one horse, myocardial function recovered fully. This corresponds to a previous study in which the long-term assessment of horses after exposure to a sublethal dose of monensin was described (Hughes et al., 2009). Eleven horses and ponies showed a reduced (<28%) or low-normal (28-32%) FS at 2 to 4 months after ingestion of contaminated feed, which improved significantly after a period of rest of more than 11 months. In contrast, the second horse in our study had a FS value of only 27% at one year after admission due to severe myocardial fibrosis. Similarly, in an experimental study with intragastric administration of sodium monensin, one horse demonstrated a FS of only 23% after seven months, which was caused by myocardial fibrosis confirmed at necropsy (Divers et al., 2009; Kraus et al., 2010).

The amount of lasalocid ingested could not be quantified as the concentrate batch fed at the onset of clinical signs was no longer available. Large between-horse variations of the lasalocid concentrations are likely due to unequal partitioning of the ionophore in the feed and variable intestinal absorption (Divers et al., 2009). This might explain the large variations of cTnI and LV systolic function in the 67 horses and the low number of severely affected horses. Unfortunately, the first horses could only be examined 30 days after the suspected onset of exposure and the sixty horses from the premises were presented for examination one month later. At this time, the myocardial damage might have resolved. Therefore, categorization of horses as having myocardial damage was based on the cTnI concentration which was measured in all horses at approximately the same time, between day 30 and 37. The categorization of severe versus mild myocardial damage was based on the ECG results and may be biased by the time of examination. In the horses that were repeatedly examined, the lowest value for each measurement was reported for comparison with the control group. This method was chosen because not all measurements showed their lowest value on the same day and there is no gold standard measurement of LV systolic function available, which made it difficult to define the worst examination for each horse. However, this approach might have favored the inclusion of outlying values. Another limitation is that only two horses were followed up for more than 10 months. A larger number of affected horses would have allowed a more extensive statistical analysis. However, despite the low number of horses we were able to demonstrate a significant correlation between cTnI concentrations and LV function and between all TDI and 2DST measurements and FS.

In conclusion, this study describes the presence of long-term myocardial dysfunction after accidental lasalocid intoxication. The measurements of LV systolic function correlated well with plasma cTnI concentrations. Left ventricular function was quantified both by FS and by TDI and 2DST, which could also detect regional wall motion abnormality in one horse with myocardial fibrosis. Future clinical studies should be performed to investigate the use of TDI and 2DST to detect myocardial dysfunction in horses with other cardiac diseases.

References

Blessberger H, Binder T (2010). Two dimensional speckle tracking echocardiography: Clinical applications. Heart 96, 2032-2040

Blomme EAG, La Perle KMD, Wilkins PA, Del Piero F, Hayes J (1999). Ionophore toxicity in horses. Equine Vet Educ 11, 153-158

Colan SD, Borow KM, Neumann A (1984). Left ventricular end-systolic wall stress-velocity of fiber shortening relation: A load-independent index of myocardial contractility. J Am Coll Cardiol 4, 715-724

Decloedt A, Verheyen T, De Clercq D, van Loon G (2012). Acute and long-term cardiomyopathy and delayed neurotoxicity after accidental lasalocid poisoning in horses. J Vet Intern Med 2012, accepted for publication

Decloedt A, Verheyen T, Sys S, De Clercq D, van Loon G (2011). Quantification of left ventricular longitudinal strain, strain rate, velocity, and displacement in healthy horses by 2-dimensional speckle tracking. J Vet Intern Med 25, 330-338

Divers TJ, Kraus MS, Jesty SA, Miller AD, Mohammed HO, Gelzer AR, Mitchell LM, Soderholm LV, Ducharme NG (2009). Clinical findings and serum cardiac troponin I concentrations in horses after intragastric administration of sodium monensin. J Vet Diagn Invest 21, 338-343

Ganame J, Claus P, Uyttebroeck A, Renard M, D'hooge J, Bijnens B, Sutherland GR, Eyskens B, Mertens L (2007). Myocardial dysfunction late after low-dose anthracycline treatment in asymptomatic pediatric patients. J Am Soc Echocardiogr 20, 1351-1358

Gehlen H, Iversen C, Stadler P (2009). Tissue Doppler echocardiographic examinations at rest and after exercise in horses with atrial fibrillation. Pferdeheilkunde 25, 11-16

Geyer H, Caracciolo G, Abe H, Wilansky S, Carerj S, Gentile F, Nesser HJ, Khandheria B, Narula J, Sengupta PP (2010). Assessment of myocardial mechanics using speckle tracking echocardiography: Fundamentals and clinical applications. J Am Soc Echocardiogr 23, 351-369; quiz 453-355

Hanson LJ, Eisenbeis HG, Givens SV (1981). Toxic effects of lasalocid in horses. Am J Vet Res 42, 456-461

Hare JL, Brown JK, Leano R, Jenkins C, Woodward N, Marwick TH (2009). Use of myocardial deformation imaging to detect preclinical myocardial dysfunction before conventional measures in patients undergoing breast cancer treatment with trastuzumab. Am Heart J 158, 294-301

Hughes KJ, Hoffmann KL, Hodgson DR (2009). Long-term assessment of horses and ponies post exposure to monensin sodium in commercial feed. Equine Vet J 41, 47-52

Jesty SA, Kraus M, Gelzer A, Rishniw M, Moise NS (2009). Effect of transvenous electrical cardioversion on plasma cardiac troponin I concentrations in horses with atrial fibrillation. J Vet Intern Med 23, 1103-1107

Kraus MS, Jesty SA, Gelzer AR, Ducharme NG, Mohammed HO, Mitchell LM, Soderholm LV, Divers TJ (2010). Measurement of plasma cardiac troponin I concentration by use of a point-of-care analyzer in clinically normal horses and horses with experimentally induced cardiac disease. Am J Vet Res 71, 55-59

Long KJ, Bonagura JD, Darke PG (1992). Standardised imaging technique for guided M-mode and Doppler echocardiography in the horse. Equine Vet J 24, 226-235

Mahler F, Ross J, Jr., O'Rourke RA, Covell JW (1975). Effects of changes in preload, afterload and inotropic state on ejection and isovolumic phase measures of contractility in the conscious dog. Am J Cardiol 35, 626-634

Matsuoka T (1976). Evaluation of monensin toxicity in the horse. J Am Vet Med Assoc 169, 1098-1100

Neilan TG, Jassal DS, Perez-Sanz TM, Raher MJ, Pradhan AD, Buys ES, Ichinose F, Bayne DB, Halpern EF, Weyman AE, Derumeaux G, Bloch KD, Picard MH, Scherrer-Crosbie M (2006). Tissue Doppler imaging predicts left ventricular dysfunction and mortality in a murine model of cardiac injury. Eur Heart J 27, 1868-1875

Peek SF, Marques FD, Morgan J, Steinberg H, Zoromski DW, McGuirk S (2004). Atypical acute monensin toxicosis and delayed cardiomyopathy in Belgian draft horses. J Vet Intern Med 18, 761-764

Sawaya H, Sebag IA, Plana JC, Januzzi JL, Ky B, Cohen V, Gosavi S, Carver JR, Wiegers SE, Martin RP, Picard MH, Gerszten RE, Halpern EF, Passeri J, Kuter I, Scherrer-Crosbie M (2011). Early detection and prediction of cardiotoxicity in chemotherapy-treated patients. Am J Cardiol 107, 1375-1380

Schefer KD, Bitschnau C, Weishaupt MA, Schwarzwald CC (2010). Quantitative analysis of stress echocardiograms in healthy horses with 2-dimensional (2D) echocardiography, anatomical M-mode, tissue Doppler imaging, and 2D speckle tracking. J Vet Intern Med 24, 918-931

Schefer KD, Hagen R, Ringer SK, Schwarzwald CC (2011). Laboratory, electrocardiographic, and echocardiographic detection of myocardial damage and dysfunction in an Arabian mare with nutritional masseter myodegeneration. J Vet Intern Med 25, 1171-1180

Schwarzwald CC, Schober KE, Berli AS, Bonagura JD (2009a). Left ventricular radial and circumferential wall motion analysis in horses using strain, strain rate, and displacement by 2D speckle tracking. J Vet Intern Med 23, 890-900

Schwarzwald CC, Schober KE, Bonagura JD (2007). Echocardiographic evidence of left atrial mechanical dysfunction after conversion of atrial fibrillation to sinus rhythm in 5 horses. J Vet Intern Med 21, 820-827

Schwarzwald CC, Schober KE, Bonagura JD (2009b). Methods and reliability of tissue Doppler imaging for assessment of left ventricular radial wall motion in horses. J Vet Intern Med 23, 643-652

Sepulveda MF, Perkins JD, Bowen IM, Marr CM (2005). Demonstration of regional differences in equine ventricular myocardial velocity in normal 2-year-old Thoroughbreds with Doppler tissue imaging. Equine Vet J 37, 222-226

Simunek T, Klimtova I, Adamcova M, Gersl V, Hrdina R, Sterba M, Kaplanova J, Mazurova Y (2003). Cardiac troponin T as an indicator of reduced left ventricular contractility in experimental anthracycline-induced cardiomyopathy. Cancer Chemother Pharmacol 52, 431-434

Varga A, Schober KE, Holloman CH, Stromberg PC, Lakritz J, Rings DM (2009). Correlation of serum cardiac troponin I and myocardial damage in cattle with monensin toxicosis. J Vet Intern Med 23, 1108-1116

Chapter 6

Cardiac changes in horses with atypical myopathy

Adapted from:

Verheyen T, Decloedt A, De Clercq D, van Loon G

Department of Large Animal Internal Medicine, Faculty of Veterinary Medicine, Ghent University, Belgium.

Cardiac changes in horses with atypical myopathy.

Journal of Veterinary Internal Medicine (2012). Accepted for publication.

Part of these results were presented at the 4th Congress of the European College of Equine Internal Medicine, February 4-5 2011, Hannover, Germany.

Summary

Background: Atypical myopathy (AM) is an acute, highly fatal rhabdomyolysis in grazing horses which mainly affects the skeletal muscles. Although post-mortem exams have demonstrated myocardial damage, limited information is available on the effect of AM on cardiac function in alive and surviving horses.

Objectives: To describe cardiac changes associated with AM in the acute stage of the disease and after follow-up.

Animals: Horses (n=12) diagnosed with AM in which blood biochemistry, echocardiography and ECG recording were available.

Methods: All horses underwent a clinical exam, biochemical analysis, echocardiography including tissue Doppler imaging (TDI) and two-dimensional speckle tracking (2DST) and ECG. Four surviving horses underwent follow-up examinations after two to ten weeks.

Results: All but one horse showed elevated cardiac troponin I (cTnI) concentrations and ten horses showed ventricular premature depolarizations (VPDs). All horses presented a prolonged corrected QT (QT_{cf}) interval at the day of admission and an abnormal left ventricular (LV) wall motion pattern which could be detected by conventional echocardiography, TDI and 2DST. TDI measurements revealed abnormal LV relaxation with prolonged contraction duration (CD), increased isovolumic relaxation time (IVRT) and decreased ratio of early to late diastolic (E/A) LV radial velocities. Decreased LV global longitudinal strain and increased mechanical dispersion between myocardial segments could be detected by 2DST. After ten weeks follow-up, one of the surviving horses still showed VPDs and a mildly prolonged QT_{cf} although the wall motion abnormality had disappeared.

Conclusions and clinical importance: AM can result in characteristic echocardiographic and electrocardiographic changes and may be associated with increased cTnI and VPDs. TDI and 2DST can detect a prolonged contraction duration, decreased longitudinal strain, increased mechanical dispersion between segments and abnormal LV relaxation. In survivors, abnormal cardiac function may still be found at ten weeks follow-up.

Introduction

Atypical myopathy (AM) is a highly fatal disease occurring in grazing horses especially during autumn and spring. The disease causes an acute degeneration of skeletal muscle, characterized clinically by weakness, stiffness, recumbency and a mortality rate of about 70% (Votion and Serteyn, 2008). The disease was first described in the United Kingdom in 1984 (Linklater, 1984) but is now recognized in many other European countries. A similar seasonal pasture myopathy has been described in the United States (Finno et al., 2006). The exact etiology of the disease remains uncertain, but recent research points towards an unknown toxin causing mitochondrial damage and multiple acyl-CoA dehydrogenase (ADD) deficiency (Westermann et al., 2008; Unger-Torroledo et al., 2010; Van Der Kolk et al., 2010).

Post-mortem examinations have revealed that AM not only causes degeneration of the skeletal muscles but also affects the heart. At necropsy, diffuse or multifocal pale areas may be observed in the myocardium, as well as focal areas of hemorrhage (Finno et al., 2006; Cassart et al., 2007; Votion and Serteyn, 2008). Histopathological changes in the myocardium are moderate to severe granular myocardial degeneration and necrosis, with lipid accumulation in the myocytes. This severe myocardial degeneration suggests that cardiac damage may represent a cause for sudden death in AM-affected horses (Cassart et al., 2007). Most horses affected by AM show an increased concentration of plasma cardiac troponin I (cTnI), a specific biomarker of myocardial injury (Votion et al., 2007). Previous studies have shown that tachycardia, dysrhythmias or cardiac murmurs can be found in AM horses, but in-depth information is not available (Votion et al., 2007; Votion and Serteyn, 2008). It is also unknown to what extent the myocardium recovers in surviving horses.

The aim of this study was to investigate cardiac function in horses with AM using biomarker analysis, echocardiography and ECG. In addition to conventional echocardiography, tissue Doppler imaging (TDI) and two-dimensional speckle tracking (2DST) were used to detect myocardial dysfunction.

Material and methods

Case selection

Horses referred to the Department of Large Animal Internal Medicine, Ghent University (Belgium) with AM between 2009 and 2011 were included in this study. Inclusion criteria were housing on pasture, acute nonexertional rhabdomyolysis (myoglobinuria, stiffness, trembling, sweating, weakness, recumbency, depression), rapid aggravation and even sudden death, elevated plasma creatine kinase (CK) activity (>10,000 IU/L) and availability of both echocardiography and ECG before initiation of medical treatment.

Drugs given at home (flunixin meglumine, butyl scopolamine and/or saline) were confirmed not to affect QT interval. The diagnosis of AM was confirmed on post-mortem in non-survivors. Survivors were followed up after two to ten weeks. At this time, they no longer received any treatment.

Table 1: Breed, sex, age, body weight, clinical status and clinical course of twelve horses with atypical myopathy

Horse	Sex	Age (years)	Body weight (kg)	Clinical status		Clinical course	Position for echocardiography and ECG	Follow-up (days)
				HR (bpm)	PCV (%)			
1	mare	3	480	44	56	euthanasia within 1 day	left lateral recumbency	
2	mare	3	500	44	50	euthanasia within 2 days	left lateral recumbency	
3	mare	6	560	48	53	death within 1 day	right lateral recumbency	
4	mare	8	394	52	39	survived	standing	
5	mare	8	433	68	44	euthanasia within 2 days	standing	
6	gelding	8	450	60	42	survived	standing	72
7	gelding	1.5	350	60	52	euthanasia within 3 days	left lateral recumbency	
8	mare	3	380	44	43	survived	standing	44
9	mare	1.5	464	42	40	survived	standing	64
10	stallion	1.5	150	68	41	survived	standing	12
11	stallion	1.5	466	64	44	death within 2 days	standing	
12	stallion	1.5	370	40	43	death within 4 days	left lateral recumbency	

bpm, beats per minute; HR, heart rate; PCV, packed cell volume

Biochemical analysis

Ionized calcium, potassium and sodium concentrations were measured (AVL 9180 Electrolyte Analyser, Roche Diagnostics, Vilvoorde, Belgium) on lithium heparine blood samples. Magnesium and CK concentrations were determined in serum (Spotchem SP-4420, Arkray Europe, Amstelveen, The Netherlands). Cardiac troponin I (cTnI) concentration was measured in lithium heparin plasma (Acces Accu-TnI, Beckman Coulter Inc, Fullerton, CA).

Echocardiography

Echocardiography was performed (GE Vivid 7 Dimension, GE Healthcare, Horten, Norway) from a right and left parasternal window (n=7), or from only one side in recumbent horses (n=5). Standardized two-dimensional and M-mode images were obtained using a phased array transducer (3S Phased Array Transducer, GE Healthcare, Horten, Norway) at a frequency of 1.7/3.4 MHz (octave harmonics). Atrial and left ventricular (LV) dimensions and fractional shortening (FS) were measured in a conventional manner (Patteson et al., 1995). Time to mitral valve opening (MVO_{MM}) was measured in a short-axis M-mode image at mitral level as the time interval between the R wave on the ECG and mitral valve opening. LV pre-ejection period (LVPEP) was measured as the time interval between the R wave and aortic valve opening in a long-axis LV outflow tract M-mode recording. LV ejection time (LVET) was measured as the time interval between aortic valve opening and closure. Isovolumic relaxation time ($IVRT_{MM}$) was calculated as the time from aortic valve closure to mitral valve opening.

For color-coded TDI, images were recorded from a right parasternal short axis view at papillary muscle level. Image width was reduced to 30° and the velocity scale ranged from -32 to +32 cm/s, resulting in a frame rate of 183 frames per second (fps). During off-line analysis (EchoPAC Software Version 108.1.5, GE Healthcare, Horten, Norway), a sample area was placed in the interventricular septum (IVS) and the left ventricular free wall (LVFW) with an adapted length (11-17 mm) and width (4-6 mm) depending on wall thickness. The sample area was anchored inside the myocardium throughout the cardiac cycle. The cine compound function was used to convert the last cycle into the average of three consecutive cycles per loop. Radial peak velocities (V) were measured during systole (Syst), early diastole (E) and late diastole (A) and the E/A ratio was calculated. Contraction duration (CD) was determined as time from the R wave to onset of E. The isovolumic relaxation time ($IVRT_{TDI}$) was measured as the time from end Syst to onset E. The preceding RR interval was recorded.

For 2DST, images were recorded from a right parasternal long-axis modified four-chamber view and a right parasternal short-axis view at papillary muscle level (Decloedt et al., 2011). Image width was reduced to 55°, resulting in a frame rate of 41 fps. Off-line analysis was performed semi-automated using the "2D Strain" application of the ultrasound software. A region of interest (ROI) was drawn along the LV endocardial border in a frame at end-systole and ROI width was adjusted to wall thickness. Speckle tracking started automatically, dividing the ROI into 6 segments. Global peak longitudinal (SL) strain was measured from the long-axis image, global circumferential (SC) and averaged radial (SR) strain were measured from the short-axis image. Contraction duration was measured as the average time to peak longitudinal (CD_{SL}), circumferential (CD_{SC}) and radial (CD_{SR}) strain in the different LV segments. The mechanical dispersion of contraction was calculated as the standard deviation (SD) of CD between the segments per loop and as the synchrony time index (STI), defined as the time difference between the shortest and longest CD of the different segments per loop (Schwarzwald et al., 2009).

All measurements were compared to a control group of ten healthy horses (seven mares, three geldings, 9.6 ± 4.4 years, 509 ± 58 kg).

Electrocardiography

A base-apex ECG was obtained (Televet 100® Version 4.1.3., Kruuse, Marslev, Denmark) at the time of echocardiographic examination in standing (n=7) or recumbent (n=5) position. From twenty consecutive cardiac cycles, the QT interval was measured as the time from the onset of the QRS complex to the end of the T wave and the associated preceding RR interval was determined. Measurements from the control group of ten healthy horses at rest were used as normal control values.

Data analysis and statistics

The QT interval was corrected for heart rate using Fridericia's correction method: $QT_{cf} = QT/RR^{1/3}$ (Davey, 2002; Schwarzwald et al., 2007). The same formula was used to correct all echocardiographic time measurements, as described in human medicine (Haugaa et al., 2010). Data are reported as mean ± standard deviation SD. Comparisons of means from AM horses and control horses were performed by the Student's t-test (level of significance $P<0.05$). Comparisons of the cTnI and CK concentrations from AM survivors and non-survivors were performed using the Mann-Whitney rank-sum test (level of significance $P<0.05$).

Results

Twelve horses with AM were examined. Breed, sex, age, body weight, clinical status and clinical course are shown in Table 1. Four surviving horses were followed up after a period of 12 to 72 days.

Biochemical analysis

Ten horses showed hyponatremia, eleven hypocalcemia and one hypomagnesemia, while potassium was elevated in two horses (Table 2). CK concentrations were elevated in all horses. All but one horse showed cTnI concentrations exceeding the reference value of 0.10 ng/ml (Jesty et al., 2009). At follow-up, cTnI values in surviving horses had returned to normal (Table 2). The cTnI and CK concentrations at admission did not differ significantly between survivors and non-survivors (P=0.639 and P=0.202, respectively).

Table 2: Results of biochemical analysis of twelve horses with atypical myopathy

		Blood biochemistry					
Horse	**Day**	**CK**	**cTnI**	**Na**	**K**	**Ca_i**	**Mg**
		mU/ml	mmol/l	mmol/l	mmol/l	mmol/l	mmol/l
		10-146	<0.10	137-143	2.9-4.4	1.5-1.8	0.6-0.9
1	1	629000	4.11	136	4.1	1.2	0.9
2	1	143100	1.81	135	3.5	1.3	0.7
3	1	787000	2.14	128	4.1	1.4	0.8
4	1	76000	0.81	138	3.2	1.3	0.6
5	1	432000	>99.99	130	3.6	1.2	0.8
6	1	29900	62.28	131	3.8	1.3	0.8
	72	85	0.04	140	3.8	1.1	0.7
7	1	482500	0.42	130	3.8	1.7	0.9
8	1	14290	0.55	131	5.2	1.4	0.6
	44	123	<0.03	NA	NA	NA	NA
9	1	149700	1.01	120	3.7	1.3	0.8
	64	104	<0.03	135	3.3	1.5	0.6
10	1	521000	8.95	128	4.3	0.9	0.6
	12	908	0.03	136	2.5	1.4	0.7
11	1	346000	0.05	139	4.5	1.2	0.6
12	1	21770	0.31	125	4.1	1.3	0.3

CK, creatine kinase; cTnI, plasma cardiac troponin I; NA, not available

Echocardiography

M-mode measurements for AM and control horses are shown in Table 3. The atrial dimensions, LV dimensions and FS were within reference values in the AM horses. Visual inspection of the two-dimensional and M-mode images showed a systolic wall motion abnormality in all cases. In eight horses, a biphasic contraction could be observed as shown in Fig. 1A. This was most obvious in the IVS, but was also present in the LVFW in six cases. In the remaining four horses, the IVS showed a "plateau-like" morphology during contraction. The $MVO_{cf,MM}$ and $IVRT_{cf,MM}$ were significantly longer in AM horses (P=0.017 and P<0.001, respectively), while $LVPEP_{cf}$ and the ratio LVPEP/LVET were significantly decreased (P<0.001). $LVET_{cf}$ was not significantly different from control horses (P=0.363).

The wall motion abnormality could be clearly demonstrated by TDI (Fig. 1B, Fig. 2A-B). In AM horses, CD_{cf} was significantly longer in IVS (P=0.004) but not in LVFW (P=0.2). $IVRT_{cf,TDI}$ was significantly longer in both IVS and LVFW (P<0.001). V_{Syst} was significantly higher in IVS (P<0.001) and LVFW (P<0.035). The E/A ratio was significantly lower in LVFW (P<0.001) but not in IVS (P=0.071), while V_E was significantly decreased in both IVS (P<0.001) and LVFW (P=0.005).

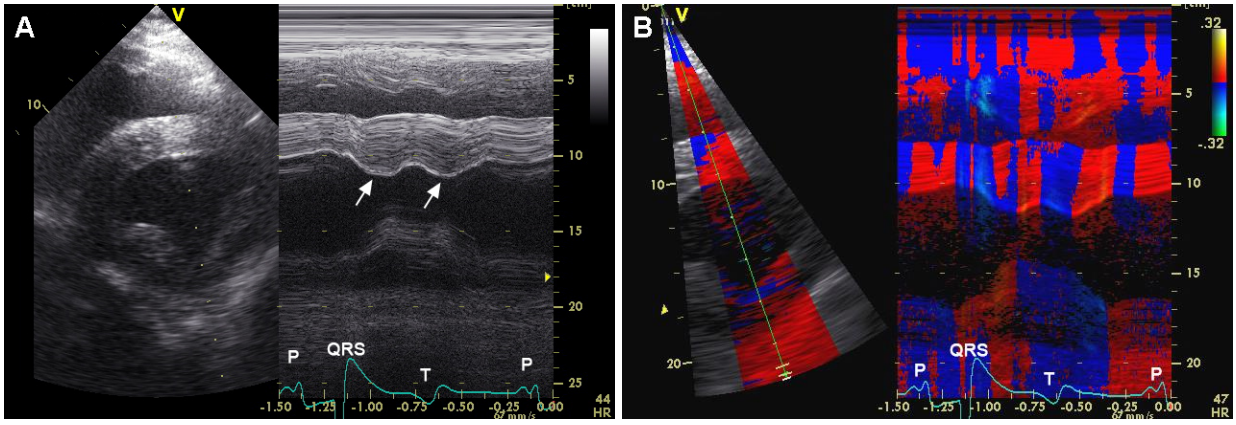

Figure 1: Short-axis two-dimensional (left panel) and M-mode (right panel) image at papillary muscle level in a horse with atypical myopathy. The ECG is displayed at the bottom. (A) Conventional M-mode image. The biphasic contraction of the interventricular septum is indicated by white arrows; (B) M-mode image with tissue Doppler imaging (TDI) color codes. The biphasic wall motion in the interventricular septum is characterized by the alternation of red and blue TDI color codes. This indicates alternating wall motion velocities towards and away from the transducer, respectively.

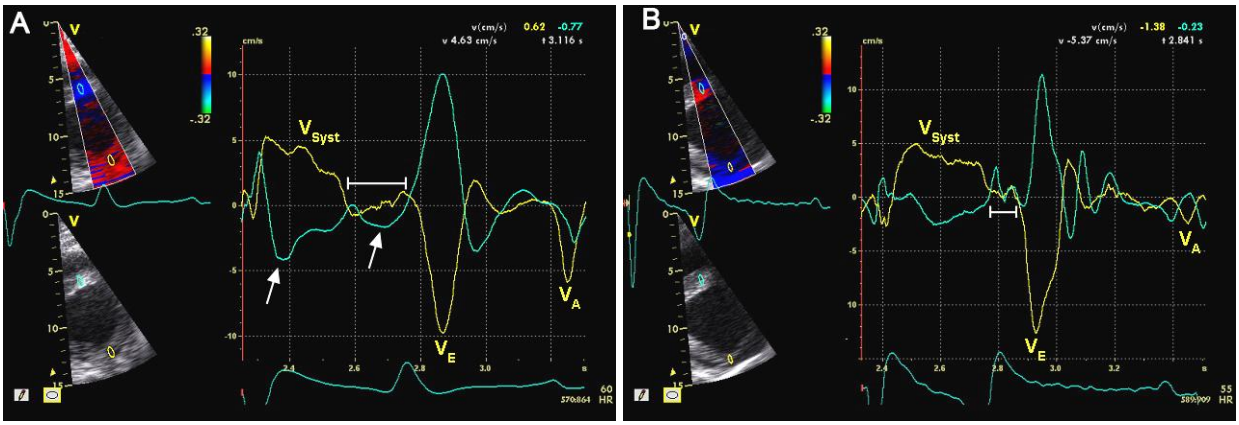

Figure 2: Wall motion velocity curve (cm/s) obtained by tissue Doppler imaging (TDI) in a short-axis image at papillary muscle level in a horse with atypical myopathy. The ECG is displayed at the bottom. A sample area has been placed in the left ventricular myocardium (yellow) and the interventricular septum (green). V_{Syst}, V_E and V_A represent peak radial wall motion velocity during systole, early diastole and late diastole, respectively. (A) At the time of admission, the biphasic contraction of the septum is seen as two separate negative velocity peaks during systole, demonstrated by white arrows. The prolonged isovolumic relaxation time (IVRT) is shown by a white horizontal bar. The E/A ratio is decreased; (B) On day 12, the biphasic contraction and prolonged IVRT are no longer present. The E/A ratio has returned to normal.

The prolonged contraction and biphasic wall motion were also visible in the 2DST strain curves (Fig. 3A-B). Peak SC and SR were not different from the control group, but SL was significantly lower in AM horses (P=0.009). Although the global CD_{SL}, CD_{SC} and CD_{SR} were not prolonged, there was increased mechanical dispersion of contraction between the six segments per view. Both the SD and STI of CD_{SL} and CD_{SC} were significantly longer in AM horses, while the SD and STI of CD_{SR} were not significantly different.

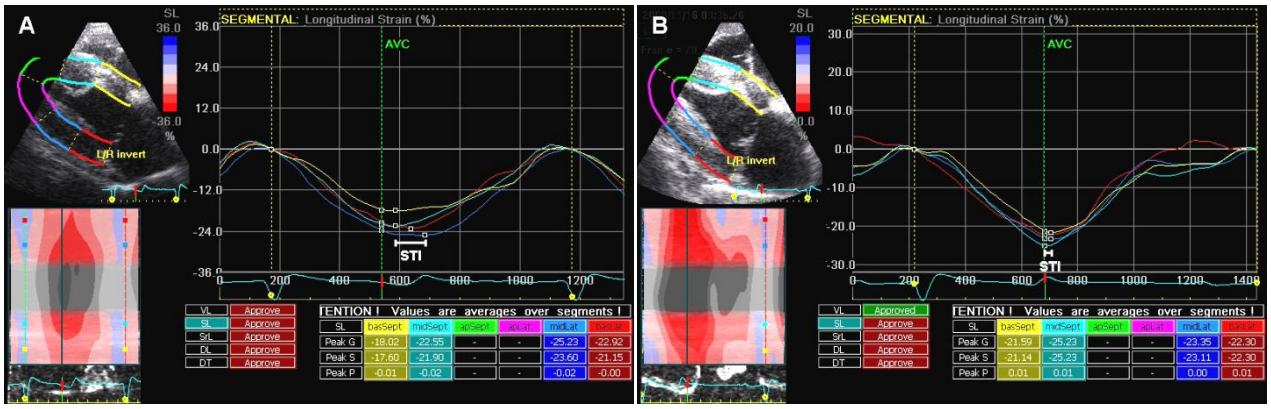

Figure 3: Longitudinal strain curves (%) obtained by two-dimensional speckle tracking (2DST) from a modified four-chamber view in a horse with atypical myopathy. The ECG is displayed at the bottom. A region of interest (ROI) has been positioned on the myocardium, which is automatically divided into six segments. (A) At the time of admission, the mechanical dispersion is visible as the large difference between the shortest and longest time to peak strain of the four segments, indicated by the large synchrony time index (STI); (B) On day 14, the contraction in the four segments is synchronous and the STI is small.

Table 3: M-mode, TDI and 2DST echocardiographic measurements of horses with atypical myopathy compared to a healthy control group

Ultrasound mode	Variable	Atypical myopathy		Controls (n=10)	P
		n	Mean ± SD	Mean ± SD	
M-mode	MVO_{cf} (ms)	9	568 ± 38	532 ± 20	0.02
	$IVRT_{cf}$ (ms)	9	165 ± 42	90 ± 17	<0.001
	$LVPEP_{cf}$ (ms)	9	53 ± 9	78 ± 8	<0.001
	$LVET_{cf}$ (ms)	9	353 ± 38	365 ± 9	0.36
	LVPEP/LVET	9	0.15 ± 0.03	0.20 ± 0.02	<0.001
	FS (%)	11	39.0 ± 3.8	36.1 ± 2.7	0.06
	LVIDd (cm)	11	9.6 ± 1.3	11.3 ± 0.8	0.002
TDI	CD_{cf} LVFW (ms)	11	554 ± 45	533 ± 25	0.2
	CD_{cf} IVS (ms)	11	563 ± 30	526 ± 21	0.004
	$IVRT_{cf}$ LVFW (ms)	11	199 ± 57	92 ± 18	<0.001
	$IVRT_{cf}$ IVS (ms)	11	224 ± 52	133 ± 26	<0.001
	V_{Syst} LVFW (cm/s)	11	7.9 ± 2.9	5.8 ± 0.81	0.04
	V_{Syst} IVS (cm/s)	11	-6.9 ± 1.4	-4.3 ± 1.1	<0.001
	V_E LVFW (cm/s)	11	-10.8 ± 3.1	-14.4 ± 1.8	0.005
	V_E IVS (cm/s)	11	7.9 ± 2.9	13.2 ± 2.2	<0.001
	V_A LVFW (cm/s)	11	-10.9 ± 4.0	-7.3 ± 2.0	0.02
	V_A IVS (cm/s)	10	5.0 ± 3.4	3.5 ± 2.7	0.31
	E/A LVFW	11	1.1 ± 0.4	2.1 ± 0.7	<0.001
	E/A IVS	10	2.7 ± 2.6	7.2 ± 6.3	0.07
2DST	SL (%)	7	-22.6 ± 1.2	-24.6 ± 1.5	0.009
	SC (%)	7	-19.5 ± 2.8	-20.0 ± 1.8	0.67
	SR (%)	7	63.8 ± 7.8	62.7 ± 3.6	0.70
	$CD_{SL,cf}$ (ms)	7	418 ± 32	443 ± 14	0.1
	$CD_{SC,cf}$ (ms)	7	395 ± 65	426 ± 18	0.27
	$CD_{SR,cf}$ (ms)	7	404 ± 75	457 ± 18	0.12
	SD of $CD_{SL,cf}$ (ms)	7	47 ± 17	29 ± 15	0.04
	SD of $CD_{SC,cf}$ (ms)	7	83 ± 40	21 ± 7	0.007
	SD of $CD_{SR,cf}$ (ms)	7	36 ± 30	19 ± 10	0.18
	STI of $CD_{SL,cf}$ (ms)	7	102 ± 38	57 ± 29	0.02
	STI of $CD_{SC,cf}$ (ms)	7	201 ± 101	52 ± 20	0.008
	STI of $CD_{SR,cf}$ (ms)	7	80 ± 64	43 ± 23	0.18

2DST, two-dimensional speckle tracking; A, late diastolic peak radial velocity; CD, contraction duration; cf, Fridericia correction for heart rate; E, early diastolic peak velocity; IVRT, isovolumic relaxation time; IVS, interventricular septum; LVET, left ventricular ejection time; LVFW, left ventricular free wall; LVPEP, left ventricular pre-ejection period; S, systolic peak velocity; SC, peak circumferential strain; SD, standard deviation; SL, peak longitudinal strain; SR, peak radial strain; STI, synchrony time index; TDI, tissue Doppler imaging; MVO, time to mitral valve opening

Electrocardiography

The QT_{cf} interval was significantly longer in horses with AM ($P<0.001$) compared to control horses (Fig. 4, Table 4).

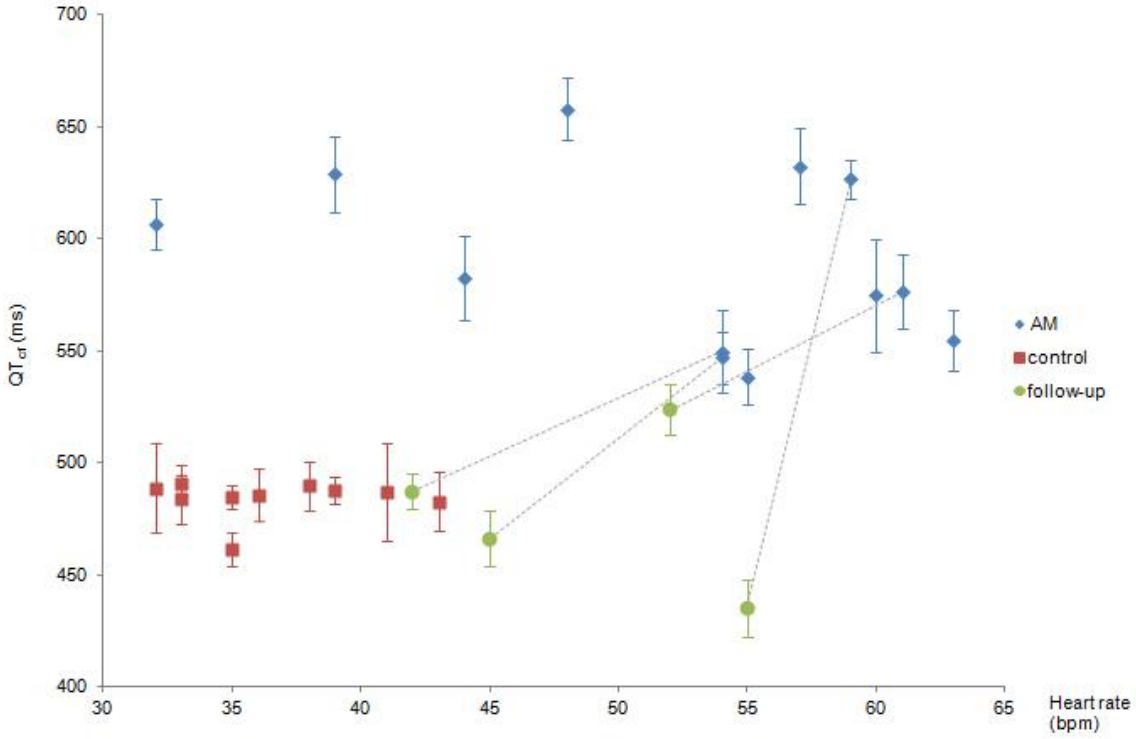

Figure 4: QT_{cf} (mean ± standard deviation) in horses with atypical myopathy compared to healthy control horses. Y-axis shows the corrected QT interval by Fridericia's method (QT_{cf}). X-axis shows heart rate. Blue symbols represent AM horses, red symbols control horses. Green symbols represent QT_{cf} at follow-up in surviving horses.

In three surviving horses, the QT_{cf} interval had returned to normal at follow-up examination. QT_{cf} in horse 6 shortened but was still above control group level at ten weeks follow-up. The fifth surviving horse (horse 4) was lost for follow-up. Ten horses showed ventricular premature depolarizations (VPDs) at admission and one horse also paroxysmal ventricular tachycardia (VT). One of the surviving horses (horse 6) still showed VPDs at rest and during exercise at two months follow-up.

Table 4: ECG results of twelve horses with atypical myopathy

Horse	Day	Duration min	ECG Dysrhythmias	QT_{cf} ms <490
1	1	15	3 VPD	583±19
2	1	15	1 VPD	538±12
3	1	15	none	555±14
4	1	15	2 VPD	575±25
5	1	15	17 VPD, pm	632±17
6	1	15	13 VPD, pm, 2 APD	576±17
	72	120	45 VPD, pm	523±11
7	1	15	10 VPD, pm	606±12
8	1	15	16 VPD, pm, VT	547±12
	44	75	none	466±12
9	1	15	1 VPD	550±19
	64	30	none	487±8
10	1	15	2 VPD, pm, 3 APD	627±9
	12	120	2 APD	435±13
11	1	15	1 VPD	658±14
12	1	15	none	629±17

APD, atrial premature depolarization; pm, polymorphic; VPD, ventricular premature depolarization; VT, ventricular tachycardia; QT_{cf}, QT interval with Fridericia's correction method

Discussion

This study confirms the presence of cardiac damage in horses with AM, as previously described (Cassart et al., 2007). Ten of twelve horses showed VPDs and all but one horse showed elevated concentrations of cTnI on admission, indicating cardiac cellular injury. In addition, all horses showed abnormal LV systolic wall motion in association with a prolonged QT_{cf} interval.

The QT interval represents the time between the onset of ventricular depolarization and end of repolarization. In man, the QT interval is known to increase with age and body mass index (Mangoni et al., 2003). AM horses were younger and had a lower body weight than control horses but still showed a significantly longer QT_{cf} interval, indicating prolonged ventricular repolarization. To the authors knowledge, this is the first time that long QT_{cf} interval has been reported in horses with cardiomyopathy. In human medicine, two forms of the long QT syndrome (LQTS) are well described: inherited LQTS and acquired QT prolongation. Inherited LQTS is caused by mutations in genes that encode ion channel proteins, causing a maintained inward current of sodium at depolarized voltages or a decrease in delayed rectifier potassium channel currents (Finley et al., 2003). Both defects lead to a prolonged ventricular repolarization. The acquired form is associated with exposure to a wide variety of cardiac and noncardiac drugs, but also with electrolyte imbalances and toxins (Khan, 2002).

The origin of the long QT in AM horses is uncertain. Drug-induced prolongation seems unlikely since no known QT prolonging drug had been administered before examination. Electrolyte imbalances such as hypokalemia and hypocalcemia are known to cause QT prolongation and dysrhythmia (Khan, 2002; Borer and Corley, 2006a; b). However, none of the horses showed hypokalemia and one horse with normocalcemia also showed QT prolongation, suggesting that other mechanisms might play a role. The exact etiology of AM remains unknown but recent research points towards a myopathy of toxic origin, affecting the mitochondria and resulting in acquired multiple ADD (Cassart et al., 2007; Westermann et al., 2008; van der Kolk et al., 2010). Interestingly, a recent study found a link between ADD and long QT interval in mice (Gelinas et al., 2011). The mice also showed a cardiac specific reduction of docosahexaenoic acid (DHA), an omega-3 polyunsaturated fatty acid which could have a protective effect against QT prolongation (Billman et al., 1999; Mozaffarian et al., 2006). Another study in ADD mice reported altered intracellular Ca^{2+} homeostasis and an elevated Ca^{2+} load in the sarcoplasmatic reticulum, which was thought to be induced by decreased ATP production as a consequence of ADD (Werdich et al., 2007).

An elevated Ca^{2+} load in the sarcoplasmatic reticulum may increase spontaneous Ca^{2+} release and lead to dysrhythmias, which were present in ten out of twelve AM horses. Another explanation for the dysrhythmias are early afterdepolarizations (EADs). EADs are membrane potential oscillations that occur when the action potential duration is increased long enough for ion channels such as the L-type Ca^{2+} channels to reactivate during repolarisation (Finley et al., 2003). EADs can trigger ectopic premature beats, but also increase electric heterogeneity and hence favor the development of reentrant ventricular tachycardia (VT) and Torsade de Pointes (El-Sherif and Turitto, 1999). Runs of VT were present in two AM horses.

Abnormal ionic currents might also explain the wall motion abnormality seen on echocardiography. The 'plateau-like' prolonged ventricular contraction has also been demonstrated in human LQTS patients as the mechanical expression of a prolonged action potential duration. Due to the delayed repolarization, Ca^{2+} inward current and release by the sarcoplasmatic reticulum may be increased, resulting in a higher intracellular calcium concentration which leads to prolonged contraction (Nador et al., 1991; Haugaa et al., 2010). This is supported by the fact that Ca^{2+} channel blockade by verapamil in LQTS patients normalized the wall motion abnormality (De Ferrari et al., 1994). The biphasic contraction shape which was present in eight horses has also been recognized in human LQTS patients. This was proposed to be the mechanical equivalent of an electrical EAD (De Ferrari et al., 1994). However, the biphasic contraction was usually present in each cardiac cycle in the same segments, making EAD less likely. Another possibility is what is known in human medicine as postsystolic motion (Citro and Galderisi, 2005). Postsystolic motion has been demonstrated in ischemic myocardium and may also occur in healthy individuals (Voigt et al., 2003). It has also been described in healthy horses (Schwarzwald et al., 2009; Decloedt et al., 2011), but the duration of postsystolic contraction was much longer in AM horses. In ischemic myocardium, pronounced postsystolic contraction can occur in affected segments due to a delayed active contraction or a passive inward movement caused by tethering by adjacent normal contractile segments, which occurs after unloading caused by aortic valve closure and hence during regional wall stress decrease (Citro and Galderisi, 2005). However, a coexisting reduction in ejection velocity is obligate (Voigt et al., 2003), which was not present in AM horses. Therefore ischemic postsystolic motion is an unlikely explanation for the observed contraction abnormality. Based on the morphology and timing of the biphasic contraction, we suggest that it might be associated with aortic valve closure, causing a biphasic instead of 'plateau-like' contraction pattern in certain segments.

TDI and 2DST measurements confirmed that the abnormal wall motion pattern was caused by delayed repolarization and thus abnormal relaxation. Similar to human LQTS patients, the rapidity of early contraction was unaffected, as demonstrated by the shorter LVPEP and faster V_{Syst} (Nador et al., 1991; Savoye et al., 2003). The prolonged contraction duration was explained by a longer IVRT duration, with a normal ejection time. This explains why the CD by TDI were increased, while the CD by 2DST were normal. The CD by TDI was defined as the time to onset of early diastole, which included IVRT. The CD by 2DST was defined as the time to peak strain. This often did not include IVRT because peak strain occurred at the end of ejection, followed by a plateau during IVRT. The impaired LV relaxation was also reflected by the reduced V_E and decreased E/A ratio, indicating diastolic dysfunction (Rivas-Gotz et al., 2003; Schefer et al., 2011). These findings are in concordance with findings in human LQTS patients (Haugaa et al., 2009).

Mechanical dispersion of contraction duration could be demonstrated by TDI and 2DST. By TDI, CD was significantly longer in IVS but not in LVFW. By 2DST, the SD and STI of longitudinal and circumferential CD were significantly longer in AM horses. This mechanical dispersion has also been found in human LQTS patients and probably reflects electric dispersion of repolarization (Nakayama et al., 1998). The ion channels are not homogeneously distributed throughout the myocardium and thus an inhomogeneous prolongation of action potential duration occurs. The dispersion of repolarization increases the risk of ventricular dysrhythmias such as Torsade de Pointes. Mechanical dispersion was higher in LQTS patients with a history of dysrhythmia, syncope or cardiac arrest compared to asymptomatic LQTS patients (Haugaa et al., 2009; Haugaa et al., 2010). In the AM horses, CD was longer in IVS compared to LVFW. Similar results were found in human LQTS patients, and this is attributed to longer action potential duration of the subendocardial Purkinje cells and midmyocardial M-cells which are located in the interventricular septum (Haugaa et al., 2009).

This transmural dispersion probably explains why longitudinal function was more affected both in human LQTS patients and AM horses. While FS, SR and SC were normal, SL was significantly lower in AM horses, although still within reference values. The longitudinal fibres are predominantly located subendocardially and have been shown to be most vulnerable in various cardiac diseases. The value of longitudinal strain for detection of subclinical myocardial dysfunction is well described in human medicine (Geyer et al., 2010). However, this is the first time that longitudinal strain is reported to be more sensitive than other measurements for detection of myocardial damage in horses.

Four of the surviving horses were followed up after a variable period. In all horses, cTnI concentrations returned to normal and the abnormal myocardial motion disappeared. One of the horses still showed VPDs and a QT_{cf} interval that remained above reference level. There was no indication for myocardial fibrosis on repeated echocardiographic examinations in this horse.

The number of surviving horses for follow-up was very limited, so conclusions on surviving horses must be interpreted with caution. Further research in a larger group of horses with a longer follow-up period is necessary to evaluate the long-term consequences of AM on cardiac function and the contribution of cardiac damage to the low survival rate. ECG recordings at the time of death might elucidate causes of sudden death associated with AM. Another limitation was the relatively low number of horses in which a full cardiac exam could be performed before initiation of treatment. However, findings were very consistent in all AM horses. Horses in the control group were not age and body weight matched to AM horses, which might be important as the QT interval was demonstrated to be positively correlated to age and body weight in healthy human subjects (Mangoni et al., 2003). However, AM horses had longer QT intervals even though they were younger and smaller.

In conclusion, this study demonstrated that AM induces myocardial damage which can lead to characteristic echocardiographic and electrocardiographic abnormalities. The AM horses showed increased cTnI, VPDs and an abnormal LV systolic wall motion pattern in association with a prolonged QT_{cf} interval. TDI and 2DST could demonstrate a prolonged contraction duration, decreased longitudinal strain, increased mechanical dispersion between segments and abnormal LV relaxation, similar to human LQTS patients. The exact pathophysiology remains to be elucidated, but ADD and abnormal ionic currents might play an important role. Further research is needed to determine the long-term consequences of AM on cardiac function.

References

Billman GE, Kang JX, Leaf A (1999). Prevention of sudden cardiac death by dietary pure omega-3 polyunsaturated fatty acids in dogs. Circulation 99, 2452-2457

Borer KE, Corley KTT (2006a). Electrolyte disorders in horses with colic. Part 1: Potassium and magnesium. Equine Vet Educ 18, 266-271

Borer KE, Corley KTT (2006b). Electrolyte disorders in horses with colic. Part 2: Calcium, sodium, chloride and phosphate. Equine Vet Educ 18, 320-325

Cassart D, Baise E, Cherel Y, Delguste C, Antoine N, Votion D, Amory H, Rollin F, Linden A, Coignoul F, Desmecht D (2007). Morphological alterations in oxidative muscles and mitochondrial structure associated with equine atypical myopathy. Equine Vet J 39, 26-32

Citro R, Galderisi M (2005). Myocardial postsystolic motion in ischemic and not ischemic myocardium: The clinical value of tissue Doppler. Echocardiography 22, 525-532

Davey P (2002). How to correct the QT interval for the effects of heart rate in clinical studies. J Pharmacol Toxicol 48, 3-9

De Ferrari GM, Nador F, Beria G, Sala S, Lotto A, Schwartz PJ (1994). Effect of calcium channel block on the wall motion abnormality of the idiopathic long QT syndrome. Circulation 89, 2126-2132

Decloedt A, Verheyen T, Sys S, De Clercq D, van Loon G (2011). Quantification of left ventricular longitudinal strain, strain rate, velocity, and displacement in healthy horses by 2-dimensional speckle tracking. J Vet Intern Med 25, 330-338

El-Sherif N, Turitto G (1999). The long QT syndrome and Torsade de Pointes. PACE 22, 91-110

Finley MR, Lillich JD, Gilmour RF, Freeman LC (2003). Structural and functional basis for the long QT syndrome: Relevance to veterinary patients. J Vet Intern Med 17, 473-488

Finno CJ, Valberg SJ, Wunschmann A, Murphy MJ (2006). Seasonal pasture myopathy in horses in the midwestern United States: 14 cases (1998-2005). J Am Vet Med Assoc 229, 1134-1141

Gelinas R, Thompson-Legault J, Bouchard B, Daneault C, Mansour A, Gillis M-A, Charron G, Gavino V, Labarthe F, Des Rosiers C (2011). Prolonged QT interval and lipid alterations beyond beta-oxidation in very long-chain acyl-CoA dehydrogenase null mouse hearts. Am J Physiol Heart Circ Physiol 301, H813-H823

Geyer H, Caracciolo G, Abe H, Wilansky S, Carerj S, Gentile F, Nesser HJ, Khandheria B, Narula J, Sengupta PP (2010). Assessment of myocardial mechanics using speckle tracking echocardiography: Fundamentals and clinical applications. J Am Soc Echocardiogr 23, 351-369

Haugaa KH, Amlie JP, Berge KE, Leren TP, Smiseth OA, Edvardsen T (2010). Transmural differences in myocardial contraction in long-QT syndrome: Mechanical consequences of ion channel dysfunction. Circulation 122, 1355-1363

Haugaa KH, Edvardsen T, Leren TP, Gran JM, Smiseth OA, Amlie JP (2009). Left ventricular mechanical dispersion by tissue Doppler imaging: A novel approach for identifying high-risk individuals with long QT syndrome. Eur Heart J 30, 330-337

Jesty SA, Kraus M, Gelzer A, Rishniw M, Moise NS (2009). Effect of transvenous electrical cardioversion on plasma cardiac troponin I concentrations in horses with atrial fibrillation. J Vet Intern Med 23, 1103-1107

Khan IA (2002). Clinical and therapeutic aspects of congenital and acquired long QT syndrome. Am J Med 112, 58-66

Linklater KA (1984). Myopathy in horses and ponies. Vet Rec 115, 666-666

Mangoni AA, Kinirons MT, Swift CG, Jackson SH (2003). Impact of age on QT interval and QT dispersion in healthy subjects: A regression analysis. Age Ageing 32, 326-331

Mozaffarian D, Prineas RJ, Stein PK, Siscovick DS (2006). Dietary fish and n-3 fatty acid intake and cardiac electrocardiographic parameters in humans. J Am Coll Cardiol 48, 478-484

Nador F, Beria G, De Ferrari GM, Stramba-Badiale M, Locati EH, Lotto A, Schwartz PJ (1991). Unsuspected echocardiographic abnormality in the long QT syndrome. Diagnostic, prognostic, and pathogenetic implications. Circulation 84, 1530-1542

Nakayama K, Yamanari H, Otsuka F, Fukushima K, Saito H, Fujimoto Y, Emori T, Matsubara H, Uchida S, Ohe T (1998). Dispersion of regional wall motion abnormality in patients with long QT syndrome. Heart 80, 245-250

Patteson MW, Gibbs C, Wotton PR, Cripps PJ (1995). Echocardiographic measurements of cardiac dimensions and indices of cardiac function in normal adult Thoroughbred horses. Equine Vet J 27, 18-27

Rivas-Gotz C, Khoury DS, Manolios M, Rao LY, Kopelen HA, Nagueh SF (2003). Time interval between onset of mitral inflow and onset of early diastolic velocity by tissue Doppler: A novel index of left ventricular relaxation - experimental studies and clinical application. J Am Coll Cardiol 42, 1463-1470

Savoye C, Klug D, Denjoy I, Ennezat PV, Le Tourneau T, Guicheney P, Kacet S (2003). Tissue Doppler echocardiography in patients with long QT syndrome. Eur J Echocardiogr 4, 209-213

Schefer KD, Hagen R, Ringer SK, Schwarzwald CC (2011). Laboratory, electrocardiographic, and echocardiographic detection of myocardial damage and dysfunction in an Arabian mare with nutritional masseter myodegeneration. J Vet Intern Med 25, 1171-1180

Schwarzwald CC, Hamlin RL, Bonagura JD, Nishijima Y, Meadows C, Carnes CA (2007). Atrial, SA nodal, and AV nodal electrophysiology in standing horses: Normal findings and electrophysiologic effects of quinidine and diltiazem. J Vet Intern Med 21, 166-175

Schwarzwald CC, Schober KE, Berli AS, Bonagura JD (2009). Left ventricular radial and circumferential wall motion analysis in horses using strain, strain rate, and displacement by 2D speckle tracking. J Vet Intern Med 23, 890-900

Unger-Torroledo L, Straub R, Lehmann AD, Graber F, Stahl C, Frey J, Gerber V, Hoppeler H, Baum O (2010). Lethal toxin of Clostridium sordellii is associated with fatal equine atypical myopathy. Vet Microbiol 144, 487-492

van der Kolk JH, Wijnberg ID, Westermann CM, Dorland L, de Sain-van der Velden MGM, Kranenburg LC, Duran M, Dijkstra JA, van der Lugt JJ, Wanders RJA, Gruys E (2010). Equine acquired multiple acyl-CoA dehydrogenase deficiency (MADD) in 14 horses associated with ingestion of maple leaves (Acer pseudoplatanus) covered with European tar spot (Rhytisma acerinum). Mol Genet Metab 101, 289-291

Voigt JU, Lindenmeier G, Exner B, Regenfus M, Werner D, Reulbach U, Nixdorff U, Flachskampf FA, Daniel WG (2003). Incidence and characteristics of segmental postsystolic longitudinal shortening in normal, acutely ischemic, and scarred myocardium. J Am Soc Echocardiogr 16, 415-423

Votion D-M, Linden A, Saegerman C, Engels P, Erpicum M, Thiry E, Delguste C, Rouxhet S, Demoulin V, Navet R, Sluse F, Serteyn D, van Galen G, Amory H (2007). History and clinical features of atypical myopathy in horses in Belgium (2000-2005). J Vet Intern Med 21, 1380-1391

Votion D-M, Serteyn D (2008). Equine atypical myopathy: A review. Vet J 178, 185-190

Werdich AA, Baudenbacher F, Dzhura I, Jeyakumar LH, Kannankeril PJ, Fleischer S, LeGrone A, Milatovic D, Aschner M, Strauss AW, Anderson ME, Exil VJ (2007). Polymorphic ventricular tachycardia and abnormal Ca^{2+} handling in very-long-chain acyl-CoA dehydrogenase null mice. Am J Physiol Heart Circul Physiol 292, H2202-H2211

Westermann CM, Dorland L, Votion DM, de Sain-van der Velden MGM, Wijnberg ID, Wanders RJA, Spliet WGM, Testerink N, Berger R, Ruiter JPN, van der Kolk JH (2008). Acquired multiple acyl-CoA dehydrogenase deficiency in 10 horses with atypical myopathy. Neuromusc Disord 18, 355-364

Chapter 7: General discussion

1. Feasibility and reliability of tissue Doppler imaging and two-dimensional speckle tracking in horses

In human medicine, tissue Doppler imaging (TDI) and two-dimensional speckle tracking (2DST) allow an objective and more extensive quantification of left ventricular (LV) function compared to conventional two-dimensional (2D) and M-mode echocardiographic measurements such as fractional shortening (FS). Little information was available on the use of both techniques in horses at the start of this research. Therefore, a fixed protocol for image acquisition and off-line analysis was developed based on the knowledge from human and small animal medicine. Several adaptations were made in order to apply TDI and 2DST in horses.

The main problem in equine ultrasonography is the cardiac size. In human medicine, the image depth is approximately 15-16 cm for parasternal views. In adult horses, a depth of 26-30 cm is required for imaging the entire LV from a right parasternal view. As a result, the frame rate of conventional 2D echocardiographic images with an image width of 90° is only 16 frames per second (fps) in horses, while the optimal frame rate for 2DST is about 40-80 fps (Mor-Avi et al., 2011) and for color TDI strain rate calculations >180 fps (Sutherland et al., 2006). In order to apply 2DST in horses, the image width was reduced to 55° to increase the 2D grayscale frame rate. This allowed visualization of the entire LV cross-section in short-axis but not in long-axis images. In the modified four-chamber view, the apical segments were not included in the image. Still, velocity and deformation values were calculated in these segments by the 2D Strain algorithm (EchoPAC^{TM}, GE Healthcare, Horten, Norway). These calculations are based on the presumption that longitudinal motion is largest in the atrioventricular plane. This motion is then distributed by spline smoothing over the whole region of interest (ROI), including the apical segments. However, tracking quality in the apical segments was not approved by the software, as expected, and these results were not used for analysis. The achieved frame rate for 2DST was 41 fps which is within the recommended guidelines. Higher frame rates will probably be needed to achieve adequate tracking at increased heart rates, e.g. during stress echocardiography (Teske et al., 2007) or to resolve the high wall motion velocity during early diastole. The frame rate can be further enhanced by reducing the number of ultrasound beams for building up the sector.

This reduced line density was not applied for 2DST as it results in decreased lateral resolution. This is detrimental for tracking speckles in the lateral direction, particularly in the far field.

For TDI, the frame rate was increased to >180 fps by decreasing the image width to 30°, narrowing the TDI sector maximally and reducing line density. The decreased image width is no limitation for TDI as accurate measurements can only be performed in a narrow sector with optimal alignment of the ultrasound beam and myocardial wall motion. A low lateral resolution is also no real drawback using parasternal images. Even in the far field, only myocardial tissue is included within the beam width. A low lateral resolution might even decrease measurement variability because the signal of a larger myocardial segment is averaged.

The second important limitation for the use of TDI and 2DST in horses is that apical images are impossible to acquire due to anatomical constraints. In human medicine, longitudinal velocity and deformation assessed from apical images are the most commonly used TDI and 2DST measurements because the thin LV walls cause difficulty for measuring radial strain from parasternal images. Using TDI, strain is preferably calculated over an offset distance or strain length of 12 mm. A shorter offset distance results in more noise (Marwick, 2006). However, a strain length of 12 mm often exceeds the human LV wall thickness. Similarly, radial strain measurements by 2DST do not correlate well with sonomicrometry and demonstrate a larger variability compared to longitudinal and circumferential strain (Reant et al., 2008; Koopman et al., 2010a). This can also be explained by the thin wall thickness, combined with the relatively poor lateral resolution. In contrast, radial strain measurements in horses were feasible both by TDI and 2DST. Radial measurements are facilitated by the large equine myocardial wall thickness, which is about 2.5 cm at end-diastole and 4 cm at end-systole (Patteson et al., 1995). Furthermore, image quality is generally better in horses compared to humans.

The image quality is crucial for TDI and 2DST analysis and should be optimized during image acquisition. Second harmonic imaging results in a reduction of noise and sidelobe artifacts (Hanekom et al., 2004). Therefore, a frequency of 1.6/3.2 MHz was used for 2DST and 1.7/3.4 MHz for TDI, with optimal gain and contrast for imaging the myocardium. A thorough visual evaluation of image quality was performed during acquisition. For 2DST, the entire myocardial cross-section should be well-defined throughout the whole cardiac cycle.

In short-axis images, attention must be paid to avoid rib or lung edge shadows which cause reduced lateral resolution. In long-axis images, image quality of the mitral ring area needs to be carefully checked as the basal segments were often excluded due to presence of drop-out caused by a rib or the coronary region. For TDI images, optimal alignment of the ultrasound beam to myocardial wall motion should be attained. Homogeneous coloring of the myocardium is important as this indicates the absence of artifacts and aliasing. Artifacts result in biased velocity estimates, which in turn lead to wrong strain rate calculations (Heimdal et al., 1998). If aliasing velocities are present, the velocity scale should be increased. A fixed velocity scale of +32/-32 cm/s was used throughout all studies. This might not be sufficient for horses with cardiac dilatation, since a larger heart size is associated with higher TDI velocities. In children, TDI velocities are positively correlated to LV end-diastolic dimension (Eidem et al., 2004). In dogs, a clear association between breed and TDI velocities was found with the largest breed having 1.5 to 3.1-fold higher velocities compared to the smallest breed (Chetboul et al., 2005).

Pulsed-wave TDI was not used in this work although this technique has been proposed as the most reliable modality of TDI in horses (Schwarzwald et al., 2009b). The main advantage of PW TDI is that the curves are visualized during acquisition, allowing correction of the sample area position until good quality curves are obtained. However, the sample area is positioned at a fixed distance from the transducer. As a consequence, the myocardial segment is moving through the sample area during contraction. In parasternal views, velocities of the endocardial border are measured during early systole while mid-myocardial to epicardial velocities are measured during late systole. Off-line analysis of color TDI allows repositioning of the sample area in order to follow the myocardial motion throughout the cardiac cycle. In addition, color TDI allows the simultaneous evaluation of different myocardial segments and calculation of strain and strain rate indices (Galderisi et al., 2007). Therefore, this modality was preferred over PW TDI.

Off-line analysis was performed following the guidelines provided by the software manufacturer (EchoPAC^{TM}, GE Healthcare, Horten, Norway). Some specific points of attention apply for the post-processing of TDI and 2DST images acquired in horses. For TDI, the size of the region of interest (ROI) should be adapted to the large myocardial wall thickness. A ROI length of 11-17 mm was applied. The data acquisition area using the EchoPAC^{TM} software extends ½ strain length above and below the ROI edges (Davidsen et al., 2010).

Using a fixed strain length of 12 mm, a free zone of minimally 6 mm should be kept between the ROI edges and the endocardium or epicardium to avoid inclusion of blood velocities in the strain calculations. However, the ROI position can vary substantially using this guideline alone, since myocardial wall thickness often exceeds 4 cm at end-systole. Therefore, the ROI should always be positioned in the mid-myocardium. Slight deviations from this position result in different peak values of velocity because of the transmural velocity gradient (Fleming et al., 1994; Uematsu et al., 1995). Peak strain and strain rate values are also influenced since transmural differences are present with higher endocardial and lower epicardial radial deformation (Delfino et al., 2008; Ishizu et al., 2010).

An additional complication for TDI off-line analysis in horses is the large image depth. During off-line analysis, the velocity curves showed more random noise in the LV free wall segment, which is situated at an image depth of about 26-28 cm. As a result, the strain rate and strain curves were of insufficient quality for accurate measurements. Deformation measurements were feasible in all other segments, although careful manual positioning of the ROI in order to track the myocardium during the cardiac cycle was a prerequisite for obtaining qualitative curves.

In contrast, off-line analysis of 2DST images is semi-automated. Only the detection of the endocardial border and determination of ROI width need to be performed manually. The ROI width should be adjusted to myocardial wall thickness without exceeding the epicardial limits. A narrow ROI width should be avoided, as this results in significantly higher radial strain measurements (Biaggi et al., 2011). Circumferential strain measurements are also influenced by ROI width, as endocardial circumferential shortening is higher than epicardial shortening (Adamu et al., 2009). The 2DST curves should always be interpreted with caution. Visual evaluation of tracking quality is essential as the curves can look normal even in poorly tracked segments due to the extensive smoothing applied by the software algorithm. Furthermore, the technical limitations of the technique should be kept in mind. For instance, circumferential strain measurements were often lower in the LV free wall segments. This was probably caused by the low lateral resolution at this level. Similar segmental differences caused by low lateral resolution have been described in myocardial infarction patients (Sjoli et al., 2009).

As for any diagnostic technique, the evaluation of repeatability and reproducibility is of major importance before the use can be assessed in clinical studies. Chapter 3 describes the reliability of TDI and 2DST measurements of equine LV function.

Both acquisition and measurement variability were determined in order to obtain a close estimate of the true variability as encountered in clinical practice. In contrast, most variability studies in human medicine only calculated measurement variability (Fraser et al., 2003; Lorch et al., 2008; Margulescu et al., 2010). In these studies, loops acquired by one observer were measured off-line by two or more observers in order to determine interobserver measurement variability, and repeatedly measured by one observer in order to determine intra-observer measurement variability. However, the acquisition variability is of equal or even higher importance, as this encompasses not only differences in image acquisition and analysis but also the biological variability over time (Vinereanu et al., 1999; Thorstensen et al., 2010). For TDI measurements in horses, peak values generally showed a higher variability than timing measurements. Similar results were found in a previous study in horses (Schwarzwald et al., 2009b). The higher variability of peak values can be explained by the angle-dependency of TDI and the influence of manual positioning of the ROI, which both affect peak velocity and deformation measurements but not timing. As expected, the within- and between-day acquisition variability was higher than the measurement variability. In addition to biological variability, TDI image acquisition under a slightly different angle might result in variation of the peak values (D'hooge et al., 2006). In general, 2DST measurements showed a better repeatability and reproducibility than TDI measurements, similar to what is found in human medicine (Amundsen et al., 2009; Van Dalen et al., 2009). The semi-automated off-line analysis reduces observer variability and the curves are smoothed more extensively than TDI curves. In contrast to human medicine, radial strain showed a lower variability than circumferential strain. This is probably explained by the larger wall thickness of the equine myocardium and the low lateral resolution in the far field, as discussed above.

In order to reduce variability, it is recommended that the same observer acquires and measures all exams. As this is practically difficult in clinical settings, different observers should use a standardized protocol for image acquisition and off-line analysis. The second important source of variability is the type of ultrasound machine and software package (Koopman et al., 2010b; Biaggi et al., 2011). Velocity and deformation measurements may differ significantly between ultrasound systems, but also when the same scanner acquisition is post-processed on two different workstations (Martensson et al., 2011). Throughout the studies described in Chapter 3-6, the same ultrasound machine and software package were used in order to minimize this variability.

2. Do TDI and 2DST measure myocardial contractility?

Myocardial contractility is the intrinsic capability of active force development by the myocytes. In an isolated myocardial fiber, contractility is described by the maximal velocity of fiber shortening at zero load (Bombardini, 2005). The myocyte force development results in increased intracavitary pressure needed for aortic valve opening, which is followed by wall deformation causing ejection of blood into the circulation. The force development during the isovolumic period reflects actual contractility but is very difficult to measure. In contrast, systolic wall deformation is easier to measure and directly related to ejection and thus stroke volume. However, wall deformation is not only influenced by intrinsic force development but also by tissue elasticity and local wall stress. The wall stress is determined by the local geometry, interaction with adjacent myocardial segments and pressure and volume loading (Bijnens et al., 2009). An ideal measurement of myocardial contractility should be sensitive to changes in inotropy but independent of load, heart size and geometry (Carabello, 2002).

The traditional measurements of LV function are calculations based on the LV internal dimensions, such as FS and ejection fraction (EF). However, these ejection-phase indices are load-dependent and do not provide direct information about LV contractility (Carabello and Spann, 1984). For example, mitral regurgitation results in a decreased afterload as the LV empties into the low-pressure left atrium. This gives rise to an increased EF, irrespective of inotropic changes. In chronic mitral regurgitation, an increase of the LV end-diastolic diameter occurs due to LV volume overload and thus increased preload. In this situation, the EF returns to normal values, although significant myocardial dysfunction might be present (O'Gara et al., 2008). In contrast, aortic stenosis causes an increased afterload which often reduces EF in presence of normal myocardial function. Another disadvantage of EF and particularly FS is the fact that assessment of global LV function is derived from a focal measurement based on geometric assumptions. This does not take into account regional differences. Furthermore, FS is based on radial wall thickening and does not consider longitudinal shortening. Longitudinal function was demonstrated to be a more sensitive measurement of subclinical changes in systolic function because the subendocardial longitudinal myocardial fibres are more vulnerable in many cardiac diseases (Blessberger and Binder, 2010).

In human medicine, TDI was introduced as a superior technique for quantification of myocardial function because myocardial velocity measurements were sensitive to changes in inotropy, could quantify regional motion both in radial and longitudinal direction and were correlated to invasive measurements of contractility (Gorcsan et al., 1997). However, systolic and diastolic TDI velocities have been experimentally demonstrated to be preload- and afterload-dependent (Ama et al., 2004; Borlaug et al., 2007). Velocity measurements are additionally influenced by overall heart motion and tethering by the adjacent segments, which can be overcome by using deformation indices like strain and strain rate. The effect of load on strain and strain rate measurements has been extensively studied. In animal models, strain correlated directly with EF and stroke volume and was strongly influenced by changes in preload and afterload. Increasing afterload resulted in impairment of predominantly longitudinal deformation and thus in lower strain values (Donal et al., 2009). Increasing preload by volume loading resulted in higher deformation due to the Frank-Starling mechanism (Urheim et al., 2000). Strain rate measurements were less load-dependent and correlated better with changes in contractility (Greenberg et al., 2002; Weidemann et al., 2002; Ferferieva et al., 2012). Therefore, strain measurements can be used as an indicator of stroke volume, while strain rate gives an estimate of contractility. However, an experimental study demonstrated that both strain and strain rate measurements are also influenced by heart size (Rosner et al., 2009). A lower amount of myocardial deformation is needed to generate the same stroke volume in enlarged hearts. Since the LV adapts to chronic volume overload by an increase of the LV internal diameter, the combination of increased preload and larger heart size will result in normal strain values. As a consequence, the influence of both loading and cardiac geometry should be taken into account when evaluating strain rate and particularly strain measurements. Despite these limitations, the predictive value of strain measurements has been extensively studied and is often better than that of EF (Antoni et al., 2010; Mignot et al., 2010; Sawaya et al., 2011). This is probably due to the fact that strain measurements usually assess longitudinal function.

In the pursuit of a non-invasive load-independent measurement of myocardial contractility, several studies have investigated the isovolumic contraction phase. As all valves are closed in this phase, the effect of loading was thought to be minimal. Still, the peak isovolumic contraction velocity by TDI was demonstrated to be influenced by changes in preload and afterload (Meco and Cirri, 2010). Isovolumic acceleration (IVA) was proposed as a true load-independent measurement (Vogel et al., 2003). Although it is currently still used in some

studies as a parameter of contractility, it has been demonstrated experimentally that IVA shows a rather low reproducibility and is load-dependent (Lyseggen et al., 2005; Margulescu et al., 2010).

This confirms the results of the study described in Chapter 4, where the influence of the atrioventricular (AV) interval on isovolumic peak velocity and acceleration was investigated. The atrioventricular delay influenced the mechanism and timing of mitral valve closure. As a result, the peak isovolumic velocity and IVA were significantly higher when the mitral valve was still open at the onset of LV contraction, which occurred during pacing at short AV delays and ventricular pacing without preceding atrial contraction. This probably reflects the load-dependency of this parameter. In horses at rest, large variations of the AV interval are physiological (McGuirk and Muir, 1985). As a consequence, the peak isovolumic velocity and IVA will vary accordingly and cannot be used as a measurement of contractility.

Up till now, myocardial contractile function can only be assessed load-independently by invasive pressure-volume loop measurements. These determine the end-systolic pressure-volume relationship, of which the slope reflects end-systolic elastance (Bombardini, 2005). This has only been described once in horses using a large-size conductance catheter (Kerkhof, 1999). Non-invasive measurement of the pressure/volume ratio might be an alternative. The LV pressure can be estimated by Doppler or peripheral blood pressure measurements. This can be combined with 2D or 3D echocardiographic measurements of LV volume and timing of the cardiac cycle in order to obtain pressure/volume loops (Kim et al., 2007). Up till now, reproducible measurements that can be used in routine clinical practice are not yet available in human medicine. In horses, these measurements are particularly difficult as LV volume cannot be assessed by apical 3D echocardiography, and 2D estimates of LV volume from parasternal images are based on geometric assumptions which might not apply in horses with cardiac dilatation. Non-invasive blood pressure measurements in adult horses can be performed using a coccygeal cuff, but this measurement is not very sensitive (Parry and Anderson, 1984). Therefore, conventional echocardiography using 2D and M-mode measurements is currently the most commonly used tool for quantification of myocardial function in horses. TDI and 2DST might provide important additional information.

3. Quantification of left ventricular function in horses: TDI versus 2DST

The current quantification of equine LV function is most often limited to the calculation of FS, which is a one-dimensional, focal and load-dependent measurement. In human medicine, measurements of global systolic longitudinal LV function and transmitral flow measurements for evaluation of diastolic function are performed from apical images. In adult horses, these images cannot be acquired. The evaluation of longitudinal LV function is not possible from conventional 2D and M-mode parasternal images and optimal alignment with transmitral flow is difficult to achieve. Accurate transmitral inflow measurements are hampered because peak values vary according to the insonation angle (Reef et al., 1989; Schwarzwald et al., 2007b). In addition, there is no objective method for evaluation of regional myocardial function in horses, although a subjective wall motion scoring system has been proposed (Gehlen et al., 2005). TDI and 2DST measurements might overcome some of these limitations and provide additional insights in equine LV function.

Because of the high temporal resolution, TDI is well suited for measurements of time intervals. As described in Chapter 3.3, the TDI time intervals in horses showed a low variability and were correlated to conventional measurements of mitral and aortic valve motion using M-mode and PW-Doppler. The main advantage of TDI is that both systolic and diastolic time intervals can be obtained from one single view. In human medicine, a good correlation was found between invasive hemodynamic measurements and TDI-derived time intervals (Zamorano et al., 1997). TDI also allows measuring the myocardial performance index (MPI) or Tei-index, which is calculated as the sum of the isovolumic contraction time and isovolumic relaxation time, divided by the ejection time. The MPI obtained by TDI in human patients correlated well with conventional PW Doppler and invasive measurements (Tekten et al., 2003; Su et al., 2007). An increased MPI and increased ratio of pre-ejection period over ejection time (PEP/ET) could be detected by TDI in a mare with nutritional masseter myodegeneration. This indicated systolic myocardial dysfunction (Schefer et al., 2011). In Chapter 6, TDI timing measurements were used to describe the myocardial wall motion abnormality caused by abnormal ventricular repolarization in horses with a prolonged QT interval. The prolonged isovolumic relaxation time (IVRT) and contraction duration reflected the abnormal repolarization.

Because of the high temporal resolution, TDI can also be used to evaluate diastolic function in horses. In human medicine, the E/E' ratio of early diastolic PW Doppler mitral inflow velocity (E) to early diastolic TDI mitral annular velocity (E') is used to estimate LV filling pressure. Although this ratio has been used in horses, it is rather unreliable because of the lack of accurate transmitral flow measurements (Schwarzwald et al., 2009b). Other possible measurements of diastolic function include the isovolumic relaxation time (IVRT), the peak E velocity and the ratio of early to late diastolic velocity (E/A). The horses with atypical myopathy described in Chapter 6 showed a prolonged IVRT, lower peak E velocities and decreased E/A-ratio by TDI, indicating LV diastolic dysfunction. Similar changes were found in a mare with nutritional masseter myodegeneration. In that horse, TDI findings were consistent with measurements of transmitral flow (Schefer et al., 2011). TDI measurements in horses with atrial fibrillation showed absence of the A wave and an increased E wave in comparison to a control group (Gehlen et al., 2009). In addition, TDI was used for the assessment of atrial myocardial function in horses, allowing follow-up of atrial contractile dysfunction after conversion of atrial fibrillation (Schwarzwald et al., 2007a; b).

When evaluating LV systolic function, TDI velocity, strain rate and strain measurements should be interpreted with caution. Although the repeatability and reproducibility of timing measurements is good, peak values show a larger variability. Alterations of the insonation angle during image acquisition can result in important changes of the peak values. The off-line analysis is also an important source of variability as it is performed manually. The analysis is time-consuming and requires considerable experience. In addition, TDI is a focal and one-dimensional measurement, like FS. In order to assess global function, several LV segments should be evaluated, which further prolongs the time for off-line analysis.

As 2DST is a semi-automated technique, the time for off-line analysis is significantly shorter and the measurements are more robust. Because the entire LV cross-section is used for calculating the deformation indices, 2DST is more suited for evaluation of global LV function than TDI. Based on the feasibility and repeatability described in Chapter 3.2, global circumferential and radial LV function is preferably assessed from a short-axis image at papillary muscle instead of chordal level. In addition, 2DST also allowed the evaluation of LV longitudinal function from a modified four-chamber view (Chapter 3.1). Longitudinal function often deteriorates first in case of myocardial dysfunction in human medicine, because the subendocardial longitudinal fibres are most vulnerable in many cardiac diseases (Geyer et al., 2010).

Using conventional 2D and M-mode echocardiography from parasternal views, longitudinal LV shortening cannot be assessed in horses. By 2DST, longitudinal myocardial velocity, strain rate and strain could be measured. All horses with severe myocardial damage described in Chapter 5 demonstrated decreased longitudinal strain values as well as alterations of FS. Remarkably, 4/15 horses with mild myocardial damage described in this chapter had decreased longitudinal strain values whereas FS was below reference range in only 1/15 horses. Similarly, in the group of horses with atypical myopathy described in Chapter 6, global longitudinal strain was decreased whereas FS, circumferential strain and radial strain were not significantly different from the control group. Further research is needed to evaluate whether longitudinal strain can reveal subclinical myocardial dysfunction in horses with other cardiac diseases such as valvular regurgitation and whether it has a prognostic value.

The main disadvantage of 2DST is the low frame rate. The low temporal resolution hampers precise time measurements and detection of isovolumic peaks. In horses, tracking quality is often poor in early diastole because of the fast myocardial motion in this phase combined with the relatively low frame rate. This results in a frame-to-frame displacement of the speckles which exceeds the search window of the software algorithm, causing unreliable measurements (Sivesgaard et al., 2009). Therefore, 2DST can only be reliably used for measurements of global systolic function in horses but not for diastolic function (Schwarzwald et al., 2009a).

Regional LV function can be evaluated by comparing segmental measurements, both by TDI and 2DST. In human medicine, this is mainly important for diagnosis of coronary artery disease and myocardial ischemia and for detection of mechanical dyssynchrony in patients undergoing cardiac resynchronization therapy (CRT) (Nesser and Winter, 2009). Changes in preload and afterload in valvular disease or hypertension can also result in regional changes of myocardial function. Due to the asymmetrical LV geometry, some segments develop increased local wall stress as a response to altered loading while others are less affected. Pressure overload causes increased wall stress in the basal septal segment because this segment is less curved than the LV free wall. As a result, decreased deformation and localized hypertrophy can be observed in this segment before other segments are involved (Bijnens et al., 2009). Regional changes have not yet been described in horses with valvular disease. In Chapter 5, TDI and 2DST could detect local myocardial dysfunction in a horse with severe myocardial fibrosis. Lower longitudinal and radial strain values were found in the interventricular septum compared to the LV free wall. Autopsy confirmed that the fibrosis was predominantly located in the septum.

Physiological segmental differences should always be taken into account when evaluating regional function. As described in Chapter 3, segmental differences of TDI and 2DST peak values and timing measurements were present in healthy horses. For example, longitudinal and radial strain by 2DST were lower in the basal septal segment, whereas circumferential strain was higher in the septal segments compared to the LV free wall. The isovolumic relaxation measured by TDI was often absent in the velocity curves at chordal level and the time to peak E was significantly longer at papillary muscle level. This reflects the physiological base-to-apex sequence of LV relaxation (Sengupta et al., 2006).

In summary, TDI and 2DST can be considered complimentary for the quantification of LV function. TDI allows reliable measurements of both systolic and diastolic cardiac time intervals from one cardiac cycle. Systolic LV function can be assessed by quantification of radial myocardial velocity, strain rate and strain in different LV segments. Furthermore, TDI is suited for the evaluation of diastolic LV function. However, off-line analysis is time-consuming and measurements of peak velocity and deformation are more variable than timing measurements. In contrast to TDI, 2DST allows calculation of myocardial velocities and deformation in the two dimensions of the ultrasound image, using the entire LV cross-section. Therefore, 2DST is well suited for measurements of longitudinal, radial and circumferential global systolic LV function. Longitudinal strain seems particularly interesting for detection of subtle myocardial dysfunction. However, the temporal resolution of 2DST is much lower and diastolic measurements are unreliable. Regional function and dyssynchrony can be assessed both by TDI and 2DST, but caution is needed as segmental differences are also present in healthy horses.

4. Future prospects

TDI and 2DST allow an objective and more extensive quantification of myocardial function in horses. Currently, both techniques are mainly used as research tools which can provide additional insights into the physiology and pathophysiology of the equine heart. In the future, TDI and 2DST are likely to become available in an increasing number of equine referral practices. The fast evolution of ultrasound technology and postprocessing software will probably solve many of the current disadvantages. For example, higher frame rates might be achieved without loss of lateral resolution, resulting in improved quality of the TDI and 2DST curves and lower measurement variability. This will also facilitate the use of both techniques at high heart rates during stress echocardiography. In addition, new technology such as 3D echocardiography and 3D strain analysis might become available in equine cardiology. At present, the off-line analysis of TDI and 2DST is time-consuming and produces a large number of measurements, of which the clinical significance is often unknown. More research is needed to identify those measurements with the best diagnostic and prognostic value. These measurements might become part of the clinical routine for evaluating horses with cardiac disease or poor performance.

The clinical studies using TDI and 2DST in horses with cardiomyopathy and atypical myopathy demonstrated that both techniques can detect myocardial dysfunction. In the future, TDI and 2DST could be used to investigate subclinical LV dysfunction in horses with valvular disease. This would certainly improve the objective assessment of the severity of regurgitation and might aid in providing a more accurate prognosis. In human medicine, TDI and 2DST are currently used to differentiate the physiological "athlete's heart" from hypertrophic cardiomyopathy. In horses, TDI and 2DST might be used to evaluate the effect of training on myocardial function. In addition, these techniques might aid in providing a better assessment of right ventricular and atrial function.

In conclusion, TDI and 2DST offer many opportunities for better quantification of LV function. However, no single measurement is perfect. Ideally, the quantification of LV function should be based on a complete echocardiographic examination with conventional, TDI and 2DST measurements.

References

Adamu U, Schmitz F, Becker M, Kelm M, Hoffmann R (2009). Advanced speckle tracking echocardiography allowing a three-myocardial layer-specific analysis of deformation parameters. Eur J Echocardiogr 10, 303-308

Ama R, Segers P, Roosens C, Claessens T, Verdonck P, Poelaert J (2004). The effects of load on systolic mitral annular velocity by tissue Doppler imaging. Anesth Analg 99, 332-338

Amundsen BH, Crosby J, Steen PA, Torp H, Slordahl SA, Stoylen A (2009). Regional myocardial long-axis strain and strain rate measured by different tissue Doppler and speckle tracking echocardiography methods: A comparison with tagged magnetic resonance imaging. Eur J Echocardiogr 10, 229-237

Antoni ML, Mollema SA, Delgado V, Atary JZ, Borleffs CJ, Boersma E, Holman ER, van der Wall EE, Schalij MJ, Bax JJ (2010). Prognostic importance of strain and strain rate after acute myocardial infarction. Eur Heart J 31, 1640-1647

Biaggi P, Carasso S, Garceau P, Greutmann M, Gruner C, Tsang W, Rakowski H, Agmon Y, Woo A (2011). Comparison of two different speckle tracking software systems: Does the method matter? Echocardiography 28, 539-547

Bijnens BH, Cikes M, Claus P, Sutherland GR (2009). Velocity and deformation imaging for the assessment of myocardial dysfunction. Eur J Echocardiogr 10, 216-226

Blessberger H, Binder T (2010). Two-dimensional speckle tracking echocardiography: Clinical applications. Heart 96, 2032-2040

Bombardini T (2005). Myocardial contractility in the echo lab: Molecular, cellular and pathophysiological basis. Cardiovasc Ultrasound 3, 27

Borlaug BA, Melenovsky V, Redfield MM, Kessler K, Chang HJ, Abraham TP, Kass DA (2007). Impact of arterial load and loading sequence on left ventricular tissue velocities in humans. J Am Coll Cardiol 50, 1570-1577

Carabello BA (2002). Evolution of the study of left ventricular function: Everything old is new again. Circulation 105, 2701-2703

Carabello BA, Spann JF (1984). The uses and limitations of end-systolic indexes of left ventricular function. Circulation 69, 1058-1064

Chetboul V, Sampedrano CC, Concordet D, Tissier R, Lamour T, Ginesta J, Gouni V, Nicolle AP, Pouchelon JL, Lefebvre HP (2005). Use of quantitative two-dimensional color tissue Doppler imaging for assessment of left ventricular radial and longitudinal myocardial velocities in dogs. Am J Vet Res 66, 953-961

Davidsen ES, Moen CA, Matre K (2010). Radial deformation by tissue Doppler imaging in multiple myocardial layers. Scand Cardiovasc J 44, 82-91

Delfino JG, Fornwalt BK, Eisner RL, Leon AR, Oshinski JN (2008). Determination of transmural, endocardial, and epicardial radial strain and strain rate from phase contrast MR velocity data. J Magn Reson Imaging 27, 522-528

D'hooge J, Bijnens B (2006). The principles of ultrasound based motion and deformation estimation. In: Sutherland GR, Hatle L, Claus P, D'hooge J, Bijnens B, editors. Doppler myocardial imaging: A textbook, BSWK Scientific Consulting and Publishing, 23-48

Donal E, Bergerot C, Thibault H, Ernande L, Loufoua J, Augeul L, Ovize M, Derumeaux G (2009). Influence of afterload on left ventricular radial and longitudinal systolic functions: A two-dimensional strain imaging study. Eur J Echocardiogr 10, 914-921

Eidem BW, McMahon CJ, Cohen RR, Wu J, Finkelshteyn I, Kovalchin JP, Ayres NA, Bezold LI, O'Brian Smith E, Pignatelli RH (2004). Impact of cardiac growth on Doppler tissue imaging velocities: A study in healthy children. J Am Soc Echocardiogr 17, 212-221

Ferferieva V, Van den Bergh A, Claus P, Jasaityte R, Veulemans P, Pellens M, La Gerche A, Rademakers F, Herijgers P, D'hooge J (2012). The relative value of strain and strain rate for defining intrinsic myocardial function. Am J Physiol Heart Circ Physiol 302, H188-195

Fleming AD, Xia X, McDicken WN, Sutherland GR, Fenn L (1994). Myocardial velocity gradients detected by Doppler imaging. Br J Radiol 67, 679-688

Fraser AG, Payne N, Madler CF, Janerot-Sjoberg B, Lind B, Grocott-Mason RM, Ionescu AA, Florescu N, Wilkenshoff U, Lancellotti P, Wutte M, Brodin LA, Investigators M (2003). Feasibility and reproducibility of off-line tissue Doppler measurement of regional myocardial function during dobutamine stress echocardiography. Eur J Echocardiogr 4, 43-53

Galderisi M, Cattaneo F, Mondillo S (2007). Doppler echocardiography and myocardial dyssynchrony: A practical update of old and new ultrasound technologies. Cardiovasc Ultrasound 5, 28

Gehlen H, Iversen C, Stadler P (2009). Tissue Doppler echocardiographic examinations at rest and after exercise in horses with atrial fibrillation. Pferdeheilkunde 25, 11-16

Gehlen H, Marnette S, Rohn K, Stadler P (2005). Echocardiographic analysis of segmental left ventricular wall motion at rest and after exercise in horses with and without heart disease. J Eq Vet Sci 25, 468-479

Geyer H, Caracciolo G, Abe H, Wilansky S, Carerj S, Gentile F, Nesser HJ, Khandheria B, Narula J, Sengupta PP (2010). Assessment of myocardial mechanics using speckle tracking echocardiography: Fundamentals and clinical applications. J Am Soc Echocardiogr 23, 351-369; quiz 453-355

Gorcsan J, 3rd, Strum DP, Mandarino WA, Gulati VK, Pinsky MR (1997). Quantitative assessment of alterations in regional left ventricular contractility with color-coded tissue Doppler echocardiography. Comparison with sonomicrometry and pressure-volume relations. Circulation 95, 2423-2433

Greenberg NL, Firstenberg MS, Castro PL, Main M, Travaglini A, Odabashian JA, Drinko JK, Rodriguez LL, Thomas JD, Garcia MJ (2002). Doppler-derived myocardial systolic strain rate is a strong index of left ventricular contractility. Circulation 105, 99-105

Hanekom L, Lundberg V, Leano R, Marwick TH (2004). Optimisation of strain rate imaging for application to stress echocardiography. Ultrasound Med Biol 30, 1451-1460

Heimdal A, Stoylen A, Torp H, Skjaerpe T (1998). Real-time strain rate imaging of the left ventricle by ultrasound. J Am Soc Echocardiogr 11, 1013-1019

Ishizu T, Seo Y, Enomoto Y, Sugimori H, Yamamoto M, Machino T, Kawamura R, Aonuma K (2010). Experimental validation of left ventricular transmural strain gradient with echocardiographic two-dimensional speckle tracking imaging. Eur J Echocardiogr 11, 377-385

Kerkhof PLM (1999). Combination of millar and conductance catheter to assess equine left ventricular function. BMES/EMBS Conf Proc 1, 227

Kim YJ, Jones M, Greenberg NL, Popovic ZB, Sitges M, Bauer F, Thomas JD, Shiota T (2007). Evaluation of left ventricular contractile function using noninvasively determined single-beat end-systolic elastance in mitral regurgitation: Experimental validation and clinical application. J Am Soc Echocardiogr 20, 1086-1092

Koopman LP, Slorach C, Hui W, Manlhiot C, McCrindle BW, Friedberg MK, Jaeggi ET, Mertens L (2010a). Comparison between different speckle tracking and color tissue Doppler techniques to measure global and regional myocardial deformation in children. J Am Soc Echocardiogr 23, 919-928

Koopman LP, Slorach C, Manlhiot C, McCrindle BW, Friedberg MK, Mertens L, Jaeggi ET (2010b). Myocardial tissue Doppler velocity imaging in children: Comparative study between two ultrasound systems. J Am Soc Echocardiogr 23, 929-937

Lorch SM, Ludomirsky A, Singh GK (2008). Maturational and growth-related changes in left ventricular longitudinal strain and strain rate measured by two-dimensional speckle tracking echocardiography in healthy pediatric population. J Am Soc Echocardiogr 21, 1207-1215

Lyseggen E, Rabben SI, Skulstad H, Urheim S, Risoe C, Smiseth OA (2005). Myocardial acceleration during isovolumic contraction: Relationship to contractility. Circulation 111, 1362-1369

Margulescu AD, Thomas DE, Ingram TE, Vintila VD, Egan MA, Vinereanu D, Fraser AG (2010). Can isovolumic acceleration be used in clinical practice to estimate ventricular contractile function? Reproducibility and regional variation of a new noninvasive index. J Am Soc Echocardiogr 23, 423-431

Martensson M, Bjallmark A, Brodin LA (2011). Evaluation of tissue Doppler-based velocity and deformation imaging: A phantom study of ultrasound systems. Eur J Echocardiogr 12, 467-476

Marwick TH (2006). Measurement of strain and strain rate by echocardiography: Ready for prime time? J Am Coll Cardiol 47, 1313-1327

McGuirk SM, Muir WW (1985). Diagnosis and treatment of cardiac arrhythmias. Vet Clin North Am Equine Pract 1, 353-370

Meco M, Cirri S (2010). The effects of load on systolic mitral annulus movements by tissue Doppler imaging in cardiac surgery patients. J Cardiovasc Surg 51, 277-281

Mignot A, Donal E, Zaroui A, Reant P, Salem A, Hamon C, Monzy S, Roudaut R, Habib G, Lafitte S (2010). Global longitudinal strain as a major predictor of cardiac events in patients with depressed left ventricular function: A multicenter study. J Am Soc Echocardiogr 23, 1019-1024

Mor-Avi V, Lang RM, Badano LP, Belohlavek M, Cardim NM, Derumeaux G, Galderisi M, Marwick T, Nagueh SF, Sengupta PP, Sicari R, Smiseth OA, Smulevitz B, Takeuchi M, Thomas JD, Vannan M, Voigt JU, Zamorano JL (2011). Current and evolving echocardiographic techniques for the quantitative evaluation of cardiac mechanics: ASE/EAE consensus statement on methodology and indications endorsed by the japanese society of echocardiography. Eur J Echocardiogr 12, 167-205

Nesser HJ, Winter S (2009). Speckle tracking in the evaluation of left ventricular dyssynchrony. Echocardiography 26, 324-336

O'Gara P, Sugeng L, Lang R, Sarano M, Hung J, Raman S, Fischer G, Carabello B, Adams D, Vannan M (2008). The role of imaging in chronic degenerative mitral regurgitation. JACC Cardiovasc Imaging 1, 221-237

Parry BW, Anderson GA (1984). Importance of uniform cuff application for equine blood pressure measurement. Equine Vet J 16, 529-531

Patteson MW, Gibbs C, Wotton PR, Cripps PJ (1995). Echocardiographic measurements of cardiac dimensions and indices of cardiac function in normal adult Thoroughbred horses. Equine Vet J Suppl 19, 18-27

Reant P, Labrousse L, Lafitte S, Bordachar P, Pillois X, Tariosse L, Bonoron-Adele S, Padois P, Deville C, Roudaut R, Dos Santos P (2008). Experimental validation of circumferential, longitudinal, and radial 2-dimensional strain during dobutamine stress echocardiography in ischemic conditions. J Am Coll Cardiol 51, 149-157

Reef VB, Lalezari K, De Boo J, van der Belt AJ, Spencer PA, Dik KJ (1989). Pulsed-wave Doppler evaluation of intracardiac blood flow in 30 clinically normal Standardbred horses. Am J Vet Res 50, 75-83

Rosner A, Bijnens B, Hansen M, How OJ, Aarsaether E, Muller S, Sutherland GR, Myrmel T (2009). Left ventricular size determines tissue Doppler-derived longitudinal strain and strain rate. Eur J Echocardiogr 10, 271-277

Sawaya H, Sebag IA, Plana JC, Januzzi JL, Ky B, Cohen V, Gosavi S, Carver JR, Wiegers SE, Martin RP, Picard MH, Gerszten RE, Halpern EF, Passeri J, Kuter I, Scherrer-Crosbie M (2011). Early detection and prediction of cardiotoxicity in chemotherapy-treated patients. Am J Cardiol 107, 1375-1380

Schefer KD, Hagen R, Ringer SK, Schwarzwald CC (2011). Laboratory, electrocardiographic, and echocardiographic detection of myocardial damage and dysfunction in an Arabian mare with nutritional masseter myodegeneration. J Vet Intern Med 25, 1171-1180

Schwarzwald CC, Schober KE, Bonagura JD (2007a). Echocardiographic evidence of left atrial mechanical dysfunction after conversion of atrial fibrillation to sinus rhythm in 5 horses. J Vet Intern Med 21, 820-827

Schwarzwald CC, Schober KE, Bonagura JD (2007b). Methods and reliability of echocardiographic assessment of left atrial size and mechanical function in horses. Am J Vet Res 68, 735-747

Schwarzwald CC, Schober KE, Berli AS, Bonagura JD (2009a). Left ventricular radial and circumferential wall motion analysis in horses using strain, strain rate, and displacement by 2D speckle tracking. J Vet Intern Med 23, 890-900

Schwarzwald CC, Schober KE, Bonagura JD (2009b). Methods and reliability of tissue Doppler imaging for assessment of left ventricular radial wall motion in horses. J Vet Intern Med 23, 643-652

Sengupta PP, Khandheria BK, Korinek J, Wang J, Jahangir A, Seward JB, Belohlavek M (2006). Apex-to-base dispersion in regional timing of left ventricular shortening and lengthening. J Am Coll Cardiol 47, 163-172

Sivesgaard K, Christensen SD, Nygaard H, Hasenkam JM, Sloth E (2009). Speckle tracking ultrasound is independent of insonation angle and gain: An in vitro investigation of agreement with sonomicrometry. J Am Soc Echocardiogr 22, 852-858

Sjoli B, Orn S, Grenne B, Ihlen H, Edvardsen T, Brunvand H (2009). Diagnostic capability and reproducibility of strain by Doppler and by speckle tracking in patients with acute myocardial infarction. JACC Cardiovasc Imaging 2, 24-33

Su HM, Lin TH, Voon WC, Lee KT, Chu CS, Yen HW, Lai WT, Sheu SH (2007). Correlation of Tei index obtained from tissue Doppler echocardiography with invasive measurements of left ventricular performance. Echocardiography 24, 252-257

Sutherland GR, Hatle L, Claus P, Herbots L, Separovic J (2006). Normal data. In: Sutherland GR, Hatle L, Claus P, D'hooge J, Bijnens B, editors. Doppler myocardial imaging: A textbook, BSWK Scientific Consulting and Publishing, 49-102

Tekten T, Onbasili AO, Ceyhan C, Unal S, Discigil B (2003). Novel approach to measure myocardial performance index: Pulsed-wave tissue Doppler echocardiography. Echocardiography 20, 503-510

Teske AJ, De Boeck BW, Melman PG, Sieswerda GT, Doevendans PA, Cramer MJ (2007). Echocardiographic quantification of myocardial function using tissue deformation imaging, a guide to image acquisition and analysis using tissue Doppler and speckle tracking. Cardiovasc Ultrasound 5, 27-45

Thorstensen A, Dalen H, Amundsen BH, Aase SA, Stoylen A (2010). Reproducibility in echocardiographic assessment of the left ventricular global and regional function, the HUNT study. Eur J Echocardiogr 11, 149-156

Uematsu M, Miyatake K, Tanaka N, Matsuda H, Sano A, Yamazaki N, Hirama M, Yamagishi M (1995). Myocardial velocity gradient as a new indicator of regional left ventricular contraction: Detection by a two-dimensional tissue Doppler imaging technique. J Am Coll Cardiol 26, 217-223

Urheim S, Edvardsen T, Torp H, Angelsen B, Smiseth OA (2000). Myocardial strain by Doppler echocardiography. Validation of a new method to quantify regional myocardial function. Circulation 102, 1158-1164

van Dalen BM, Bosch JG, Kauer F, Soliman OI, Vletter WB, Ten Cate FJ, Geleijnse ML (2009). Assessment of mitral annular velocities by speckle tracking echocardiography versus tissue Doppler imaging: Validation, feasibility, and reproducibility. J Am Soc Echocardiogr 22, 1302-1308

Vinereanu D, Khokhar A, Fraser AG (1999). Reproducibility of pulsed wave tissue Doppler echocardiography. J Am Soc Echocardiogr 12, 492-499

Vogel M, Cheung MM, Li J, Kristiansen SB, Schmidt MR, White PA, Sorensen K, Redington AN (2003). Noninvasive assessment of left ventricular force-frequency relationships using tissue Doppler-derived isovolumic acceleration: Validation in an animal model. Circulation 107, 1647-1652

Weidemann F, Jamal F, Sutherland GR, Claus P, Kowalski M, Hatle L, De Scheerder I, Bijnens B, Rademakers FE (2002). Myocardial function defined by strain rate and strain during alterations in inotropic states and heart rate. Am J Physiol Heart Circ Physiol 283, H792-799

Zamorano J, Wallbridge DR, Ge J, Drozd J, Nesser J, Erbel R (1997). Non-invasive assessment of cardiac physiology by tissue Doppler echocardiography. A comparison with invasive haemodynamics. Eur Heart J 18, 330-339

Summary

The equine heart is extremely adapted to athletic performance. However, the large cardiac size and enormous cardiovascular pressures during exercise also entail negative consequences such as the high prevalence of exercise-induced pulmonary hemorrhage, exercise-related dysrhythmia and valvular insufficiency. In horses with cardiac disease or poor performance, echocardiography is an essential tool for non-invasive evaluation of myocardial function. Left ventricular (LV) function is usually quantified by calculating fractional shortening. This measurement is based on focal radial myocardial wall thickening and is therefore only a rough estimator of global LV function, which consists of radial, circumferential and longitudinal wall motion. In contrast to human medicine, measurements of longitudinal LV function and diastolic transmitral flow are difficult because apical views are impossible to acquire in adult horses. Tissue Doppler imaging (TDI) and two-dimensional speckle tracking (2DST) are two echocardiographic techniques that might overcome the above mentioned limitations.

TDI measures myocardial velocities based on the Doppler principle. Using parasternal images, radial myocardial velocities can be assessed and myocardial deformation can be calculated from the velocity gradient between the endo- and epicardium. The total amount of wall deformation relative to the end-diastolic state is described as strain (%), the speed of deformation as strain rate (s^{-1}). Using 2DST, acoustic speckle patterns which are unique for each myocardial region are tracked in the two dimensions of the ultrasound image. As a result, longitudinal and circumferential shortening can be measured in addition to radial wall thickening. Although TDI and 2DST have been extensively described in human and small animal medicine, little is known on the use of both techniques in horses.

The aim of this study was to evaluate the use of TDI and 2DST for quantification of LV function in horses. First, the feasibility and repeatability of both techniques were determined in healthy horses and preliminary reference values were established (Chapter 3). Next, Chapter 4 describes the influence of the atrioventricular delay on peak LV velocity and acceleration during isovolumic contraction.

The clinical use of TDI and 2DST was assessed in horses with toxic cardiomyopathy caused by accidental lasalocid intoxication (Chapter 5). Finally, Chapter 6 describes the use of TDI and 2DST for detection of subtle myocardial dysfunction in horses with atypical myopathy.

In Chapter 3, the feasibility and reproducibility of TDI and 2DST measurements were described in ten healthy trotter horses. A fixed protocol for image acquisition and off-line analysis was developed. Repeated echocardiography and off-line measurements were performed by two independent observers. The inter- and intra-observer acquisition and measurement variability were assessed by calculating the coefficients of variation for repeated measurements. TDI and 2DST analyses were feasible in all horses. Using a modified four-chamber view, 2DST allowed quantification of global and segmental longitudinal LV velocity, displacement, strain rate and strain (Chapter 3.1). Significant segmental differences could be demonstrated. The longitudinal velocity and displacement curves presented a prominent base-to-midwall gradient, while strain rate and strain were similar in all segments except for a lower peak strain in the basal septal segment. Using short-axis images acquired at chordal and papillary muscle level, circumferential and radial LV function could be assessed by 2DST (Chapter 3.2). The interventricular septum showed a higher circumferential and lower radial strain compared to the LV free wall. Both in the four-chamber view and the short-axis images, tracking was often visually inadequate during diastole. Global systolic longitudinal, circumferential and radial strain and strain rate could be determined with low variability. Segmental function could be assessed with low variability using longitudinal and radial strain measurements, whereas circumferential measurements showed a higher variability. Using TDI, radial velocity, strain rate and strain measurements were feasible from left and right parasternal short-axis views at chordal and papillary muscle level, although strain rate and strain could often not be measured in the LV free wall from right parasternal views (Chapter 3.3). The high frame rate allowed measurements of systolic and diastolic time intervals, which could be determined with low to moderate variability and were significantly correlated to M-mode and pulsed wave Doppler measurements. The variability of measurements of peak velocity, strain rate and strain ranged from low to high and segmental differences were present.

Chapter 4 describes the influence of the atrioventricular (AV) delay on mitral valve closure (MVC) and LV peak velocity and acceleration (IVA) during isovolumic contraction (IVC). Six unsedated horses were evaluated during dual-chamber pacing at AV delays ranging from 150 to 350 ms, right ventricular pacing without preceding atrial contraction (RVP) and sinus rhythm. From a modified four-chamber view, MVC was measured simultaneously with LV pre-ejectional peak velocity and IVA. During sinus rhythm and long AV delays (≥300 ms), two positive pre-ejectional velocity peaks were present. The first peak was identified as LV recoil during atrial relaxation and consistently preceded MVC. The second peak occurred after MVC and was thus true isovolumic LV contraction. However, during short AV delays (<300 ms) and RVP, MVC occurred significantly later. Only one pre-ejectional peak was present, of which the end coincided with MVC. This suggests MVC caused by LV contraction. Since the mitral valve was still open at the onset of LV contraction, peak pre-ejectional velocity and IVA were significantly higher. As a consequence, the influence of AV interaction should be kept in mind when using peak pre-ejectional velocity and IVA as parameters of LV contractility.

The clinical use of TDI and 2DST was evaluated in horses with myocardial damage caused by an ionophore intoxication (Chapter 5.1). Accidental lasalocid poisoning had occurred on a farm in Belgium with eighty-one horses. Fourteen horses had demonstrated clinical signs such as inappetance, lethargy, sweating and muscular weakness between day 0 and 21 after being fed a new concentrate batch. Sixty-seven horses underwent a detailed cardiac examination consisting of echocardiography, electrocardiography (ECG) and determination of plasma cardiac troponin I (cTnI) concentration at admission and during follow-up between day 30 and 490. The echocardiographic study (Chapter 5.2) included twenty horses with signs of myocardial damage, which was defined as having a plasma cTnI concentration above reference range at one or more occasions. Based on the ECG results, five horses showed severe myocardial damage (increased cTnI and ventricular tachycardia) and fifteen mild myocardial damage (increased cTnI without ventricular tachycardia). Radial systolic LV velocity and strain were measured by TDI.

Using 2DST, longitudinal strain (SL) and circumferential (SC) and radial strain (SR) at chordal and papillary muscle level were measured. LV fractional shortening (FS) was calculated for comparison. Horses with severe myocardial damage showed severely decreased TDI, 2DST and FS measurements, indicating reduced LV function. Long-term follow-up of two surviving horses demonstrated full recovery in one horse and permanent regional myocardial fibrosis in the other. TDI and 2DST could detect regional alterations of myocardial function caused by the predominant presence of fibrosis in the interventricular septum. TDI and 2DST measurements in horses with mild myocardial damage showed few significant differences compared to a control group, although 4/15 horses had decreased SL values whereas only 1/15 horses had a FS value below reference range. Over all horses, TDI measurements, SL, SR at chordal level and FS correlated significantly with maximal cTnI. Over all examinations, TDI and 2DST measurements correlated well with FS.

The ability of TDI and 2DST to detect myocardial dysfunction in horses with normal FS was investigated in Chapter 6. Atypical myopathy (AM) is an acute, highly fatal rhabdomyolysis in grazing horses that mainly affects the skeletal muscles, although myocardial damage has been described at necropsy. Twelve horses with AM underwent a clinical exam, echocardiography, ECG and determination of plasma cTnI concentration. Eleven horses had elevated cTnI concentrations and ten horses ventricular premature depolarizations (VPDs). All horses presented a prolonged corrected QT (QT_{cf}) interval and an abnormal LV wall motion pattern. FS was normal in all horses. TDI measurements revealed abnormal LV relaxation with prolonged contraction duration, increased isovolumic relaxation time and decreased ratio of early to late diastolic (E/A) LV radial velocities. Decreased LV global longitudinal strain and increased mechanical dispersion between myocardial segments could be detected by 2DST. One of four surviving horses still showed VPDs and a mildly prolonged QT_{cf} after ten weeks follow-up, although the wall motion abnormality had disappeared.

The final chapter (Chapter 7) presents the general discussion and conclusions. TDI and 2DST can be considered complimentary for the comprehensive quantification of LV function.

Because of the high frame rate, TDI offers reliable measurements of cardiac time intervals and can be used for quantification of both systolic and diastolic radial LV function, while 2DST is well suited for measurements of global systolic longitudinal, circumferential and radial LV function. Regional function and synchrony can be assessed by TDI and 2DST, taking into account physiological segmental differences.

Currently, TDI and 2DST are mainly research tools, providing new insights into the physiology and pathophysiology of the equine heart. The clinical studies using TDI and 2DST in horses with toxic cardiomyopathy and with atypical myopathy demonstrated that both techniques can detect myocardial dysfunction, even in horses with normal FS. In the future, TDI and 2DST are likely to become available in an increasing number of equine referral practices. The fast evolution of ultrasound technology and postprocessing software will probably solve many of the current disadvantages. More research is needed to evaluate the clinical use of both techniques and to identify those measurements with the best diagnostic and prognostic value. TDI and 2DST might be applied for detection of subclinical myocardial dysfunction in horses with valvular disease, for evaluating the effect of training or for quantification of right ventricular and atrial function.

Samenvatting

Het paard staat bekend om zijn superieure atletische capaciteit. De extreme hartgrootte en hoge cardiovasculaire drukken tijdens inspanning hebben echter ook negatieve gevolgen zoals het optreden van longbloedingen en hartritmestoornissen en de verhoogde prevalentie van kleplekken. Echocardiografie is een essentieel diagnostisch instrument bij het onderzoek van paarden met een hartaandoening of verminderde prestaties. De myocardfunctie wordt meestal beoordeeld aan de hand van de radiale verkortingsfractie van het linker ventrikel (LV). Deze meting is gebaseerd op de focale radiale verdikking van het myocard en geeft dus slechts een ruwe inschatting van de globale hartspierfunctie, die bestaat uit radiale, circumferentiële en longitudinale beweging van het LV. Metingen van de longitudinale LV functie en diastolische bloedstroom over de mitraalklep zijn moeilijk bij volwassen paarden doordat een apicale benadering van het hart onmogelijk is. Tissue Doppler imaging (TDI) en two-dimensional speckle tracking (2DST) zijn twee echocardiografische technieken die bij de mens en kleine huisdieren reeds gebruikt worden voor een meer uitgebreide beoordeling van de LV functie.

Met TDI wordt de snelheid van de myocardbeweging gemeten op basis van het Doppler-principe. Door middel van parasternale beelden kan de radiale myocardsnelheid worden beoordeeld. Aan de hand van de gradiënt tussen de endo- en epicardiale snelheid kan de deformatie van het myocard berekend worden. De totale deformatie ten opzichte van de einddiastolische toestand is de strain (%), de snelheid van vervorming is de strain rate (s^{-1}). Met 2DST wordt de beweging van akoestische speckle patronen in het myocard gevolgd doorheen de hartcyclus (‘tracking’) in de twee dimensies van het echobeeld. Hierdoor kan niet enkel de radiale wandverdikking, maar ook de longitudinale en circumferentiële verkorting gemeten worden. Hoewel TDI en 2DST uitvoerig beschreven zijn in de humane geneeskunde en bij kleine huisdieren, is er weinig bekend over het gebruik van beide technieken bij paarden.

Het doel van deze studie was om het gebruik van TDI en 2DST voor het meten van LV functie bij paarden te evalueren. Eerst werden de haalbaarheid en herhaalbaarheid bepaald bij gezonde paarden en werden referentiewaarden vastgelegd (Hoofdstuk 3).

Hoofdstuk 4 beschrijft de invloed van het atrioventriculair interval op de LV pieksnelheid en acceleratie tijdens de isovolumetrische contractie. Het klinisch gebruik van TDI en 2DST werd beoordeeld bij paarden met toxische cardiomyopathie als gevolg van een accidentele lasalocid intoxicatie (Hoofdstuk 5). Tot slot werd in Hoofdstuk 6 het gebruik van TDI en 2DST voor de detectie van subklinische myocarddysfunctie bij paarden met atypische myopathie onderzocht.

In Hoofdstuk 3 werden de haalbaarheid en herhaalbaarheid van TDI en 2DST metingen bepaald bij tien gezonde dravers. Een vast protocol voor de acquisitie en het uitmeten van TDI en 2DST curves werd opgesteld. Herhaalde beeldacquisitie en metingen werden uitgevoerd door twee onafhankelijke waarnemers. De inter- en intra-observer acquisitie- en meetvariabiliteit werden bepaald door de berekening van variatiecoëfficiënten voor herhaalde metingen. TDI en 2DST metingen konden uitgevoerd worden bij alle paarden. Met behulp van een aangepast vierkamerbeeld kon de globale en regionale longitudinale LV snelheid, verplaatsing, strain en strain rate gemeten worden (Hoofdstuk 3.1). Significante regionale verschillen konden worden aangetoond. De longitudinale snelheid en verplaatsing vertoonden een duidelijke gradiënt van de mitraalring naar de apex terwijl de strain en strain rate vergelijkbaar waren in alle segmenten, met uitzondering van lagere strain waarden in het basale septum. Op basis van korte-as beelden op chordae- en papillairspierniveau kon de circumferentiële en radiale LV functie worden beoordeeld met 2DST (Hoofdstuk 3.2). Het interventriculaire septum had een hogere circumferentiële en lagere radiale strain ten opzichte van de LV vrije wand. Zowel in het vierkamerbeeld als in de korte-as beelden was de tracking vaak visueel onvoldoende tijdens diastole. Globale systolische longitudinale, circumferentiële en radiale strain en strain rate konden wel worden bepaald met een lage variabiliteit. Ook regionale longitudinale en radiale LV functie konden worden gemeten met een lage variabiliteit, terwijl de circumferentiële metingen een grotere variabiliteit vertoonden. Met TDI konden de radiale snelheid, strain rate en strain vanuit linker en rechter parasternale korte-as beelden op chordae- en papillairspierniveau gemeten worden. Strain rate en strain konden echter vaak niet bepaald worden in de LV vrije wand van rechts parasternaal uit (Hoofdstuk 3.3).

De hoge frame rate van TDI maakte metingen van systolische en diastolische tijdsintervallen mogelijk met een lage tot matige variabiliteit. Deze metingen waren significant gecorreleerd met conventionele M-mode en pulsed wave Doppler metingen. De variabiliteit van de metingen van pieksnelheid, strain rate en strain varieerde van laag naar hoog en net als bij 2DST waren regionale verschillen waren aanwezig.

In Hoofdstuk 4 werd de invloed van het atrioventriculair (AV) interval op de mitraalklepsluiting (MVC) en de linker ventriculaire pieksnelheid en acceleratie (IVA) tijdens de isovolumetrische contractie (IVC) nagegaan. Zes ongesedeerde paarden werden onderzocht tijdens pacen aan AV intervallen van 150 tot 350 ms, rechter ventriculaire pacing zonder voorafgaande atriale contractie (RVP) en sinusritme. Met behulp van een aangepast vierkamerbeeld kon MVC gelijktijdig gemeten worden met de IVC pieksnelheid en IVA. Tijdens sinusritme en lange AV intervallen ($\geq$ 300 ms) waren 2 snelheidspieken aanwezig in de pre-ejectie periode. De eerste piek werd geïdentificeerd als beweging van het LV tijdens atriale relaxatie en werd gevolgd door MVC. De tweede piek kwam na MVC en was dus een echte isovolumetrische LV contractie. Tijdens korte AV intervallen (<300 ms) en RVP trad de MVC significant later op. Slechts 1 snelheidspiek was aanwezig tijdens de pre-ejectie periode, waarvan het einde samenviel met MVC. Dit suggereert dat MVC werd veroorzaakt door LV contractie. Aangezien de mitraalklep nog open was bij het begin van de LV contractie waren de IVC pieksnelheid en IVA significant hoger. Bij de interpretatie van de IVC pieksnelheid en IVA als parameter voor LV contractiliteit moet dus rekening gehouden worden met de invloed van de AV interactie.

Het klinisch gebruik van TDI en 2DST werd geëvalueerd bij paarden met myocardschade veroorzaakt door ionoforen (Hoofdstuk 5.1). Accidentele lasalocid intoxicatie had plaatsgevonden op een paardenhouderij in België met eenentachtig paarden. Veertien paarden hadden tussen dag 0 en 21 na het eten van een nieuwe levering krachtvoeder klinische verschijnselen vertoond zoals gebrek aan eetlust, lusteloosheid, zweten en spierzwakte. Zevenenzestig paarden ondergingen tussen dag 30 en 490 een uitgebreid hartonderzoek, bestaande uit echocardiografie, elektrocardiografie (ECG) en bepaling van plasma cardiale troponine I (cTnI) concentratie.

Twintig paarden werden opgenomen in de echocardiografische studie (Hoofdstuk 5.2) omdat ze tekenen van myocardschade vertoonden. Dit werd gedefinieerd als een plasma cTnI concentratie boven de referentiewaarden bij een of meerdere onderzoeken. Op basis van de ECG-resultaten werden de paarden verder onderverdeeld. Vijf paarden vertoonden ernstige myocardschade (verhoogde cTnI en ventriculaire tachycardie) en vijftien lichte myocardschade (verhoogde cTnI zonder ventriculaire tachycardie). De radiale systolische myocardsnelheid en strain werden gemeten met TDI. Met 2DST werden de longitudinale strain (SL) en de circumferentiële en radiale strain (SR) op chordae- en papillairspierniveau gemeten. De LV radiale verkortingsfractie (FS) werd berekend door middel van M-mode. De paarden met ernstige myocardschade hadden sterk afwijkende TDI, 2DST en FS metingen, wat wees op een verminderde LV functie. Opvolging van twee overlevende paarden toonde volledig herstel aan bij een paard en permanente regionale myocardfibrose bij het andere. TDI en 2DST konden bij dit laatste paard regionale veranderingen detecteren die veroorzaakt werden door de gelokaliseerde aanwezigheid van fibrose in het interventriculaire septum. TDI en 2DST metingen bij paarden met lichte myocardschade waren niet significant verschillend in vergelijking met een controlegroep, hoewel 4/15 paarden een verlaagde SL hadden terwijl slechts 1/15 paarden een verlaagde FS waarde had. De TDI metingen, SL, SR op chordae niveau en FS waren significant gecorreleerd met de maximale cTnI concentratie. Over het geheel van alle onderzoeken waren de TDI en 2DST metingen gecorreleerd met FS.

Het vermogen van TDI en 2DST om myocarddysfunctie op te sporen bij paarden met een normale FS werd onderzocht in Hoofdstuk 6. Atypische myopathie (AM) is een acute en vaak fatale spierziekte die enkel voorkomt bij paarden met weidegang. Vooral de skeletspieren worden aangetast, maar bij autopsie wordt ook myocardschade gezien. Twaalf paarden met AM werden onderzocht door middel van echocardiografie, ECG en bepaling van plasma cTnI concentratie. Elf paarden hadden verhoogde cTnI concentraties en tien paarden ventriculaire premature depolarisaties (VPDs). Alle paarden hadden een verlengd gecorrigeerd QT (QT_{cf}) interval en een abnormaal LV contractiepatroon. FS was normaal bij alle paarden. TDI metingen toonden een verlengde contractieduur, een verlengde isovolumetrische relaxatietijd en een verlaagde verhouding van vroeg- tot laat-diastolische myocardsnelheid aan, wat wees

op abnormale LV relaxatie. Met 2DST kon een verminderde LV globale longitudinale strain en verhoogde spreiding van de contractieduur tussen myocardsegmenten gedetecteerd worden. Een van de vier overlevende paarden vertoonde nog steeds VPDs en een milde verlenging van het QT_{cf} interval na tien weken follow-up, hoewel het abnormale LV contractiepatroon was verdwenen.

Het laatste hoofdstuk (Hoofdstuk 7) omvat de algemene discussie en conclusies. TDI en 2DST vullen elkaar aan bij het meten van LV functie. Door de hoge frame rate is TDI uitermate geschikt voor metingen van systolische en diastolische tijdsintervallen en kan zowel systolische als diastolische radiale LV functie beoordeeld worden. Met 2DST kan de globale systolische longitudinale, circumferentiële en radiale LV functie gemeten worden. Beide technieken kunnen worden gebruikt voor de beoordeling van regionale functie en synchronie, waarbij rekening moet gehouden worden met fysiologische regionale verschillen.

Momenteel worden TDI en 2DST voornamelijk gebruikt voor wetenschappelijk onderzoek. Beide technieken verschaffen nieuwe inzichten in de fysiologie en pathofysiologie van het paardenhart. De klinische studies bij paarden met toxische cardiomyopathie en met atypische myopathie hebben reeds aangetoond dat TDI en 2DST myocarddysfunctie kunnen detecteren, zelfs bij paarden met normale FS. Meer onderzoek is nodig om het klinisch gebruik van beide technieken te evalueren en de metingen met de beste diagnostische waarde te identificeren. Mogelijke toepassingen zijn het opsporen van subklinische myocarddysfunctie bij paarden met kleplekken, het evalueren van het effect van training op de myocardfunctie en het meten van rechter ventriculaire en atriale functie.

Curriculum vitae

Annelies Decloedt werd geboren op 16 februari 1986 te Gent.

Na het beëindigen van het secundair onderwijs aan het Emmäusinstituut in Aalter begon zij in 2002 met de studies diergeneeskunde aan de Universiteit Gent. In 2008 behaalde ze het diploma van dierenarts (optie paard) met grootste onderscheiding. Haar scriptie, getiteld "MestpH bij het paard: vergelijking bij gezonde paarden en bij paarden met digestiestoornissen", werd bekroond met de prijs van de Belgian Equine Practitioners Society.

Gefascineerd door wetenschappelijk onderzoek, startte zij op 1 oktober 2008 een doctoraatsstudie over de evaluatie van de myocardfunctie bij het paard aan de vakgroep Interne Geneeskunde en Klinische Biologie van de Grote Huisdieren. Deze studie werd gefinancierd door het Fonds Wetenschappelijk Onderzoek - Vlaanderen (FWO). Naast haar onderzoek was zij ook betrokken bij het klinisch werk op de dienst Inwendige Ziekten. Tevens vervolledigde zij in 2012 het trainingsprogramma van de Doctoral School of Life Sciences and Medicine van de Universiteit Gent.

Annelies Decloedt is auteur of mede-auteur van meerdere wetenschappelijke (A1) publicaties. Zij was eveneens spreker op verschillende internationale congressen.

Bibliography

Publications

Verheyen T, Decloedt A, De Clercq D, van Loon G (2012). Ventricular response during lunging exercise in horses with atrial fibrillation. In preparation.

Decloedt A, Verheyen T, Sys S, De Clercq D, Bijnens B, van Loon G (2012). The influence of atrioventricular interaction on mitral valve closure and left ventricular isovolumic contraction. Ready for submission.

Decloedt A, Verheyen T, Sys S, De Clercq D, van Loon G (2012). Tissue Doppler imaging for regional quantification of radial left ventricular wall motion in healthy horses. Am J Vet Res, submitted.

Verheyen T, Decloedt A, De Clercq D, van Loon G (2012). Cardiac changes in equine atypical myopathy. J Vet Int Med, accepted for publication.

Decloedt A, Verheyen T, Sys S, De Clercq D, van Loon G (2012). Tissue Doppler imaging and two-dimensional Speckle Tracking detect left ventricular hypocontractility in horses exposed to ionophores. J Vet Int Med, submitted.

Decloedt A, Verheyen T, De Clercq D, Sys S, Vercauteren G, Ducatelle R, Delahaut P, van Loon G. Acute and long-term cardiomyopathy and delayed neurotoxicity after accidental lasalocid poisoning in horses. J Vet Int Med, Epub 2012/04/21, DOI: 10.1111/j.1939-1676.2012.00933.x

Decloedt A, Verheyen T, Sys S, De Clercq D, van Loon G (2012). Two-dimensional speckle tracking for quantification of left ventricular circumferential and radial wall motion in horses. Eq Vet J, Epub 2012/02/20, DOI: 10.1111/j.2042-3306.2012.00549.x

Verheyen T, Decloedt A, Sys S, De Clercq D, van Loon G (2012). Oesophageal electrocardiography in healthy horses. Eq Vet J, Epub 2011/12/14, DOI: 10.1111/j.2042-3306.2011.00526.x

Decloedt A, Verheyen T, Sys S, De Clercq D, van Loon G (2011). Quantification of left ventricular longitudinal strain, strain Rate, velocity, and displacement in healthy horses by two-dimensional speckle tracking. J Vet Int Med 25, 330–338

Verheyen T, Decloedt A, De Clercq D, Deprez P, Sys S, van Loon G (2010). Electrocardiography in horses, part 2: how to read the equine ECG. Vlaams Dierg Tijdschrift 79, 337-344

Verheyen T, Decloedt A, De Clercq D, Deprez P, Sys S, van Loon G (2010). Electrocardiography in horses, part 1: how to make a good recording. Vlaams Dierg Tijdschrift 79, 331-336

Conference contributions

Verheyen T, Decloedt A, Van Der Vekens N, Smiet E, De Clercq D, van Loon G (2012). Extreme tachycardia and QRS broadening during exercise in horses with atrial fibrillation. Oral abstract presentation, Proceedings 45th European Veterinary Conference (Voorjaarsdagen) 2012, Amsterdam, The Netherlands, p302

De Clercq D, Verheyen T, Decloedt A, Lefere L, van Loon G (2012). Atrial standstill in a horse with cardiac glycoside intoxication. Oral abstract presentation, Proceedings 45th European Veterinary Conference (Voorjaarsdagen) 2012, Amsterdam, The Netherlands, p302

van Loon G, De Witte M, Rossel N, Decloedt A, Verheyen T, De Clercq D, Saey V, Chiers K, Segers P (2012). Measurement of arterial diameter distension to assess arterial wall stiffness in horses: preliminary results. Oral abstract presentation, 5th Congress of the European College of Equine Internal Medicine 2012, Edinburgh, UK, J Vet Int Med 2012;26:425-426

Decloedt A, Verheyen T, Sys S, De Clercq D, van Loon G (2011). Peak left ventricular isovolumic velocity: determined by atrioventricular interaction and not always isovolumic? Oral abstract presentation, EUROECHO & other Imaging Modalities Congress 2011, Budapest, Hungary, Eur J Echocardiogr. 12 (Suppl 2), p84

van Loon G, Decloedt A, Verheyen T, De Clercq D, Van Der Vekens N, Deprez P (2011). Accidental lasalocid intoxication on a farm with eighty-one horses. Clinical research presentation, 50th BEVA Congress 2011, Liverpool, United Kingdom, p90-91

Decloedt A, Verheyen T, De Clercq D, van Loon G (2011). Quantification of left ventricular function in horses with aortic valve insufficiency by tissue Doppler imaging and 2D speckle tracking. Clinical research presentation, 50th BEVA Congress 2011, Liverpool, United Kingdom, p84-85

van Loon G, Verheyen T, Decloedt A, Delesalle C, Schauvliege S, De Wolf D (2011). Use of a transcatheter occlusion device in a 9-year old Friesian gelding with aortopulmonary fistula. Oral abstract presentation, Proceedings 44th European Veterinary Conference (Voorjaarsdagen) 2011, Amsterdam, The Netherlands, p365

Decloedt A, Verheyen T, van Loon G (2011). TDI and 2DST detect left ventricular hypocontractility in horses exposed to ionophores. Oral abstract presentation, Proceedings 44th European Veterinary Conference (Voorjaarsdagen) 2011, Amsterdam, The Netherlands, p365-366

Verheyen T, Decloedt A, van Loon G (2011). Electrocardiographic and echocardiographic evidence of cardiac muscle involvement in horses with atypical myopathy. Poster presentation, 5th European Equine Nutrition and Health Congress 2011, Waregem, Belgium

Verheyen T, Decloedt A, De Clercq D, van Loon G (2011). Oesophageal electrocardiography in horses. Oral abstract presentation, 4th Congress of the European College of Equine Internal Medicine 2011, Hannover, Germany, J Vet Intern Med 25, 625

Verheyen T, Decloedt A, De Clercq D, van Loon G (2011). Electrocardiographic and echocardiographic findings in horses with atypical myopathy. Oral abstract presentation, 4th Congress of the European College of Equine Internal Medicine 2011, Hannover, Germany, J Vet Intern Med 25, 625-626

Verheyen T, Decloedt A, De Clercq D, van Loon G (2010). Do arrhythmias on a twenty-four hour ECG recording predict atrial fibrillation recurrence after successful transvenous electrical cardioversion? Oral abstract presentation, Proceedings 38th AVEF congress 2010, Bordeaux, France, p323-324

Decloedt A, Sys S, Deprez P, De Clercq D, van Loon G (2010). Echocardiographic assessment of equine left ventricular function: tissue Doppler versus 2-dimensional strain analysis. Poster presentation, 8th International Conference on Equine Exercise Physiology 2010, Cape Town, South Africa

van Loon G, De Clercq D, de Bruin CM, Chiers K, Verheyen T, Decloedt A, Deprez P (2010). Clinical findings and diagnosis of aortopulmonary fistula in four Friesian horses. Oral abstract presentation, Proceedings 49th BEVA congress 2010, Birmingham, United Kingdom, p215

van Loon G, Decloedt A, Verheyen T, De Clercq D, Deprez P (2010). Noninvasive determination of atrial fibrillation cycle length by means of tissue Doppler imaging. Poster presentation, Proceedings 49th BEVA congress 2010, Birmingham, United Kingdom, p230

Decloedt A, Deprez P, van Loon G (2009). Left ventricular longitudinal strain and strain rate in healthy horses. Clinical research presentation, Proceedings 48th BEVA Congress 2009, Birmingham, United Kingdom, p169

Decloedt A, van Loon G (2009). TDI: a new way to visualise the equine heart. Oral abstract presentation, Proceedings 42nd European Veterinary Conference (Voorjaarsdagen) 2009, Amsterdam, The Netherlands, p366

Decloedt A, van Loon G (2009). Tissue Doppler and speckle tracking in horses: can we quantify equine myocardial function? Poster Presentation, Symposium 75 Years of Veterinary Medicine at Ghent University, Merelbeke, Belgium

Dankwoord

Een doctoraat schrijven doe je niet alleen en dit wordt weerspiegeld in het dankwoord, wat waarschijnlijk meteen het meest gelezen stuk van dit boekje is.

De bovenstaande zin bevat de twee grootste clichés die in een dankwoord gebruikt worden, maar ze kloppen dan ook als een bus. Om te beginnen hebt u, beste lezer, wellicht niet eerst het hele boekje doorgelezen, maar bent u snel doorgebladerd naar deze pagina. En inderdaad, ik had dit doctoraat nooit kunnen maken zonder de hulp en steun van vele anderen, die hun plaatsje in dit dankwoord meer dan verdiend hebben.

Dit doctoraat zou er nooit gekomen zijn zonder mijn promotor, prof. Dr. Gunther van Loon. Bij het begin van dit onderzoek kende ik net het verschil tussen een systolisch en diastolisch bijgeruis, maar dankzij uw onmetelijke enthousiasme werd ik al snel gepassioneerd door de cardiologie. Zelfs als alle dossiers en to do-lijstjes zich opstapelden op uw bureau was er toch steeds tijd voor het bespreken van nieuwe resultaten of om mee te kijken naar iets interessants dat te zien was op de echo. Bedankt voor de begeleiding en alle advies, maar ook voor de vrijheid die ik kreeg om mijn onderzoek zelf in een bepaalde richting te sturen. Ook mijn co-promotor, Prof. Dr. Piet Deprez wil ik graag bedanken. Als vakgroepvoorzitter weet u steeds met zachte hand alles in goede banen te leiden op Inwendige.

Prof. Dr. Johan De Sutter, terwijl wij ons blindstaarden op de vele piekjes in de curves gaf u als tip dat ik mij vooral moest focussen op die dingen die we wel goed konden meten, met als resultaat dit doctoraat. Bedankt om deel uit te maken van mijn begeleidingscommissie!

Prof. Dr. Bart Bijnens, uw enthousiasme voor het onderzoek werkt zeer aanstekelijk. Ik ben dan ook vereerd dat u lid bent van de examencommissie. Prof. Dr. Jimmy Saunders en Dr. Valerie Bavegems, bedankt voor het nalezen van dit werk en voor de opbouwende kritieken. Dr. Bavegems wil ik ook graag bedanken om mij in te wijden in de cardiologie van hond en kat. Prof. Dr. Amory and Prof. Dr. Schwarzwald, thank you for your remarks and suggestions. They have certainly improved the quality of this thesis.

Prof. Dr. Stanislas Sys, bedankt voor de hulp bij de statistische analyses.

De voorbije jaren mocht ik deel uitmaken van het enige echte ‘cardio-team’. Dominique, bedankt voor alle hulp bij het praktische werk van dit doctoraat. Tussen het vele werk in de kliniek en het studeren voor je diplomate-status door wist je toch steeds tijd te vinden om me nuttige tips te geven. Tinne, wat was ik blij toen ik op de vakgroep kwam en bleek dat er nog iemand een doctoraat over cardiologie deed. Drie jaar lang waren we met ons twee ‘partners in crime’ als het over cardiologie-onderzoek ging. De echo’s en inspanningstesten die we samen gedaan hebben zijn ondertussen al niet meer te tellen. Hopelijk blijven we elkaar nog zien als we (binnenkort) allebei “doctor” zijn. Nicky, jij bent er laatst bijgekomen maar ondertussen zijn jij en je biomarkers niet meer weg te denken. Behalve een veelbelovende doctoraatsstudente ben je vooral een heel toffe bureaugenote!

Tijdens mijn doctoraat kon ik mij volledig toeleggen op dit onderzoek, en dat was alleen mogelijk dankzij de collega’s die de kliniek draaiende hielden, ook ’s nachts en in het weekend. Bedankt dus aan Laurence, Caroline, Sara, Kirsten, Barbara en de vroegere collega’s Heidi, Katleen en Inge. (Bijna) ieder paard met een bijgeruis of aritmie werd gemeld zodat ik nog een echootje bij kon doen voor mijn onderzoek. Ter afwisseling was er af en toe eens een kalfje of koe om te scannen, met dank aan de rundercollega’s Bart, Peter en Bonnie. Daarnaast verleenden ook de interns en studenten vele uurtjes assistentie. Zeggen dat paarden vasthouden voor een hartecho niet de meest favoriete job op kliniek was is een understatement. Toch werd dit met de glimlach gedaan. Ook alle collega’s van de andere vakgroepen wil ik bedanken voor de fijne samenwerking. Een belangrijke schakel in de kliniekwerking zijn natuurlijk ook alle niet-dierenartsen op onze dienst. Dankzij Elvin waren de katheters steeds op tijd gesteriliseerd, terwijl Saar altijd lachend en enthousiast de paarden verzorgde. Hans, door jouw vrolijke goeiemorgen is het altijd aangenaam toekomen op het werk. Daarnaast moet ik je natuurlijk ook bedanken voor de IT-hulp. Na het crashen van mijn 2 eerste computers bleek de derde de juiste te zijn voor het afwerken van dit doctoraat! Sylvie, bedankt voor het regelen van alle geldzaken. In alle rust en stilte verzet je toch bergen werk. Sabrina, jou kwamen we meestal pal op de middag lastigvallen met bloed voor het ‘cardio-bakje’ in de diepvries. Bedankt voor de fijne samenwerking de afgelopen jaren! Tot slot wil ik ook de stalknechten graag bedanken voor de goede verzorging van de proefpaarden.

Voor het uitvoeren van dit onderzoek was het echotoestel van groot belang. Bedankt dus aan Johan Vandeweghe van GE Healthcare voor de goede samenwerking en de vlotte service. Dankzij GE kreeg ik ook de kans om naar Wenen te gaan voor de cursus ‘Deformation Imaging for Research and Clinical Practice’, een zeer leerrijke ervaring.

Daarnaast wil ik ook nog alle paardeneigenaren bedanken die ons toestonden om bij hun paard de extra TDI en 2DST beelden te nemen, ook al duurde het onderzoek dan wat langer. Vooral de eigenaars en vrijwilligers van de paardenhouderij uit hoofdstuk 5 wil ik bedanken voor hun medewerking. Ze brachten meer dan 60 paarden naar Merelbeke voor de nodige onderzoeken, zelfs al moesten sommige paarden tot drie maal toe terugkomen voor een hercontrole. Bedankt hiervoor!

Voor de financiële kant van dit doctoraat wil ik graag het Fonds Wetenschappelijk Onderzoek Vlaanderen bedanken voor de beurs waarvan ik 4 jaar mocht genieten.

Natuurlijk is er meer in het leven dan cardiologie alleen, en dankzij mijn vrienden kon ik de afgelopen jaren ook eens over iets anders praten dan mijn doctoraat. Omdat het niet de bedoeling is dat dit dankwoord langer wordt dan de rest van het boekje zal ik niet teveel uitweiden, maar weet dat jullie mij allemaal heel nauw aan het hart liggen. Om te beginnen mijn collega-dierenartsen, de 'liefste vriendjes', vier jaar na afstuderen zijn we uitgezwermd in allerlei richtingen, de ene al wat verder dan de andere. Toch hoop ik dat we elkaar nog lang regelmatig zullen zien, al wordt de groep steeds groter met alle partners en kinderen. Daarnaast kon ik op vrijdagavond stoom afblazen dankzij de bende van het Brouwershuys. Het doet elke keer deugd om over van alles en nog wat te kunnen babbelen. Ook de vrienden van Emmaüs en van Rapid Aalter konden af en toe mijn gedachten verzetten. En alle mensen van Horse Mania, bedankt voor jullie steun, vooral tijdens het voorbije jaar.

Een speciale dankjewel gaat naar mijn ouders. Dankzij jullie kon ik zorgeloos opgroeien, bezig zijn met de paarden, diergeneeskunde studeren, … Bedankt om er altijd voor Anneleen en mij te zijn.

En tot slot: Xavier, bedankt voor alles wat je voor mij doet, maar vooral gewoon om wie je bent.

Annelies

UNIVERSITEIT GENT

Ghent University
Faculty of Veterinary Medicine
Department of Large Animal Internal Medicine
Salisburylaan 133, 9820 B-Merelbeke

ISBN 978-90-5864-293-6